

DEVELOPING A STABLE ISOTOPE APPROACH TO TRACE THE SOURCES AND METABOLISM OF PHOSPHORUS IN FRESHWATERS

Ceri Louise Davies

MSci (Hons), MSc

This thesis is submitted in accordance of the requirements for the degree of
Doctor of Philosophy

September 2016

Lancaster
Environment Centre

Lancaster
University



ABSTRACT

The oxygen isotope ratio of dissolved inorganic phosphate ($\delta^{18}\text{O}_p$) represents a novel and potentially powerful stable isotope tracer for biogeochemical research. Analysis of $\delta^{18}\text{O}_p$ may offer new insights into the relative importance of different sources of phosphorus within natural ecosystems. Due to the isotope fractionations that occur alongside metabolism of phosphorus-containing compounds, $\delta^{18}\text{O}_p$ could also be used to better understand the intracellular and extracellular reaction mechanisms that control phosphorus cycling.

In this thesis, new methods were developed and tested for the extraction of dissolved inorganic phosphate (P_i) from freshwaters and its isolation from other oxygen-containing compounds, including nitrate, sulfate and dissolved organic matter. Excluding contaminant sources of oxygen during $\delta^{18}\text{O}_p$ analysis is a critical analytical challenge that has constrained $\delta^{18}\text{O}_p$ research in freshwaters to date. These new methods were evaluated against existing protocols for analysis of $\delta^{18}\text{O}_p$. While the protocol developed in this thesis exhibited greater accuracy and precision for freshwater matrices compared to the traditional approach reported by McLaughlin *et al.* (2004), further development work is required to increase the accuracy of this protocol compared to that reported by Gooddy *et al.* (2016).

Through the application of $\delta^{18}\text{O}_p$ within two exemplar freshwater ecosystems in this thesis, the in-stream fate of P_i derived from the effluent of a wastewater treatment plant and from groundwater discharge was examined. Within both ecosystems, $\delta^{18}\text{O}_p$ revealed the occurrence of metabolic processes that influenced the in-stream fate of P yet were masked in the hydrochemical data. In addition, the data reported here increase the worldwide groundwater $\delta^{18}\text{O}_p$ dataset nearly threefold. These groundwater data highlight the important potential differences in $\delta^{18}\text{O}_p$ due to bedrock geology, alongside the potential to use $\delta^{18}\text{O}_p$ to better understand the importance of groundwater-derived P following discharge to surface water ecosystems.

- Gooddy, D.C., D.J. Lapworth, S.A. Bennett, T.H.E. Heaton, P.J. Williams & B.W.J. Surridge. 2016. A multi-stable isotope framework to understand eutrophication in aquatic ecosystems. *Water Research*. **88**, 623
- McLaughlin, K., S. Silva, C. Kendall, H. Stuart-Williams & A. Paytan. 2004. A precise method for the analysis of $\delta^{18}\text{O}$ of dissolved inorganic phosphate in seawater. *Limnology and Oceanography: Methods*. **2**, 202

DECLARATION

I hereby declare that the work presented in this thesis is my own, except where acknowledged, and has not been submitted for the award of a higher degree or qualification at this or any other institution.

A handwritten signature in black ink, reading "Ceri Louise Davies", written over a horizontal dotted line.

Ceri Louise Davies

30th September 2016

CONTENTS

List of equations.....	iv
List of tables.....	v
List of figures.....	vi
Symbols and abbreviations.....	viii
Acknowledgements.....	ix
Chapter 1: Introduction and aims of the thesis.....	1
1.1 Introduction.....	1
1.2 Aims and objectives.....	6
Chapter 2: A synthesis and review of phosphate oxygen isotope research within aquatic ecosystems.....	8
2.1 Stable isotopes and P biogeochemistry: theoretical background.....	9
2.2 Isotope effects controlling $\delta^{18}\text{O}_p$ during biogeochemical cycling of P.....	11
2.2.1 <i>Intracellular metabolism of P_i</i>	11
2.2.2 <i>Uptake of extracellular P_i</i>	14
2.2.3 <i>Extracellular hydrolysis of organic P compounds</i>	14
2.3 Analytical protocols for determining $\delta^{18}\text{O}_p$.....	17
2.3.1 <i>P_i extraction protocols for aqueous matrices</i>	19
2.3.2 <i>Determination of $\delta^{18}\text{O}_p$ through TCEA-IRMS</i>	22
2.4 Synthesis of global $\delta^{18}\text{O}_p$ data from aquatic ecosystems.....	24
2.4.1 <i>Marine ecosystems</i>	25
2.4.2 <i>Estuarine ecosystems</i>	29
2.4.3 <i>Sediments within aquatic ecosystems</i>	29
2.5 Freshwater ecosystems.....	31
2.5.1 <i>Application of $\delta^{18}\text{O}_p$ to identify sources of P in freshwater ecosystems</i>	31
2.5.2 <i>Evidence from $\delta^{18}\text{O}_p$ analysis of P metabolism in freshwater ecosystems</i>	35
2.6 Concluding remarks.....	36
Chapter 3: Development and evaluation of new protocols for the robust determination of $\delta^{18}\text{O}_p$ in freshwaters.....	37
3.1 Introduction.....	37
3.2 Potential P_{org} contamination during brucite precipitation.....	41
3.2.1 <i>Selection of P_{org} compounds</i>	42

3.2.2 Analytical approach.....	44
3.2.3 Results and discussion	45
3.3 Brucite-P_{org} susceptibility toward acid hydrolysis	47
3.3.1 Analytical methods.....	48
3.3.2 Results and discussion	49
3.4 Revisions to the Method 1 protocol to minimise DOM-contamination of Ag₃PO₄ 53	
3.4.1 Standardisation of matrix for loading onto an anion exchange resin	56
3.4.2 Dissolved organic matter removal.....	59
3.4.3 Anion exchange resin elution profiles.....	62
3.4.4 Method 3 protocol.....	65
3.5 Comparison of Ag₃PO₄ extraction methods	67
3.5.1 Experimental approach.....	67
3.5.2 Results.....	69
3.5.3 Summary: selecting an appropriate Ag ₃ PO ₄ protocol for freshwater matrices.....	76

Chapter 4: Evaluating the utility of $\delta^{18}\text{O}_p$ as a tracer of point source inputs and in-stream cycling of P in a freshwater river system 78

4.1 Introduction.....	78
4.2 Methodology	83
4.2.1 Study site description.....	83
4.2.2 Field sampling	86
4.2.3 Sample collection and field measurements	86
4.2.4 Analysis of nutrient concentrations	87
4.2.5 $\delta^{18}\text{O}_p$ and $\delta^{18}\text{O}_w$ measurements	88
4.3 Results.....	90
4.4 Discussion	98
4.4.1 In-river phosphorus biogeochemistry revealed by bulk hydrochemical data.....	99
4.4.2 Insights into the sources and biogeochemical cycling of P through stable isotope analysis	101
4.5 Conclusions.....	112

Chapter 5: Application of $\delta^{18}\text{O}_p$ to understand phosphorus sources and cycling within groundwater and a groundwater-fed stream..... 113

5.1 Introduction.....	113
5.2 Methodology	117
5.2.1 Geological setting.....	117
5.2.2 Groundwater survey	120
5.2.3 In-river sampling for analysis of $\delta^{18}\text{O}_p$	122
5.2.4 Field sampling campaigns	125
5.2.5 Sample collection and field measurements	125
5.2.6 Analysis of nutrient concentrations	126

5.2.7	<i>Upper Greensand rock extracts</i>	127
5.2.8	$\delta^{18}O_p$ and $\delta^{18}O_w$ measurements.....	127
5.3	Results	128
5.3.1	<i>Analysis of groundwater samples and Upper Greensand bedrock extracts</i>	128
5.3.2	<i>Hydrochemical and isotopic data from surface water samples</i>	135
5.4	Discussion	141
5.4.1	<i>Characterising $\delta^{18}O_p$ within groundwater and assessing microbially-mediated cycling of P_i in groundwater using $\delta^{18}O_p$</i>	141
5.4.2	<i>Evidence for sources and biogeochemical cycling of P within the Caker stream</i>	146
5.5	Conclusions	151
Chapter 6: Discussion and consideration of future requirements for $\delta^{18}O_p$ research		
		152
6.1	Development of robust analytical protocols for $\delta^{18}O_p$ in freshwater matrices	153
6.2	Constraining $\delta^{18}O_p$ within sources of P_i to freshwater ecosystems	161
6.3	Providing insights into biogeochemical processes controlling P cycling with $\delta^{18}O_p$	164
6.4	Future priorities to develop research using $\delta^{18}O_p$	169
6.4.1	<i>The utility of $\delta^{18}O_p$ to provide insight into biogeochemical processes controlling P cycling</i>	169
6.4.2	<i>Determination of $\delta^{18}O$ in P_{org} molecules</i>	171
6.4.3	<i>Couple $\delta^{18}O_p$ with parallel techniques to develop an integrated isotope framework across C, N and P cycles</i>	172
	References.....	173
	Appendix.....	195
A.1	Supplementary elution profiling for Chapter 3	195
A.2	Supplementary field data for Chapter 5	196

LIST OF EQUATIONS

- 1
$$\delta^{18}O_{sample} = 1000 \left[\frac{\left(\frac{^{18}O}{^{16}O} \right)_{sample}}{\left(\frac{^{18}O}{^{16}O} \right)_{standard}} - 1 \right] \text{‰}_{\text{VSMOW}}$$
- 2
$$T(^{\circ}C) = 111.4 - 4.3(\delta^{18}O_p - \delta^{18}O_w)$$
- 3
$$T(^{\circ}C) = 118.7(\pm 4.9) - 4.3(\pm 0.20)(\delta^{18}O_p - \delta^{18}O_w)$$
- 4
$$1000 \ln \alpha_{p-w} = \left(14.43(\pm 0.39) \times \frac{1000}{T(K)} \right) - 26.54(\pm 1.33)$$
- 4a
$$\alpha_{p-w} = \frac{(\delta^{18}O_p + 1000)}{(\delta^{18}O_w + 1000)}$$
- 5
$$BiPO_4 + \frac{8}{3}BrF_3 \rightarrow BiF_3 + PF_5 + \frac{4}{3}Br_2 + 2O_2$$
- 6
$$2Ag_3PO_4 + Br_2 \rightarrow Ag_4P_2O_7 + \frac{1}{2}O_2 + 2AgBr$$
- 7
$$\%P_i \text{ from } P_{org} \text{ remineralisation} = \frac{(\delta^{18}O_{sample} - \delta^{18}O_{eq})}{(\delta^{18}O_{rem} - \delta^{18}O_{eq})} \times 100\%$$
- 8
$$F = \frac{(\delta^{18}O_p - \delta^{18}O_{recycled})}{(\delta^{18}O_{fertiliser} - \delta^{18}O_{recycled})} \times 100\%$$
- 9
$$Co - precipitation \text{ extent } (\%) = \frac{100[Supernatant TP]}{[Initial TP]}$$
- 10
$$RCOOR' + H_2O \xrightarrow{H^+(aq)} RCOOH + R'OH$$
- 11
$$Ca_5(PO_4)_3OH + 4H_2CO_3 \leftrightarrow 5Ca^{2+} + 3HPO_4^{2-} + 4HCO_3^- + H_2O$$

LIST OF TABLES

2.1	Global $\delta^{18}\text{O}_p$ data synthesis for aquatic ecosystems	28
2.2	Observed $\delta^{18}\text{O}_p$ values for potential P sources to freshwaters	32
3.1	P_{org} compound speciation in freshwaters	44
3.2	P_{org} compounds selected for analysis within Chapter 3	45
3.3	Extent of P_{org} co-precipitation with brucite	46
3.4	Two factor ANOVA analysis output for TP acid hydrolysis	49
3.5	DOC and SRP analysis of DOM-resin eluates	61
3.6	DOC analysis of eluates from a natural river matrix	62
3.7	Comparison of spiked Ag_3PO_4 precipitates with Methods 1 and 3	71
4.1	Site descriptions for surface water samples in the Beult catchment	86
4.2	Dissolved nutrient concentrations for Beult surface water samples	91
4.3	Isotopic compositions for Beult surface water samples	95
4.4	Comparison of key variables with Goddy <i>et al.</i> (2016)	102
5.1	Site descriptions for groundwater borehole and spring samples	121
5.2	Site descriptions for Caker stream surface water samples	124
5.3	Dissolved nutrient concentrations for groundwater samples	130
5.4	Isotope composition and geological descriptions for groundwaters	131
5.5	Dissolved nutrient concentration for Caker stream samples	136
5.6	Isotopic compositions for Caker stream samples	139
6.1	Summary of sample sites used for in-field method comparison	155
A.1	Supplementary field data for Chapter 5	196

LIST OF FIGURES

1.1	Peak phosphorus model	2
2.1	Schematic diagram for isotope effects associated with metabolism	11
2.2	Dephosphorylation of ATP	12
2.3	Schematic diagram for extracellular metabolism involving P_i	16
2.4	Published protocols for Ag_3PO_4 precipitation from aqueous samples	20
3.1	Method 1 protocol	39
3.2	Percentage of spiked P_{org} that co-precipitated with brucite	46
3.3	Percentage of TP mass hydrolysed to SRP following dissolution	50
3.4	Extent of ATP hydrolysis following co-precipitation and dissolution	50
3.5	Comparison of hydrolysis in excess vs minimum acetic acid volume	51
3.6	Kinetic study of ATP and phytic acid hydrolysis	52
3.7	Method 2 protocol	54
3.8	Method 3 - new sample preparation stages	56
3.9	Anion exchange resin elution profile for 0.25M KCl and 1 mL.min ⁻¹	64
3.10	Anion exchange resin elution profile for 0.3M KCl and 1 mL.min ⁻¹	64
3.11	Anion exchange resin elution profile for 0.3M KCl and 0.5 mL.min ⁻¹	65
3.12	Method 3 protocol	66
3.13	“Black” precipitate formed in the River 2 matrix with Method 1	70
3.14	Method comparison with $\delta^{18}O_p$ for Methods 1 and 3	72
3.15	Method comparison with O yields for Methods 1 and 3	74
3.16	Method comparison for Methods 1 and 3 - $\delta^{18}O_p$ vs. O yield	74
3.17	Method comparison with $\delta^{18}O_p$ for Methods 1 and 2	76
4.1	Conceptual diagram for in-river responses to WWTP effluent input	80

4.2	Location of sample sites along the River Beult, Kent	84
4.3	View downstream from site A	85
4.4	Surface water temperature profiles	92
4.5	SRP concentration profiles	93
4.6	Molar N:P profiles	94
4.7	$\delta^{18}\text{O}_p$ profiles	96
4.8	$\delta^{18}\text{O}_w$ profiles	97
4.9	$\delta^{18}\text{O}_p - \delta^{18}\text{O}_{eq}$ profiles	98
5.1	Geological map of the Alton and Godalming area, UK	119
5.2	Geographical location of Caker stream water samples	123
5.3	Underlying geological setting for Caker stream water samples	124
5.4	Groundwater SRP concentrations vs. Cl^- , SO_4^{2-} and NO_3^-	132
5.5	Groundwater $\delta^{18}\text{O}_p$ vs. $\delta^{18}\text{O}_w$ and water temperature	133
5.6	Groundwater $\delta^{18}\text{O}_p - \delta^{18}\text{O}_{eq}$ vs. water temperature	133
5.7	Caker stream SRP concentration profile	137
5.8	Caker stream surface water temperature profile	138
5.9	Caker stream $\delta^{18}\text{O}_p$ profile	139
5.10	Caker stream $\delta^{18}\text{O}_w$ profile	140
5.11	Caker stream $\delta^{18}\text{O}_p - \delta^{18}\text{O}_{eq}$ profile	140
5.12	Global $\delta^{18}\text{O}_p$ ratios in relation to data from Chapters 4 and 5	143
6.1	Boxplots for in-field method comparison	157
6.2	Scatterplot of $\delta^{18}\text{O}_p$ generated from Method 3 vs. Method 2	157
6.3	In-field method comparison using a $\delta^{18}\text{O}_p$ profile	160
6.4	In-field method comparison using a $\delta^{18}\text{O}_p - \delta^{18}\text{O}_{eq}$ profile	160
A.1	Anion exchange resin elution profile for 0.3M KCl and 1 mL.min ⁻¹	195

SYMBOLS AND ABBREVIATIONS

P_i	Dissolved inorganic phosphate
δ¹⁸O_p	Isotopic composition of P _i -oxygen
δ¹⁸O_w	Isotopic composition of water-oxygen
δ¹⁸O_{eq}	Theoretical δ ¹⁸ O _p when in thermodynamic equilibrium with δ ¹⁸ O _w
VSMOW	Vienna Standard Mean Ocean Water
‰ or ‰_{VSMOW}	Per mille notation – calibrated to the VSMOW scale
SRP	Soluble reactive phosphorus, analogous to P _i
P_{org}	Organic phosphorus containing compounds
TDP	Total dissolved phosphorus (0.45μm filtered)
DOM	Dissolved organic matter
DOC	Dissolved organic carbon
c.AA	Concentrated acetic acid
ATP	Adensine-5'-triphosphate
DAX-8	Supelite™ DAX-8, solid-phase organic exchange/absorbent resin
ENV+	ISOLUTE® ENV+, solid-phase organic exchange/absorbent resin
TCEA-IRMS	Thermal conversion elemental analyser-isotope ratio mass spectrometer
MagIC	Magnesium induced co-precipitation
Brucite	A form of magnesium hydroxide
WWTP	Wastewater treatment plant
MilliQ	18.2 MΩ H ₂ O

ACKNOWLEDGEMENTS

I would like to sincerely thank Dr Ben Surridge for the exceptional support and guidance he gave me throughout this process, and for always turning my “pessimistic” realism into optimism. I am also very grateful to Prof. Daren Goody for his continued help, encouragement and invaluable second opinions. I also wish to thank the staff of the Lancaster Environment Centre, in particular Mr Dave Hughes and Drs Peter Wynn, Montse Auladell-Mestre, Catherine Wearing and Paddy Keenan, for their advice, laboratory assistance, and patience.

This Ph.D. thesis would not have been possible without the funding and opportunities provided to me through a Natural Environment Research Council (NERC) CASE studentship (NE/K501001/1) with the British Geological Survey (BGS). Further thanks must go to Dan Lapworth from the BGS for his teaching and patience during all the fieldwork, and for making it such an enjoyable experience. I would also like to thank Craig Hampton at the Environment Agency for providing knowledge and assistance to support the groundwater work presented in Chapter 5.

Finally, I would like to thank my family, and the staff and Ph.D. students at both LEC and CEH Lancaster, in particular Verity Green, Laura Deeprise, Amy Anderson and the Friday Night Dinner crew, for keeping me relatively sane.

Chapter 1:

Introduction and aims of the thesis

1.1 Introduction

Phosphorus (P) is an essential element for all life, being integral to the structure and function of key biomolecules including deoxyribonucleic acid (DNA), ribonucleic acid (RNA), adenosine-5'-triphosphate and phospholipids. Under ambient conditions in natural ecosystems, P is tightly cycled within the biosphere and can limit or co-limit primary producer and microbial communities (Ruttenberg, 2003). Therefore, due to the essential role played by P in the biosphere, alterations to the natural biogeochemical cycles of P have been linked to undesirable ecosystem changes, particularly following inputs of bioavailable P from anthropogenic sources. Within aquatic ecosystems, these changes include increases in primary production, shifts in community composition, increased frequency of algal blooms and hypoxia, and reduced biodiversity (Sondergaard and Jeppesen, 2007; Smith and Schindler, 2009).

Although bioavailable P enters aquatic ecosystems from a range of sources, models have indicated that, globally, over 50% of dissolved inorganic phosphate (P_i) exported to surface waters is derived from anthropogenic sources and that in Europe anthropogenic sources account for 92% of the $0.27 \text{ Tg } P_i\text{-P}\cdot\text{yr}^{-1}$ that is exported by rivers to coastal regions (Harrison *et al.*, 2010). Anthropogenic sources are dominated by agricultural P (e.g. associated with export of inorganic fertiliser from agricultural land) and waste water (both human and industrial in origin) (Ott and Rechberger, 2012; Withers *et al.*, 2015). Fluxes of P from anthropogenic sources have increased significantly as a result of global population growth and attempts to expand and intensify food production for human society (Filippelli, 2008; Liu *et al.*, 2008; Haygarth *et al.*, 2014).

Despite an increased awareness of the adverse effects that could result from the input of bioavailable P to ecosystems, and recent attempts to reduce P inputs through regulation, including under the European Union Water Framework Directive (WFD), the Urban Waste Water Treatment Directive and the United States Clean Water Act (U.S. Senate, 1972; Council Directive (EC), 1991; European Parliament, 2000), recent research has highlighted the potential for long-term effects of the pool associated with legacy P that has accumulated within the environment, particularly within agricultural soils following a prolonged period of excessive P inputs given crop demand (Jarvie *et al.*, 2013; Haygarth *et al.*, 2014; Rowe *et al.*, 2015). Global estimates suggest that 815 Tg of legacy P has accumulated within soils between 1965 and 2007, with Western Europe having the highest cumulative P input at an average of approximately 1115 kg P.ha⁻¹ (Sattari *et al.*, 2012; Rowe *et al.*, 2015). Remobilisation of P from this legacy pool may continue to input significant quantities of P into aquatic ecosystems, for years to decades after the initial input of P to a terrestrial ecosystem (Haygarth *et al.*, 2014; Powers *et al.*, 2016).

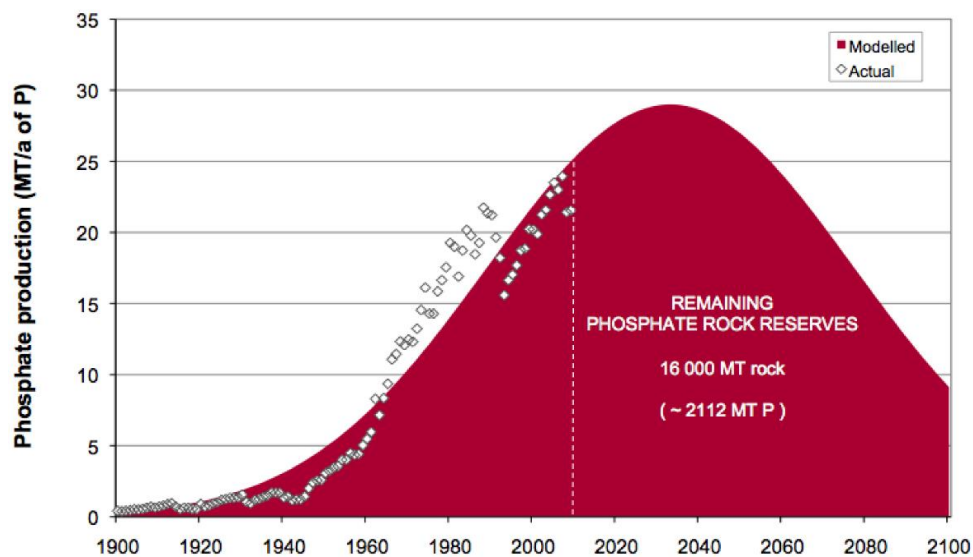


Figure 1.1: A model describing a possible peak in phosphorus production from rock reserves in 2033, due to the finite supplies of these reserves. Figure taken from Cordell and White (2011).

Beyond the potential for adverse impacts of enhanced P availability within aquatic ecosystems, human society has become increasingly concerned over the long-term sustainability of global P rock reserves (**Figure 1.1**), with future exhaustion of reserves being likely without major advances in P mining and recycling technologies (Cordell *et al.*, 2011; Cordell and White, 2011; Vaccari and Strigul, 2011; Seyhan *et*

al., 2012). Whilst estimates of mineral P reserves have increased dramatically in recent years, estimates of the size of remaining mineral P reserves remain highly uncertain and yet these reserves are critical for supporting future food production (Cordell *et al.*, 2009; Childers *et al.*, 2011; Elser and Bennett, 2011; Jasinski, 2012). At present there is a lack of alternative sources for P beyond mineral reserves and, globally, only a small fraction of P is recovered from waste streams, such as urine, and reused through recycling schemes (Cordell *et al.*, 2009; Vaccari and Strigul, 2011; Seyhan *et al.*, 2012). Therefore, while steps to address inefficient P use are being enforced, securing future access to P remains a globally-significant issue due to the lack of effective P recycling within urban and agricultural areas, the lack of a suitable alternative source beyond phosphorite deposits, and the limited range of geographical locations within which economically viable mineral P reserves are found (Beardsley, 2011).

However, despite the fundamental importance of P to human society and the implications of perturbations to the P cycle for natural ecosystems, understanding of the sources and reaction mechanisms controlling biogeochemical cycling of P within natural ecosystems remains relatively limited (Blake *et al.*, 2005; Slomp, 2011). A critical reason for this is the lack of inherent tracers for analysing the sources and the metabolism of P in natural ecosystems (Karl, 2000). For example, quantifying the importance of different sources of P in aquatic ecosystems has relied on mass flux budgets, spatial and temporal analysis of P concentration, export coefficient models and indirect tracers, such as boron, as a marker for waste water treatment plant (WWTP) effluent, or microbial source tracking to identify human versus agricultural sources of faecal contamination (Dillon and Kirchner, 1975; Smith *et al.*, 1989; Neal *et al.*, 2000a; Jarvie *et al.*, 2002; Scott *et al.*, 2002; Simpson *et al.*, 2002; Holt *et al.*, 2003; Bowes *et al.*, 2008). However, none of these approaches provide an inherent label for P. As a result, none offer a direct means of tracing specific sources or biogeochemical processes relevant to the P cycle.

Analysis of the stable isotope ratio of an element in a molecule can potentially represent an inherent label for that molecule, and a label that is not altered by the same radioactive decay processes which would occur in radioisotope studies. Stable isotope ratios have been widely used to understand long-term trends and processes in both

local and global biogeochemical cycles (Beveridge and Shackleton, 1994; Newton and Bottrell, 2007 and references therein). This analysis requires an element to have a minimum of two naturally occurring stable isotopes, with changes in the ratio of individual isotopes of an element in a sample, against a known ratio in a reference, providing insight into biogeochemical processes controlling the cycle of that element. Carbon (C), nitrogen (N) and oxygen (O) are commonly used in stable isotope research on the basis of ratios of $^{13}\text{C}/^{12}\text{C}$, $^{15}\text{N}/^{14}\text{N}$ and $^{18}\text{O}/^{16}\text{O}$ respectively. Stable isotope analyses cannot be conducted on the P atom in P-containing compounds, because ^{31}P is the only stable P isotope. However, in natural aquatic ecosystems P is often bound strongly to O in the form of the dissolved inorganic phosphate ion (Blake *et al.*, 2001), defined hereafter as P_i . Under typical temperature and pressure conditions in the Earth's surface water and groundwater ecosystems, the P-O bonds in P_i are resistant to inorganic hydrolysis (O'Neil *et al.*, 2003). Therefore, under most ambient conditions and given only abiotic reactions, the stable isotope ratio of oxygen within the P_i molecule will remain constant. However, biological mediation can cause the P-O bond to break and reform, potentially causing isotope exchange between oxygen in P_i and oxygen in water within an ecosystem (Tudge, 1960; Blake *et al.*, 2001). Therefore, the stable oxygen isotope ratio within P_i (hereafter, $\delta^{18}\text{O}_p$) has recently emerged as a novel and potentially powerful inherent tracer for the sources and metabolism of P in natural ecosystems (McLaughlin *et al.*, 2004; Elsbury *et al.*, 2009; Young *et al.*, 2009; Goldhammer *et al.*, 2011a; Li *et al.*, 2011).

In recent research, a protocol was established to extract P_i from marine water matrices, convert P_i to silver phosphate (Ag_3PO_4) and measure $\delta^{18}\text{O}_p$ (McLaughlin *et al.*, 2004). Subsequent research has applied this method to determine biogeochemical processing of P within marine environments (McLaughlin *et al.*, 2004; Colman *et al.*, 2005; McLaughlin *et al.*, 2006a; McLaughlin *et al.*, 2006b; McLaughlin *et al.*, 2006c; Goldhammer *et al.*, 2011a; McLaughlin *et al.*, 2013). Adaptation of the McLaughlin *et al.* (2004) protocol (Weiner *et al.*, 2011) or the development of a new extraction protocol (Tamburini *et al.*, 2010) has also allowed the application of $\delta^{18}\text{O}_p$ to soil and plant systems (Angert *et al.*, 2011; Angert *et al.*, 2012; Tamburini *et al.*, 2012; Tamburini *et al.*, 2014). However, beyond a relatively intensive study of Lake Erie reported by Elsbury *et al.* (2009), the catalogue of $\delta^{18}\text{O}_p$ data for freshwater ecosystems remains much more constrained than for marine and terrestrial

ecosystems. A limited number of initial studies have sought to use $\delta^{18}\text{O}_p$ to explore the sources and metabolism of P_i in freshwater ecosystems (Blake *et al.*, 2001; Gruau *et al.*, 2005; McLaughlin *et al.*, 2006a; McLaughlin *et al.*, 2006c; Young *et al.*, 2009; Li *et al.*, 2011). One critical reason for the relative lack of application of $\delta^{18}\text{O}_p$ to freshwater ecosystems lies in the uncertainty that surrounds the use of an extraction protocol initially developed for marine environments to freshwater matrices. Some research has applied the McLaughlin *et al.* (2004) protocol without modification to freshwater matrices, whilst other research has adapted the Ag_3PO_4 precipitation protocol to include clean-up stages for samples containing high concentrations of particulate and dissolved organic matter (DOM). In organic-rich sample matrices, including many freshwaters, inefficient removal of DOM could significantly influence measured $\delta^{18}\text{O}_p$, because DOM can consist of up to 45% O by weight and has been shown to persist until the precipitation of Ag_3PO_4 (Ma *et al.*, 2001; Lécuyer, 2004; McLaughlin *et al.*, 2004; Zohar *et al.*, 2010). For accurate determination of $\delta^{18}\text{O}_p$, all O-containing contaminants, especially DOM, must be removed from an Ag_3PO_4 precipitate prior to $\delta^{18}\text{O}_p$ analysis. This remains a significant challenge for research seeking to apply $\delta^{18}\text{O}_p$ to complex freshwater matrices.

Therefore, if a robust protocol for extracting P_i from freshwater matrices can be developed and tested, this would potentially support far more extensive application and evaluation of $\delta^{18}\text{O}_p$ within research to understand biogeochemical cycling of P within freshwater ecosystems. This research could range from better constraining the relative importance of different sources of P within freshwater ecosystems, to the extent to which P from individual sources is linked to metabolic activity within an ecosystem. Such research would have potentially important implications for understanding the reaction mechanisms controlling P biogeochemistry in natural ecosystems, and for the design and targeting of future policies and practices to deliver more sustainable stewardship of P. This provides the broad context for the research reported within this thesis.

1.2 Aims and objectives

This thesis firstly aims to develop a robust method for the accurate determination of $\delta^{18}\text{O}_p$ in freshwater matrices and, subsequently, to apply $\delta^{18}\text{O}_p$ as an inherent tracer of P within two exemplar freshwater ecosystems. In order to achieve these aims, the following objectives have been developed for this thesis:

1. To develop, optimise and test extraction protocols for analysis of $\delta^{18}\text{O}_p$ in surface water and groundwater matrices.
2. To determine $\delta^{18}\text{O}_p$ in river water, wastewater treatment plant (WWTP) effluent and groundwater to constrain $\delta^{18}\text{O}_p$ in potential sources of P_i to freshwater stream ecosystems.
3. To examine changes in $\delta^{18}\text{O}_p$ within river water as an indicator for the in-river fate of P_i derived from sources including WWTP final effluent and groundwater.
4. To determine whether $\delta^{18}\text{O}_p$ within groundwater can act as a tracer for the sources and metabolism of P_i within groundwater and the discharge of groundwater-derived P_i to surface water ecosystems.

This thesis will be structured in two main sections followed by a concluding discussion chapter. The first section (**Chapters 2 and 3**) focuses on the development of $\delta^{18}\text{O}_p$ extraction protocols and their potential application to freshwaters. **Chapter 2** provides a synthesis of the current application of $\delta^{18}\text{O}_p$ in aquatic ecosystems and the development of methodologies for $\delta^{18}\text{O}_p$ analysis within aqueous matrices. **Chapter 3** reports research that developed and tested a new $\delta^{18}\text{O}_p$ extraction protocol, specifically designed to support the application of $\delta^{18}\text{O}_p$ within freshwater ecosystems. This chapter also reports work to validate and compare previously published protocols against those developed within this thesis.

The second section (**Chapters 4 and 5**) reports the application of protocols that were established in **Chapter 3** to freshwater ecosystems. **Chapter 4** explores the initial application of $\delta^{18}\text{O}_p$ as a tracer of P cycling following the input of P_i -enriched WWTP effluent into a headwater river system. **Chapter 5** investigates the potential use of

$\delta^{18}\text{O}_p$ as a label of sources of P within groundwater and as a tracer of P sources and cycling within streams that are potentially fed by groundwater discharge.

Chapter 6 concludes the thesis with a discussion of the potential applications of $\delta^{18}\text{O}_p$ to address questions surrounding P biogeochemistry within freshwater ecosystems. In addition, a comparison of multiple methods for $\delta^{18}\text{O}_p$ determination is provided, based on samples collected and analysed as part of the research reported in **Chapters 4** and **5**.


Chapter 2: A synthesis and review of phosphate oxygen isotope research within aquatic ecosystems

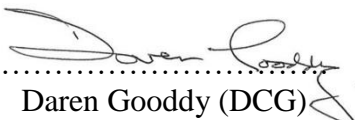
The chapter presented here has been modified from a paper published in 2014 in
Science of the Total Environment:

Davies, C.L., Surridge, B.W.J. & Goody, D.C. 2014. Phosphate oxygen
isotopes within aquatic ecosystems: Global data synthesis and future
research priorities. *Science of the Total Environment*. **496**, 563-575.

CLD performed analysis on all samples, interpreted data and wrote the manuscript.
BWJS and DCG supervised the development of work, helped in data interpretation
and edited the manuscript.


.....
Ceri Davies (CLD)


.....
Ben Surridge (BWJS)


.....
Daren Goody (DCG)

This review focuses on the use of $\delta^{18}\text{O}_p$ in aquatic ecosystems and particularly within freshwater ecosystems. The objectives are to: i) examine the theoretical basis to the use of $\delta^{18}\text{O}_p$ in P research; ii) consider the methodological challenges involved in the analysis of $\delta^{18}\text{O}_p$ in aquatic ecosystems; and iii) synthesise global data from initial application of $\delta^{18}\text{O}_p$ within aquatic ecosystems.

2.1 Stable isotopes and P biogeochemistry: theoretical background

Biogeochemical cycling of P in aquatic ecosystems has previously been explored using two radioactive isotopes ^{32}P ($t_{1/2}=14.36$ days) and ^{33}P ($t_{1/2} = 25.34$ days, Salonen *et al.*, 1994; Benitez-Nelson, 2000; Smith *et al.*, 2011). Although studies have been conducted using P radioisotopes at natural abundance (Benitez-Nelson and Buesseler, 1998; Benitez-Nelson and Buesseler, 1999), the combination of a trace natural abundance of both ^{32}P and ^{33}P with such short half-lives limits the use of radioisotopes as an inherent tracer of P in ecosystems, such as freshwaters, in which P concentrations may be relatively low. Therefore, the use of radioisotopes in P biogeochemical studies is constrained by short isotope half-lives, perturbation of experimental systems associated with labelling, or the use of incubations which omit irregular events in natural ecosystems, such as seasonal algal blooms (Levine *et al.*, 1986; Thingstad *et al.*, 1993; Salonen *et al.*, 1994; Benitez-Nelson, 2000). Stable isotope studies analyse the ratio between two individual stable isotopes of the same element. Whilst P has three major isotopes, ^{31}P constitutes the majority of the natural P pool (100%) and is its only stable isotope (de Laeter *et al.*, 2003). Consequently, stable isotope analyses cannot be conducted on the P atom in P-containing compounds.

In natural aquatic ecosystems, P is often bound strongly to O in the form of the dissolved inorganic phosphate ion (Blake *et al.*, 2001), defined hereafter as P_i . Therefore, attention has recently focussed on whether the stable isotope composition of O in P_i can be used to gain insight into the biogeochemical cycling of P. Isotope fractionation involves the preferential incorporation of one isotope over another from a starting material into a reaction product. Kinetic fractionation describes a process

that preferentially selects one isotope (generally the lighter isotope) due to a faster reaction rate in a unidirectional reaction. In contrast, equilibrium fractionation is a thermodynamic effect in which a system has time to exchange isotopes continuously in order to achieve the lowest energy system, wherein the heavier isotope forms the strongest bond possible (Hoefs, 2008). The P-O bonds in P_i are resistant to inorganic hydrolysis under typical temperature and pressure conditions in the Earth's surface water and groundwater ecosystems (O'Neil *et al.*, 2003). Therefore, without biological mediation, negligible isotope exchange occurs between P_i and water within these ecosystems (Tudge, 1960; Blake *et al.*, 2001). Whilst the initial stages of some abiotic reactions, including the sorption of P_i to solid-phase iron-oxide or the formation of apatite, may be associated with kinetic fractionation, this does not persist and through time the stable isotope composition of the solid-phase P_i approaches that of the aqueous-phase P_i (Liang and Blake, 2007; Jaisi *et al.*, 2010; Jaisi *et al.*, 2011). In contrast, enzyme-catalysed processes cleave P-O bonds leading to fractionation between the isotopes of O in P_i and O in a surrounding fluid, either within a cell or within the extracellular environment (Blake *et al.*, 2005). The fractionation between the stable isotopes of O (^{16}O and ^{18}O) within a sample is expressed as $\delta^{18}\text{O}$, relative to Vienna Standard Mean Ocean Water (VSMOW), defined as 0‰_{VSMOW} on the $\delta^{18}\text{O}$ scale (**Equation 1**).

$$\delta^{18}\text{O}_{\text{sample}} = 1000 \left[\frac{\left(\frac{^{18}\text{O}}{^{16}\text{O}} \right)_{\text{sample}}}{\left(\frac{^{18}\text{O}}{^{16}\text{O}} \right)_{\text{standard}}} - 1 \right] \text{‰}_{\text{VSMOW}} \quad (1)$$

Phosphate oxygen isotopes have previously been used within both the archaeological and environmental communities to determine palaeoclimate conditions at the time of formation of biogenic phosphatic material, such as apatite in fossil bones and teeth, as well as to reconstruct historical salinity and water temperatures from biogenic phosphate derived from fish remains (Longinelli and Nuti, 1973; Bryant *et al.*, 1994; Fricke and O'Neil, 1996; Lécuyer *et al.*, 1996; Stephan, 2000). Recent methodological advances in the analysis of $\delta^{18}\text{O}_p$ now provide the opportunity to use $\delta^{18}\text{O}_p$ as both a tracer of source and of the extent of metabolism of P in aquatic ecosystems (McLaughlin *et al.*, 2004; Elsbury *et al.*, 2009; Goldhammer *et al.*, 2011b).

2.2 Isotope effects controlling $\delta^{18}\text{O}_p$ during biogeochemical cycling of P

A range of isotope effects associated with metabolic processes have the potential to influence $\delta^{18}\text{O}_p$. These effects are summarised in **Figure 2.1** and described in **Sections 2.2.1 to 2.2.3**.

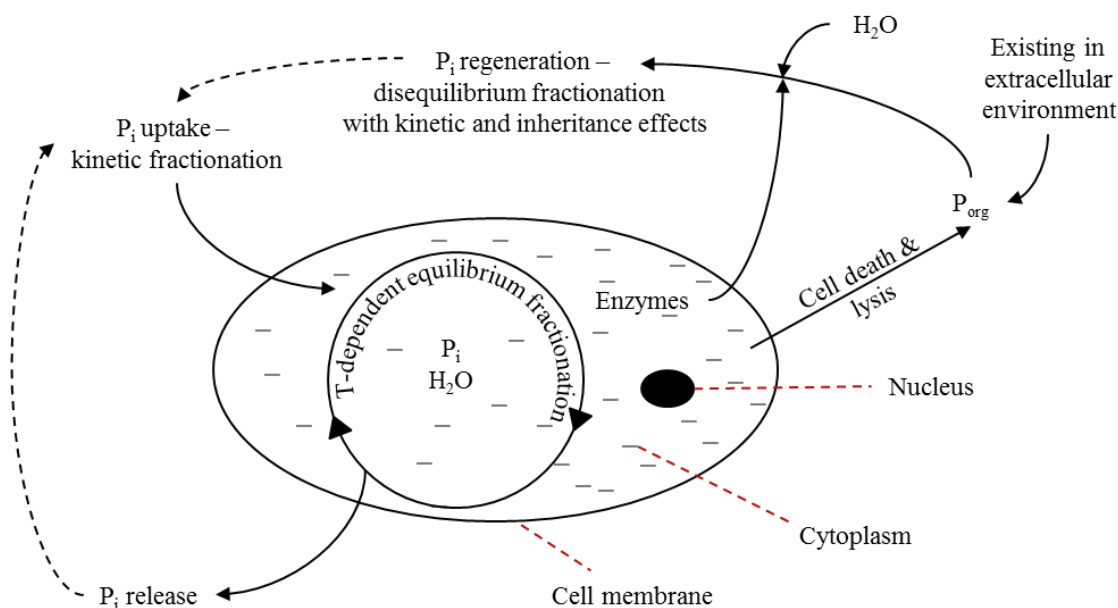


Figure 2.1: Schematic diagram describing the major isotope effects that can occur within the intracellular or extracellular environment due to metabolic processes. P_{org} = organic P compounds; P_i = dissolved inorganic phosphate ion; H_2O = water molecule.

2.2.1 Intracellular metabolism of P_i

A variety of P-containing compounds are present within aquatic ecosystems, including P_i , inorganic polyphosphates and organic compounds such as proteins, sugars and phospholipids (Karl and Tien, 1997). However, P_i is the species preferentially utilised by organisms as it is capable of diffusion across cytoplasmic cell membranes (Björkman and Karl, 1994; Liang and Blake, 2006b). Consequently, P_i is required for a number of intracellular reactions, including cellular signalling through phosphorylation and dephosphorylation, as well as being incorporated within biomass during cell growth (Blake *et al.*, 1997; Blake *et al.*, 2005). The major enzyme that catalyses intracellular P cycling is inorganic pyrophosphatase, due to its ability to mediate reversible reactions such as the cleavage of adenosine-5'-triphosphate to

adenosine-5'-diphosphate (**Figure 2.2**, Cohn, 1958; Blake *et al.*, 2005). Intracellular reactions catalysed by inorganic pyrophosphatase cause complete and very rapid (in the order of minutes) O isotope exchange between O atoms in P_i and O atoms in surrounding water molecules that donate O atoms to newly produced P_i molecules (Kolodny *et al.*, 1983; Blake *et al.*, 1997). Thermodynamic fractionation characterises the exchange of O between P_i and the surrounding fluid, resulting in temperature-dependent equilibrium between O in P_i and O within intracellular water ($\delta^{18}O_w$, expected to be identical to extracellular $\delta^{18}O_w$ (Fricke *et al.*, 1998)).

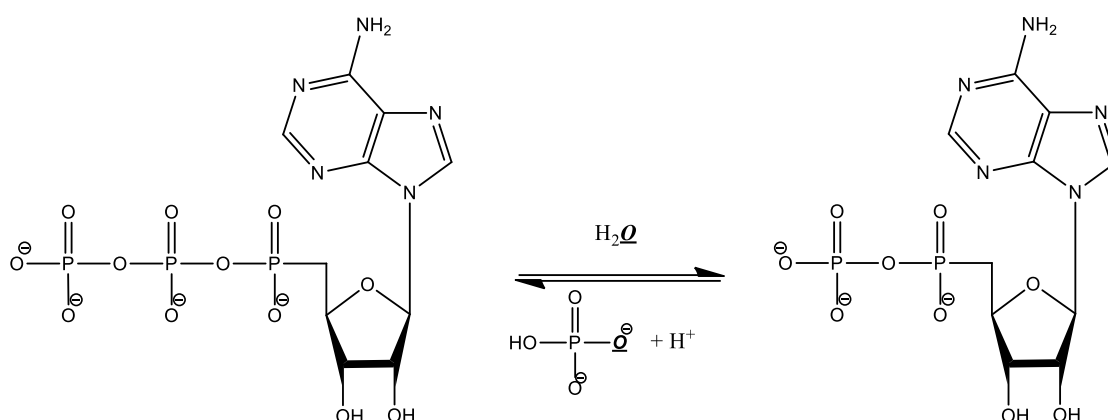


Figure 2.2: Reversible reaction of the dephosphorylation of adenosine-5'-triphosphate to adenosine-5'-diphosphate, in which P_i is generated as a by-product (Gajewski *et al.*, 1986).

Release of P from biomass into the extracellular environment is driven by two mechanisms. Firstly, from live biomass as a by-product of uptake and intracellular metabolic reactions, in order to maintain constant intracellular P concentrations (Cooperman *et al.*, 1992), and secondly, following death and lysis of cells. Within environments in which P_i is extensively taken up and recycled through live biomass, an initially distinctive $\delta^{18}O_p$ composition in the extracellular environment, potentially reflecting sources of P, could be overprinted following intracellular, equilibrium fractionation and release of P_i to the extracellular environment. The $\delta^{18}O$ value of a P_i molecule in equilibrium with surrounding water can be predicted, based on the measured $\delta^{18}O_w$ and temperature of the surrounding water, using empirically-derived **Equation 2** (Longinelli and Nuti, 1973). This is the basis for using historical $\delta^{18}O_p$ in solid-phase samples, such as tooth enamel, as a palaeothermometer, given an ecosystem in equilibrium *via* intracellular metabolism (Kolodny *et al.*, 1983; Fricke *et al.*, 1998).

$$T(^{\circ}C) = 111.4 - 4.3(\delta^{18}O_p - \delta^{18}O_w) \quad (2)$$

where T is the average growth temperature and $\delta^{18}O_p$ and $\delta^{18}O_w$ refer to the isotopic compositions of P_i and environmental water (at 25.2°C) respectively. Whilst predominantly based on biogenic apatite from marine organisms, one freshwater species, *Unio pictorum*, was included in the empirically-derived **Equation 2**, suggesting no significant difference between seawater and freshwater equilibria equations. Although **Equation 2** has been used widely, more recent development of techniques for purification of P_i from solid materials and for determination of $\delta^{18}O_p$ has led Pucéat *et al.* (2010) to propose a revised phosphate–water fractionation equation based on empirical analysis of biogenic apatite samples (**Equation 3**) and, most recently, Chang and Blake (2015) to form **Equation 4** for the fractionation of P_i with water under controlled laboratory conditions:

$$T(^{\circ}C) = 118.7(\pm 4.9) - 4.3(\pm 0.20)(\delta^{18}O_p - \delta^{18}O_w) \quad (3)$$

$$1000 \ln \alpha_{p-w} = \left(14.43(\pm 0.39) \times 1000 / T(K) \right) - 26.54(\pm 1.33) \quad (4)$$

where,

$$\alpha_{p-w} = \frac{(\delta^{18}O_p + 1000)}{(\delta^{18}O_w + 1000)} \quad (4a)$$

Based on empirical equations **2**, **3** or **4**, if both the ambient water temperature and $\delta^{18}O_w$ are determined then the expected equilibrium value for $\delta^{18}O_p$ can be calculated. Therefore, comparing the theoretical value for $\delta^{18}O_p$ at equilibrium with $\delta^{18}O_p$ observed in an environmental sample can provide insight into the extent to which P_i has been recycled through intracellular metabolic reactions, assuming that $\delta^{18}O_p$ in the sources of P to an ecosystem were originally at disequilibrium. **Equation 4** will be used to determine $\delta^{18}O_p$ at thermodynamic equilibrium for **Chapters 3-6** within this thesis.

2.2.2 Uptake of extracellular P_i

Many biologically-mediated processes associated with isotope effects are kinetically controlled, for example bacterial sulfate reduction and methanogenesis (Nakai and Jensen, 1964; Whiticar, 1999). During bacterial sulfate reduction, bacteria preferentially reduce ^{32}S - and ^{16}O -containing sulfate molecules, because these molecules have lower bond energies due to a lower combined mass. Thus, bacteria can metabolise isotopically lighter sulfate at a faster rate, resulting in the formation of isotopically light sulfide relative to the starting sulfate pool, assuming that only partial reduction of the available sulfate occurs (Nakai and Jensen, 1964; Habicht and Canfield, 1997). A similar kinetic fractionation may also be imparted on the P_i pool during biological uptake of P_i from the extracellular environment. For example, initial research reported by Blake *et al.* (2005) has shown that *Escherichia coli* grown in controlled laboratory conditions preferentially take up $^{31}\text{P}^{16}\text{O}_4^{3-}$ compared to the isotopically-heavier $^{31}\text{P}^{18}\text{O}_4^{3-}$, resulting in enrichment of the extracellular environment with $^{31}\text{P}^{18}\text{O}_4^{3-}$. If this kinetic isotope effect operates more widely in natural ecosystems, the effect would only be observed given unidirectional reactions in which the reactants are not fully consumed and where competing fractionations do not overprint that associated with biological uptake of P_i .

2.2.3 Extracellular hydrolysis of organic P compounds

Organic P (P_{org}) compounds can be used to support metabolism given low bioavailable P_i concentrations within the extracellular environment. However, P_{org} compounds are too large for direct diffusion across cytoplasmic cell membranes (Liang and Blake, 2006b). Therefore, P_{org} must be hydrolysed through enzyme-mediated reactions involving phosphohydrolases that are either attached to the outside of a cell membrane or are secreted by organisms into the extracellular environment (Liang and Blake, 2006b). These extracellular metabolic reactions release P_i as a by-product (**Figure 2.3**) that can be transported into a cell via diffusion or via ATP-driven pumps or transport proteins (Ammerman, 1991).

During enzyme-catalysed hydrolysis of P_{org} , P-O bonds are cleaved and O atoms within the original P_{org} compound are replaced with O atoms from surrounding water

molecules in the newly created P_i . The specific enzyme and associated hydrolysis pathway will influence the extent of O isotope exchange. For hydrolysis catalysed by a phosphomonoesterase, one O atom within the newly produced P_i will be incorporated from the surrounding water-O and the remaining three O atoms are inherited from the P_{org} compound. With hydrolysis catalysed by a phosphodiesterase, two O atoms will be incorporated from the surrounding water-O (in a two-stage process involving incorporation of one O atom due to the action of the phosphodiesterase and the second O atom due to phosphomonoesterase-catalysed hydrolysis of the newly produced monoester), with the remaining two O atoms inherited from the P_{org} compound. Therefore, because extracellular hydrolysis of P_{org} does not result in complete exchange of all four O atoms in P_i with O atoms in water, inheritance isotope effects occur in which $\delta^{18}O_p$ of the newly produced P_i lies between that of the starting P_{org} compound and $\delta^{18}O_w$ (Blake *et al.*, 1997; Colman *et al.*, 2005). Incorporation of water-O within P_i during extracellular hydrolysis of P_{org} is also accompanied by a large kinetic fractionation, due to more rapid incorporation of the isotopically lighter ^{16}O atom compared to the ^{18}O atom from water molecules in the resulting P_i (Blake *et al.*, 2005). To date however, the magnitude of the fractionation factor associated with this process has only been quantified for a small number of enzyme–substrate combinations (e.g. Liang and Blake (2006b)).

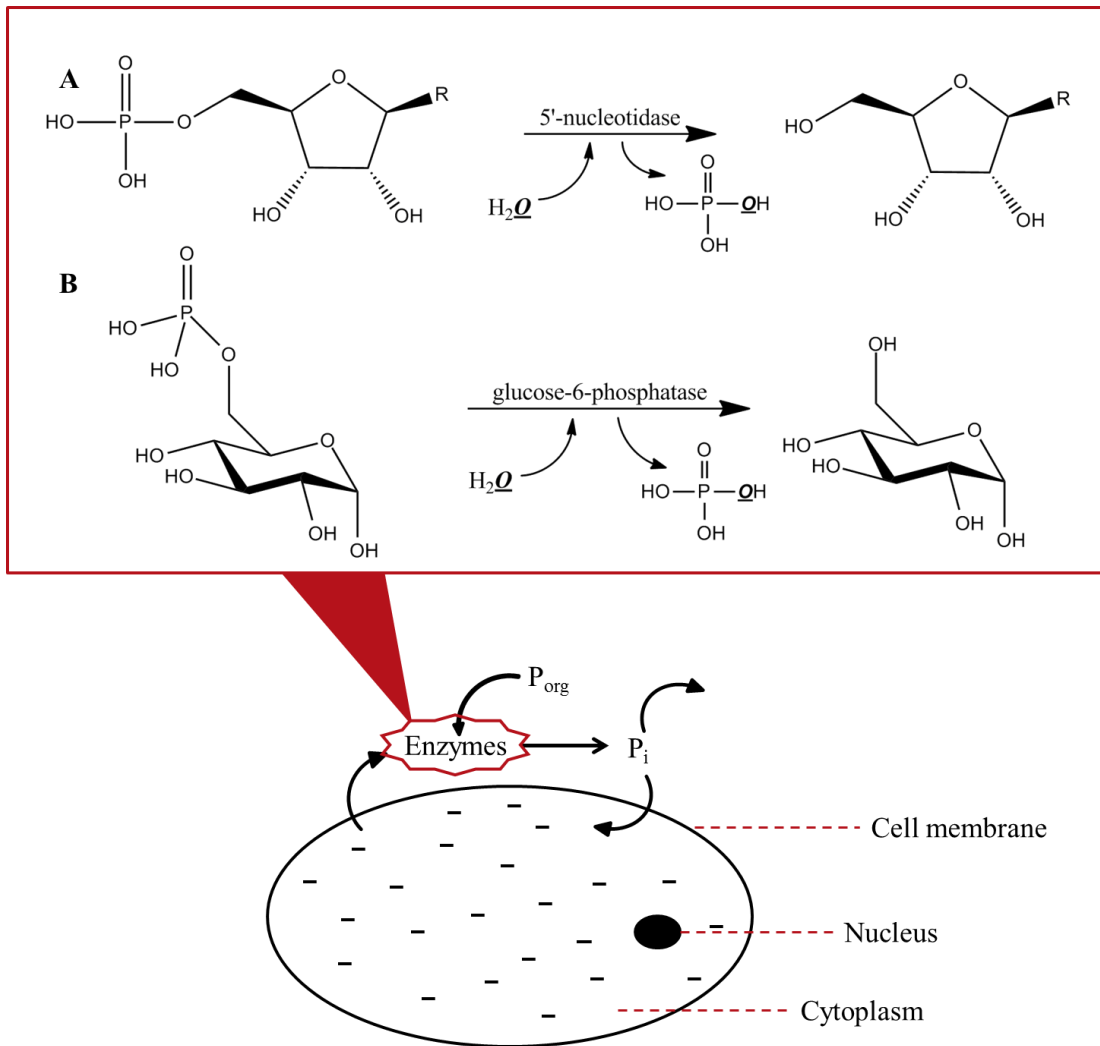


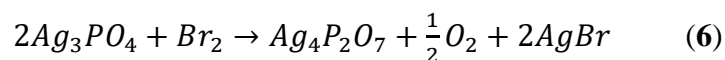
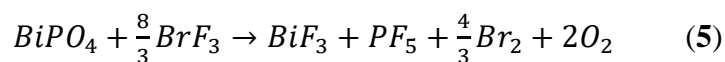
Figure 2.3: Schematic diagram representing extracellular metabolism of P_i , in which enzymes are released to the extracellular environment beyond the cytoplasmic membrane to metabolise P_{org} and release P_i which is subsequently transported across the cell membrane. Reactions include: **A:** Hydrolysis of a 5'-nucleotide molecule through the action of 5'-nucleotidase; and **B:** Hydrolysis of glucose-6-phosphate through the action of glucose-6-phosphatase. Both reactions yield a P_i molecule as a by-product.

In aquatic environments, extracellular hydrolysis is significant in the regeneration of P_i (Ammerman and Azam, 1985; Chróst, 1991; Colman *et al.*, 2005; Goldhammer *et al.*, 2011a). The fate of P_i regenerated from P_{org} depends on the initial driver for P_i regeneration from organic matter. Under conditions of P_i limitation, regenerated P_i is required to meet the metabolic demand for P among heterotrophic microorganisms. Alternatively, dephosphorylation of particulate or dissolved P_{org} may be required prior to uptake of C compounds to meet intracellular energy or C requirements among heterotrophic organisms (Colman *et al.*, 2005; Goldhammer *et al.*, 2011a). Because C rather than P demand drives dephosphorylation under these conditions, not all P_i

regenerated from P_{org} is necessarily taken up and recycled extensively through biomass. For example, it has been estimated that in coastal waters only 10-15% of P_i produced through the action of secreted 5'-nucleotidase was taken up by microorganisms (Ammerman and Azam, 1985). The remaining 85-90% may enter the P_i pool of the water column and affect the bulk $\delta^{18}O_p$ value of the extracellular environment. Effects on extracellular $\delta^{18}O_p$ due to regeneration of P_i from P_{org} that is driven by C-limitation have also been observed in deep-ocean water and in marine sediment porewater (Colman *et al.*, 2005; Goldhammer *et al.*, 2011a).

2.3 Analytical protocols for determining $\delta^{18}O_p$

Historically, $\delta^{18}O_p$ has been determined through fluorination or bromination of a phosphate precipitate, traditionally bismuth(III) phosphate ($BiPO_4$), or more recently silver(I) phosphate (Ag_3PO_4) (Lécuyer, 2004). Fluorination (**Equation 5**) and bromination (**Equation 6**) halogenate the metal ion, reducing the bromine present and releasing gaseous O_2 which can be quantitatively converted into CO_2 for analysis (Vennemann *et al.*, 2002; Lécuyer, 2004). However, fluorination (which can also be achieved using BrF_5) and bromination reactions can suffer from the use of hazardous materials, poor O_2 yields, time intensive preparation (e.g. precipitation of $BiPO_4$ requires 6 days of extraction time relative to the 3 days of the Ag_3PO_4 precipitation method) and the requirement for large sample sizes in both methods (typically 4-5 mg Ag_3PO_4) (Lécuyer *et al.*, 1993; Vennemann *et al.*, 2002; Lécuyer, 2004; Gruau *et al.*, 2005).



Isotope ratio mass spectrometry (IRMS) allows for the precise measurement of small mass differences between different isotopes within a compound and, when coupled to a thermal conversion/elemental analyser (TCEA), the system can carry out relatively rapid on-line measurements of isotope ratios (LaPorte *et al.*, 2009). These systems have been automated, while retaining both precision and accuracy, for $\delta^{13}C$, $\delta^{15}N$ and $\delta^{18}O$ solid sample analysis. A further advantage of TCEA-IRMS is the relatively small

sample mass required for analysis (typically 400-500 $\mu\text{g Ag}_3\text{PO}_4$). To establish similar TCEA-IRMS protocols for $\delta^{18}\text{O}$ measurements in P_i , aqueous samples containing P_i must be converted from dissolved to solid form. In this conversion, particular care must be taken to ensure that: i) the original isotope composition of P_i is retained by using non-fractionating reactions or ensuring reactions go to completion; ii) P_i is not introduced through hydrolysis within P_{org} -rich natural samples; and iii) other O-bearing compounds including dissolved organic carbon (DOC), nitrate (NO_3^-), sulfate (SO_4^{2-}) and calcium carbonate (CaCO_3) are excluded from the final solid product.

Bismuth(III) phosphate (BiPO_4) is a hygroscopic material, with full rehydration after dehydration possible after 15 minutes in air. The BiPO_4 precipitate requires significant preparation before isotopic analysis to remove adsorbed water which can otherwise increase O yields by up to 12.5% in $\delta^{18}\text{O}_p$ analysis (Karhu and Epstein, 1986), with $\delta^{18}\text{O}_p$ enrichment possible when drying at temperatures greater than 200 °C (Mooney-Slater, 1962; Shemesh and Kolodny, 1988). Such constraints limit the utility of BiPO_4 , leading to consideration of alternative solid-phase compounds for analysis of $\delta^{18}\text{O}_p$. Silver(I) phosphate (Ag_3PO_4) has been identified as a suitable alternative, due to its weakly hygroscopic nature, stability, low solubility and relatively short preparation time (Lécuyer, 2004; McLaughlin *et al.*, 2004; Tamburini *et al.*, 2010). Firsching (1961) was among the first to precipitate Ag_3PO_4 in order to gravimetrically determine the phosphate concentration of a homogeneous solution. Whilst silicates and multivalent ions were observed to interfere with Ag_3PO_4 precipitation, ions with lower valences did not significantly interfere (e.g. NO_3^- , ammonium (NH_4^+) and potassium (K^+)), or exerted only a slight effect at high concentrations (sodium (Na^+) and SO_4^{2-}). However, Ag_3PO_4 has only more recently become a viable basis for analysis of $\delta^{18}\text{O}_p$ in aqueous environmental samples, following advances in extraction protocols that enable the precipitation of a sufficient mass of Ag_3PO_4 for analysis from complex matrices that often contain low concentrations of P_i (Colman, 2002; McLaughlin *et al.*, 2004).

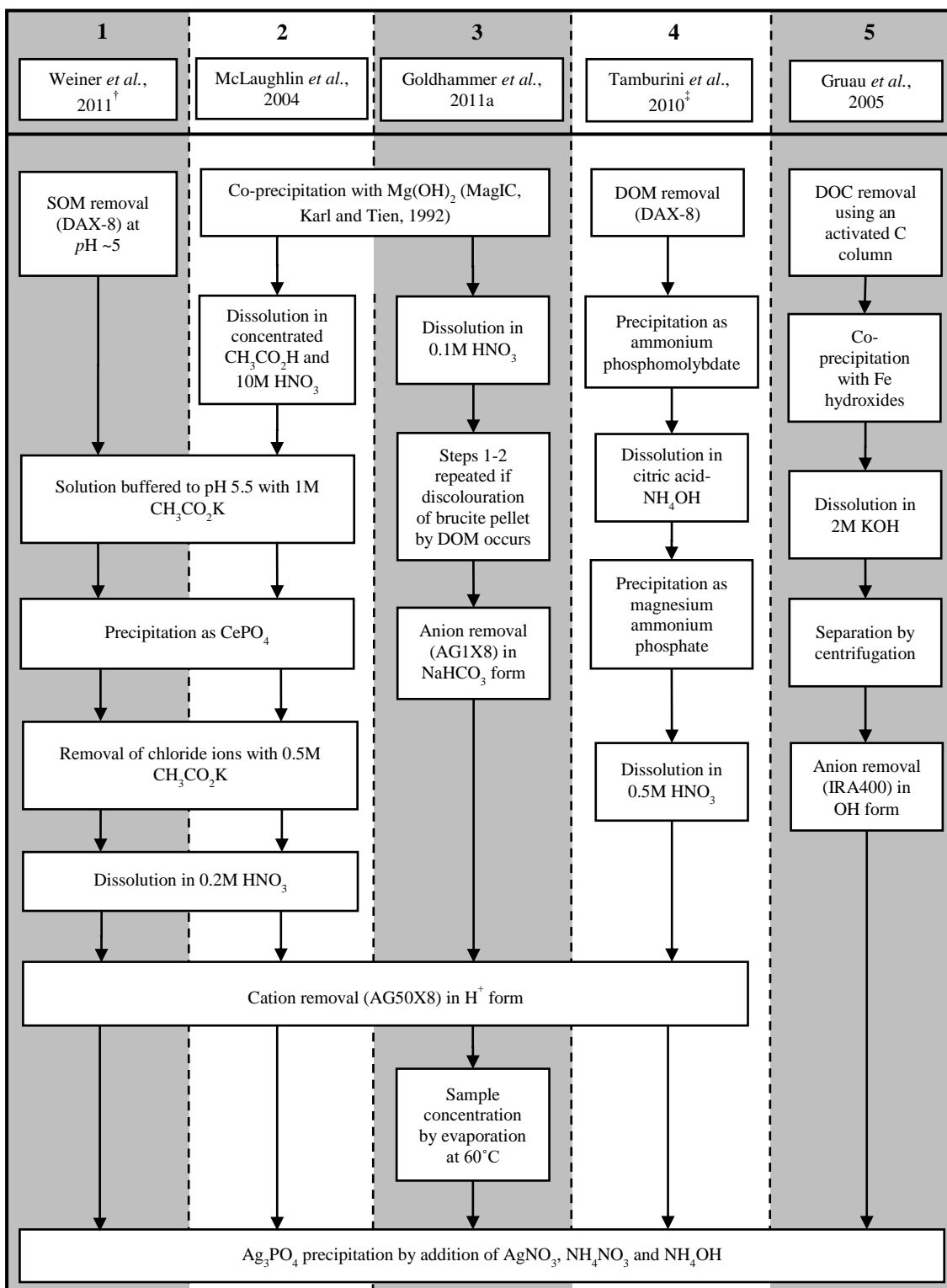
2.3.1 P_i extraction protocols for aqueous matrices

The major published protocols for extraction of P_i via precipitation of Ag_3PO_4 are summarised in **Figure 2.4**. None of the protocols in **Figure 2.4** currently represents a definitive approach for all aquatic matrices. Development and evaluation of extraction protocols is required across the range of aquatic samples in which $\delta^{18}O_p$ research is undertaken, to ensure that accurate determination of $\delta^{18}O_p$ is achieved within these complex matrices.

There are commonalities across these protocols, particularly across procedures 1-4:

- i) concentration of P_i through co-precipitation of P_i with brucite following the magnesium-induced co-precipitation (MagIC) method of Karl and Tien (1992);
- ii) redissolution of the brucite precipitate in an acid matrix;
- iii) removal of other potential sources of O using anion exchange resins and/or sequential precipitations;
- iv) removal of cations that have the potential to interfere with Ag_3PO_4 precipitation, using a cation exchange resin;
- iv) precipitation of Ag_3PO_4 .

The method of Gruau *et al.* (2005) in **Figure 2.4** was developed for freshwaters and includes an initial dissolved organic matter (DOM) removal step using activated carbon. This protocol is based on the $BiPO_4$ method of Longinelli *et al.* (1976), with the benefit of a weakly hygroscopic end precipitate (Ag_3PO_4) relative to $BiPO_4$.



SOM: soil organic matter; DOM: dissolved organic matter; DOC: dissolved organic carbon; DAX-8, AG1X8, AG50X8 and IRA400 are all types of solid phase exchange resins.

[†]Weiner *et al.* (2011) method is based on soil extracts using anion-exchange membranes

[‡]Tamburini *et al.* (2010) method is based on HCl extracts of soil samples.

Figure 2.4: Categorisation of published protocols for the precipitation of Ag₃PO₄ from aqueous samples.

Final precipitation of Ag_3PO_4 is accomplished using either ‘slow’ or ‘fast’ approaches. Both precipitation methods involve the addition of silver nitrate (AgNO_3), ammonium hydroxide (NH_4OH) and ammonium nitrate (NH_4NO_3) to form a near-neutral pH solution. Whilst ‘slow’ precipitation is achieved by holding a solution at $\sim 50^\circ\text{C}$ over several days to allow large Ag_3PO_4 crystals to grow, ‘fast’ precipitation can achieve full precipitation in a matter of minutes (Dettman *et al.*, 2001; Tamburini *et al.*, 2010). The ‘fast’ precipitation also has the added advantage of 100% Ag_3PO_4 yields independent of sample sizes, whereas lower recovery has been observed using the ‘slow’ precipitation, particularly for smaller P_i masses (Dettman *et al.*, 2001). However, the isotopic difference in Ag_3PO_4 generated by the two methods has been found to be within expected interlaboratory variation (Dettman *et al.*, 2001).

Some research has applied the McLaughlin *et al.* (2004) protocol that was originally developed for marine systems without modification to freshwater matrices, whilst other research has adapted one of the major Ag_3PO_4 precipitation protocols to include clean-up stages for samples containing high concentrations of particulate organic matter and DOM. Particulate organic matter in environmental samples is typically removed through filtration at a maximum filter pore size of $0.45\ \mu\text{m}$ (Elsbury *et al.*, 2009; Li *et al.*, 2011). In organic-rich sample matrices, including many freshwaters, inefficient removal of DOM could significantly influence measured $\delta^{18}\text{O}_p$, because DOM can consist of up to 45% O by weight and has been shown to persist until the precipitation of Ag_3PO_4 (Ma *et al.*, 2001; Lécuyer, 2004; McLaughlin *et al.*, 2004; Zohar *et al.*, 2010). For accurate determination of $\delta^{18}\text{O}_p$, all O-containing contaminants, especially DOM, must be removed from the Ag_3PO_4 precipitate prior to TCEA-IRMS. This remains a significant challenge for research seeking to apply $\delta^{18}\text{O}_p$ to complex freshwater matrices. Removal of DOM from samples has been attempted through adsorption of organic compounds to activated carbon (Gruau *et al.*, 2005), washing the final Ag_3PO_4 precipitate with hydrogen peroxide to oxidise organic compounds (Tamburini *et al.*, 2010; Zohar *et al.*, 2010), using resins to specifically remove DOM (Tamburini *et al.*, 2010), repetition of precipitation steps such as MagIC in order to isolate P_i from a matrix of potential contaminants (Goldhammer *et al.*, 2011b), and pH-specific precipitations to remove fulvic and/or humic acids (Zohar *et al.*, 2010).

Beyond a source of contaminant O, DOM includes P_{org} compounds that may undergo acid hydrolysis during the protocols described in **Figure 2.4**, for example during the dissolution of brucite. Hydrolysis of P_{org} that is co-precipitated with brucite can yield P_i , with potential incorporation of water-O from the extracellular environment during acid hydrolysis (McLaughlin *et al.*, 2006d). The P_i generated from hydrolysis of P_{org} will subsequently be incorporated within an Ag_3PO_4 precipitate, potentially altering the bulk $\delta^{18}\text{O}_p$ composition. Therefore, if the original $\delta^{18}\text{O}_p$ of P_i is to be retained, effective removal of DOM must be achieved prior to introduction of conditions that could hydrolyse P_{org} compounds.

Although research to date has focussed on analysis of $\delta^{18}\text{O}_p$ in P_i , the oxygen isotope composition of the phosphate moieties within P_{org} compounds ($\delta^{18}\text{O}_{P_{\text{org}}}$) is also of significant interest, both as a constraint on inheritance effects on $\delta^{18}\text{O}_p$ in P_i regenerated from P_{org} , but also, potentially, as an inherent tracer of P_{org} cycling within aquatic ecosystems. Analysis of $\delta^{18}\text{O}_{P_{\text{org}}}$ requires extraction of P_i from P_{org} followed by precipitation of a solid-phase P compound. Following a review of several extraction methods, Liang and Blake (2006a) concluded that extraction using UV radiation does not result in significant isotope effects on $\delta^{18}\text{O}_{P_{\text{org}}}$. However, there is a lack of any published research that has sought to characterise $\delta^{18}\text{O}$ in P_{org} compounds from aquatic samples using the apparently robust UV radiation extraction method, and only one study has been found to apply it to aqueous samples of phosphonate in a laboratory setting (Sandy *et al.*, 2013).

2.3.2 Determination of $\delta^{18}\text{O}_p$ through TCEA-IRMS

On-line TCEA-IRMS has been utilised for analysis of Ag_3PO_4 . Dried samples (typically 400-500 μg) are introduced in silver capsules as the traditional and cheaper tin alternatives can lead to significant deterioration of chromatography results (Lécuyer *et al.*, 2007). Conversion of Ag_3PO_4 to CO for analysis is achieved through pyrolysis at 1270 to 1450 °C in the presence of a carbon source to aid full conversion, typically nickelised graphite and/or glassy carbon (Vennemann *et al.*, 2002; Lécuyer *et al.*, 2007; Halas *et al.*, 2011). Water vapour is removed through a water trap and CO is separated from other gaseous impurities through gas chromatography using purge-and-trap technology or a packed GC column (Meier-Augenstein, 1999; Fourel *et al.*,

2011). Helium is used as a carrier gas to transfer the sample gas into a mass spectrometer *via* a continuous flow mode. Mass signals of 28 ($^{12}\text{C}^{16}\text{O}$) and 30 ($^{12}\text{C}^{18}\text{O}$; $^{14}\text{C}^{16}\text{O}$; $^{13}\text{C}^{17}\text{O}$) are integrated and compared to those in an independently introduced pulse of pure CO reference gas to calculate the $^{18}\text{O}/^{16}\text{O}$ ratio. Subsequently, these ratios are calibrated to the VSMOW scale in per mille notation (‰_{VSMOW}) using international reference materials, typically benzoic acids and barium sulfates (LaPorte *et al.*, 2009; Halas *et al.*, 2011). The precision for isotopic analysis is generally quoted as better than $\pm 0.3\text{‰}_{\text{VSMOW}}$ (1 standard deviation) (Lécuyer *et al.*, 2007; LaPorte *et al.*, 2009; Halas *et al.*, 2011). For the purposes of this thesis, the notation ‰_{VSMOW} will be abbreviated to ‰.

A major analytical challenge remains the lack of internationally certified Ag_3PO_4 standards, despite the long-term use of Ag_3PO_4 in the determination of $\delta^{18}\text{O}_p$ in archaeological and palaeoclimate studies (Stephan, 2000; Vennemann *et al.*, 2002; Halas *et al.*, 2011). Using materials other than Ag_3PO_4 as calibration standards, such as benzoic acids, can introduce matrix effects in which differences in chemical composition between materials can influence the analysis, for example through differing temperatures at which efficient pyrolysis is achieved (Lécuyer *et al.*, 2007). Some researchers have produced internal synthetic Ag_3PO_4 standards from either internationally recognised $\delta^{18}\text{O}$ standards such as NBS120c (phosphate rock (Florida), distributed by NIST), or KH_2PO_4 solutions equilibrated with ^{18}O -enriched water (Lécuyer *et al.*, 2007; Fourel *et al.*, 2011; Halas *et al.*, 2011). These synthetic Ag_3PO_4 materials have been shown to be stable over long periods (at least 8 years), a key requirement for any international reference material (Lécuyer *et al.*, 2007). A number of these uncertified compounds have been distributed to other laboratories and initial inter-laboratory comparison undertaken (Lécuyer *et al.*, 2007; Halas *et al.*, 2011). However, the finite availability of such material and the lack of a quality control network in the production of these materials represent significant challenges for broader use of these materials.

Linearity effects, referring to a change in the reported isotope ratio due to a change in sample mass introduced to the TCEA-IRMS and thus the peak size of the CO ion in the mass spectrometer (Brand, 2004), can also affect determination of $\delta^{18}\text{O}_p$. If this effect is consistent and can be quantified then the measured isotope ratios can be

corrected (Brand, 2004). One alternative solution to address linearity effects is to match CO ion peak heights across a run for both samples and standards by using a narrow sample mass range. However this is made more complicated by variable Ag_3PO_4 pyrolysis efficiency and CO yield between samples, which can cause variations in peak heights. Difficulties have been found in ensuring complete conversion of Ag_3PO_4 to CO in the TC/EA, with Ag_3PO_4 requiring pyrolysis in the hot spot of a furnace (LaPorte *et al.*, 2009). While many compounds can achieve complete conversion easily (especially at temperatures exceeding 1400 °C), ensuring accurate analysis of the bulk $\delta^{18}\text{O}$, incomplete conversion of other matrices, such as carbonates, has been implicated in isotope fractionation (Koziet, 1997; Kornexl *et al.*, 1999). If conversion to CO is not complete then the reaction order of the O atoms in a compound becomes significant, with those being most strongly bound to the P atom being under-represented in the CO product. If this fractionation can be shown to affect all samples equally then the results can be properly calibrated. However, if the kinetic fractionation is not equivalent across all samples due to variable conversion to CO then correction becomes problematic. This highlights the need to ensure the pyrolysis of Ag_3PO_4 is efficient and standardised across a sample run, which requires that samples are pyrolysed within the hot spot of a furnace.

2.4 Synthesis of global $\delta^{18}\text{O}_p$ data from aquatic ecosystems

Recent research has highlighted the potential to use $\delta^{18}\text{O}_p$ as both a tracer of P sources and as a dynamic tracer of metabolic processes affecting P cycling in aquatic ecosystems (McLaughlin *et al.*, 2004; Elsbury *et al.*, 2009; Goldhammer *et al.*, 2011b). The characterisation of significant sources of P_i within an ecosystem can be achieved using $\delta^{18}\text{O}_p$ assuming:

- i) $\delta^{18}\text{O}_p$ for major sources of P_i is constrained;
- ii) individual sources of P_i possess distinct $\delta^{18}\text{O}_p$ signatures;
- iii) $\delta^{18}\text{O}_p$ for P_i sources is not equal to the theoretical equilibrium;
- iv) $\delta^{18}\text{O}_p$ signatures for P_i sources are maintained and not rapidly overprinted by fractionation associated with metabolic processes.

Given these prerequisites, if $\delta^{18}\text{O}_p$ within an ecosystem tends towards the value of a particular source, inferences regarding the dominant P_i sources within ecosystems can be made. However, under conditions in which iv) above is not met and $\delta^{18}\text{O}_p$ tends towards the theoretical equilibrium (**Equations 2-4**), $\delta^{18}\text{O}_p$ can then be used to probe the extent of intracellular metabolism of P_i . Insights into other metabolic processes, including P_i uptake by cells and extracellular hydrolysis of P_{org} , may be gained through the kinetic and disequilibrium isotope effects associated with these processes. **Table 2.1** synthesises published $\delta^{18}\text{O}_p$ data currently available across a range of aquatic ecosystems. Below, ways in which recent research has begun to explore the use of $\delta^{18}\text{O}_p$ in aquatic ecosystems have been considered, highlighting the insights into P biogeochemistry that can be derived using this stable isotope technique.

2.4.1 Marine ecosystems

Marine upwelling zones, in which nutrient-rich bottom water is driven towards the surface, are areas of enhanced primary production and potentially rapid P turnover (Pennington and Chavez, 2000). Research in upwelling zones has reported $\delta^{18}\text{O}_p$ values that approach equilibrium with water-O, indicating substantial intracellular metabolism of P_i in these coastal ecosystems (Colman *et al.*, 2005; McLaughlin *et al.*, 2006b). However, the lack of complete equilibrium between $\delta^{18}\text{O}_p$ and water-O in upwelling zones suggests biological turnover of P_i relative to inputs from terrestrial and deep-water sources is lower in coastal upwelling zones compared to the open ocean (McLaughlin *et al.*, 2006b).

In the surface water of the open ocean, P_i concentrations in the photic zone can be extremely low (e.g. 0.2 – 1 nM in the Sargasso Sea), often limiting or co-limiting primary production (Wu *et al.*, 2000). Under these conditions, $\delta^{18}\text{O}_p$ values that tend towards temperature-dependent equilibrium with water-O have been reported, indicating extensive cycling of P_i through biomass (Colman *et al.*, 2005). Insights into temporal variations in P sources and the extent of biological turnover of P within marine ecosystems can also be gained through $\delta^{18}\text{O}_p$. For example, in Monterey Bay, California, McLaughlin *et al.* (2006b) observed $\delta^{18}\text{O}_p$ values in the upper water column (<200m) that were significantly influenced by source contributions from terrestrial freshwater and from deeper water (500-800m) inputs. However, during the

spring-summer periods of upwelling, $\delta^{18}\text{O}_p$ in the upper water column was isotopically heavier relative to non-upwelling autumn/winter periods, and more closely reflected the $\delta^{18}\text{O}_p$ value expected at theoretical equilibrium. The most likely explanation for this trend is enhanced intracellular cycling of P_i by phytoplankton relative to P_i inputs during periods of upwelling. Upwelling periods provide nutrients to the surface zone that, combined with a greater intensity of sunlight in the spring-summer months, can enhance productivity and consequently biological turnover of P_i (McLaughlin *et al.*, 2006b). Extensive extracellular-intracellular-extracellular cycling of P_i during the upwelling periods would lead to an over-printing of source $\delta^{18}\text{O}_p$ signatures and a shift of $\delta^{18}\text{O}_p$ in the extracellular environment towards equilibrium values. However, the data reported by McLaughlin *et al.* (2006b) suggest that the extent of extracellular-intracellular-extracellular cycling was still not sufficient, even in the spring-summer period, to establish complete equilibrium between $\delta^{18}\text{O}_p$ and water-O.

The preferential remineralisation of P over C from dissolved organic compounds has been observed in marine ecosystems, particularly in the euphotic zone (Clark *et al.*, 1998; Aminot and Kerouel, 2004). This selective remineralisation of P_{org} is caused by the presence of extracellular enzymes and their action on P_{org} substrates, meaning that the turnover rate of P_{org} molecules in this environment is dependent on the specific enzymes and P_{org} compounds present. For example, it has been shown that the flux of dissolved ATP through an oligotrophic ocean ecosystem can be up to five-fold greater than for the bulk P_{org} compound pool (Bjorkman and Karl, 2005). McLaughlin *et al.* (2013), in research conducted in the Sargasso Sea, used $\delta^{18}\text{O}_p$ to investigate the role of P_{org} hydrolysis in P-cycling in marine ecosystems. Based on the fractionation imparted on $\delta^{18}\text{O}_p$ when P_i is regenerated from a specific P_{org} molecule following a specific hydrolysis pathway, McLaughlin *et al.* used **Equation 7** to estimate the fraction of P_i in samples that had been regenerated from P_{org} :

$$\%P_i \text{ from } P_{\text{org}} \text{ remineralisation} = \frac{(\delta^{18}\text{O}_{\text{sample}} - \delta^{18}\text{O}_{\text{eq}})}{(\delta^{18}\text{O}_{\text{rem}} - \delta^{18}\text{O}_{\text{eq}})} \times 100\% \quad (7)$$

where $\delta^{18}\text{O}_{\text{rem}}$ is the calculated value of $\delta^{18}\text{O}_p$ based on a particular combination of P substrate and hydrolysis pathway; $\delta^{18}\text{O}_{\text{eq}}$ is the expected equilibrium value of $\delta^{18}\text{O}_p$ and $\delta^{18}\text{O}_{\text{sample}}$ is the measured $\delta^{18}\text{O}_p$ in a sample. McLaughlin *et al.* concluded that 5-

80% of P_i present in the upper 200m of an oligotrophic marine ecosystem was the product of P_{org} remineralisation, dependent on which enzyme/substrate system was used in **Equation 7**. These data, combined with expressed enzyme activity and low P_i concentration, suggest that P_i regeneration from P_{org} was coupled with uptake by organisms to support metabolism. The proportion of P_i thought to derive from P_{org} remineralisation was significantly reduced (12-35%) at a monitoring station closest to the shoreline, suggesting increased P_i availability in this region and thus reduced requirement for P_{org} mineralisation. Despite the limited number of samples and large contrasts between differing enzyme/substrate systems, the research highlights the potential for using $\delta^{18}O_p$ to gain new insights into P cycling within the marine ecosystem, without the need to directly determine the concentrations or fluxes affecting P_i and P_{org} pools.

Colman *et al.* (2005) also demonstrated that $\delta^{18}O_p$ was also close to or at theoretical equilibrium in deep water samples from both the Atlantic (900-4000 m) and Pacific (300-3000 m) oceans. These data are consistent with intracellular equilibration between $\delta^{18}O_p$ and water-O in surface waters, followed by advection of P_i to depth. However, small offsets from the expected theoretical equilibrium (-1.5‰) in P_i from deep-ocean samples collected below the thermocline were used by Colman *et al.* (2005) to infer that significant P_{org} mineralisation occurred in this zone, imparting a disequilibrium fractionation on $\delta^{18}O_p$. The disequilibrium effects were not fully overprinted by equilibrium fractionations, supporting estimates that 80-95% of the remineralised P_i was not utilised by the surrounding microorganisms in these deep-ocean waters to meet their P requirements, because metabolism in these zones is hypothesised to be limited by C and energy rather than by P. However, the size of the $\delta^{18}O_p$ offset from equilibrium was smaller than that expected on the basis of P_i regeneration from P_{org} through the action of phosphohydrolases, suggesting partial biological turnover of P_i in these deep ocean environments (Colman *et al.*, 2005).

Table 2.1: Synthesis of global $\delta^{18}\text{O}_p$ data derived from a range of aquatic ecosystems.

Type	Setting	Min $\delta^{18}\text{O}_p$ ‰	Max $\delta^{18}\text{O}_p$ ‰	Mean $\delta^{18}\text{O}_p$ ‰	1 σ	Number of samples	Geographical Locations	Reference
Marine	Coastal surface waters	15.9	22.3	20.0	1.34	141	Monterey Bay, California; Long Island Sound, USA	McLaughlin <i>et al.</i> (2004); Colman <i>et al.</i> (2005); McLaughlin <i>et al.</i> (2006b)
	Open ocean surface (<200m depth)	13.8	23.7	18.5	3.27	17	Monterey Bay, California; Sargasso Sea	McLaughlin <i>et al.</i> (2004); McLaughlin <i>et al.</i> (2013)
	Deep ocean (>200 m depth)	17.4	25.4	22.6	2.08	31	North Atlantic and Pacific Ocean tropical gyres; Sargasso Sea	McLaughlin <i>et al.</i> (2004); Colman <i>et al.</i> (2005); McLaughlin <i>et al.</i> (2013)
Estuarine		7.8	20.3	15.9	2.78	54	North San Francisco Bay California; Elkhorn Slough, California;	McLaughlin <i>et al.</i> (2004); McLaughlin <i>et al.</i> (2006a); McLaughlin <i>et al.</i> (2006c)
Freshwater	River (main)	8.6	15.2	12.4	1.46	32	San Joaquin River and Lake Tahoe California; Lake Erie, USA	Elsbury <i>et al.</i> (2009); McLaughlin <i>et al.</i> (2006a); Young <i>et al.</i> (2009)
	River (tributaries)	9.2	17.2	12.5	2.03	32	Elkhorn Slough, San Joaquin River and Lake Tahoe California; Lake Erie, USA	McLaughlin <i>et al.</i> (2006a); Young <i>et al.</i> (2009)
	Groundwater	15.1	22.4	18.6	2.13	9	Elkhorn Slough and San Joaquin River, California	Blake <i>et al.</i> (2001); McLaughlin <i>et al.</i> (2006a); Young <i>et al.</i> (2009)
	Lake (surface water – 1 m)	10	17.1	14.1	1.57	34	Lake Erie, USA	Elsbury <i>et al.</i> (2009)
	Lake (5.5 - 22 m)	8.4	15.8	13.6	1.58	25	Lake Erie, USA	Elsbury <i>et al.</i> (2009)
	Lake (58 m)	-	-	12.7	-	1	Lake Erie, USA	Elsbury <i>et al.</i> (2009)
	WWTP final effluent	8.4	18.4	12.9	4.02	14	Brittany, France;	Gruau <i>et al.</i> (2005); Young <i>et al.</i> (2009); McLaughlin <i>et al.</i> (2006c)
	Constructed wetlands (canals, inlet, interior and outlet)	20.0	25.5	21.5	1.32	25	Florida Everglades, USA	Li <i>et al.</i> (2011)
Marsh	21.6	25.1	23.5	1.61	4	Florida Everglades, USA	Li <i>et al.</i> (2011)	
Sediments	Marine porewater	12.8	26.6	22.2	2.59	119	Benguela Upwelling, South Atlantic	Goldhammer <i>et al.</i> (2011a)

2.4.2 Estuarine ecosystems

Source $\delta^{18}\text{O}_p$ signatures have been shown to be retained within some estuarine ecosystems (e.g. McLaughlin *et al.*, 2006a). Source signals representing inputs derived from surrounding land (e.g. chemical fertilisers associated with runoff from agricultural land) and from other aquatic ecosystems (e.g. groundwater and surface water tributaries) are thought to dominate the bulk $\delta^{18}\text{O}_p$ composition in many estuarine ecosystems, due to the short residence time of P compounds in tidal estuaries (McLaughlin *et al.*, 2006a). The limited contact time with biomass in these ecosystems constrains the opportunity for metabolism of P, increasing the potential for source $\delta^{18}\text{O}_p$ signatures to be retained. McLaughlin *et al.* (2006a) demonstrated that towards the mouth of Elkhorn Slough in California, $\delta^{18}\text{O}_p$ was dominated by that of oceanic-derived P_i (~20%) due to tidal flushing of the ecosystem in this area. Similar $\delta^{18}\text{O}_p$ values were also found upstream in the estuary. However, these were attributed to chemical fertilisers, entering the estuarine ecosystem through agricultural field runoff, that have an isotopic composition similar to that of the marine ore from which the fertilisers were formed. One mid-estuary site had a significantly lower $\delta^{18}\text{O}_p$ composition. This observation, combined with the use of other natural tracers, suggested that groundwater discharge significantly affected bulk $\delta^{18}\text{O}_p$ at this sampling location. $\delta^{18}\text{O}_p$ can also provide insights into the presence of temporal and spatial patterns in P_i sources to estuaries. For example, it was observed that $\delta^{18}\text{O}_p$ composition throughout the main estuary channel was not affected by either tidal or seasonal variations (McLaughlin *et al.*, 2006a). However, a nearby harbour, close to the mouth of the estuary, did show evidence of tidal patterns through $\delta^{18}\text{O}_p$, with high tide displaying $\delta^{18}\text{O}_p$ values higher and closer to that of oceanic-derived P_i and low tide exhibiting lower $\delta^{18}\text{O}_p$ values towards those observed upstream in the estuary.

2.4.3 Sediments within aquatic ecosystems

$\delta^{18}\text{O}_p$ has also been used as a tracer of particulate inorganic P sources and sinks within aquatic ecosystems (Markel *et al.*, 1994; Jaisi and Blake, 2010). The first major lacustrine site for this application was Lake Kinneret, situated in the Dead Sea Rift Valley (Markel *et al.*, 1994). Markel *et al.* (1994) showed that $\delta^{18}\text{O}_p$ in sediment bound- P_i varied significantly with sediment grain size, with clay bound- P_i having a

significantly heavier $\delta^{18}\text{O}_p$ than silt or sand bound- P_i . These $\delta^{18}\text{O}_p$ signatures enabled an internal P-cycling model of Lake Kinneret to be developed, which included major processes such as the sedimentation of both detrital and authigenic apatite and CCP ($\text{Ca}_3(\text{HCO}_3)_3(\text{PO}_4)$), as well as the dissolution of these materials. In conjunction with other internal P-cycling studies of Lake Kinneret, $\delta^{18}\text{O}_p$ was used as a tool to both elucidate the interaction pathways that P can undergo in this environment and support the quantitative analyses of sediment-lake interactions found in other studies. Further work has also shown that $\delta^{18}\text{O}_p$ may act as a tracer of P source and as a paleotemperature proxy (particularly in detrital and authigenic P phases) in other ecosystems, such as continental margins (Jaisi and Blake, 2010).

More recent methodological advances that enable accurate measurements of $\delta^{18}\text{O}_p$ in samples containing a small mass of P_i have underpinned studies of $\delta^{18}\text{O}_p$ within porewaters of deep marine sediments (Goldhammer *et al.*, 2011a; Goldhammer *et al.*, 2011b). These studies demonstrate that $\delta^{18}\text{O}_p$ in extracted porewater, P_i concentration profiles and two-endmember isotope mixing models can be used to determine whether marine sediments are dominated by P release (regeneration of P_i during microbial respiration of organic matter and the desorption of P_i from mineral phases), P burial from sources in the overlying water column, or P_i movement within the sediment column, through advection or diffusion (Goldhammer *et al.*, 2011a; Goldhammer *et al.*, 2011b). In particular, it was shown that marine sediments demonstrate significant disequilibrium in $\delta^{18}\text{O}_p$, reflecting the dominance of disequilibrium effects associated with P_i regeneration from organic matter (Goldhammer *et al.*, 2011a). However, it was noted that simple isotope mass balance models can overlook processes which could be significant within these environments and thus improvements need to be made for future analyses, including the construction of more complex and realistic isotope models that allow for the incorporation of physical mixing processes such as diffusion and advection.

2.5 Freshwater ecosystems

Beyond the relatively intensive study of Lake Erie reported by Elsbury *et al.* (2009), the catalogue of $\delta^{18}\text{O}_p$ data for freshwater ecosystems remains more constrained than for marine and terrestrial ecosystems. However, a limited number of initial studies have explored $\delta^{18}\text{O}_p$ to assess sources and metabolism of P_i in freshwater ecosystems.

2.5.1 Application of $\delta^{18}\text{O}_p$ to identify sources of P in freshwater ecosystems

A range of potential sources of P to freshwater ecosystems may be distinguished on the basis of $\delta^{18}\text{O}_p$, as long as the source isotopic signature is not rapidly over-printed by isotopic fractionations associated with metabolism (e.g. Young *et al.* (2009); Li *et al.* (2011)). However, this emerging dataset also shows potential for significant overlap in $\delta^{18}\text{O}_p$ between a number of individual sources. For example, whilst $\delta^{18}\text{O}_p$ may be used to distinguish P derived from fertilisers compared to WWTP effluents, no significant differences were found between $\delta^{18}\text{O}_p$ across other potential sources, such as vegetation and detergents (Young *et al.*, 2009). **Table 2.2** synthesises currently available data regarding $\delta^{18}\text{O}_p$ in potential sources of P to freshwaters, with average $\delta^{18}\text{O}_p$ in these sources ranging from 13.2 to 21.5‰. However, note that for many of these sources, the size of the available dataset is currently small and geographically constrained.

Table 2.2: Observed $\delta^{18}\text{O}_p$ values for potential P sources to freshwater ecosystems (Ayliffe *et al.*, 1992^(A); Gruau *et al.*, 2005^(S); McLaughlin *et al.*, 2006a^(#); Young *et al.*, 2009^(*); Li *et al.*, 2011⁽⁻⁾; Gross *et al.*, 2013^(E)).

Source	Min $\delta^{18}\text{O}_p$ /‰	Max $\delta^{18}\text{O}_p$ /‰	Mean $\delta^{18}\text{O}_p$ /‰	1σ	Number of samples	Geographical location
Chemical fertilisers ^{*#S~}	15.5	25.3	22.1	2.32	33	--
Fertiliser ore and processing [*]	18.2	21.6	20	1.43	5	Israel
†Aerosols and dust ^{*E}	14.2	24.9	20.1	2.17	17	Israel
WWTP final effluent and during processing ^{*S}	8.4	18.4	13.5	3.5	18	USA; France
Detergent [*]	13.3	18.6	16.8	1.83	7	--
Toothpaste [*]	--	--	17.7	--	1	--
†Animal faeces ^{*A}	15.7	23.1	20	1.82	11	South Pacific; California, USA
†Soil leachate [*]	17.9	19.1	18.5	0.474	5	Israel
Compost [#]	23.3	27	25.2	2.62	2	California, USA
†Vegetation leachate (Live, Dead and Decayed) [*]	14.2	23.1	16.8	2	27	California, USA

†Water soluble P_i fractions

Gruau *et al.* (2005) compared $\delta^{18}\text{O}_p$ across three commonly-used inorganic P fertilisers and effluent samples from three WWTPs in France. The origin of the phosphatic rock used in the production of the fertilisers was found to be significant in the resulting $\delta^{18}\text{O}_p$ value with the samples analysed in this study lying in the range 19.6 to 23.1‰, which is consistent with the typical ranges for the two largest phosphatic rock suppliers to France – Morocco (18.5‰ to 20.5‰) and Florida (17.2‰ to 23.2‰) respectively. Laboratory dissolution experiments demonstrated no significant fractionation of $\delta^{18}\text{O}_p$ within the bulk fertiliser, suggesting that fertiliser $\delta^{18}\text{O}_p$ could be preserved in runoff from agricultural land (Gruau *et al.*, 2005). Phosphate in WWTP effluents from the study by Gruau *et al.* was assumed to originate from two main sources: human waste, including faeces, urine and waste food disposal (30-50%) and phosphate-based detergents (50-70%). For the same WWTP effluents, $\delta^{18}\text{O}_p$ values fell in a narrow range of 16.6 to 18.1‰_{VSMOW}, whilst $\delta^{18}\text{O}_p$ for a phosphate builder used in detergents fell within the same range (17.9‰_{VSMOW}), indicating a possible maintenance of source $\delta^{18}\text{O}_p$ composition in the final WWTP effluent. However, the $\delta^{18}\text{O}_p$ composition of WWTP effluents could also reflect the result of microbial metabolism of P_{org} , as reported values also fall in the $\delta^{18}\text{O}_p$ range expected following fractionation due to mineralisation of P_{org} (Blake *et al.*, 1997; Gruau *et al.*, 2005). The difference between $\delta^{18}\text{O}_p$ ranges for fertiliser- and sewage-derived phosphate (<2‰) reported by Gruau *et al.* (2005) was statistically significant.

However, given the relatively small absolute difference, and the variability in $\delta^{18}\text{O}_p$ of the two sources (ranges for both sources were $\geq 1.5\%$), these authors conclude that $\delta^{18}\text{O}_p$ may not be suitable for distinguishing between sources of anthropogenic phosphate.

However, the $\delta^{18}\text{O}_p$ of other potentially significant sources of P_i to freshwaters have not been thoroughly characterised, including soil leachate, waste from aquaculture and, in particular, groundwater and septic tank discharge. Where sources such as inorganic fertiliser or WWTP effluent have begun to be characterised, available data tend to focus on specific geographical regions such as California (USA) (Young *et al.*, 2009), the Great Lakes (USA) (Elsbury *et al.*, 2009; Young *et al.*, 2009) and Brittany (France) (Gruau *et al.*, 2005). A larger body of research is required to extend the isotopic characterisation of sources of P_i to other geographical locations. Further, the majority of existing studies provide only snapshots in time, and the potential for temporal changes in $\delta^{18}\text{O}_p$ of sources has not been fully constrained, for example within WWTP effluent in which the dominant sources and treatment efficiency may change significantly over annual, seasonal or daily timescales.

Analysis of $\delta^{18}\text{O}_p$ in natural freshwater samples has demonstrated that disequilibrium isotopic compositions can persist in these environments (Young *et al.*, 2009; Li *et al.*, 2011). Young *et al.* (2009) compared $\delta^{18}\text{O}_p$ in the tributaries to three major US freshwater bodies, Lake Erie, the San Joaquin River and Lake Tahoe, to a theoretical equilibrium value. Only two of the 40 samples analysed in the study fell within the 95% confidence limit for the theoretical isotopic equilibrium. This was also true for two groundwater samples in the San Joaquin catchment, in which data indicated that both groundwater samples were enriched in ^{18}O relative to the expected equilibrium isotopic composition.

Similar conclusions were reached by Li *et al.* (2011) who showed that anthropogenic phosphate fertilisers could be traced within a freshwater wetland in the Everglades National Park, USA. Inputs of P from artificial fertilisers in the Everglades Agricultural Area (EAA) have contributed to mean concentrations of P in runoff being 20-fold greater than in non-agricultural areas of the national park. The average $\delta^{18}\text{O}$ value of fertilisers used within the EAA was found to be $24.4 \pm 0.7\%$ between April

2005 and March 2006. Analysis revealed that $\delta^{18}\text{O}_p$ was at equilibrium with the ambient water in one constructed wetland (April 2005), although later sampling in July and March 2006 determined that the $\delta^{18}\text{O}_p$ values were strongly governed by fertiliser inputs, being enriched with $\delta^{18}\text{O}$ compared to the expected equilibrium, particularly close to the inlet from the EAA. Seasonal variation was also observed, with $\delta^{18}\text{O}_p$ being enriched in the colder, winter months relative to samples collected in July. These observations may reflect differences in metabolic activity between summer and winter months, or alternatively reflect the timing of fertiliser applications. At least within the specific catchments reported in research by Li *et al.* (2011), disequilibrium isotope composition was shown to be maintained in P_i under certain circumstances. However, the maintenance or otherwise of disequilibrium $\delta^{18}\text{O}_p$ remains to be evaluated across a wider range of spatial and temporal scales for freshwater ecosystems.

If disequilibrium isotope compositions do persist in freshwater ecosystems and the major P_i sources have statistically different $\delta^{18}\text{O}_p$ values, then it would be possible to utilise $\delta^{18}\text{O}_p$ in source apportionment calculations. Li *et al.* (2011) estimated the proportion of P_i derived from artificial fertiliser inputs (F) using a two-system mass balance model (**Equation 8**), the theoretical equilibrium isotope composition ($\delta^{18}\text{O}_{\text{recycled}}$), the isotopic composition of fertiliser ($\delta^{18}\text{O}_{\text{fertiliser}}$) and the isotopic composition of P_i measured in a sample ($\delta^{18}\text{O}_p$).

$$F = \frac{(\delta^{18}\text{O}_p - \delta^{18}\text{O}_{\text{recycled}})}{(\delta^{18}\text{O}_{\text{fertiliser}} - \delta^{18}\text{O}_{\text{recycled}})} \times 100\% \quad (8)$$

This mass balance equation is based on the assumption that only fertiliser inputs and biologically recycled phosphate make up the P_i of the wetland. Using this equation, it was estimated that artificial fertiliser inputs into the wetland contributed between 15-100% of the total dissolved P_i content, with the lowest and highest proportions found in samples collected in April and in March respectively. Clearly, more complicated mass balance approaches would be required for more complex ecosystems with multiple sources. If sources, and any fractionation effects, could be sufficiently well constrained, then it would be theoretically possible to build mixing models to estimate the relative contribution from different sources to P within receiving waters.

2.5.2 Evidence from $\delta^{18}\text{O}_p$ analysis of P metabolism in freshwater ecosystems

Evidence of temperature-dependent equilibrium fractionation between $\delta^{18}\text{O}_p$ and $\delta^{18}\text{O}_w$ has also been used to infer evidence of full or partial metabolism of P_i in some freshwater ecosystems (Blake *et al.*, 2001; Elsbury *et al.*, 2009). For example, Blake *et al.* (2001) analysed $\delta^{18}\text{O}_p$ within groundwater samples from a shallow P_i -rich aquifer in Cape Cod, Massachusetts, USA. Significant inputs of P_i to groundwater resulted from sewage contamination, causing P_i concentrations to rise to 30-108 $\mu\text{mol.L}^{-1}$. Full equilibration between $\delta^{18}\text{O}_p$ and $\delta^{18}\text{O}_w$ in the surrounding groundwater was not achieved, probably due to a low DOC concentration meaning that elevated P_i concentrations were above metabolic requirements. However, a strong positive correlation was found between $\delta^{18}\text{O}_p$ and $\delta^{18}\text{O}_w$, suggesting partial metabolism of P and that $\delta^{18}\text{O}_p$ could be used to provide insights into metabolism of P_i in groundwater.

The first major study of the application of $\delta^{18}\text{O}_p$ in the water column of a lacustrine setting was conducted in Lake Erie, USA (Elsbury *et al.*, 2009) and emphasises the potential to use $\delta^{18}\text{O}_p$ within freshwater P cycling studies to identify trends that cannot be observed by determining concentration alone. Despite strict regulations on point sources of P since the 1970s and no observed increase in influx to the lake, P_i concentration in the Central Basin of Lake Erie has increased since 1990 (Elsbury *et al.*, 2009). As changes in inflow P_i fluxes could not explain the observed increase in P_i concentration, analysis of $\delta^{18}\text{O}_p$ was initially applied to identify additional sources of P_i .

Weighted riverine $\delta^{18}\text{O}_p$ average feeding the lake was considerably depleted in ^{18}O compared to that of the theoretical equilibrium $\delta^{18}\text{O}_p$, whereas the $\delta^{18}\text{O}_p$ values observed in Lake Erie were generally enriched in ^{18}O compared to those of the seven sampled tributaries, particularly in the Central Basin. Any samples with $\delta^{18}\text{O}_p$ between that of the theoretical equilibrium and the weighted riverine signal (+11‰) could potentially be attributed to incomplete equilibration of the O within riverine phosphate with water-O in the lake through metabolism of P_i . Consequently, Elsbury *et al.* (2009) concluded that samples with $\delta^{18}\text{O}_p$ values outside of the potential mixing region must be derived from an additional (unconstrained) source of P_i . Potential sources included smaller tributaries that were not sampled in the study; however this was deemed

improbable given the large P_i fluxes required to achieve the observed concentration increase in the Central Basin. Alternatively, disequilibrium isotopic effects could be operating in the lake, leading to an increase of $\delta^{18}O_p$ in lake P_i through processes associated with a kinetic fractionation (Blake *et al.*, 2005). However, the most likely explanation for the observed increase in P_i concentration was concluded to be end-member mixing of riverine P_i with an isotopically enriched source(s) of P_i ($>+17\text{‰}$), which was suggested by Elsbury *et al.* to be associated with remineralisation of ^{18}O -enriched P_{org} within the bed sediments, followed by release of P_i from the lake sediment to the water column.

2.6 Concluding remarks

The use of $\delta^{18}O_p$ in research examining P cycling in natural ecosystems is at an embryonic stage, particularly with respect to freshwater ecosystems. This stable isotope tracer has the potential to offer new insights into both the relative importance of different sources of P to ecosystems, and the extent to which P from individual sources is linked to metabolic activity within ecosystems. These insights would have important implications for understanding the reaction mechanisms controlling P biogeochemistry in nature, and for the design and targeting of future policies and practices to deliver more sustainable stewardship of P.

Given the review reported above, and the importance of analytical protocols that are specifically designed to address the challenges of determining $\delta^{18}O_p$ in freshwater matrices, **Chapter 3** reports the development and testing of new techniques for the precipitation of Ag_3PO_4 from these matrices.

Chapter 3:

Development and evaluation of new protocols for the robust determination of $\delta^{18}\text{O}_p$ in freshwaters

3.1 Introduction

This chapter reports the development and testing of new protocols for the determination of $\delta^{18}\text{O}_p$ within freshwater environments. Specifically, new sample preparation stages have been combined with the McLaughlin *et al.* (2004) protocol (**Method 1, Figure 3.1**), in order to more robustly apply $\delta^{18}\text{O}_p$ analyses to freshwater matrices. The protocol in **Method 1** was first designed for use within shallow and deep marine waters (McLaughlin *et al.*, 2004). The first step (1a) in this protocol extracts P_i from the bulk 0.45 μm filtered sample using a magnesium-induced co-precipitation (MagIC) step, to form a solid-phase brucite ($\text{Mg}(\text{OH})_2$) pellet with co-precipitated P_i , thereby removing P_i from the remaining sample matrix. The intermediate steps (2a-7a) in **Method 1** were included in an attempt to ensure the removal of any species that might chemically interfere with step 8a, the precipitation of Ag_3PO_4 , which is subsequently analysed *via* TCEA-IRMS. In addition, these steps were included to minimise the incorporation of contaminant O in the final Ag_3PO_4 precipitate. However, this chapter presents data to show that these steps do not necessarily remove contaminants effectively from the Ag_3PO_4 when applied to freshwater matrices.

Species that might chemically interfere with step 8a include both cations and anions that either prevent the formation of Ag_3PO_4 , e.g. by participating in competing reactions that prevent the full conversion of P_i into Ag_3PO_4 , or reduce its purity by forming insoluble compounds which could be a source of contaminant O. For example, a cerium phosphate (CePO_4) precipitation at *pH* 5.5 (steps 2a-4a) is included

to isolate P_i from Cl^- anions that may have derived from the original sample matrix or from the addition of magnesium chloride as part of the MagIC precipitation; step 5a ensures the precipitate is washed thoroughly to achieve full removal of Cl^- ions. This is imperative because any Cl^- ions present in step 8a can competitively react with Ag^+ ions to form a very poorly soluble $AgCl$ precipitate in water ($1.334 \times 10^{-5} \text{ mol.L}^{-1}$ at 25°C (Davies and Jones, 1955)). This competitive reaction would cause the final Ag_3PO_4 precipitate to be impure, potentially interfering with the TCEA-IRMS analysis by reducing the mass of O within the measured sample; although a reduced O yield should not alter the measured $\delta^{18}O_p$, it is possible that with sufficiently low O yields, a linearity effect could be imparted, in which $\delta^{18}O_p$ is altered due to a change in sample mass introduced to the TCEA-IRMS and thus the peak size of the CO ion in the mass spectrometer (Brand, 2004). Furthermore, if there is incomplete precipitation of P_i during step 8a due to an insufficient concentration of Ag^+ ions remaining in solution after $AgCl$ precipitation, a potential kinetic isotope effect could be imparted on the P_i pool, introducing an error into the measured $\delta^{18}O_p$.

Step 6a in **Figure 3.1**, like step 2a, re-dissolves the precipitate formed in the previous step of the protocol. This is an efficient way to solubilise P_i ; however, any other ions or molecules contained within, or bound to, the precipitate will also be released into solution. Removal of cations that have the potential to interfere with Ag_3PO_4 precipitation, such as Ce^{3+} , is achieved using an H^+ -form cation exchange resin to exchange cations present with H^+ ions in solution (7a). However, the risk that oxyanions that are co-adsorbed or co-precipitated alongside P_i in the MagIC step are also released on redissolution of a precipitate and remain in solution until the Ag_3PO_4 precipitation is not addressed through the use of a cation exchange resin. As these oxyanions could introduce error to the $\delta^{18}O_p$ measurement in the TCEA-IRMS, this issue needs to be addressed. Finally, the final step (8a) in the **Method 1** protocol is a ‘fast’ precipitation of Ag_3PO_4 , achieved by the addition of silver nitrate ($AgNO_3$) when the solution is at a near-neutral pH. The ‘fast’ precipitation allows the Ag_3PO_4 to form within minutes with 100% yields, ensuring that the bulk P_i is precipitated and analysed for $\delta^{18}O_p$ in the TCEA-IRMS (Dettman *et al.*, 2001; Tamburini *et al.*, 2010).

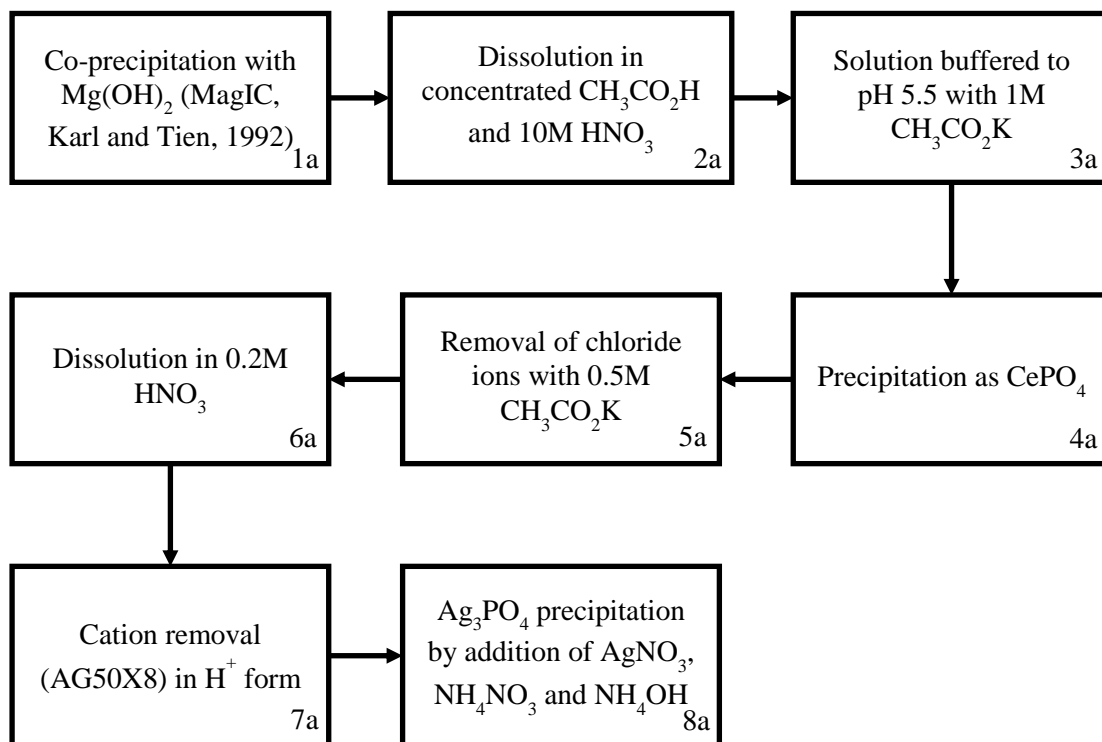


Figure 3.1: Method 1 – a protocol developed for P_i extraction from $0.45\mu\text{m}$ filtered seawater prior to determination of the stable oxygen isotope composition of P_i (McLaughlin *et al.*, 2004).

Chapter 2 highlighted that a priority for future applications of $\delta^{18}\text{O}_p$ analyses within freshwaters was to consider how the effects of potential sources of contaminant O can be minimised within analytical protocols. Inaccurate $\delta^{18}\text{O}_p$ data can result from two types of oxygen contamination: incorporation of contaminant oxygen within the PO_4 moiety of the Ag_3PO_4 molecule itself, or the pyrolysis of impure Ag_3PO_4 in which the impurity(s) contains an additional source of O. Impurities could include oxyanions (other than P_i) and organic compounds, each of which may have co-precipitated during Ag_3PO_4 formation or adsorbed to the surface of, or become incorporated within, the precipitate. These impurities have the potential to act as sources of O within the TCEA-IRMS determination that are not associated with P_i . These contaminants could include nitrate and sulfate oxyanions which are both frequently present in freshwater matrices. Like P_i , nitrate is a key concern because of its potentially controlling role in primary production within marine and freshwater ecosystems. However, average nitrate concentrations are geographically highly variable, with many areas exceeding the $50\text{ mg NO}_3^-\cdot\text{L}^{-1}$ World Health Organisation drinking water standard (Neal *et al.*, 2006; Stuart *et al.*, 2007; SI 2000 No. 3184). It has been estimated that for some rural English rivers up to 97% of the in-stream

nitrate concentration is derived from diffuse sources and attributed to agricultural practices, for example following the application of N fertilisers such as NH_4NO_3 (Neal *et al.*, 2006). Sulfate is also a potential source of oxyanion contamination; although the sulfate concentration in many UK surface waters has decreased in recent decades due to a reduction of anthropogenic inputs from acid rain, concentrations are still variable with some sites averaging more than $170 \mu\text{eq SO}_4^{2-} \cdot \text{L}^{-1}$ of anthropogenically-derived sulfate between 2003 and 2008 (Monteith *et al.*, 2014).

Incorporation of contaminant oxygen in the PO_4 moiety of the Ag_3PO_4 molecule itself either results from an exchange of oxygen atoms between the water molecules and the P_i molecules originally present in a sample, or from the generation of new P_i prior to the precipitation of Ag_3PO_4 within a protocol. The source of P in any newly generated P_i is typically from P-containing organic compounds (P_{org}), and thus P_{org} is a potentially important contributor to this form of contamination. For example, hydrolysis of P_{org} (see **Section 2.2.3**) can yield P_i that has incorporated water-O from the extracellular environment and/or inherited O from the source P_{org} compound (McLaughlin *et al.*, 2006d). Thus, the $\delta^{18}\text{O}_p$ ratio of a sample may be altered, because the final Ag_3PO_4 precipitate is derived from an unknown mixture of the original sample P_i pool and P_i derived from the hydrolysis of P_{org} . Therefore, a robust protocol for $\delta^{18}\text{O}_p$ would remove any potential contaminants before the TCEA-IRMS stage, without degrading them to a product that could contribute to the Ag_3PO_4 formed at the end of the protocol.

Freshwater matrices, in comparison to marine matrices for which the original $\delta^{18}\text{O}_p$ protocol described in **Figure 3.1** was developed, typically contain higher concentrations of dissolved organic matter (DOM) compounds (Harvey *et al.*, 2015; Kubo *et al.*, 2015). Inefficient removal of DOM could significantly influence measured $\delta^{18}\text{O}_p$, because DOM can consist of up to 45% O by weight and has been shown to persist until the precipitation of Ag_3PO_4 (Ma *et al.*, 2001; Lécuyer, 2004; McLaughlin *et al.*, 2004; Zohar *et al.*, 2010). In addition, samples that contain a larger mass of DOM are also likely to have a larger mass of P_{org} . Consequently, there is a greater risk in freshwater, compared to marine, matrices of $\delta^{18}\text{O}_p$ being affected due to the generation of new P_i from P_{org} during a protocol. A more complete discussion of

typical P_{org} compounds found in freshwaters in the context of their potential influence on $\delta^{18}\text{O}_p$ can be found in **Section 3.2.1**.

In light of the considerations described above, this chapter aims to develop and evaluate a range of modifications to **Method 1** – the McLaughlin *et al.* (2004) protocol – in order to improve the protocol in the context of application to freshwater matrices. Particular consideration is given to the effect that P_{org} and DOM compounds within a sample could have on $\delta^{18}\text{O}_p$, including the potential for hydrolysis of P_{org} that leads to the production of contaminant P_i .

3.2 Potential P_{org} contamination during brucite precipitation

In each of the previously published protocols for the precipitation of Ag_3PO_4 from an aqueous matrix (**Figure 2.4**), an initial precipitate is formed from the bulk sample matrix that is subsequently re-dissolved. In the case of **Method 1** and the Goldhammer *et al.* (2011b) protocol, this precipitate is brucite (MgOH_2) which has been shown to co-precipitate P_i through a magnesium-induced co-precipitation (MagIC) (Karl and Tien, 1992). However, it is assumed in these protocols that no other P-containing molecules (particularly P_{org}) are co-precipitated alongside the brucite. In effect, the MagIC step in these previously published protocols is the primary route through which P_i is deemed to be isolated from sources of contaminant O within a sample matrix. Whilst this assumption may be valid within marine sample matrices, the greater concentration and range of possible sources of contaminant O within freshwater matrices means that direct translation of protocols between marine and freshwater matrices may not be feasible. Therefore, the first stage in the development of a revised protocol in this thesis was to evaluate the extent to which the MagIC step could isolate P_i from other constituents in a freshwater sample matrix.

Previous work by Thomson-Bulldis and Karl (1998), prior to any of the published protocols for $\delta^{18}\text{O}_p$ determination in aqueous samples, did begin to consider whether P-containing molecules other than P_i co-precipitated in the MagIC process in seawater and tap water matrices. This work primarily focused on modifying MagIC to more

accurately determine P_i concentrations within seawater samples. Standard procedures to measure P_i often involved measuring what is termed as soluble reactive phosphate (SRP) concentrations, in which P_i may only account for 30-75% of the measured P concentration, with the remaining concentration being a mixture of other dissolved inorganic and organic P compounds (Thomson-Bulldis and Karl, 1998). Thomson-Bulldis and Karl (1998) used radio-labelled $^{32}P_i$ to show that certain P_{org} molecules did co-precipitate with brucite and modified the original Karl and Tien (1992) method to alter to the ratio of NaOH volume to sample volume used within the MagIC method and added radio-labelled $^{32}P_i$ compounds to the system. This modification was performed in order to more accurately measure the concentration of the non-precipitated P pool in marine matrices. The research reported within this current chapter first aims to quantify the extent of P_{org} contamination of brucite that could potentially result from the co-precipitation of a range of non-labelled P_{org} compounds typically found within freshwater matrices, under the same MagIC reagent conditions as **Method 1**.

3.2.1 Selection of P_{org} compounds

In natural freshwaters, the main P_{org} compounds that are likely to be present can be grouped in five main classes: phosphonates, orthophosphate diesters, polyphosphates, pyrophosphates and orthophosphate monoesters (Worsfold *et al.*, 2008; Monbet *et al.*, 2009). Phosphonates are a class of compound with the general structure of $RPO(OR')(OR'')$ and are found in water industry processes, including water softening and through their use as anti-scalants and chelating agents (Nowack, 2003; Demadis *et al.*, 2007). Orthophosphate diesters – $PO_2(OR)(OR')$ – support the functionality of many biological molecules, for example as a key component of the backbone of DNA and RNA, and can form the majority of P_{org} inputs into agricultural soils (Turner and Haygarth, 2005). Polyphosphates are constructed of chains of $[PO_3]$ units that can form compounds by themselves, for example when chains are ended by hydroxyl groups, or form sections of larger molecules, such as adenosine-5'-triphosphate (ATP) a key compound in biological energy transfers (Kornberg, 1999). ATP acts as a coenzyme in many biological reactions and plays a key role in energy storage, respiration and metabolism within cells. One of the compounds that ATP interacts

with during the process of energy transfer within the cell is pyrophosphate. Pyrophosphate is the common name for the $P_2O_7^{4-}$ anion which can form salts, which allows it to act as a metal complexing agent (Manahan, 2004). Finally, orthophosphate monoesters are a general class of P_{org} compounds in the form of $RO-PO(OH)_2$ and, for example within freshwater sediments, are typically found in higher abundance than orthophosphate diesters (Jorgensen *et al.*, 2011). This class of P_{org} compound can also be separated into two major subclasses - labile orthophosphate monoesters and inositol hexakisphosphate (phytic acid salt). Labile orthophosphate monoesters, such as glucose-6-phosphate, can be highly biologically-active compounds and can undergo dephosphorylation reactions in the presence of enzymes to act as, or release, energy stores within the body. Phytic acid has a similar role within plant biology and can also play a role in DNA repair.

Compared to the volume of research that has focussed on P_i , much less is known about the concentration or the cycling of specific groups of P_{org} compounds in natural freshwater environments. A summary of research that has determined the relative concentrations of these P_{org} classes in natural samples is reported in **Table 3.1** (Espinosa *et al.*, 1999; Turner *et al.*, 2002; Toor *et al.*, 2003; Cade-Menun *et al.*, 2006; Koopmans *et al.*, 2007). However, there remains insufficient research that has fully speciated the P_{org} compounds found in freshwaters (Monbet *et al.*, 2009). This gap remains to be addressed by future research, particularly considering the potential role of P_{org} as a factor influencing $\delta^{18}O_p$ in freshwaters. However, for the purposes of the experiments reported in this chapter, the choice of appropriate P_{org} compounds was determined on the basis of the research reported in **Table 3.1**.

Table 3.1: Relative concentrations of P_{org} compounds in a range of freshwater matrices for which suitable speciation work has been undertaken

Study	Type of sample	Units	Phosphonates	Orthophosphate monoesters		Orthophosphate diesters	Polyphosphates	Pyrophosphates
				Labile	Inositol hexakis-phosphate			
Cade-Menun <i>et al.</i> (2006)	River inlet of PeeDee River	% DP	2.1	8.3		0.7	2.1	4.1
Espinosa <i>et al.</i> (1999)	Grassland soil leachates	%TP	1.2 ¹	4.1 ²	3.3	---	1.2 ³	---
Turner <i>et al.</i> (2002)	Water extracts of air-dried soils	%MUP	---	<0.1-4.8	12.3-33.5	9-23	---	---
Koopmans <i>et al.</i> (2007)	NaOH-EDTA extracted from unfertilised soils	%TP	<0.1	60.2		0.7		<0.1
Toor <i>et al.</i> (2003)	Soil leachate from treated soils	%TUP	---	23	20	15	---	---

As: ¹(±)1-aminoethylphosphonic acid, ²D-glucose-6-phosphate, ³Adenose-5'-triphosphate
 DP = dissolved P, TP = total P, MUP = molybdate-unreactive P and TUP = total unreactive P.

3.2.2 Analytical approach

In order to evaluate the potential extent of co-precipitation of P_{org} compounds with brucite, six P_{org} compounds were selected that were representative of the five major P_{org} classes identified above (**Table 3.2**). Tests were conducted to determine the extent to which each compound co-precipitated with brucite. Brucite was precipitated by the addition of 1M NaOH to n x 0.1M MgCl₂ solutions (n given in **Table 3.3**) made in MilliQ (18.2 MΩ) water and containing a known concentration (~4 mg P.L⁻¹) of each P_{org} compound in **Table 3.2** and one inorganic P_i source (KH₂PO₄). The resulting mixture was allowed to stand for 10 minutes before being separated by centrifugation at 3500 RCF for 10 minutes, with the supernatant decanted and stored at ≤4 °C until analysis. The supernatant from this precipitation was analysed for SRP and total P concentration using a Seal Analytical AQ2 discrete autoanalyser (LOD = 0.005 mg P.L⁻¹; matrix-matched calibration of 0 – 1 mg P.L⁻¹; analytical quality controls: SPEX CertiPrep WR1 (0.6 mg P.L⁻¹) and WR2 (0.3 mg P.L⁻¹)), following digestion of the samples in a sulfuric acid (H₂SO₄) and potassium persulfate (K₂S₂O₈) matrix for TP analyses.

Table 3.2: P_{org} compounds selected for analysis within this chapter

Class	Compound	Further information
Phosphonate	2-aminoethylphosphonic acid	
Labile orthophosphate monoester	D-glucose-6-phosphate	As a disodium salt hydrate
Inositol hexakisphosphate	Inositol hexakisphosphate (phytic acid salt)	As a sodium salt hydrate; from rice
Orthophosphate diester	DNA	As a sodium salt; from herring testes
Polyphosphate	Adenosine-5'-triphosphate (ATP)	As a disodium salt hydrate; microbial source
Pyrophosphate	Sodium pyrophosphate decahydrate	

The extent of co-precipitation for each P_{org} compound was calculated as a percentage, using the difference between the TP concentration in the supernatant following brucite precipitation and the initial TP concentration in the original solutions (**Equation 9**).

$$Co - precipitation\ extent\ (\%) = \frac{100[Supernatant\ TP]}{[Initial\ TP]} \quad (9)$$

3.2.3 Results and discussion

Significant co-precipitation of all P_{org} compounds with brucite was observed in the experiments described above, ranging from 34.5% (2-aminoethylphosphonic acid) to 97.5% (sodium pyrophosphate decahydrate) of the original spiked P_{org} concentration (**Figure 3.2**). From **Table 3.3** it can be seen that the extent of co-precipitation for those compounds which were also analysed in the Thomson-Bulldis and Karl (1998) study is broadly similar in both MilliQ and seawater matrices. However, substantially greater co-precipitation of 2-aminoethylphosphonic acid with brucite was observed in the research reported in this chapter for a MilliQ matrix than was observed previously for a seawater matrix. These observations clearly indicate that the use of MagIC as the initial step in protocols for the precipitation of Ag₃PO₄ does not ensure that P_i is the only species removed from solution to be carried forward to later stages of a protocol. In particular, the data reported in **Figure 3.2** and **Table 3.3** demonstrate that a wide range of P_{org} compounds may co-precipitate with brucite. In freshwater matrices this is of particular concern as absolute concentrations of P_{org} may be considerably greater than in other matrices (Smith *et al.*, 1999).

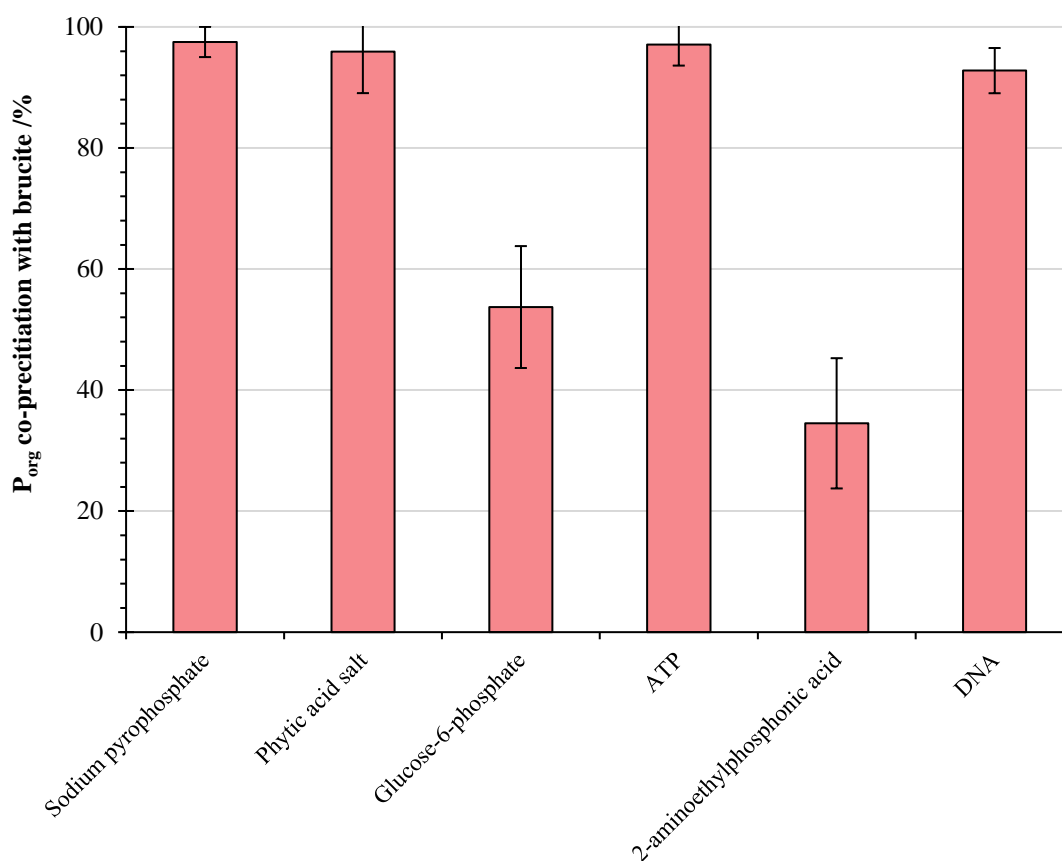


Figure 3.2: Percentage of spiked P_{org} co-precipitated with brucite. Error bars based on $\pm 1\sigma$ (n is given in **Table 3.3**).

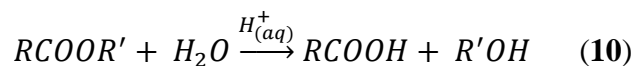
Table 3.3: Extent of P_{org} co-precipitation with brucite in a MilliQ water matrix and comparison with co-precipitation extents reported by Thomson-Bulldis and Karl (1998) when precipitated from a seawater matrix.

Compound	Measured co-precipitation extent in MilliQ matrix (3sf) $\pm 1\sigma$ /%	n	Co-precipitation extent in seawater (n=3) /% (Thomson-Bulldis and Karl, 1998)
P _i	97.0 \pm 0.6	8	99.9 \pm 0.9
2-aminoethylphosphonic acid	34.5 \pm 10.8	18	26.9 \pm 1.7
Glucose-6-phosphate	53.7 \pm 10.1	18	n.d.
Phytic acid salt	95.9 \pm 6.8	32	95.7 \pm 5.7 [†]
DNA	92.8 \pm 3.7	3	n.d.
Adenosine-5'-triphosphate (ATP)	97.1 \pm 3.5	30	97.1 \pm 1.3
Sodium pyrophosphate decahydrate	97.5 \pm 2.5	17	99.5 \pm 1.2 [‡]

[†]named phytic acid; [‡] named pyrophosphate; n.d. not determined

3.3 Brucite-P_{org} susceptibility toward acid hydrolysis

The potential importance of the data reported in **Figure 3.2** and **Table 3.3** is that previously published protocols for $\delta^{18}\text{O}_p$ analysis that include an initial step of brucite precipitation, also include a subsequent step that involves the re-dissolution of the brucite pellet in a strongly acidic matrix. However, many P_{org} compounds can undergo acid hydrolysis, yielding P_i that is derived from the original P_{org} compound. Therefore, co-precipitation of P_{org} with brucite has the potential to generate P_i within an acidic matrix in later stages of any extraction protocol. Acid hydrolysis involves the breaking of a chemical bond through a nucleophilic substitution of a water molecule, catalysed by surrounding aqueous protons, i.e. **Equation 10** (Bender, 1960; Cox Jr and Ramsay, 1964).



In the case of P_{org} compounds, this reaction is of particular importance, due to the formation of a free P_i molecule. The formation of free P_i from P_{org} could alter the final $\delta^{18}\text{O}_p$ determined for a sample through two mechanisms. Firstly, a proportion of the oxygen atoms included in the new P_i molecule would be derived from the extracellular water molecules. This could be associated with a kinetic fractionation, in which ^{16}O atoms are preferentially incorporated into the newly formed P_i, due to a faster reaction rate during hydrolysis compared to ^{18}O atoms. The second mechanism is an inheritance effect, in which the $\delta^{18}\text{O}_p$ of the newly formed P_i will partially reflect the $\delta^{18}\text{O}$ ratio of the P moiety in the original P_{org} compound, because some oxygen atoms within the newly generated P_i will be inherited from the parent material, without any exchange with water-O (McLaughlin *et al.*, 2006d). The relative importance of kinetic fractionation *versus* inheritance isotope effects depends on the P_{org} compound in question and its hydrolysis pathway (**Sections 2.2.3**). Both effects are likely to generate P_i that differs in terms of $\delta^{18}\text{O}_p$ from the “true” $\delta^{18}\text{O}_p$ of P_i that was originally present in a sample (Liang and Blake, 2006a; McLaughlin *et al.*, 2006d). Therefore, the material in this section reports the outcomes of experiments that were designed to test whether the acidic solution used to re-dissolve brucite can be optimised, specifically in order to reduce any potential hydrolysis of P_{org} that is co-precipitated with brucite from the original sample matrix.

3.3.1 Analytical methods

A range of analytical grade acids of different molarities and strengths were selected and 3 x 100 mL 0.4 mg P.L⁻¹ MgCl₂ solutions were produced for each P_{org} and acid system combination. The volumes of each acid to be used were determined experimentally by the minimum volume required to consistently result in the full dissolution of the brucite pellet formed from a 100 mL 0.4 mg P.L⁻¹ MgCl₂ solution. This resulted in the following final acid systems being selected:

- 2M hydrochloric acid (HCl, 2 mL);
- 0.1M nitric acid (HNO₃, 3 mL);
- concentrated acetic acid (c.AA, 0.5 mL and 4 mL);
- the standard **Method 1** (McLaughlin *et al.* (2004)) conditions (1 mL c.AA and 1 mL 10M HNO₃);
- concentrated aqua regia (0.2 mL). 0.4 mL was required to dissolve the brucite pellet, however this concentration adversely affected the formation of the phosphomolybdate compound for the colorimetric analysis of SRP concentration, so the mass of brucite was reduced two-fold to enable 0.2 mL of aqua regia to be used without changing the relative concentrations of reagents. Aqua regia was freshly made prior to analysis as a 3:1 mixture of c.HCl to c.HNO₃.

Within the **Method 1** protocol, it is possible that a “standing time” will exist between the addition of the acid and the subsequent pH adjustment (steps 2a and 3a in **Figure 3.1**). Therefore, a kinetic study was also conducted on the ATP and phytic acid salt compounds as exemplars, using the same acid systems described above, to determine whether the length of time that a P_i solution is at a low pH has an effect on the extent of P_{org} hydrolysis. These exemplar compounds were chosen because they had exhibited the greatest extent of acid hydrolysis in the preliminary stages of the experiment reported in **Section 3.3.2**, meaning that differences between standing times were more likely to be identified. Standing time periods from 5 to 60 mins between the dissolution of brucite in acid and the addition of molybdenum blue method reagents for SRP determination were evaluated. All solutions were shaken after the addition of acid to dissolve the brucite pellet but were kept still between the

dissolution of brucite and the addition of the colour reagents. However, to determine whether agitation could also affect the extent of hydrolysis, three additional replicates were continuously shaken for the samples that had a standing time of 15 minutes. Soluble reactive P concentrations in the re-dissolved acidic matrices were determined using a modified matrix-matched Murphy and Riley (1962) molybdenum blue method. Thirty mins after the reagents were added, the solutions were analysed colourimetrically using a Jenway UV-vis 6300 spectrophotometer (882 nm, LOD = 0.025 P.L⁻¹; matrix-matched calibration of 0-1 mg P.L⁻¹; analytical quality controls: SPEX CertiPrep WR1 (0.6 mg P.L⁻¹) and WR2 (0.3 mg P.L⁻¹)).

3.3.2 Results and discussion

Figure 3.3 illustrates clearly that individual P_{org} compounds differ in terms of their susceptibility to acid hydrolysis and, therefore, P_i production following the MagIC and acid dissolution stages of the protocol for Ag₃PO₄ precipitation. For example, when a brucite precipitate was dissolved in c.AA, up to 17% and 5% of the mass of TP that co-precipitated with brucite underwent hydrolysis to yield SRP (assumed to be P_i) for the ATP and pyrophosphate compounds respectively. In contrast, when a 2M HCl acid system was used to dissolve the brucite, P_i concentrations were below the limit of detection for 2-aminoethylphosphonic acid and sodium pyrophosphate and the ATP conversion was reduced to 11%. A two factor analysis of variance (ANOVA) test was undertaken, establishing that the extent of SRP production following co-precipitation with brucite varied significantly with both the P_{org} compound and the acid system used. There was also a significant interaction between the two factors (**Table 3.4**).

Table 3.4: Two factor ANOVA analysis output for the extent of TP hydrolysis after co-precipitation with, and dissolution of, brucite across six different acid systems.

	SS (3sf)	df	MS (3sf)	F (3sf)	p-value (3sf, α = 0.05)	Significant?
P _{org} compound	1310	4	328	3630	6.85 x 10 ⁻⁶⁷	yes
Acid system	76.0	5	15.2	168	2.12 x 10 ⁻³²	yes
Inter	132	20	6.58	72.6	7.96 x 10 ⁻³³	yes
Within	5.07	56	0.0905			
Total	1550	85	18.3			

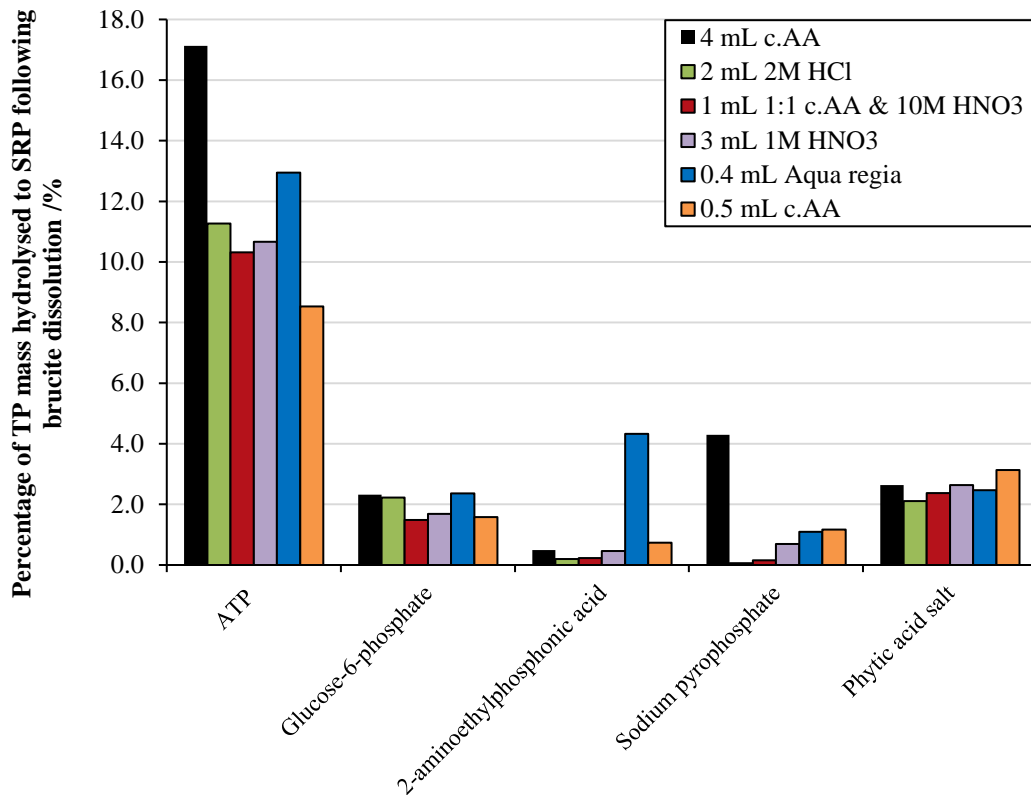


Figure 3.3: Mean percentage of total starting P from five individual P_{org} compounds that formed SRP following brucite precipitation and acidic dissolution across a range of acid systems ($n \geq 3$ for each bar).

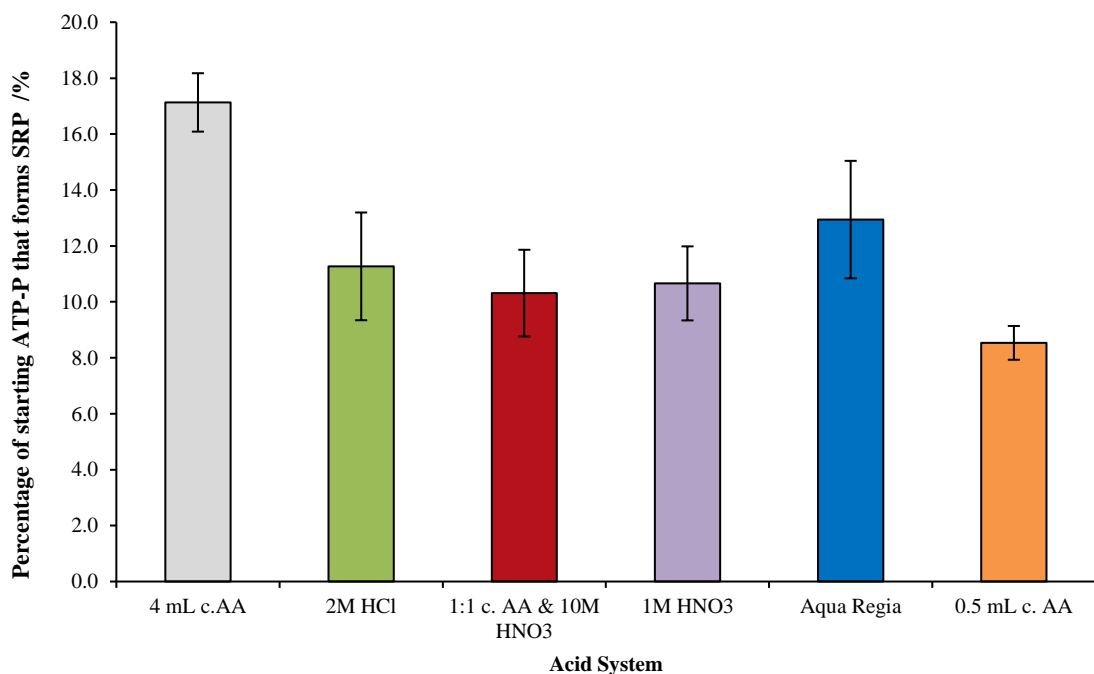


Figure 3.4: A more detailed expansion for the extent of ATP hydrolysis after co-precipitation with, and dissolution of, brucite using minimum volumes (for complete dissolution) of five different acid systems, and one system when an 8-fold volume excess of acid was used (4 mL c.AA). Mean values given, error bars show $\pm 1\sigma$ ($n = 3$ for each acid system).

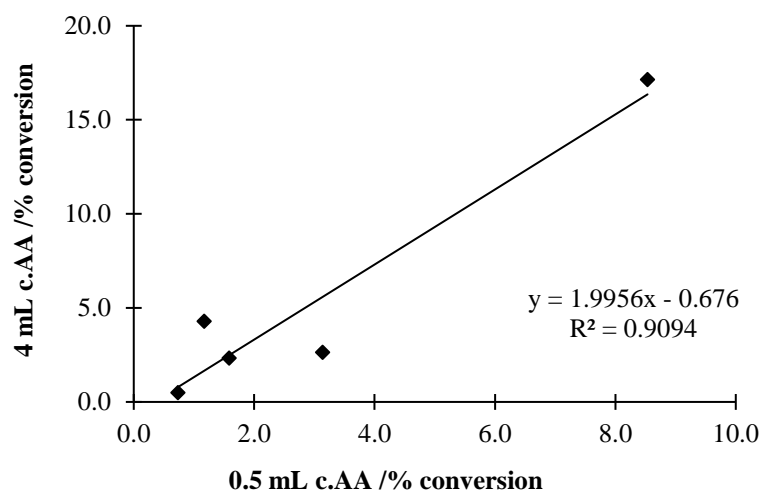


Figure 3.5: Comparison of mean percentage conversions of P in P_{org} compounds to form SRP, using the minimum volume of c.AA (x-axis) and an 8-fold excess volume (y-axis). Individual data points represent individual P_{org} compounds in **Table 3.2**.

A more focussed study dealing only with ATP, chosen as the P_{org} compound most susceptible to acid hydrolysis based on **Figure 3.3**, was also undertaken to further evaluate the effect on P_{org} hydrolysis of the acid system used for brucite re-dissolution. **Figure 3.4** demonstrates that the conversion of P_{org} to P_1 can be reduced when using concentrated acetic acid to levels similar to, if not lower than, those following the use of 1:1 c.AA and 10M HNO_3 (the acid system in the **Method 1** protocol), but only assuming that the minimum volume of concentrated acetic acid required to dissolve the brucite pellet is used. These results highlight the importance of using the minimum acid volume possible for complete brucite dissolution, in order to minimise the risk of acid hydrolysis of any co-precipitated P_{org} . This is further highlighted when considering the extent of P_{org} hydrolysis within both acid systems (minimum volumes of c.AA and 8-fold excess of c.AA) across all five P_{org} compounds used in these experiments (**Figure 3.5**).

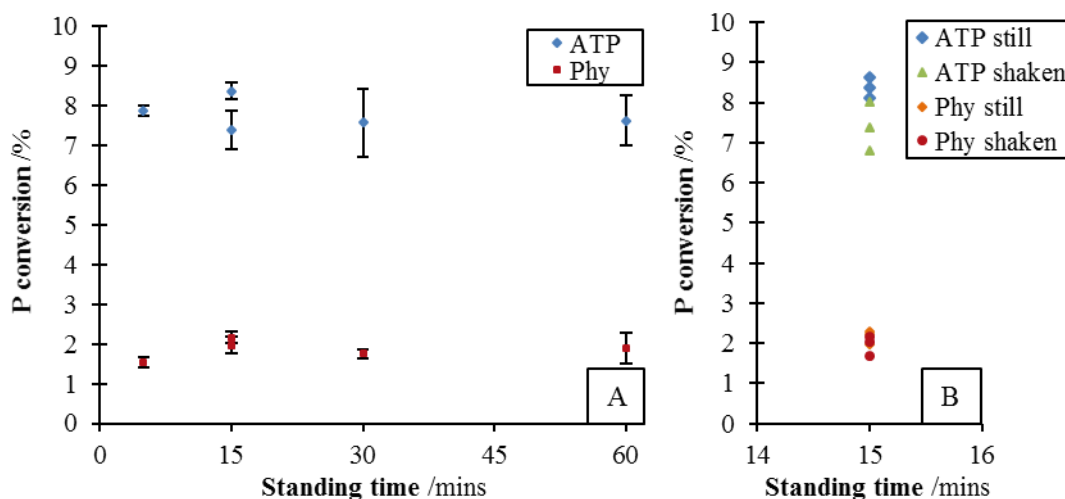


Figure 3.6: a) Results of the kinetic study focussed on ATP and phytic acid salt hydrolysis using the acid system used in **Method 1** - 1 mL c.AA and 1 mL 10M HNO₃. The two data points at t = 15 mins represent the two movement conditions (i.e. the mean points of the data displayed in **3.6b**). Mean values given, error bars show $\pm 1\sigma$ (n = 3). b) The full data set from 15 mins to illustrate the difference between 15 mins of minimal movement (still) and 15 mins of constant movement (shaken).

As shown in **Figure 3.6**, there was no significant difference in the degree of P_{org} hydrolysis over time (5-60 mins) for either ATP or the phytic acid salt. As the datasets were normally distributed, single factor ANOVA tests were performed on the dataset for each P_{org} compound resulting in ATP: $F(3, 8) = 0.891$, $p = 0.486$, and phytic acid: $F(3, 8) = 2.65$, $p = 0.120$. However, in the case of ATP there was a significant increase in hydrolysis between a sample that was constantly shaken between the addition of acid to re-dissolve the brucite pellet and the addition of reagents for SRP determination and a sample that remained still: two sample t-test, $t(4) = 2.57$, $p = 0.0308$. This was not observed in the case of phytic acid: two sample t-test, $t(4) = 1.09$, $p = 0.168$. Therefore, although the time delay between the addition of acid to re-dissolve brucite and the subsequent pH raising step (for example the addition of potassium acetate (3a in **Figure 3.1**)), should be minimised for efficiency, there appears to be no significant impact on the extent of contaminant P_{org} hydrolysis depending on how long the sample stands in an acid matrix before neutralisation (up to a 60 minute limit based on the data reported here). However, during any standing time before neutralisation, movement of the samples should be minimised to reduce the extent of P_{org} hydrolysis.

The findings reported in this section have potentially significant implications for analysis of $\delta^{18}\text{O}_p$, because any fresh P_i produced from acid hydrolysis will potentially

be subjected to inheritance effects and kinetic isotope fractionations, altering the bulk $\delta^{18}\text{O}_p$ measured within a sample. Therefore, if the original $\delta^{18}\text{O}_p$ of P_i is to be retained, P_i must be effectively isolated from a matrix containing potential sources of contaminant oxygen (whether organic C, competing oxyanions, or P_{org} compounds). In addition, this isolation from P_{org} should ideally be achieved prior to introduction of conditions that could hydrolyse P_{org} compounds that persist within a solution being carried forward to Ag_3PO_4 precipitation. In addition, consideration should be given to how hydrolysis of P_{org} , and therefore generation of new P_i , can be minimised prior to precipitation of Ag_3PO_4 .

3.4 Revisions to the Method 1 protocol to minimise DOM-contamination of Ag_3PO_4

Dissolved organic matter (DOM), particularly in the form of P_{org} compounds, has been shown above to potentially contaminate a brucite pellet and to undergo acid hydrolysis within the original **Method 1** protocol for precipitation of Ag_3PO_4 and analysis of $\delta^{18}\text{O}_p$. Consequently, within DOM-rich freshwater matrices, the original McLaughlin *et al.* (2004) methodology does not appear to be sufficiently robust to ensure the purity of an Ag_3PO_4 precipitate and the accuracy of $\delta^{18}\text{O}_p$ determined from this precipitate. In order to evaluate the utility of $\delta^{18}\text{O}_p$ within freshwaters, a revised methodology appears to be required. Therefore, significant efforts have been made to develop and evaluate initial steps in an Ag_3PO_4 precipitation protocol that are able to minimise the risk that contaminant O from DOM is incorporated into Ag_3PO_4 precipitated from freshwater matrices. This work is described in further detail below.

Previous work within the research group at Lancaster University has introduced a resin removal step prior to step 1a in **Method 1 (Figure 3.1)** – see **Method 2 (Figure 3.7)** and Goody *et al.* (2016). The resin was Supelite™ DAX-8, a solid-phase organic exchange/absorbent resin, which captures strongly hydrophobic organic matter attributed to humic and fulvic acids within DOM (Carroll *et al.*, 2000). The eluate from this resin is subsequently loaded onto a Cl^- -form anion exchange column, which sorbs P_i from solution whilst allowing hydrophilic compounds to pass through

the column to waste, providing further isolation of P_i from DOM in a sample. Finally, P_i that is sorbed to the Cl^- -form anion exchange column is further isolated from competing oxyanions and any DOM that have also been sorbed to the column through chromatographic separation. Sorbed oxyanions other than P_i and sorbed DOM will either be eluted with the KCl eluent, although predominantly in eluent fractions other than those containing P_i , or remain bound to the anion exchange resin. Hydrogen peroxide treatment of the final Ag_3PO_4 precipitate was included in this revised protocol to ensure that any organic matter remaining within the Ag_3PO_4 precipitate, despite these sample preparation stages, was removed *via* oxidation, a step which has also been included in protocols for $\delta^{18}O_p$ analysis in soils where contamination of Ag_3PO_4 with additional sources of O is of particular concern (Tamburini *et al.*, 2010; Zohar *et al.*, 2010). Further to the work reported in Gooddy *et al.* (2016), this thesis has more thoroughly tested and evaluated the use of the DAX-8 resin to remove DOM in freshwater samples and the Cl^- -form anion exchange resin to isolate P_i .

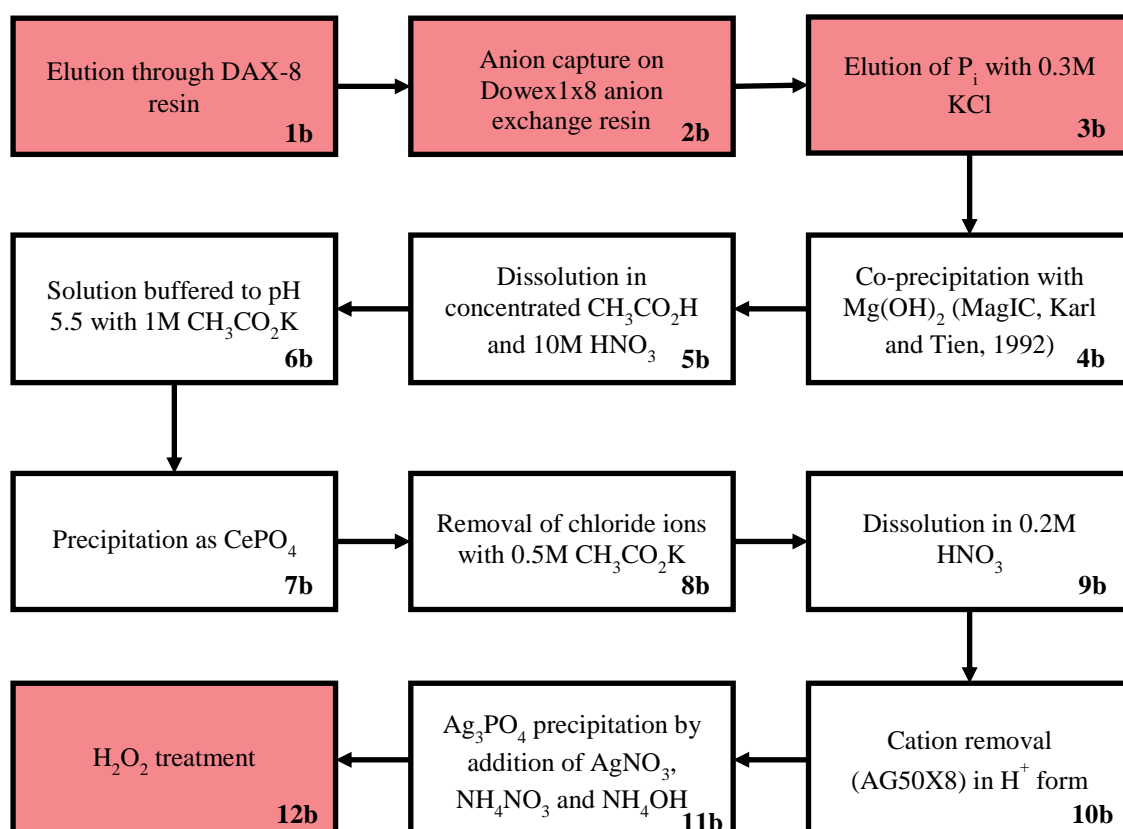


Figure 3.7: Method 2 – Modifications to the Method 1 (McLaughlin *et al.* (2004)) protocol reported in Gooddy *et al.* (2016); including DOM removal steps (1b and 12b) and steps to further isolate P_i from potential sources of contamination (2b-3b).

However, the **Method 2** protocol (**Figure 3.7**) potentially suffers from a variable sample volume and matrix composition being loaded onto the DAX-8 and anion exchange resins in steps 1-3b. This is a particular challenge in freshwaters where the P_i concentration can vary significantly across samples, meaning that the sample volume to be loaded onto the resins in order to generate sufficient Ag_3PO_4 also varies significantly, as does the composition of the sample matrix. In an attempt to address these potential challenges, the research reported within this thesis developed and evaluated further modifications to the original **Method 1** protocol for the precipitation of Ag_3PO_4 – see **Method 3** (**Figures 3.8** and **3.12**). In this protocol, a standardised matrix to be loaded onto subsequent DOM-removal and anion exchange resins is provided by the introduction of an initial MagIC precipitation. The resulting brucite precipitate is re-dissolved in a standard acidic matrix which contains P_i , Mg^{2+} ions, and any other compounds that have co-precipitated within the MagIC step. This standardised matrix is subsequently loaded onto an H^+ -form cation exchange resin, to remove magnesium ions (to prevent interference with the later $CePO_4$ precipitation stages in the protocol), and subsequent DOM-removal and anion exchange resins. Further, the protocol introduces a second organic exchange resin, in addition to DAX-8, namely ISOLUTE® ENV+. This resin was chosen to target polar analytes (Alonso *et al.*, 1999; Biotage, 2004), thus in combination with the Supelite™ DAX-8 resin, both hydrophilic and hydrophobic organic compounds were hypothesised to be captured and removed from a sample matrix.

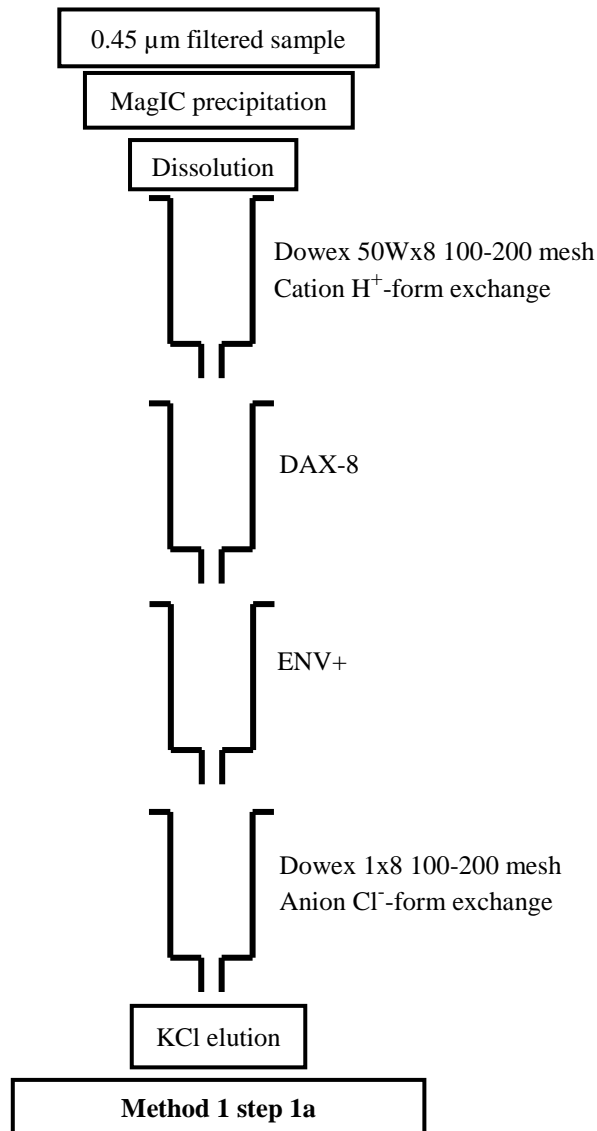


Figure 3.8: Method 3 - New sample preparation stages for Ag_3PO_4 precipitation protocol for freshwater samples developed and evaluated in this thesis.

3.4.1 Standardisation of matrix for loading onto an anion exchange resin

Anion exchange resins are designed to capture and exchange sample anions with one anionic species present on the solid-phase resin (Amer *et al.*, 1955); in the case of the research reported in this thesis, Cl^- ions were released to solution based on the use of Dowex 1x8 chloride-form resin. However, significant variations in the concentration of competing anions present within a sample matrix (e.g. chloride, nitrate, sulfate and phosphate anions) could alter the efficiency of an anion exchange resin with respect to P_i retention. Standardisation of the matrix loaded onto an anion exchange resin column should ensure that the retention efficiency and the subsequent elution profiles for P_i do not vary significantly between individual samples. Thus, two aspects that

could potentially interfere with the efficient P_i loading of the anion exchange resin were tested. Firstly, the extent of co-precipitation of nitrate and sulfate ions associated with the MagIC step. This work was undertaken to determine the probability that competing anions would co-precipitate alongside P_i during brucite precipitation, which may affect the retention efficiency of the anion exchange resin with respect to P_i . For example, if a substantial proportion of the nitrate present within a sample was shown to co-precipitate with brucite in the MagIC step, then it may be the case that the retention efficiency of the anion exchange resin for P_i would be diminished in a sample with high nitrate concentrations. The second set of tests considered how the conditions associated with brucite dissolution may affect the subsequent loading of an anion exchange resin. In particular, the acidic conditions required for brucite dissolution could impair the ability of a resin to sorb P_i , due to the potential overwhelming competition between P_i and the acid's counteranions which could create a self-elution effect and prevent P_i from binding to the resin.

3.4.1.1 Co-precipitation of competing anions with the MagIC step

In **Section 3.2**, the assumption that P_{org} compounds did not co-precipitate with brucite as part of the MagIC step was tested and found to be false. A similar test was conducted to determine the extent to which the competing anions nitrate (NO_3^-) and sulfate (SO_4^{2-}) may also co-precipitate with brucite. These anions were chosen as they are two common anions in freshwater matrices and are likely to be the most important anions to be evaluated with respect to co-precipitation with brucite. Concentrations for these anions vary significantly in freshwaters. Therefore, tests were conducted with 20 mg S- $SO_4.L^{-1}$ and 9 mg N- $NO_3.L^{-1}$ to represent typical concentrations found in UK river waters (Sutcliffe, 1998; Environment Agency, 2009). Brucite was precipitated by the addition of 1M NaOH to 0.1M $MgCl_2$ solutions, 3 x 100 mL of 20 mg S- $SO_4.L^{-1}$ and 3 x 100 mL of 9 mg N- $NO_3.L^{-1}$. The solutions were mixed occasionally to precipitate brucite over 10 mins and the resulting mixture was centrifuged at 3500 RCF for 10 mins. The supernatant was decanted and stored at ≤ 4 °C until analysis. Concentrations of N- NO_3^- were determined using a hydrazine/sulfanilamide method on a Seal Analytical AQ2 discrete autoanalyser (LOD = 0.40 mg N.L⁻¹; matrix-matched calibration of 0-20 mg N.L⁻¹; analytical quality control: SPEX CertiPrep WR1 (4 mg N.L⁻¹) and WR2 (2 mg N.L⁻¹)) and by ion chromatography on a Dionex ICS2500 (LOD = 0.02 mg N.L⁻¹; calibrated 0-10 mg N.L⁻¹; analytical quality controls:

SPEX CertiPrep WR1 (4 mg N.L⁻¹) and WR2 (2 mg N.L⁻¹). Concentrations of S-SO₄²⁻ were determined through ion chromatography on a Dionex ICS2500 (LOD = 0.07 mg S.L⁻¹; calibrated 0-25 mg S.L⁻¹; analytical quality control: SPEX CertiPrep WR1 (10 mg S.L⁻¹) and WR2 (5 mg S.L⁻¹)).

It was found that 5.4% N-NO₃ and 46.0% S-SO₄ of the original mass in solution co-precipitated with the brucite pellet. The maximum loading capacity of the anion exchange resin used in this thesis was 1.2 meq.mL⁻¹. Therefore, the addition of an initial MagIC precipitation is able to significantly reduce, although not completely exclude, the mass and concentration of SO₄²⁻ and NO₃⁻ that reaches the anion exchange resin. Thus, the introduction of this initial brucite precipitation step will significantly reduce the competition between P_i and additional anions, increasing the retention efficiency of the anion exchange resin with respect to P_i.

3.4.1.2 Dissolution of initial brucite pellet

As discussed in **Section 3.3.1** and **Figure 3.4**, a number of different acid systems could be used to re-dissolve a brucite pellet formed during the MagIC precipitation. Despite there not being an acid system that prevented all acid hydrolysis of P_{org}, the HCl- and HNO₃-based systems, such as that included in **Method 1** involving concentrated acetic acid (CH₃CO₂H) and 10M HNO₃ combination, are unsuitable for use before loading the resulting solution onto an anion exchange resin. This is due to the concentration of competing anions that would be introduced in such acid systems (i.e. NO₃⁻ in the case of 10M HNO₃), which would potentially exceed the exchange capacity of the anion exchange resin. Therefore, concentrated CH₃CO₂H was selected in order to re-dissolve the brucite pellet created in the initial MagIC step for **Method 3**. However, using an excess CH₃CO₂H has been shown to increase the hydrolysis of P_{org} compounds that are co-precipitated with brucite and the formation of new P_i molecules (see **Section 3.3**). Therefore, the minimum volume of acetic acid required to fully dissolve the brucite pellet was always used at this stage of the **Method 3** protocol.

3.4.2 Dissolved organic matter removal

Dissolved organic matter (DOM) removal is an essential stage in the adaptation of protocols for $\delta^{18}\text{O}_p$ analysis to freshwater samples, due to the organic-rich nature of many of these sample matrices. A combination of Supelite™ DAX-8 (DAX-8) and ISOLUTE® ENV+ (ENV+) were trialled separately as part of the development of the revised sample preparation methodology for Ag_3PO_4 precipitation. These trials focussed initially on the effectiveness of each resin with respect to the removal of DOM (measured as DOC) from representative freshwater matrices.

Test A: Two freshwater samples were collected from two stream sites within an upland peatland catchment in the Forest of Bowland, UK and filtered using $0.45\ \mu\text{m}$ cellulose nitrate membranes. Subsequently, $0.9521\ \text{g}\ \text{MgCl}_2 \cdot 6\text{H}_2\text{O}$ was added to $3 \times 100\ \text{mL}$ of each sample. $2.5\ \text{mL}\ 1\text{M}\ \text{NaOH}$ was added to each beaker and the solutions were mixed occasionally to precipitate brucite over 10 mins and the resulting mixture was centrifuged at 3500 RCF for 10 mins. The supernatant was decanted and stored at $\leq 4\ ^\circ\text{C}$ until DOC analysis was performed to determine the extent to which DOC was co-precipitated with brucite in the MagIC precipitation. DOC concentrations for all three tests were measured on a Thermalox TOC/TN analyser (LOD: $1.3\ \text{mg}\ \text{C.L}^{-1}$; calibration $0\text{-}50\ \text{mg}\ \text{C.L}^{-1}$; analytical quality control: EAG REF162 ($0.5, 5$ and $15\ \text{mg}\ \text{C.L}^{-1}$)) following the acidification and sparging of samples with $2\text{M}\ \text{HCl}$.

Test A was used to quantify how much DOC would co-precipitate with brucite when formed within a natural freshwater sample. The original DOC concentrations within the two stream samples were 2.47 and $2.06\ \text{mg}\ \text{C.L}^{-1}$ respectively. The mean concentrations found within the supernatant following the MagIC precipitation were 1.27 ($\sigma = 0.08$) and 1.48 ($\sigma = 0.24$) $\text{mg}\ \text{C.L}^{-1}$, corresponding to an uptake by the brucite precipitate of 54.6% ($\sigma = 2.7$) and 32.0% ($\sigma = 10.9$) of the original DOC concentration across the two sample matrices. These data emphasise that substantial co-precipitation of DOC with brucite occurs. Therefore, a potentially significant mass of contaminant-O associated with DOC compounds is taken forward to subsequent stages of an Ag_3PO_4 precipitation protocol, alongside the potential for a significant mass of P_{org} compounds which could subsequently undergo acid hydrolysis (see

Section 3.3). These data indicate that simple brucite precipitation, as used within **Method 1** (McLaughlin *et al.*, 2004), is unlikely to effectively minimise contaminant sources of O within a sample derived from a freshwater matrix prior to $\delta^{18}\text{O}_p$ analysis.

Test B: 0.4 mg P and 5%_{v/v} CH₃CO₂H solutions were made with KH₂PO₄ using the 0.45 μm -filtered sample matrix from one of the stream sites in Test A described above. The amended aqueous solutions were loaded through a combination of DAX-8 and/or ENV+ resins at 11 mL.min⁻¹ to determine how the two organic exchange resins performed, given the concentration and mass of acetic acid used to re-dissolve the brucite precipitate formed during step 1c in **Method 3 (Figure 3.12)**. Preparation is required prior to use for the DAX-8 and ENV+ resins to ensure maximum resin functionality, using methanol and MilliQ rinses. The preparation protocols for both resins were determined using DOC analysis of the waste washings and deemed to be successful when the DOC fell below the LOD. Throughout this thesis, the preparation protocol used involved 1 x 1 hr CH₃OH batch shake followed by 3 x 1 hr MilliQ water shakes for DAX-8, whilst for ENV+ 1 x 1 hr CH₃OH contact, 1 x 30 mins MilliQ water contact followed by 2 MilliQ water rinses was used. DOC was measured as described above and SRP as described in **Section 3.2.2**.

Table 3.5 shows that a variable, but generally small, proportion of the CH₃CO₂H was retained on the organic resins and that, unexpectedly, in some cases a substantial proportion of P_i was retained during a stage which aims to selectively remove DOM from a sample matrix. It should be noted that the majority of DOC measured in these experiments was associated with the added P_i-free CH₃CO₂H used to re-dissolve the brucite precipitate. It may still be possible that a significant proportion of natural DOM compounds (containing the bulk P_{org} pool) is retained on the DAX-8 or ENV+ resins due to the two different targets (hydrophilic/hydrophobic) for each resin (see test C below). The test B experiment described here was conducted with 5%_{v/v} CH₃CO₂H. Further work reported in **Section 3.4.4** established that it was not possible to run this concentration of CH₃CO₂H when loading a sample onto the anion exchange resin, and therefore this concentration was reduced to 0.6%_{v/v} for samples that were run using **Method 3** in **Chapters 4** and **5**. However, the data reported in **Table 3.5** do highlight the potential for retention of P_i on organic exchange resins. This retention has the potential to impart an isotope effect on the bulk P_i, if one isotope is

preferentially retained on the resins. No evidence has been found to support such an isotope effect, however further work is required to fully explore this issue. In addition, P_i retention on resins could be an issue if P_i concentrations are very low in a sample, meaning that an insufficient mass of P_i is ultimately eluted from the anion exchange resin and carried forward to precipitate Ag_3PO_4 .

Table 3.5: DOC and SRP analysis of eluates through ENV+ and DAX-8 resins following Test B

DAX-8 /mL	ENV+ /cartridge	Sample volume /mL	Mass of DOC loaded /mg	DOC% retained	P_i % captured
10	-	100	18700	24	16
20	-	100	17300	16	29
40	-	100	18800	42	45
-	1	50	9060	32	27
-	1	100	18100	16	18
-	1	250	50600	16	14
20	1	100	18500	37	35
20	1	250	45900	18	13

Test C: A river water sample was collected from the same location described in test A above and filtered at $0.45 \mu m$. The filtered water was pumped at $11 mL \cdot min^{-1}$ through a combination of the DAX-8 and ENV+ resins, in order to establish the optimum resin volume required to efficiently remove DOM compounds from the freshwater matrix. The original DOC concentration within the river water from this second sample collection was $36.2 \text{ mg C} \cdot L^{-1}$ (**Table 3.6**). It can be seen that whilst increasing the number of ENV+ cartridges in series does not have a substantial effect on DOC removal, the larger the ratio of sample volume to DAX-8 resin, the greater the concentration of DOC that remained in the eluate. Although the 1:5 ratio of DAX-8 to sample was the most efficient DOC removal ratio in **Table 3.6**, it can be seen in **Table 3.5** that 29% of P_i was retained on the DAX-8 resin at this ratio, which could cause a significant alteration in the $\delta^{18}O_p$ of the P_i pool remaining in solution. Therefore, a volume of 10 mL of DAX-8 was chosen for the one litre tests described in **Section 3.5** below.

Table 3.6: DOC analysis of eluates from a natural river matrix with initial concentration of 36.2 mg C.L⁻¹

Resin	Amount	Volume of river water /mL	Average [eluate DOC] /mg C.L ⁻¹	DOC % retained	DAX-8:River water
ENV+	1 cartridge	1000	21.0	42	-
ENV+	2 cartridges	1000	28.1	22	-
ENV+	3 cartridges	1000	22.4	38	-
DAX-8	20 mL	100	13.7	62	1:5
DAX-8	20 mL	200	17.7	51	1:10
DAX-8	10 mL	250	21.0	42	1:25
DAX-8	30 mL	100	10.7	70	1:33.3
DAX-8	10 mL	500	24.6	32	1:50

3.4.3 Anion exchange resin elution profiles

Step 6c of **Method 3** (**Figure 3.12**) involves loading a sample matrix onto a Cl⁻-form anion exchange resin. Following loading, it is important to ensure the elution profile separates competing anions (e.g. P_i, NO₃⁻ and SO₄²⁻) effectively and consistently, in order to isolate P_i without major loss of P_i or the need to determine P_i mass in each sample run individually. The elution profile in **Method 2** is based on a 50 mL volume of anion exchange resin per sample, with 0.3M KCl as the eluent. However, for **Method 3** a removal of significant quantities of competing anions prior to loading of the anion exchange resin will occur through the initial MagIC precipitation described in **Section 3.4.1**. Therefore, based on the 1.2 meq.mL⁻¹ binding exchange capacity of the Cl⁻-form anion exchange resin, 12.5 mL of resin was deemed sufficient to capture 0.4 mg P-P_i, with a sufficiently large excess of anion exchange capacity associated with this volume of resin to prevent competition with other competing anions, which could reduce P_i retention efficiency during loading. Due to such a major change in resin volume compared to that used in **Method 2**, new elution profiles for P_i removal from anion exchange resins were developed in the research reported in this thesis.

Six x 100 mL MilliQ solutions containing 0.4 mg P, 25.8 mg NH₄NO₃, 13.7 mg (NH₄)₂SO₄ and 5 mL CH₃CO₂H were loaded onto 12.5 mL of Cl⁻-form anion exchange resin at 5 mL.min⁻¹. Three columns were eluted with 0.25M KCl at 1 mL.min⁻¹ and the remaining three columns with 0.3M KCl. Eluent fractions were collected every minute for 110 mins and analysed for SRP, NO₃⁻ and SO₄²⁻. SRP

concentrations were measured using the techniques described in **Section 3.2.2**, and N-NO₃⁻ and S-SO₄²⁻ concentrations were determined as described in **Section 3.4.1.1**.

As reported in **Figures 3.9** and **3.10**, subtle differences between elution profiles were observed when using 0.3 and 0.25M KCl. Both eluents resulted in very similar forms for both the P_i and SO₄²⁻ profiles. However, there was a greater degree of separation between the downward tail of P_i and the upward tail of SO₄²⁻ when using the 0.25M KCl eluent compared to the 0.3M eluent. For both profiles, the NO₃⁻ concentration was below detection for the entire period during which P_i and SO₄²⁻ were eluting from the anion exchange resin. From these profiles it was determined that, in order to ensure a sufficient gap between the P_i and SO₄²⁻ tails, 12.5 mL anion exchange resin should be eluted with 0.25M KCl at 1 mL.min⁻¹. Under these conditions, the first 29 x 1 mL fractions were collected for further treatment within **Method 3**, on the basis that these fractions were assumed to contain the bulk of the P_i that could be eluted from the anion exchange resins. Analysis of the area underneath the P_i peaks in **Figure 3.9** determined that initial 0.4 mg P_i was almost fully recovered (>95%) in the 29 mL fraction using 0.25 M KCl as the eluent. In addition, a reduced elution rate of 0.5 mL.min⁻¹ was also evaluated (**Figure 3.11**). However, 1 mL.min⁻¹ was deemed to be optimum due to the increased length of time taken to collect P_i at a lower elution rate, but without an appreciably greater separation between P_i and SO₄²⁻.

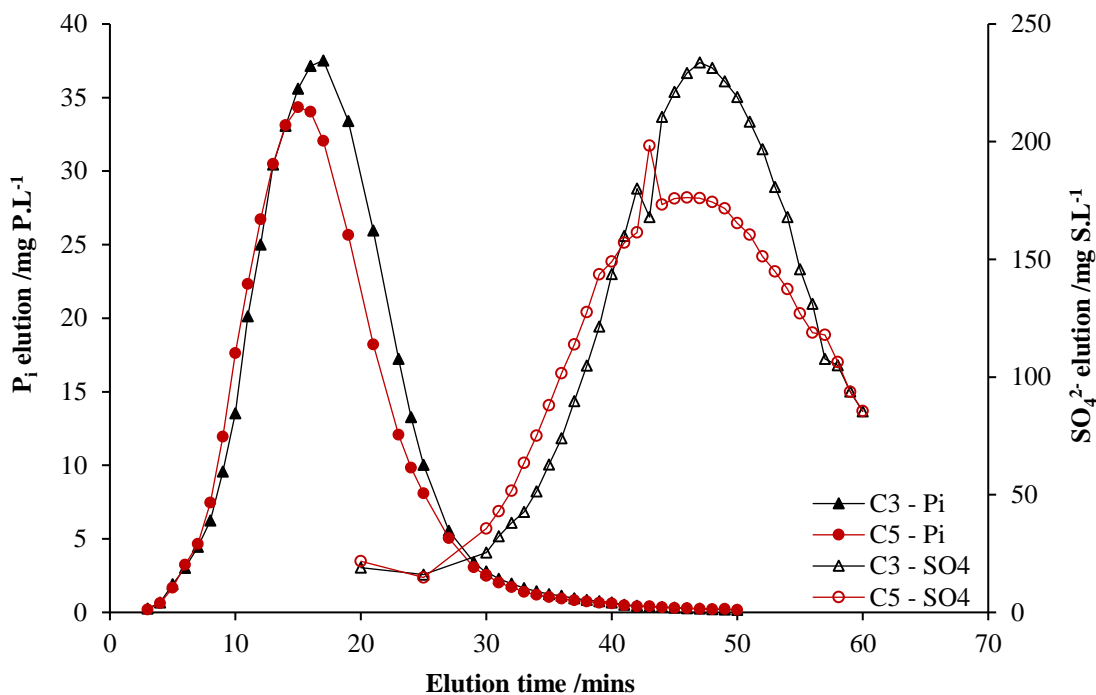


Figure 3.9: Elution profiles for Cl⁻-form anion exchange resins using 0.25M KCl with an elution rate of 1 mL.min⁻¹ in two duplicate columns - C3 and C5.

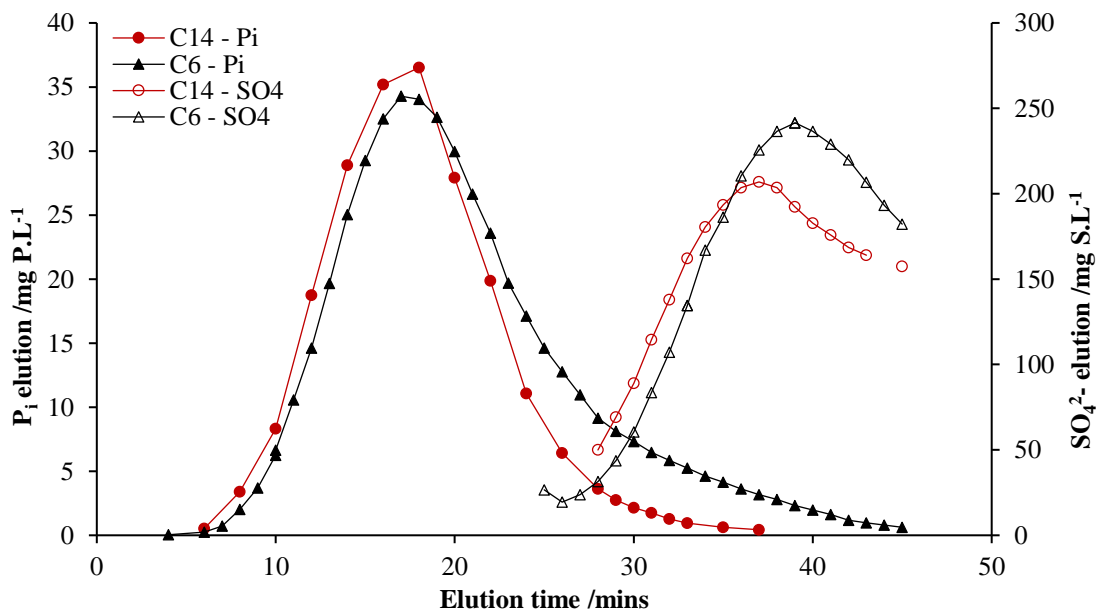


Figure 3.10: Elution profiles for Cl⁻-form anion exchange resins using 0.3M KCl with an elution rate of 1 mL.min⁻¹ in two duplicate columns - C6 and C14.

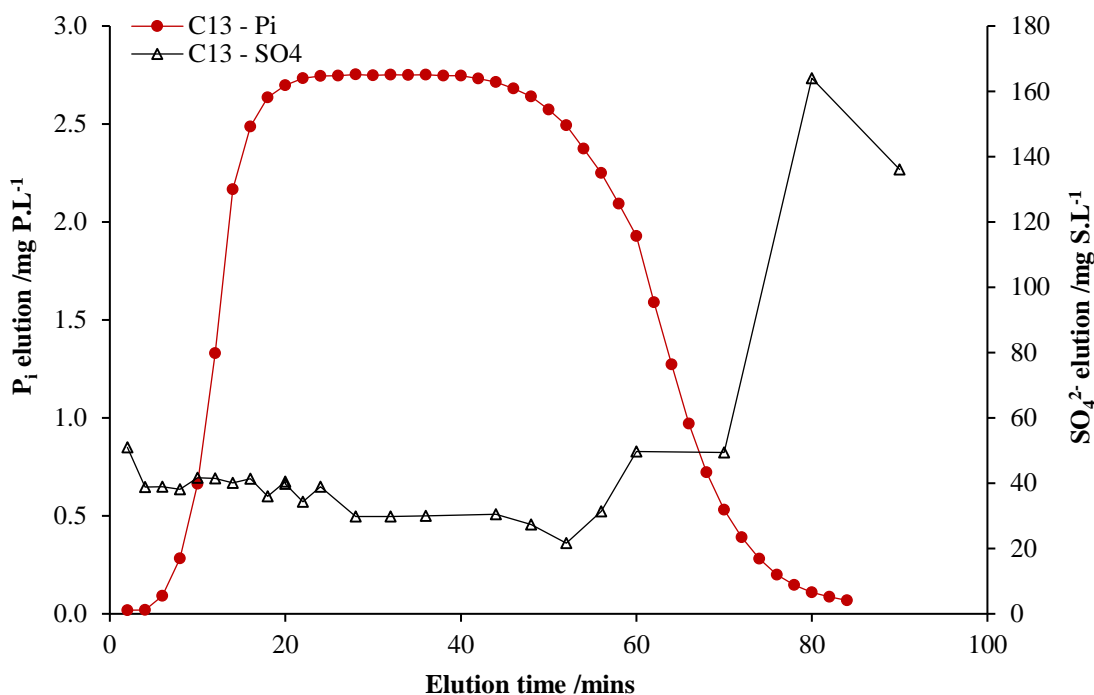


Figure 3.11: Elution profile for Cl⁻-form anion exchange resin using 0.3M KCl with an elution rate of 0.5 mL.min⁻¹. The P_i profile is not as “peaked” as in **Figures 3.9** and **3.10** as fractions that exceeded the P_i concentration range of the autoanalyser were not diluted, and yielded results of the maximum value for the instrument. However, the point at which the P_i and SO₄²⁻ tails overlap is still clearly visible.

3.4.4 Method 3 protocol

The full **Method 3** protocol that was used in **Section 3.5** is reported in **Figure 3.12**. The new sample preparation stages prior to **Method 1** are steps 1c-7c and 16c; the addition of steps 4c, 6c and 16c are consistent with the **Method 2** preparation stages. The major differences compared to **Method 2** are the introduction of a primary MagIC step to standardise the matrix before the samples are loaded onto resins (steps 1c-2c in **Figure 3.12**), and a new resin methodology (steps 3c-6c) to ensure effective DOM removal.

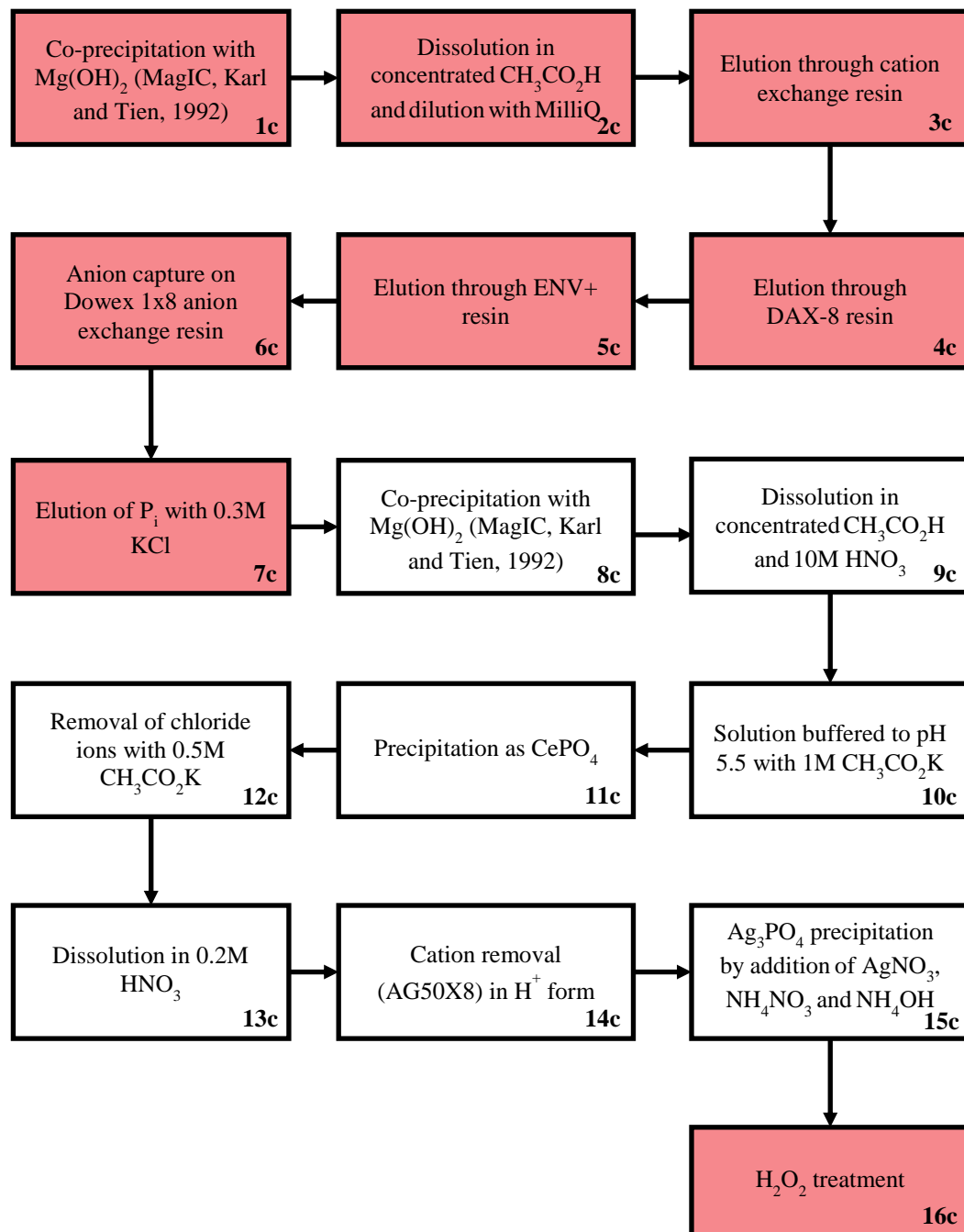


Figure 3.12: Method 3 protocol before testing.

3.5 Comparison of Ag₃PO₄ extraction methods

This section reports a comparison of the new **Method 3** protocol described in **Section 3.4** against **Method 1**. Four different matrices were employed: MilliQ water; an effluent from Lancaster wastewater treatment plant (WWTP); and two DOM-rich river waters from the upland peat catchment sampled in **Section 3.4.2** (test A). These natural matrices were chosen to represent high DOM samples from different sources, incorporating the potential for different combinations of DOM and P_{org} compounds to influence a protocol for $\delta^{18}\text{O}_p$ determination, and are choices that will likely cover a large range of P_{org} compounds found in UK freshwaters.

3.5.1 Experimental approach

In order to test whether the $\delta^{18}\text{O}_p$ determined from an individual protocol is accurate, it is important that the source $\delta^{18}\text{O}_p$ used within an experiment is known. Therefore, 10 litres of the WWTP effluent and of the two river waters were stripped of P_i prior to analysis, to prevent P_i that may have been originally present within a matrix from influencing the final $\delta^{18}\text{O}_p$ measurement. Stripping of P_i was achieved through a batch mode shake using a zirconium oxide (ZrO)/acrylamide binding gel that has been used to remove P from aqueous solutions within a diffusive gradient in thin films (DGT) technique (Zhang *et al.*, 1998; Ding *et al.*, 2010). The matrix was shaken for 24 hrs following the addition of each sheet of ZrO binding gel, until the P_i concentration in the matrix was below 0.009 mg P.L⁻¹ (equating to <2% of the P_i in the sample after the addition of the KH₂PO₄ spike). This method was chosen to minimise any potential alterations of the initial matrix; for example, chemical stripping of P using the MagIC precipitation would have stripped the matrix of P_i, however this process would have also introduced both Mg²⁺ and Cl⁻ ions into the matrix. The presence of these additional ions during the spiking experiment could have significant, and differing, effects on the performance of the two methods.

A KH₂PO₄ spike was subsequently added to 3 x 1 L of the four matrices to attain triplicate 0.4 mg P.L⁻¹ solutions for each method. KH₂PO₄ was chosen to create the P_i spike as it is readily combustible, which allows direct analysis of $\delta^{18}\text{O}$ within the

TCEA-IRMS without the need for additional chemical reactions which could alter the source $\delta^{18}\text{O}$ value. The spectator cations – K^+ and H^+ – should also have minimal interference on the protocols for Ag_3PO_4 precipitation.

Aliquots of the spiked matrices were taken throughout the initial stages of **Method 3** (steps 3c-6c in **Figure 3.12**) to determine P_i losses and pH . The concentrations of SRP and TP were measured using the techniques described in **Section 3.2.2**, and DOC concentrations as in **Section 3.4.2**. The following approaches were then used:

Method 1: 0.1 mol $\text{MgOH}_2 \cdot 6\text{H}_2\text{O}$ was added to 3 x 1 L of each P_i -spiked MilliQ water matrix and sample matrix, followed by 25 mL 1M NaOH solution, and mixed occasionally to precipitate brucite over 10 mins. The precipitate was collected through centrifugation at 3500 RCF for 10 minutes and dissolved in a 1:1 mixture of 10M HNO_3 and c. CH_3COOH . The addition of a $\text{CH}_3\text{CO}_2\text{K}$ buffer and CeNO_3 formed a CePO_4 precipitate, which was dissolved in 2 mL 1M HNO_3 . The solution was diluted to 0.2M HNO_3 with MilliQ water before the removal of Ce^+ ions using an overnight shake with Dowex 50x8 cation exchange resin in batch mode. After separation of the liquid from the resin, Ag_3PO_4 was precipitated using the fast precipitation method by addition of 0.5 g AgNO_3 , c. NH_4OH , 3M HNO_3 and 3M NH_4NO_3 . The resulting Ag_3PO_4 was captured on a 0.2 μm polycarbonate membrane filter and transferred to a glass vial and dried at 40 °C overnight.

Method 3: 0.1 mol $\text{MgOH}_2 \cdot 6\text{H}_2\text{O}$ was added to 3 x 1L of each P_i -stripped sample matrix, followed by 25 mL 1M NaOH solution and mixed occasionally to precipitate brucite over 10 mins. The precipitate was collected through centrifugation at 3500 RCF for 10 minutes and dissolved in the minimum volume of c. CH_3COOH necessary to fully dissolve the brucite pellet. The acidic solutions were loaded at 5 $\text{mL} \cdot \text{min}^{-1}$ through 1 x 7 mL cation exchange resin, 1 x 10 mL DAX-8 column, 1 x ENV+ resin and onto a 12.5 mL anion exchange resin. P_i was eluted using 0.25M KCl at 1 $\text{mL} \cdot \text{min}^{-1}$. 0.01 mol $\text{MgOH}_2 \cdot 6\text{H}_2\text{O}$ was added and diluted to form a 100 mL solution. 2.5 mL 1M NaOH solution was added to a beaker containing the 100 mL solution and mixed occasionally to precipitate brucite over 10 mins. Following the brucite precipitation, the method proceeded as for **Method 1**, as described above, from brucite centrifugation to Ag_3PO_4 collection. After the Ag_3PO_4 had dried, 0.5 mL 15%

H₂O₂ was added to each vial and left to decompose any remaining organic compounds (minimum 3 hrs) and then removed by evaporation at 40 °C overnight, and finally washed with 3 x ~1.5 mL MilliQ water, centrifuged at 3500 RCF for 20 minutes and dried at 40 °C overnight.

Ag₃PO₄ samples were analysed for δ¹⁸O_p on an IsoPrime100 mass spectrometer coupled to a varioPYRO cube elemental analyser. For each sample, 700 µg Ag₃PO₄ was weighed into a silver capsule with 800 µg carbon black, dried at 40°C overnight and converted to CO by pyrolysis in an ash crucible at 1450 °C. The resulting gases are passed through Sicapent (phosphorus pentoxide) to remove water. The CO is separated from other impurities, namely N₂, using a purge-and-trap system and helium carrier gas. ¹⁸O/¹⁶O is derived from the integrated mass 28 (¹²C¹⁶O) and 30 (¹²C¹⁸O; ¹⁴C¹⁶O; ¹³C¹⁷O) signals from the sample CO pulse, compared to those in an independently introduced pulse of pure CO reference gas. These ratios are then calibrated to the Vienna-Standard Mean Ocean Water (VSMOW) scale in per mille notation (‰) using standards – NBS127 (+9.3‰), EM Ag₃PO₄ (+21.7‰) and Acros Ag₃PO₄ (+14.2‰). The precision obtained from repeat analysis of standard materials is generally better than ±0.5‰_{VSMOW}.

3.5.2 Results

The isotopic composition of Ag₃PO₄ collected from each method applied to each matrix is reported in **Table 3.7** and **Figure 3.14**. Although triplicate spiked aliquots of each matrix were used for each method and matrix combination, isotopic analysis was not always possible for every sample due to a lack of Ag₃PO₄ yield. This was particularly the case for **Method 1** when applied to these matrices, confirming that there are severe limitations associated with this protocol when applied to freshwater matrices. For example, following the MagIC precipitation for **Method 1** in the River 2 matrix, the acidic mixture would not fully dissolve a black precipitate that had formed instead of the usual creamy white brucite pellet (**Figure 3.13**). This precipitate appeared to contain the P_i because no Ag₃PO₄ was precipitated in the final step of the **Method 1** protocol. The reason for very low Ag₃PO₄ yields within the **Method 1** protocol was not always as visibly apparent for other the matrices; however, the yields were so low that only a full set of triplicate measurements was achieved for the

Lancaster WWTP effluent, which was also associated with substantial variation in isotope composition. Therefore, it is suggested that, even if the P_i loss was not visible, freshwater matrices can prevent the full transformation of P_i into Ag_3PO_4 .

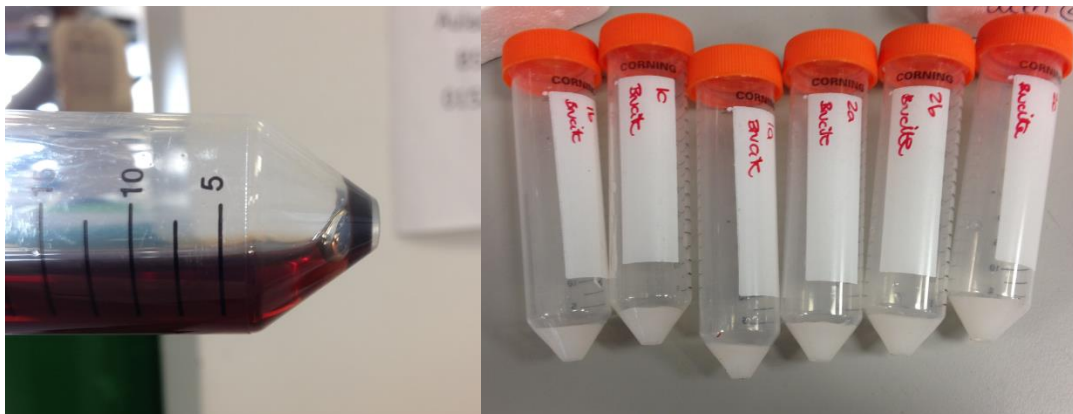


Figure 3.13: Comparison of black “brucite” precipitate formed when applying **Method 1** to the River 2 matrix, which did not fully dissolve in very low pH conditions, and typical creamy white brucite pellets formed in other matrices.

For **Method 3**, loss of P_i was found to occur consistently during the loading of the anion exchange resin. For example, using the WWTP matrix, 43.2% of the starting P_i mass was lost throughout all the resin stages (steps 3c-7c in **Figure 3.12**), of which the majority was found in the waste stream when loading the anion exchange resin (39.9% of starting mass of P_i). A similar loss was also observed in the case of the River 2 samples, with 58.1% of the original P_i mass being lost in total and 46.3% of the starting P_i mass being recovered in the waste stream from loading of the anion exchange resin. After several small-scale experiments in which the mass of acetic acid and pH were varied to determine which had the greatest effect, it was established that the increased total mass of acetic acid loaded onto the anion resin, relative to earlier trials described in **Section 3.4**, had prevented P_i from effectively sorbing to the solid phase anion exchange resin. Given the large proportion of P_i that did not bind to the anion exchange resin, an isotope effect associated with the loss of P_i during the loading of the resin cannot be ruled out, and that this potential isotope effect may have influenced the resulting $\delta^{18}O_p$ from these trials. Subsequently, within the analyses of samples collected in **Chapters 4** and **5** (and reported in **Chapter 6**), the anion exchange resin conditions at this stage of the protocol were altered, increasing the anion exchange resin volume to 50 mL and the KCl molarity to 0.3M in order to optimise the P_i elution profile. In addition for **Chapter 4** and **5** samples, to ensure the

acetic acid concentration did not affect the loading of P_i onto the anion exchange resin, re-dissolved brucite samples were diluted with MilliQ water to form a 0.6%_{v/v} solution for loading, because this concentration had been typically used without P_i losses in the previous small-scale trials described in **Section 3.4**. To ensure that these new conditions allowed full P_i adsorption to the resin and that P_i was effectively separated during the anion exchange resin elution, triplicate spiked MilliQ matrices – consisting of 0.6%_{v/v} acetic acid, 0.7 mg $P\text{-PO}_4\text{.L}^{-1}$, 11.2 mg $N\text{-NO}_3\text{.L}^{-1}$ and 3.3 mg $S\text{-SO}_4\text{.L}^{-1}$ – were loaded and eluted using the new conditions. The waste streams from the loading of the resins were collected and analysed for P_i , and were all below detection limits. The subsequent elution profiles exhibited a clear separation of P_i from SO_4^{2-} and almost complete P_i mass recovery was achieved (**Appendix A.1**).

Table 3.7: Comparison of spiked KH_2PO_4 samples in 4 matrices – MilliQ water, Lancaster WWTP effluent and two river samples taken from an upland peat catchment. The mean $\delta^{18}\text{O}_p$ of the KH_2PO_4 spike following direct pyrolysis was 15.00‰ ($1\sigma = 0.78\%$, $n = 9$). Oxygen yield refers to the EA measurement of oxygen within the Ag_3PO_4 . A pure Ag_3PO_4 sample would have an oxygen yield of 15.3%. Isotope values are given to 2 decimal places and oxygen yields to 1 decimal place.

Matrix	Method 1 - McLaughlin <i>et al.</i> (2004)					Method 3 – Revised protocol				
	Mean $\delta^{18}\text{O}_p$ /‰	1σ /‰	Oxygen yield /%	1σ /%	n	Mean $\delta^{18}\text{O}_p$ /‰	1σ /‰	Oxygen yield /%	1σ /%	n
MilliQ	14.59	-	8.4	-	1*	13.88	0.47	15.3	0.7	3
WWTP effluent	14.83	6.89	19.1	3.2	3	13.04	0.31	14.1	0.7	3
River 1	14.06	-	10.6	-	1*	16.12	-	16.0	-	1
River 2	n.d.	-	n.d.	-	0	14.23	-	12.3	-	1
Total	14.65	4.89	15.2	5.8	5	13.89	1.06	14.5	1.3	8

n.d. = not determined; * = 3 samples amalgamated to form one TCEA-IRMS analysis

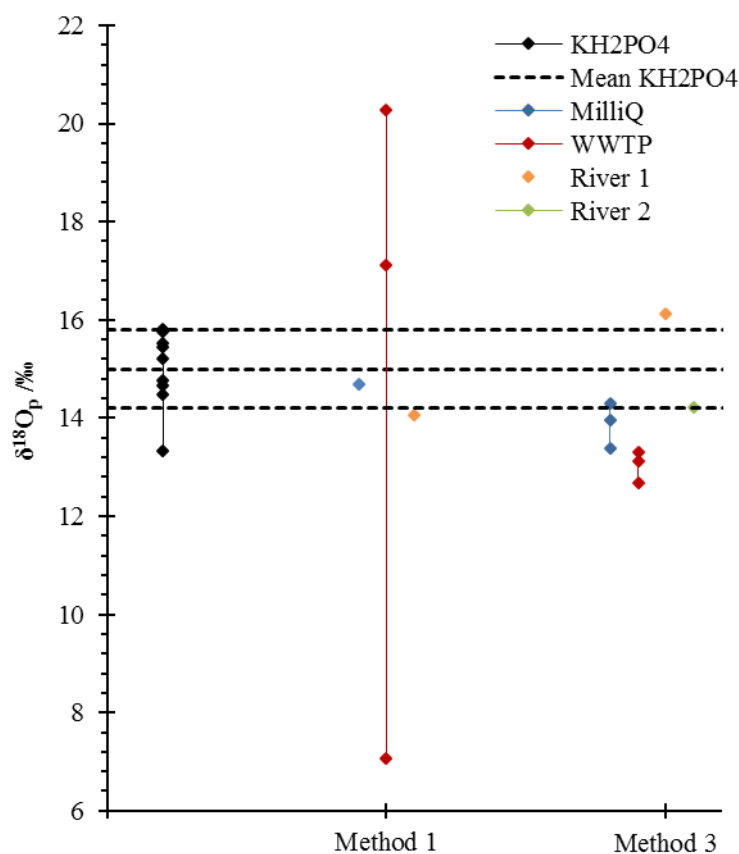


Figure 3.14: Individual $\delta^{18}\text{O}_p$ results from KH_2PO_4 spikes of four matrices across two methods – **Method 1** - McLaughlin *et al.* (2004) protocol and **Method 3** – the revised protocol (**Figure 3.12**). Black diamonds represent the $\delta^{18}\text{O}_p$ from a direct pyrolysis of KH_2PO_4 and the dashed lines for the mean ratio $\pm 1\sigma$ ($n = 9$).

Whilst neither **Method 1** nor **Method 3** consistently achieved suitable Ag_3PO_4 yields to perform isotope analyses on all triplicate subsamples, the mean $\delta^{18}\text{O}_p$ of **Method 1** ($\bar{x} = 14.65$, $\sigma^2 = 23.87$, $n = 5$) was closer to that of the directly pyrolysed KH_2PO_4 spike ($\bar{x} = 15.00$, $\sigma^2 = 0.62$, $n = 9$), compared to **Method 3** ($\bar{x} = 13.89$, $\sigma^2 = 1.13$, $n = 8$). However, **Method 3** resulted in a much smaller variance in terms of $\delta^{18}\text{O}_p$ than **Method 1** (**Figure 3.14**). For example, for WWTP effluent – the only matrix that generated sufficient Ag_3PO_4 in each triplicate subsample for TCEA-IRMS analysis using both protocols – the maximum-minimum ranges were 13.20 and 0.61‰ for **Methods 1** and **3** respectively. In addition, whilst **Method 3** did not generate a complete triplicate dataset, **Method 1** did not precipitate sufficient Ag_3PO_4 for any subsample in any matrix, except within WWTP effluent (**Table 3.7**). It should also be noted that the loss of P_i on the anion exchange resin experienced in **Method 3** (up to 58% of the starting mass of P_i), may also have created an isotope effect that could explain the substantial difference in terms of $\delta^{18}\text{O}_p$ between the KH_2PO_4 spike and the Ag_3PO_4 generated using **Method 3**. This difference may be reduced by the proposed

change in acetic acid concentrations and anion exchange resin conditions described in this section.

To determine the purity of the Ag_3PO_4 produced from an extraction protocol, the oxygen yield from TCEA-IRMS analysis can be compared to that of a pure Ag_3PO_4 precipitate. A pure Ag_3PO_4 precipitate contains a theoretical oxygen yield of 15.3%. If Ag_3PO_4 precipitates yield larger oxygen yields then this suggests that a source of contaminant O is present in the precipitate. If oxygen yields are smaller than 15.3%, the presence of an O-free contaminant might be inferred, for example AgCl , which may have prevented a full precipitation of P_i during the extraction protocol which could impart a kinetic fractionation. However, the presence of such compounds would not alter $\delta^{18}\text{O}_p$ for the Ag_3PO_4 that had been precipitated. However, the incorporation of P_i generated within a protocol as part of an Ag_3PO_4 precipitate, i.e. following hydrolysis of P_{org} , cannot be distinguished using oxygen yields.

When the oxygen yields of the Ag_3PO_4 precipitates within the TCEA-IRMS analysis were compared, it was found that the mean oxygen yield for **Method 1** was closer to that of a pure compound ($\bar{x} = 15.2\%$, $1\sigma = 5.8\%$, $n = 5$), compared to **Method 3** ($\bar{x} = 14.5$, $1\sigma = 1.3$, $n = 8$) which shows a lower oxygen yield than expected (**Table 3.7**). Despite the mean content being close to that of a pure Ag_3PO_4 molecule, no individual matrix from **Method 1** produced an oxygen yield within $\pm 25\%$ of the expected figure of 15.3% for a pure Ag_3PO_4 compound, with yields suggesting purities of 55% for the MilliQ, 125% for the WWTP effluent and 69% for the River 1 matrices. In contrast, the only matrix from **Method 3** that is outside $\pm 10\%$ of the theoretical yield is that of the River 2 matrix (20% lower than the theoretical yield). **Figure 3.15** demonstrates a substantially smaller variance for oxygen yields for the WWTP effluent matrix for **Method 3** compared to **Method 1**. Furthermore, **Figure 3.16** clearly demonstrates that there is a tighter clustering of O yields and $\delta^{18}\text{O}_p$ ratios for individual data points when using **Method 3**, suggesting that **Method 1** was not reliable in terms of O yield, particularly in combination with the fact that many of the replicates did not yield sufficient quantities of Ag_3PO_4 for isotope analysis.

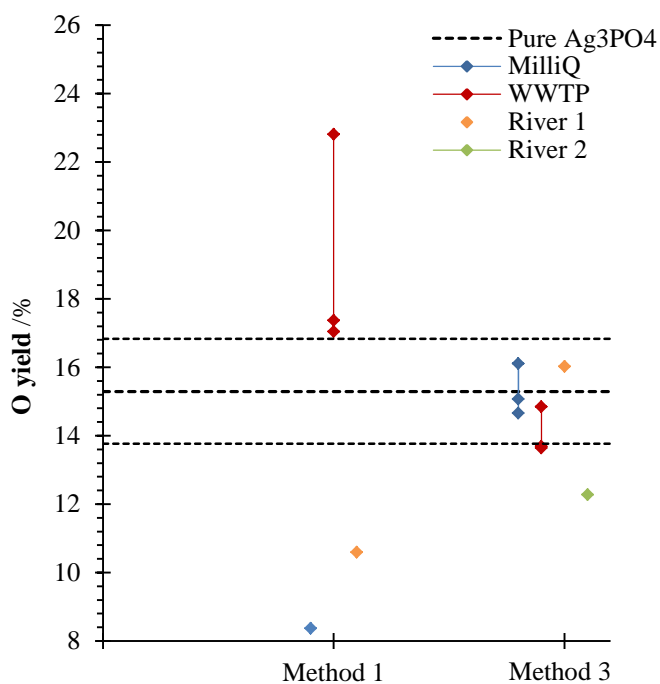


Figure 3.15: Individual oxygen yields of Ag_3PO_4 that were run in the TCEA-IRMS for **Method 1** - McLaughlin *et al.* (2004) protocol and **Method 3** - Revised protocol (**Figure 3.12**). The theoretical yield for Ag_3PO_4 – 15.3% ($\pm 10\%$) - is provided for reference as dashed lines.

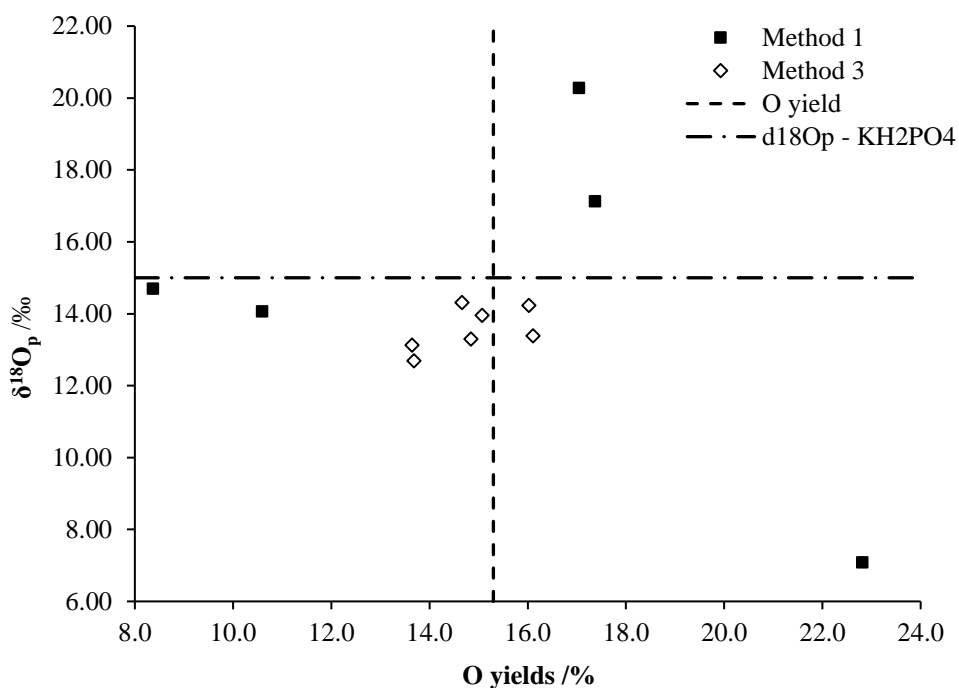


Figure 3.16: $\delta^{18}\text{O}_p$ and O yields for individual Ag_3PO_4 precipitates formed using **Methods 1** and **3** across all four matrices. The mean $\delta^{18}\text{O}_p$ of the KH_2PO_4 spike and theoretical O yield for a pure Ag_3PO_4 have been provided for reference at 15.00‰ and 15.3% respectively.

Previous work within the research group at Lancaster University has also compared **Method 1** against **Method 2** across four matrices (**Figure 3.17**). Similarly to **Method 3**, **Method 2** resulted in a much smaller variance in $\delta^{18}\text{O}_p$ than **Method 1** for across these sample matrices, although little difference between **Methods 1** and **2** was observed for the MilliQ matrix. To determine if there was a significant difference between mean $\delta^{18}\text{O}_p$ determined from the two protocols and directly pyrolysed KH_2PO_4 regardless of sample matrix, a Shapiro-Wilk test for normality was performed on all three categories (**Methods 1** and **2** and KH_2PO_4), resulting in p values greater than 0.18 showing that the data were normally distributed within each category. A test for equality of variance, the Levene's test for means, was then performed yielding a p value <0.001 , determining that variances were significantly different from each other. Based on these analyses, two one-way analyses of variance (ANOVA) were undertaken, and it was determined that there was no significant difference between **Method 2** and KH_2PO_4 at a matrix level. Conversely, there was a significant difference with **Method 1** and KH_2PO_4 at a matrix level: $F(4, 12) = 45$, $p < 0.001$. When considering the pairwise comparison for each **Method 1** matrix against KH_2PO_4 , the only matrix that was not significantly different from KH_2PO_4 in terms of $\delta^{18}\text{O}_p$ generated using **Method 1** was that of the MilliQ matrix.

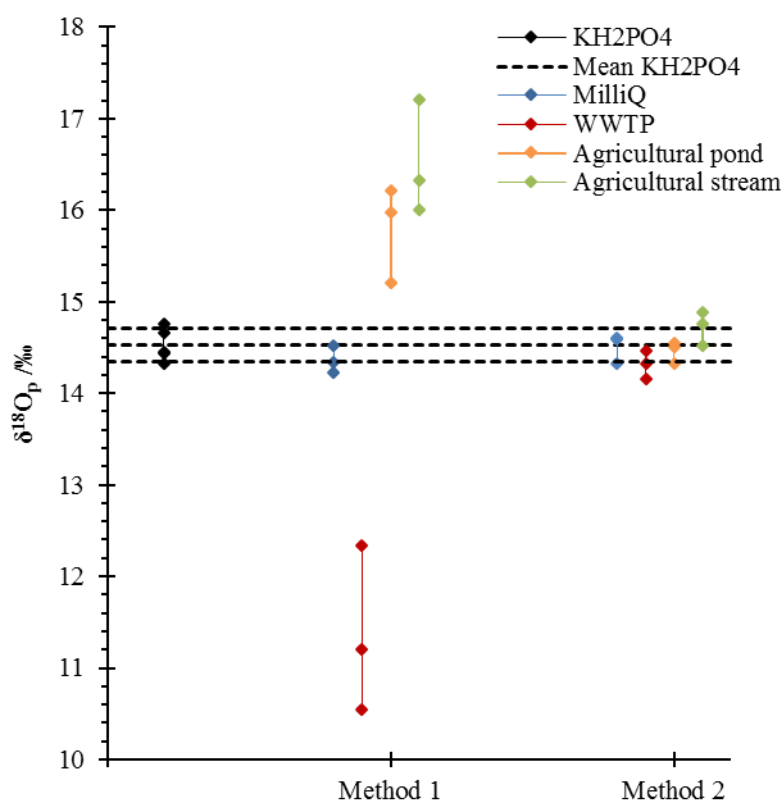


Figure 3.17: Previous comparison of **Methods 1** and **2** (data from B. Surridge, personal communication). Individual $\delta^{18}\text{O}_p$ results from KH_2PO_4 spikes of four matrices across two methods – **Method 1** - McLaughlin *et al.* (2004) protocol and **Method 2** – Goody *et al.* (2016). Black diamonds represent the $\delta^{18}\text{O}_p$ from a direct pyrolysis of KH_2PO_4 and the dashed lines for the mean ratio $\pm 1\sigma$ ($n = 5$).

3.5.3 Summary: selecting an appropriate Ag_3PO_4 protocol for freshwater matrices

This chapter has shown that there are a number of significant issues to address when applying the original McLaughlin *et al.* (2004) (**Method 1**) protocol to freshwater matrices. This is evidenced through the extent of co-precipitation with brucite of the potential contaminants P_{org} (**Section 3.2**), DOM, NO_3^- and SO_4^{2-} (**Section 3.4.1**). Therefore, the use of MagIC to isolate P_i from a sample matrix is not sufficient for freshwater matrices in which these sources of contaminant O are likely to be common. In addition, this thesis has encountered difficulties in generating sufficient masses of Ag_3PO_4 from freshwater matrices using **Method 1**, including the formation of an insoluble precipitate in the MagIC step that appears to bind or adsorb P_i and does not dissolve in the strongly acidic conditions proposed by McLaughlin *et al.* (2004). Finally, the O yield data from **Method 1** appear to be problematic, with none of the samples reported in **Figure 3.15** achieving yields with $\pm 25\%$ of the theoretical yield. Furthermore, for the WWTP effluent, a very wide range for $\delta^{18}\text{O}_p$ (13.20‰) was

observed across replicate samples. In conclusion, the research reported in this chapter emphasises that **Method 1** cannot be applied directly to freshwater matrices without any modification.

Method 3 appears to be a significant improvement over **Method 1**, particularly in terms of its potential to reduce sources of contaminant O through the combined use of organic exchange resins (**Section 3.4.2**). In addition, the O yield data are far closer to the theoretical value for a pure Ag_3PO_4 compound (**Table 3.7**), and the variances in $\delta^{18}\text{O}_p$ for replicate samples are much smaller than observed for **Method 1**. However, it should be noted that the loss of P_i on the anion exchange resin reported in **Section 3.5.2** prevented some of the replicate samples from generating sufficient Ag_3PO_4 for analysis. This loss, up to 58% of the starting P_i mass in this step, may also have created an isotope effect that could explain the substantial difference between the $\delta^{18}\text{O}_p$ from the KH_2PO_4 spike and the $\delta^{18}\text{O}_p$ in the Ag_3PO_4 generated using **Method 3**. In conclusion, **Method 3** is a significant improvement on **Method 1** and generates what appears to be pure Ag_3PO_4 . However, there is also evidence of an isotope effect that influences $\delta^{18}\text{O}_p$, which has likely been caused by the incomplete recovery of P_i through the loading of the anion exchange resin in step 6c. However, this remains a method that merits further application in **Chapters 4** and **5**, specifically following the proposed change in acetic acid concentrations and anion exchange resin conditions described above that are designed to minimise P_i loss.

Method 2 is also a significant improvement over the **Method 1** protocol, particularly in terms of the isolation of P_i from a freshwater matrix, but also importantly the consistency of generating sufficient Ag_3PO_4 for pyrolysis. **Figure 3.17** demonstrates the precision and accuracy of $\delta^{18}\text{O}_p$ measurements across a number of sample matrices using **Method 2**, in contrast to **Method 1**. Therefore, **Method 2** was selected to be applied throughout the research reported in **Chapters 4** and **5** of this thesis. Furthermore, where possible, **Method 3** was run in parallel with **Method 2** to generate data for a subsequent method comparison that will be reported in **Chapter 6**.

Chapter 4:

Evaluating the utility of $\delta^{18}\text{O}_\text{p}$ as a tracer of point source inputs and in-stream cycling of P in a freshwater river system

4.1 Introduction

Phosphate oxygen isotope analysis represents a potentially valuable tool to aid in the determination of sources and biogeochemical cycling of inorganic phosphorus (P_i) within riverine environments. Inorganic P plays a vital role in river ecosystems through its control on primary production because, typically, freshwaters are perceived to be P-limited whereas marine environments are viewed as N-limited (Schindler, 1974; Doering *et al.*, 1995). However there are exceptions to this traditional view of nutrient limitation, with some freshwater ecosystems shown to be N-limited or co-limited by both N and P, whilst some marine environments have been shown to be P-limited (Krom *et al.*, 1991; Howarth and Marino, 2006; Conley *et al.*, 2009; Xu *et al.*, 2010).

Phosphorus limitation occurs when the bioavailable pool of P is insufficient to support the demands of primary producers, including phytoplankton, phytoplankton and macrophytes in river ecosystems, compared to the availability of other nutrients. Under these circumstances, an increase in the availability of P_i would result in an increase in the rate of primary production (Hecky and Kilham, 1988). Removal of P limitation is often linked to the alteration of natural P cycles within aquatic ecosystems through inputs of bioavailable P from anthropogenic sources, resulting in undesirable ecosystem changes linked to eutrophication that include increases in primary production, shifts in community composition, increased frequency of algal blooms and hypoxia, and reduced biodiversity (Sondergaard and Jeppesen, 2007; Smith and Schindler, 2009). Although bioavailable P enters aquatic ecosystems from a

range of sources, modelling suggests that anthropogenic sources are responsible for 92% of the 0.27 Tg P_i -P.yr⁻¹ that is exported by rivers to coastal regions in Europe (Harrison *et al.*, 2010). To be able to reduce the impact of anthropogenic P_i inputs to aquatic ecosystems and restore natural P biogeochemical cycles, it is vital that sources of P_i are accurately identified and that understanding of how P is cycled within aquatic ecosystems is improved.

Traditional tools to address such questions surrounding P_i , including radioisotope labelling and modelling or monitoring of concentration changes within ecosystems, have significant limitations. These include constraints on the timescales over which processes can be investigated due to short half-lives associated with radioisotopes, disturbances to the natural systems associated with radiolabelling, or the omission of irregular natural events, such as seasonal algal blooms, during incubation experiments, see **Section 2.1** for further discussion (Thingstad *et al.*, 1993; Benitez-Nelson, 2000). However, the stable isotope composition of P_i ($\delta^{18}O_p$) has the potential to act as an inherent tracer for the sources and metabolism of P in natural ecosystems without a number of these limitations (McLaughlin *et al.*, 2004; Elsbury *et al.*, 2009; Young *et al.*, 2009; Goldhammer *et al.*, 2011a; Li *et al.*, 2011). For example, the $\delta^{18}O_p$ ratio of a wastewater treatment plant (WWTP) effluent, assuming that it is isotopically distinct from upstream sources of P_i in a river, could be used to determine how a riverine ecosystem responds to inputs of bioavailable P_i from effluent. It may be hypothesised that if the P_i concentration within a river upstream of a WWTP is low, the river may be in a state of P limitation. Under these conditions, the input of bioavailable P from a WWTP effluent could stimulate in-stream biological activity. Consequently, in-stream biota could then readily metabolise P_i derived from the effluent, resulting in rapid fractionation of $\delta^{18}O_p$ and the approach of riverine $\delta^{18}O_p$ towards a temperature-dependent isotopic equilibrium with water $\delta^{18}O$ (Scenario A in **Figure 4.1**). However, if a river had a high P_i concentration upstream of a WWTP, it may be hypothesised that metabolic activity within the river was limited by factors other than the availability of P_i . Under these conditions, in-stream biota may not respond metabolically to an input of P from WWTP effluent at all, or at least at a much slower rate than within a strongly P-limited system. Under this alternative scenario, the influence of $\delta^{18}O_p$ from a WWTP effluent on in-river $\delta^{18}O_p$ might be expected to persist over a significantly longer downstream reach (Scenario B). If further inputs of

P_i occurred downstream of WWTP, $\delta^{18}O_p$ could also be used to identify the major source of P to the river within that environment, assuming that $\delta^{18}O_p$ source signatures were maintained. Therefore, the use of $\delta^{18}O_p$ may allow the relative importance of in-stream metabolism of P_i derived from WWTP effluent to be clearly elucidated.

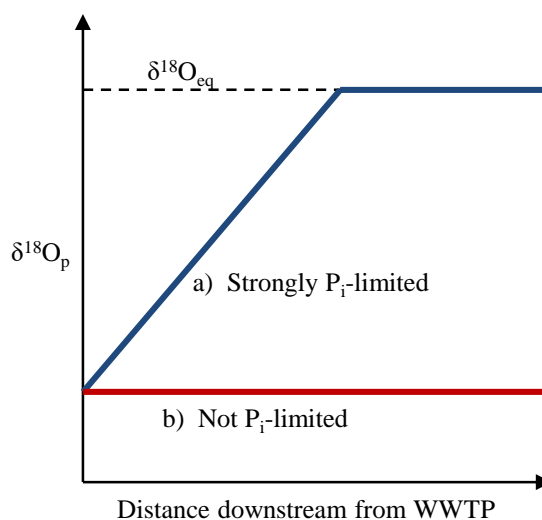


Figure 4.1: Conceptual diagram describing possible changes in in-river $\delta^{18}O_p$ following a WWTP effluent input (with a distinct $\delta^{18}O_p$ signature, lower than the theoretical equilibrium ($\delta^{18}O_{eq}$)) for two different states of P_i -limitation within the river. Scenario A depicts a strongly P_i -limited system in which $\delta^{18}O_p$ rapidly approaches $\delta^{18}O_{eq}$ downstream of the WWTP, whereas in Scenario B the $\delta^{18}O_p$ signature of the WWTP effluent is maintained downstream, for a system that is not limited by P_i .

Despite the significant potential for $\delta^{18}O_p$ to inform research into P biogeochemistry within freshwater ecosystems, only a very limited number of initial studies have explored the use of $\delta^{18}O_p$ to assess sources and metabolism of P_i in these ecosystems (Blake *et al.*, 2001; Gruau *et al.*, 2005; McLaughlin *et al.*, 2006a; McLaughlin *et al.*, 2006c; Young *et al.*, 2009; Li *et al.*, 2011; Gooddy *et al.*, 2016). A major reason for the relative lack of research in this area has been uncertainty surrounding the use of current P_i extraction protocols in freshwater environments (see **Chapter 3**). Some research has applied the McLaughlin *et al.* (2004) protocol without modification to freshwater matrices, whilst other research has adapted one of the major Ag_3PO_4 precipitation protocols to include clean-up stages for samples containing high concentrations of particulate and dissolved organic matter (DOM). The majority of studies have analysed $\delta^{18}O_p$ within rivers in the U.S.A. that represent potential sources of P_i to larger water bodies, such as Lake Erie (Elsbury *et al.*, 2009), a tidal estuary, Elkhorn Slough (McLaughlin *et al.*, 2006a), and Lake Tahoe, Lake Erie and San

Joaquin River (Young *et al.*, 2009). However, research has also shown that $\delta^{18}\text{O}_p$ may be used to determine anthropogenic fertiliser inputs into a wetland system (Li *et al.*, 2011) and to trace effluent P_i immediately downstream of a WWTP point source in a freshwater river (Gooddy *et al.*, 2016). For example, Li *et al.* (2011) used $\delta^{18}\text{O}_p$ to estimate that 15-100% of the total dissolved P_i content within a wetland system impacted by agricultural runoff was derived from fertiliser input and retained evidence of a fertiliser $\delta^{18}\text{O}_p$ signature. In contrast, in an area not impacted by agricultural runoff, P_i concentrations were substantially lower, fertiliser inputs were estimated to contribute 0-1% of the total dissolved P_i and $\delta^{18}\text{O}_p$ indicated a significantly greater extent of biological cycling of P_i , with $\delta^{18}\text{O}_p$ values close or equal to $\delta^{18}\text{O}_{eq}$.

This current chapter reports an initial application of the $\delta^{18}\text{O}_p$ technique to a headwater stream in the upper catchment of the River Beult (Kent, UK). Typically, between 60 and 85% of the total global river network length is in the form of headwater streams (Peterson *et al.*, 2001; Benda *et al.*, 2005). Therefore, understanding the sources and biogeochemical cycling of P within these systems is important for understanding nutrient cycling within river networks in general, and also for the downstream transport of nutrients from headwater reaches into lowland reaches of the network (Alexander *et al.*, 2007; Wipfli *et al.*, 2007). The River Beult was chosen as an exemplar of a rural, headwater catchment that contains a WWTP set within a predominantly agricultural system. In addition, previous work within the research group has also been conducted within the Beult catchment (Lapworth *et al.*, 2009; Gooddy *et al.*, 2016), and therefore direct comparisons can be made with historical data from the sites. Gooddy *et al.* (2016) combined $\delta^{18}\text{O}_p$ analysis with stable isotope analyses of both nitrate and ammonium to trace biogeochemical processes following the input of a WWTP effluent to this headwater stream. The research was conducted over a 200m reach, with Sutton Valence WWTP located 35m upstream of the final in-river sample site. Under low flow conditions, P_i concentrations decreased prior to the WWTP input but $\delta^{18}\text{O}_p$ remained relatively constant, suggesting that abiotic processes such as dilution or sorption of P_i , rather than biological cycling, were responsible for changes in P_i concentration. Conversely, under high flow conditions P_i concentrations and $\delta^{18}\text{O}_p$ increased prior to the WWTP, suggesting an additional P_i input or P_i regeneration from P_{org} compounds. However, under both flow conditions, $\delta^{18}\text{O}_p$ provided little evidence for in-river metabolism of P

derived from WWTP effluent within the 35m reach downstream of the WWTP. However, the relatively short reach downstream of the point source, and therefore the short residence time of water within the river, may have constrained any chance to detect evidence for in-river metabolism of WWTP-derived P_i . Longer in-river transects downstream of WWTPs are required in order to more fully assess the impact of in-river cycling on P_i derived from sources such as WWTPs.

Therefore, the aim of this chapter was to evaluate the potential for $\delta^{18}O_p$ to be used as a tracer of P_i inputs to the headwater reaches of a freshwater river network and, through $\delta^{18}O_p$ analysis, to identify the biogeochemical processes influencing the downstream transport of P_i within a river network. In comparison to the research reported by Goddy *et al.* (2016), the in-river transect was extended to 4 km and included a 2.75 km reach downstream of the WWTP effluent input. Two specific hypotheses were tested within this chapter:

- i) The input of P_i to a river from a point source (WWTP effluent) can be identified on the basis of an isotopically distinct $\delta^{18}O_p$ signature compared to upstream sources of P_i ;
- ii) Metabolic processes will influence the downstream transport of P_i following input from a point source, leading to isotope effects or isotope fractionations that will enable the specific processes to be identified through $\delta^{18}O_p$ analysis.

Hypothesis 4.ii assumes that the river is in a state of P limitation upstream of the WWTP. To indicate which nutrient is most likely to be limiting within an ecosystem, the Redfield ratio has often been used. This ratio is based on the stoichiometry of the mean chemical composition of marine plankton (both zoo- and phytoplankton) (Redfield *et al.*, 1963). According to the classic Redfield ratio, C:N:P is found as a 106:16:1 molar ratio. However, further work has questioned the consistency of the ratio spatially and temporally, and has suggested alternative ratios to represent different environments (Hecky *et al.*, 1993; Elser and Hassett, 1994; Sterner *et al.*, 2008). This thesis will use the ratio of Sterner *et al.* (2008); a 166:20:1 molar ratio which was assimilated from more than 2000 data points, including from both large

and small freshwater lakes, whereas the classic Redfield *et al.* (1963) ratio was based on marine organisms only.

A secondary aim of the chapter was to generate an in-field dataset comparison between **Methods 2** and **3** reported in **Chapter 3**. However, this comparison will be discussed in **Chapter 6**, with all data presented in the current chapter based on **Method 2**, thereby allowing direct comparison with previous research from the site reported by Lapworth *et al.* (2009) and Gooddy *et al.* (2016).

4.2 Methodology

4.2.1 Study site description

This research was undertaken within the upper Beult catchment located near Sutton Valence, Kent, South England (**Figure 4.2**). The geological setting of the study sites is the Weald Clay formation, which represents a clay and silty-clay formation within which are found outcrops of limestone and sand (Lapworth *et al.*, 2009). The section of the River Beult chosen for sampling covered approximately 4 km. At the upstream end of the reach was a working fruit farm and orchard, before the stream flowed through arable land and grassland (mainly dairy pasture) (**Table 4.1**). Located 1.38 km downstream from site A was the final effluent discharge point for Sutton Valence WWTP. Sample W was collected from the final effluent itself before entry into the river, whilst sample E was collected 40 m downstream on the assumption that the effluent would have mixed fully with the main stream by this point.

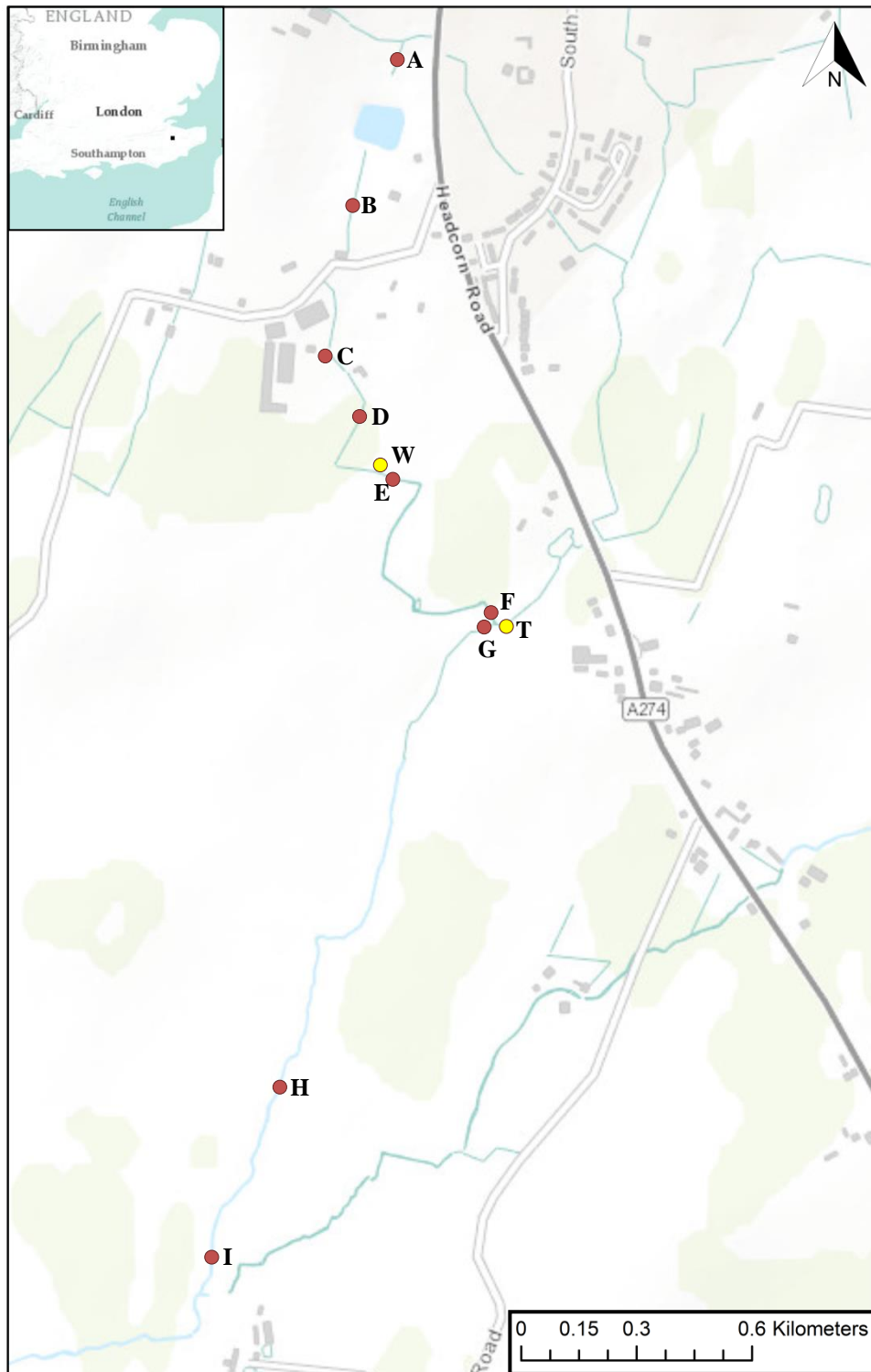


Figure 4.2: Location of sample sites along a tributary of the River Beult, Kent, UK (direction of river flow is from site A to site I). All samples were located along the main stem of the river, with the exception of samples T and W (yellow markers), which represent a tributary inflow and the final effluent from Sutton Valence WWTP respectively. Tap water sample was collected from a location 1.6km ESE from sample I. Inset shows the geographical location of the study site in southern England (given as a black marker).

As shown in **Figure 4.2**, there is an apparent break in the stream between sampling sites A and B. Based on conversations with farm workers, it was determined that the stream had been diverted underground around the side of the irrigation pond, and a pipe is visible directly south of the irrigation pond where the stream re-emerges. Typically, the stream is allowed to flow and the entrance to the irrigation pond is blocked (this was the case in the March sampling event described below). However, when water levels in the irrigation pond are low, the stream is blocked and diverted to the irrigation pond (**Figure 4.3**), as was the case during the September sampling event described below. The suspected length of the underground culvert around the edge of the irrigation pond has been included in the reported distances from site A in **Table 4.1**.

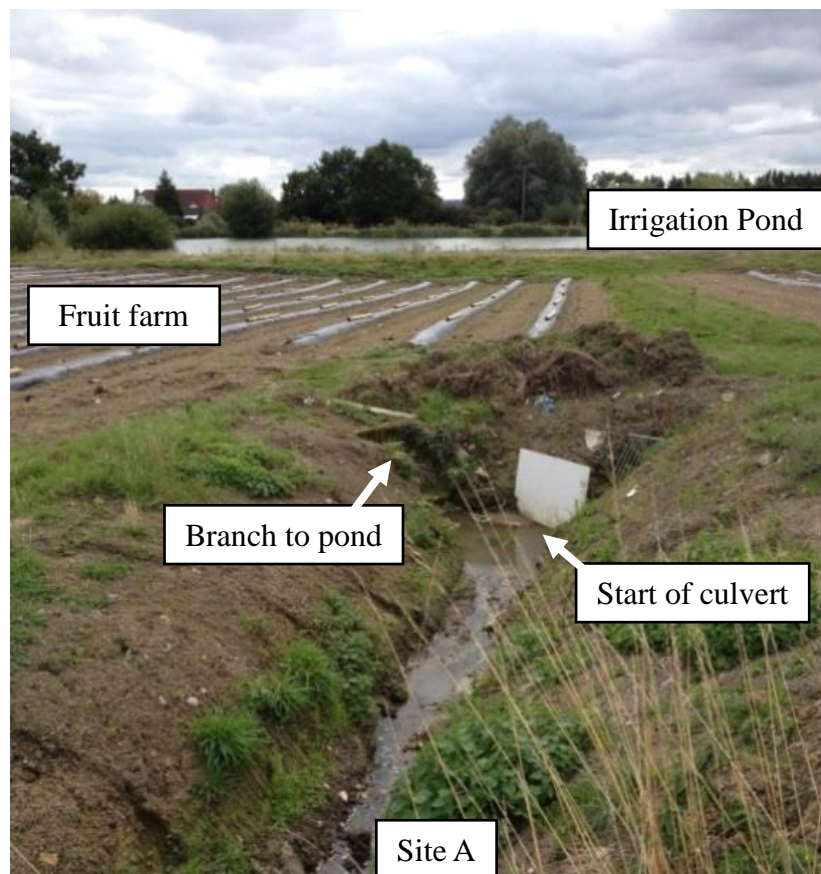


Figure 4.3: View downstream from site A towards site B (see **Figure 4.2**) on 08/09/2015. The stream is directed either to the left branch – feeding the isolated irrigation pond – or the right branch – underground culvert that emerges immediately south of the irrigation pond, upstream of site B.

Table 4.1: Site descriptions for surface water samples in the Beult catchment and predominant land use surrounding each site.

Site Number	Sample site	Distance downstream from A /km	Predominant land use
A	Main stream	0.00	Fruit farm and orchard
B	Main stream	0.49	Garden
C	Mill pond	0.93	Farm mill pond
D	Main stream	1.14	Pastoral farmland
W	WWTP effluent	1.38*	n.a.
E	Main stream	1.42	Sewage works/Arable land
F	Main stream	2.11	Arable land
T	Stream tributary	2.15*	Grassland
G	Main stream	2.18	Arable land
H	Main stream	3.63	Pastoral farmland
I	Main stream	4.13	Pastoral farmland
Tap Water	n.a.	n.a.	n.a.

*Point at which inflow enters the main stream.

4.2.2 Field sampling

Two sampling campaigns were conducted, the first over two days in March 2015 (02/03/2015 – sites C, D, F-I and T; 03/03/15 – sites A, B, E and W) and the second on 8th September 2015. March was chosen to represent late winter/early spring, high-flow conditions, whilst September was selected to be representative of late summer, low-flow conditions. These sampling events were selected to enable the impact of well-recognised seasonal differences, for example in river discharge, water temperature, nutrient concentrations and metabolic activity, on $\delta^{18}\text{O}_p$ to be evaluated. No confounding effects are expected due to the March sampling event being conducted over two days compared to the single day in the September, because weather and, therefore, flow conditions were stable over the 30 hour period during which sampling occurring, as reflected in the measured surface water temperatures.

4.2.3 Sample collection and field measurements

Water samples of 5-10 L for $\delta^{18}\text{O}_p$ analysis were collected directly from the stream using a beaker or bucket (depending on the width of the stream); with the exceptions of site W and “Tap Water” which were collected as intercepts from a pipe leaving the Sutton Valence WWTP and a local golf course’s outdoor tap respectively. Typically, the stream was sufficiently narrow to allow sampling across the full channel, where streams were larger than the width of the bucket, the most actively flowing section of the channel was sampled. The samples were filtered in the field through 0.45 μm filter

cartridges, using a peristaltic pump, into acid-washed high-density polyethylene containers and stored at 4°C in a cold store before analysis. The required volumes of sample to collect were estimated prior to sampling using previous concentrations of P_i determined from the same or nearby sites as a guide to the volume of sample that would yield approximately 0.4-0.7 mg P, thereby producing sufficient Ag_3PO_4 to run triplicate measurements on the thermal combustion/elemental analyser isotope ratio mass spectrometer (TCEA-IRMS). Water temperature was measured directly in the river using a Hanna Instruments handheld probe. An unfiltered sample was collected and analysed for conductivity, pH and dissolved oxygen (DO) in the field using calibrated Mettler Toledo probes. Alkalinity was determined in the field by a bromocresol green colorimetric titration against 1.6N H_2SO_4 . Separate unfiltered (collected in amber vials) and filtered (0.45 μm syringe filtered, collected in 50 mL centrifuge tubes) sample aliquots were collected from each site and retained for $\delta^{18}O_w$ and nutrient analysis respectively, and stored at <4 °C prior to analysis in the laboratory.

4.2.4 Analysis of nutrient concentrations

On 0.45 μm filtered sample aliquots, soluble reactive P (SRP) concentrations were determined using a phosphomolybdenum blue method on a Seal Analytical AQ2 discrete autoanalyser (LOD = 0.005 mg P.L⁻¹; analytical quality controls: matrix-matched SPEX CertiPrep WR1 (0.6 mg P.L⁻¹) and WR2 (0.3 mg P.L⁻¹)). Total dissolved P (TDP) concentrations were analysed similarly to SRP, following the digestion of samples in a 0.11M sulfuric acid (H_2SO_4) and 0.03M potassium persulfate ($K_2S_2O_8$) matrix. However, due to a time delay of several weeks in analysis for this component, the TDP concentrations indicated that sample deterioration had occurred prior to analysis, with lower TDP concentrations relative to the SRP concentrations which were processed immediately on returning to the laboratory. TDP loss is a known issue with delayed analysis (Kotlash and Chessman, 1998; Neal *et al.*, 2000); therefore, the TDP concentrations have not been included in this thesis. Analyses of dissolved organic carbon concentrations were carried out on acidified and sparged filtered samples using an Analytical Sciences Thermalox (LOD = 1.3 mg C.L⁻¹; analytical quality control: EAG REF162 (0.5, 5 and 15 mg C.L⁻¹)). Nitrate-N ($N-NO_3^-$) and sulfate-S ($S-SO_4^{2-}$) concentrations in filtered samples were

determined using ion chromatography on a Dionex ICS2500 (LOD = 0.02 mg N.L⁻¹ and 0.07 mg S.L⁻¹ respectively; calibrated 0-10 mg N.L⁻¹; analytical quality controls: SPEX CertiPrep WR1 (4 mg N.L⁻¹ and 10 mg S.L⁻¹) and WR2 (2 mg N.L⁻¹ and 5 mg S.L⁻¹)).

4.2.5 $\delta^{18}O_p$ and $\delta^{18}O_w$ measurements

After P_i concentrations had been determined, the appropriate volume of sample to generate 0.7 mg P as Ag₃PO₄ was processed using **Method 2**. If sufficient sample volume remained, the sample was also run for Ag₃PO₄ using the revised **Method 3** (see **Chapter 3**). For **Method 2**, samples were loaded at 5 mL.min⁻¹ through 2 x 50 mL DAX-8 columns and onto a 50 mL anion exchange resin column. P_i was eluted using 0.3M KCl at 1 mL.min⁻¹; 0.01 mol MgOH₂.6H₂O was added and diluted to form a 100 mL solution. 2.5 mL 1M NaOH solution was added to a beaker containing the 100 mL solution and mixed occasionally to precipitate brucite over 10 mins. The precipitate was collected through centrifugation at 3500 RCF for 10 minutes and dissolved in the minimum volume of a 1:1 mixture of 10M HNO₃ and c.CH₃COOH required for complete dissolution. The addition of a CH₃CO₂K buffer and CeNO₃ formed a CePO₄ precipitate, which was isolated and cleaned through repetitive centrifugation at 3500 RCF in 15 minute intervals with 0.5M CH₃CO₂K. CePO₄ was dissolved in 2 mL 1M HNO₃. The solution was diluted to 0.2M HNO₃ with MilliQ water before the removal of Ce³⁺ ions using an overnight shake with Dowex 50x8 cation exchange resin in batch mode. After separation of the liquid from the resin, Ag₃PO₄ was precipitated using the fast precipitation method by addition of 0.5 g AgNO₃, c.NH₄OH, 3M HNO₃ and 3M NH₄NO₃. The resulting Ag₃PO₄ was captured on a 0.2 µm polycarbonate membrane filter and transferred to a glass vial and dried at 40 °C. 0.5 mL 15% H₂O₂ was added to each vial and left to decompose any remaining organic compounds and then removed by evaporation at 40 °C overnight, and finally washed with 3 x ~1.5 mL MilliQ water, centrifuged at 3500 RCF for 20 minutes and dried.

Ag₃PO₄ samples were analysed for $\delta^{18}O_p$ on an IsoPrime100 mass spectrometer coupled to a varioPYRO cube elemental analyser. For each sample, 400-700 µg Ag₃PO₄ was weighed out into a silver capsule with 800 µg carbon black, dried at 40°C

overnight and converted to CO by pyrolysis in an ash crucible at 1450 °C. The resulting gases passed through Sicapent (phosphorus pentoxide) to remove water vapour. Subsequently, the CO is separated from other impurities, namely N₂, using a purge-and-trap system and helium carrier gas. ¹⁸O/¹⁶O is derived from the integrated mass 28 (¹²C¹⁶O) and 30 (¹²C¹⁸O; ¹⁴C¹⁶O; ¹³C¹⁷O) signals from the sample CO pulse, compared to those in an independently introduced pulse of pure CO reference gas. These ratios are then calibrated to the Vienna-Standard Mean Ocean Water (VSMOW) scale in per mille notation (‰) using standards – NBS127 (+9.3‰), EM Ag₃PO₄ (+21.7‰) and Acros Ag₃PO₄ (+14.2‰). Analytical precision based on two standard errors for repeat analysis of the quality control (Acros Ag₃PO₄) is better than ±0.3‰_{VSMOW}.

Unfiltered field samples were analysed for δ¹⁸O_w using an equilibration method on an IsoPrime100 mass spectrometer coupled to an IsoPrime Multiflow inlet. 200 µL of heated (40°C) sample was left for ~15 hours to equilibrate with the equilibration CO₂ gas. The resulting headspace gas was then sampled and passed to the Isoprime for isotopic analysis. ¹⁸O/¹⁶O ratios are then calibrated to the Vienna-Standard Mean Ocean Water (VSMOW) scale in per mille notation (‰) using standards – LEC LIGHT (-15.0‰) and LEC HEAVY (-1.5‰). The analytical precision obtained for repeat analysis of the quality control (LEC TAP) is better than ±0.15‰_{VSMOW}.

The δ¹⁸O_p value predicted for a system at thermodynamic equilibrium with δ¹⁸O_w was calculated using **Equation 4** and is denoted as δ¹⁸O_{eq} (Chang and Blake, 2015).

$$1000 \ln \alpha_{eq-w} = (14.43(\pm 0.39) \times 1000/T) - 26.54(\pm 1.33) \quad (4)$$

where T is in degrees Kelvin, and:

$$\alpha_{eq-w} = \frac{(\delta^{18}O_{eq} + 1000)}{(\delta^{18}O_w + 1000)} \quad (4a)$$

4.3 Results

Data for selected field and laboratory parameters are reported in **Table 4.2**. Across both seasons, dissolved organic carbon (DOC) concentrations tended to increase with distance downstream, particularly across sites A-D; however, substantial reductions in river DOC concentrations were associated with inputs from both the WWTP effluent and the tributary to the main river stem. In samples collected during March 2015, nitrate (NO_3^-) concentrations indicated the opposite spatial pattern compared to DOC concentrations, tending to decrease downstream including following the input of the tributary to the main stem, although with a substantial increase in nitrate concentration immediately downstream of the WWTP effluent input. However, the NO_3^- concentration profile in samples A-D from September 2015 was more variable than in March 2015 although, similarly to March 2015, NO_3^- concentrations increased substantially following the input of WWTP effluent to the river and decreased following the input of the tributary. No particularly strong or consistent trends in the dissolved oxygen (DO), pH, electrical conductivity (EC) or alkalinity profiles were observed in either season. However, DO concentrations decreased substantially between sites C and D in September 2015, a pattern that was not observed in samples collected in March 2015.

Table 4.2: Dissolved (0.45µm filtration) nutrient concentrations and temperatures of surface water samples in the Beult catchment. Soluble reactive P (SRP) concentration values are given to 3 decimal places; temperature, pH, dissolved oxygen (DO) to 1 decimal place; electrical conductivity (EC) and alkalinity to 3 significant figures; and the remaining parameters to 2 decimal places.

	Distance downstream from site A	[SRP]	[DOC]	[NO ₃ ⁻]	T	DO	pH	EC	Alkalinity	
	/km	/mg P.L ⁻¹	/mg C.L ⁻¹	/mg N.L ⁻¹	°C	mg. L ⁻¹		µS. cm ⁻¹	mg HCO ₃ .L ⁻¹	
March 2015	A	0.00	0.187	4.47	7.29	7.7	10.5	8.4	718	341
	B	0.49	0.334	7.97	5.66	6.7	9.3	8.2	742	332
	C	0.93	0.293	10.47	3.38	6.2	9.4	8.3	655	297
	D	1.14	0.293	10.06	3.71	6.1	9.2	8.2	1280	293
	W*	1.38	1.190	5.67	18.22	8.8	7.4	8.0	839	247
	E	1.42	0.839	7.73	12.39	7.4	9.4	8.1	776	261
	F	2.11	0.691	10.13	9.44	7.4	10.5	8.4	726	271
	T*	2.15	0.152	4.36	5.84	7.3	11.1	8.4	659	297
	G	2.18	0.307	5.86	6.77	7.3	10.9	8.4	681	315
	H	3.63	0.290	6.67	6.51	7.2	11.2	8.5	782	274
I	4.13	0.293	6.82	6.48	7.3	11.1	8.5	781	268	
September 2015	A	0.00	0.472	4.39	8.16	18.1	9.7	7.8	829	330
	B	0.49	0.063	8.83	2.20	14.3	9.2	7.6	1050	255
	C	0.93	0.254	15.07	14.34	13.5	13.2	8.2	812	461
	D	1.14	1.092	13.20	2.74	13.3	4.1	7.7	902	327
	W*	1.38	1.799	6.30	18.74	15.2	8.1	7.4	1020	296
	E	1.42	1.782	5.87	18.55	15.2	8.9	7.4	1030	289
	F	2.11	1.767	5.84	18.26	14.1	10.1	8.0	1010	284
	T*	2.15	0.162	2.67	8.60	13.2	10.4	8.2	796	306
	G	2.18	0.670	3.23	11.78	13.6	10.4	8.2	863	310
	H	3.63	0.620	3.65	11.29	13.3	9.7	8.2	868	307
I	4.13	0.582	3.88	11.09	13.3	10.1	8.2	866	313	
Tap water	n/a	0.146	b.d.	3.91	15.4	-	-	-	-	

*Sites T and W represent the inputs from a tributary and the WWTP effluent respectively.

b.d.: below limit of detection

There was a significant seasonal difference between surface water temperatures across March and September 2015 (**Figure 4.4**). However, the spatial pattern of water temperature along the reach was similar for both sampling events, with increases in river water temperature driven by the input of WWTP effluent in both seasons. In samples collected during the September event, river water temperature immediately downstream of the effluent input effectively equalled the water temperature within the effluent itself, whilst this was not observed to the same extent in samples collected in March 2015. Across sites G, H and I, water temperatures were relatively constant in

both March and September 2015, in contrast to sites A-D across which decreases in water temperatures were observed in both sampling events.

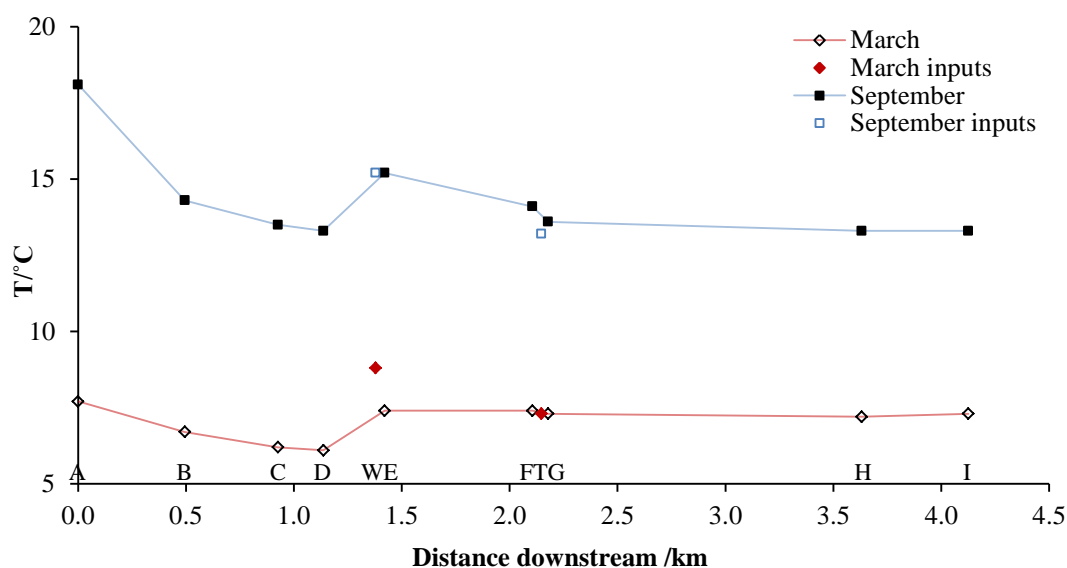


Figure 4.4: Surface water temperature in samples from the River Beult catchment collected during March and September 2015. Main stem sites are connected with lines, inputs to the river are plotted at the point at which they would enter the main stem, i.e. W = 1.38 km, and T = 2.15 km. Site labels have been added to all figures within this chapter.

Table 4.2 and **Figure 4.5** report SRP concentration data, for the purposes of this thesis taken to be analogous to the concentration of P_i . In general, a similar spatial pattern in SRP concentration emerged in both March and September sampling events, with a significant increase in concentration associated with the input of WWTP effluent to the main river stem. In samples from the March sampling event, SRP concentration within the river increased from 0.293 (site D) to 0.839 mg P.L⁻¹ (site E) following the effluent input, which itself had a SRP concentration of 1.190 mg P.L⁻¹. Despite this increase, the concentration of SRP at site E remained only approximately 70% of that in the final effluent. In contrast, in samples from September there was a significant increase in SRP concentration between sites C and D (with site D located 240 m upstream of the effluent input), followed by a further increase in SRP concentration between sites D and E, such that SRP concentration in the river at site E reached a similar value to that in the effluent. Downstream of the effluent input the SRP concentration remained elevated until the input of a tributary at 2.15 km downstream of site A with a low SRP concentration (site T, 0.152 and 0.162 mg P.L⁻¹ for March and September respectively), resulting in a decrease in SRP concentration

within the main river stem. During both the March and September sampling events, the concentration of SRP remained relatively stable between sites G and I.

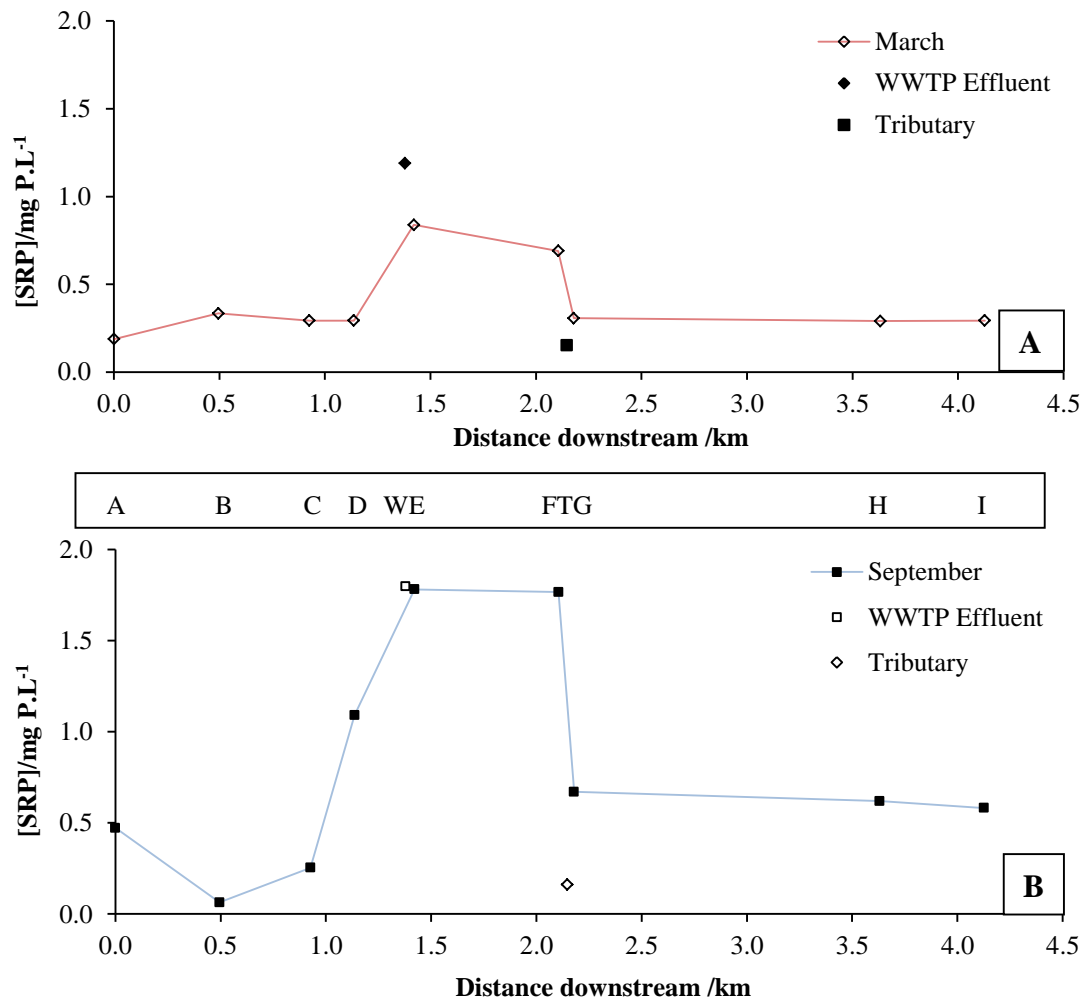


Figure 4.5: SRP concentrations in samples from the River Beult catchment in March (A) and September (B) 2015. Main stem sites are connected with lines, inputs to the river are plotted at the point at which they would enter the main stem, i.e. W = 1.38 km, and T = 2.15 km.

Figure 4.6 reports the molar ratio of dissolved inorganic N to dissolved inorganic P (with N as NO_3^- and P as SRP). All river sites, alongside the WWTP effluent and the tributary, indicated a molar ratio greater than 20, apart from site D in September 2015 where the ratio decreased to 5.54. However, typically N to P ratios also include ammonium concentrations, but these were not determined in this research meaning that site D in September may not have been considered N-limited if NO_3^- and NH_4^+ had been determined (Sander and Moore, 1979). However, regardless of the absolute value of N:P at site D in September 2015, it is clear that a substantial decrease in this molar ratio occurred compared to site C. Contrasting trends in N to P ratios were

observed along the upper 1.4 km of the River Beult (sites A-D) between the two sampling events. During March, N:P decreased across sites A-C before a small increase between sites C and D. During September, N:P exhibited a steep increase across sites A-C before a substantial decrease between sites C and D. Samples collected during both seasons revealed a stepped increase in N:P at the confluence between the main river stem and the tributary (2.15 km), with higher N:P in the tributary resulting in an increase in this molar ratio with the River Beult between sites F and G. Downstream of site G, molar N:P was relatively stable in both March and September 2015.

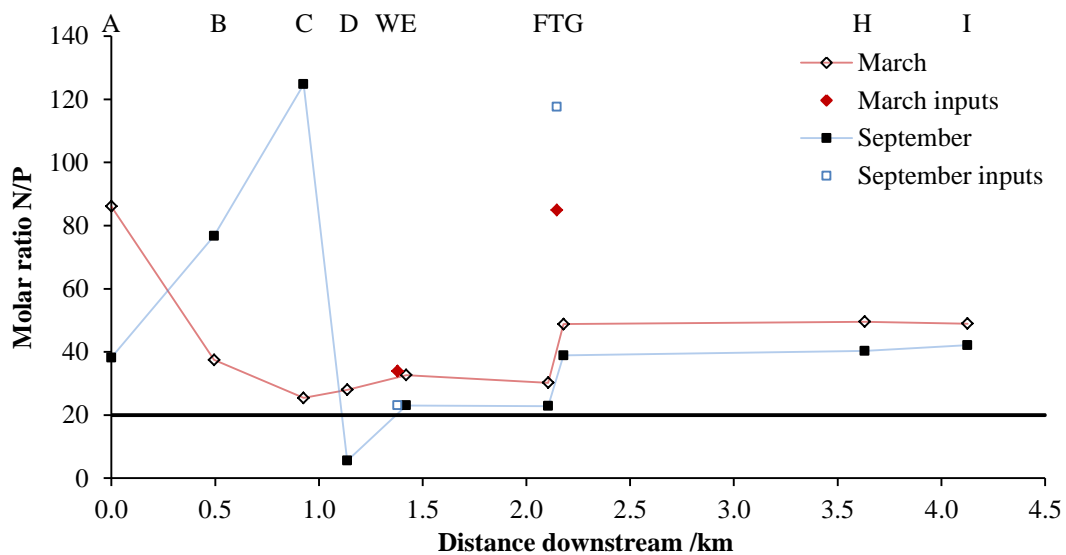


Figure 4.6: Molar N:P from samples collected in the Beult catchment during March and September 2015. Main stem sites are connected with lines, inputs to the river are plotted at the point at which they would enter the main stem, i.e. W = 1.38 km, and T = 2.15 km.

Table 4.3 reports the oxygen isotope composition of P_1 and H_2O , as well as the theoretical equilibrium $\delta^{18}O_p$ value ($\delta^{18}O_{eq}$) calculated using **Equation 4**, for both March and September sampling events. The final data column in **Table 4.3** reports the difference between the measured $\delta^{18}O_p$ and the calculated theoretical $\delta^{18}O_{eq}$.

Table 4.3: Oxygen isotope composition of phosphate ($\delta^{18}\text{O}_p$), water ($\delta^{18}\text{O}_w$) and the theoretical equilibrium ($\delta^{18}\text{O}_{eq}$) for samples in the Beult catchment. The oxygen yields of Ag_3PO_4 precipitates are given to 1 decimal place, a pure Ag_3PO_4 molecule would contain 15.3% oxygen. Isotope compositions and distances given to 2 decimal places.

		Distance downstream from site A	Mean $\delta^{18}\text{O}_p$	n	Range / $1\sigma^\dagger$	Mean O yield	Mean $\delta^{18}\text{O}_w$	n	Range / $1\sigma^\dagger$	$\delta^{18}\text{O}_{eq}$	$\delta^{18}\text{O}_p -$ $\delta^{18}\text{O}_{eq}$
		/km	/‰		/‰	%	/‰		/‰	/‰	/‰
March 2015	A	0.00	16.60	1	-	14.9	-7.06	2	0.20	17.92	-1.31
	B	0.49	17.81	1	-	14.9	-6.83	2	0.55	18.34	-0.53
	C	0.93	16.73	1	-	14.9	-6.67	2	0.81	18.60	-1.86
	D	1.14	16.63	1	-	15.0	-6.68	2	0.15	18.60	-1.97
	W*	1.38	16.15	2	0.57	15.6	-7.32	2	0.09	17.44	-1.29
	E	1.42	15.10	2	0.51	15.3	-7.06	2	0.45	17.97	-2.86
	F	2.11	15.96	2	0.83	15.0	-6.93	2	0.00	18.10	-2.14
	T*	2.15	15.86	1	-	14.5	-7.11	2	0.03	17.94	-2.08
	G	2.18	16.27	2	0.50	14.6	-7.09	2	0.11	17.95	-1.69
	H	3.63	16.49	1	-	15.5	-7.08	2	0.11	17.99	-1.49
I	4.13	15.90	1	-	15.2	-7.12	2	0.03	17.93	-2.03	
September 2015	A	0.00	17.03	3	0.08	15.6	-6.67	1	-	16.44	0.58
	B	0.49	15.62	1	-	15.2	-5.47	1	-	18.34	-2.72
	C	0.93	16.03	3	0.11	15.1	-5.36	1	-	18.59	-2.57
	D	1.14	15.90	3	0.04	15.5	-5.41	3	0.02	18.59	-2.69
	W*	1.38	16.13	3	0.12	15.5	-6.87	3	0.09	16.75	-0.62
	E	1.42	16.25	3	0.25	15.2	-6.84	1	-	16.78	-0.53
	F	2.11	16.21	3	0.16	15.4	-6.83	1	-	16.98	-0.77
	T*	2.15	16.01	3	0.08	15.2	-6.72	1	-	17.26	-1.25
	G	2.18	15.81	3	0.37	15.2	-6.70	1	-	17.21	-1.39
	H	3.63	15.70	3	0.07	15.4	-6.78	1	-	17.18	-1.48
I	4.13	15.96	3	0.27	15.1	-6.67	1	-	17.29	-1.34	
Tap water	n.a.	15.51	3	0.22	14.9	-7.46	3	0.03	16.11	-0.60	

[†]n is the number of repeats for TCEA-IRMS analysis from one Ag_3PO_4 precipitate. If n = 2, instrument range is quoted, if n = 3 the uncertainty is 1 standard deviation.

*Sites T and W characterise the inputs to the main river stem from a tributary and the WWTP effluent respectively.

Measured $\delta^{18}\text{O}_p$ shows substantial variability along the river transect during both sampling events (**Figure 4.7**). Contrasting changes in $\delta^{18}\text{O}_p$ were observed between sites A-D when comparing samples collected in March and September 2015. The transect based on samples collected in March 2015 showed an increase of 1.21‰ between sites A and B, whereas a decrease of 1.41‰ was observed between the same sites in September 2015. In March, a consistent decrease in $\delta^{18}\text{O}_p$ was observed across sites B-D, whereas in September a gradual increase in $\delta^{18}\text{O}_p$ was observed across these sites. Very little difference was observed in $\delta^{18}\text{O}_p$ within the WWTP effluent, with values only changing by 0.02‰ across the two sampling events. Whilst the input of effluent to the River Beult in September 2015 generated a $\delta^{18}\text{O}_p$ value at site E that

was very similar to $\delta^{18}\text{O}_p$ within the effluent itself, $\delta^{18}\text{O}_p$ at site E was approximately 1‰ lower than the value within the effluent for samples collected in March 2015. Downstream of site E, the variation in $\delta^{18}\text{O}_p$ followed almost completely opposite patterns in March and September 2015, although both profiles converged towards very similar absolute $\delta^{18}\text{O}_p$ values (15.90 and 15.96‰) at the most downstream site, I, in both seasons.

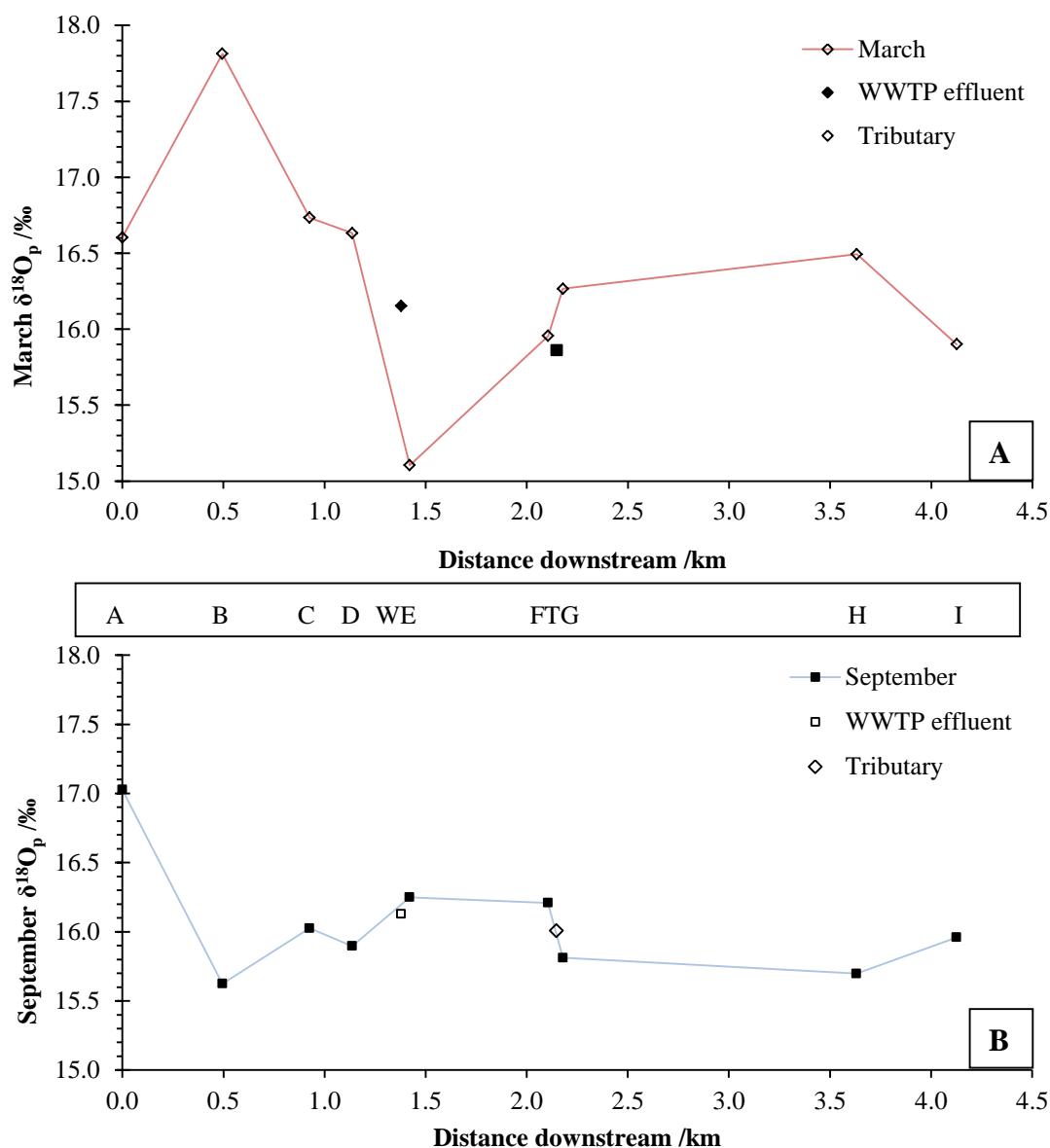


Figure 4.7: Mean $\delta^{18}\text{O}_p$ for sites in the River Beult catchment in March (A) and September (B) 2015. Main stem sites are connected with lines, inputs to the river are plotted at the point at which they would enter the main stem. Analytical uncertainty based on 2 standard errors of the Acros Ag_3PO_4 standard measurements is $\pm 0.3\text{‰}$.

A distinct pattern in $\delta^{18}\text{O}_w$ was observed within the River Beult (**Figure 4.8**), although this pattern was largely consistent across both seasons with the main difference being the magnitude of variations between individual sampling sites. Changes in $\delta^{18}\text{O}_w$ between sites D and E largely reflected the input of WWTP effluent in both seasons, whilst $\delta^{18}\text{O}_w$ of the tributary input to the River Beult is reflected in changes in $\delta^{18}\text{O}_w$ between sites F and G in both seasons. Downstream of site G, $\delta^{18}\text{O}_w$ remained relatively constant in both March and September 2015.

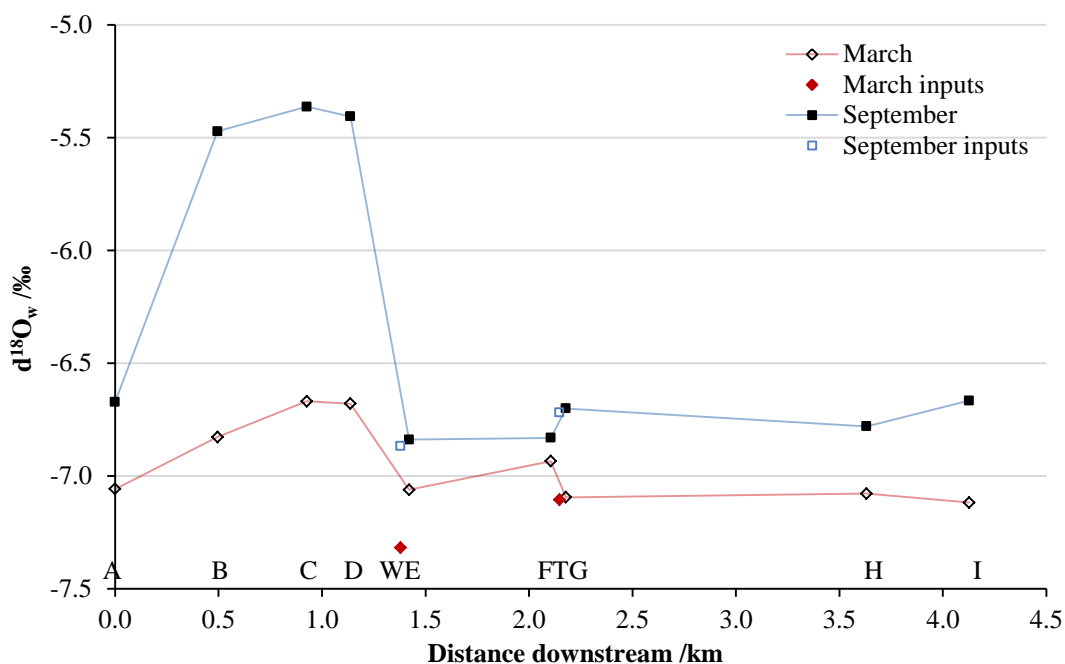


Figure 4.8: Mean $\delta^{18}\text{O}_w$ for samples collected from the River Beult catchment in March and September 2015. Analytical uncertainty based on 2 standard errors of the LEC TAP standard measurements is $\pm 0.15\%$. Main stem sites are connected with lines, inputs to the river are plotted at the point at which they would enter the main stem, i.e. W = 1.38 km, and T = 2.15 km.

Although there were significant variations in the difference between measured $\delta^{18}\text{O}_p$ and the temperature dependent equilibrium value ($\delta^{18}\text{O}_{eq}$) along both the March and September 2015 transects, measured $\delta^{18}\text{O}_p$ was always $\geq 0.5\%$ from $\delta^{18}\text{O}_{eq}$ in all samples collected during both sampling events. Only the sample from site A in September 2015 revealed $\delta^{18}\text{O}_p > \delta^{18}\text{O}_{eq}$ (**Figure 4.9**). Changes in $\delta^{18}\text{O}_p - \delta^{18}\text{O}_{eq}$ between individual sampling sites revealed almost completely opposite patterns in March compared to September 2015. These patterns indicated that, whilst WWTP effluent and tributary inputs to the main river stem played very significant roles in controlling the difference between $\delta^{18}\text{O}_p$ and $\delta^{18}\text{O}_{eq}$ in samples from September, these effects were less pronounced in samples collected during March.

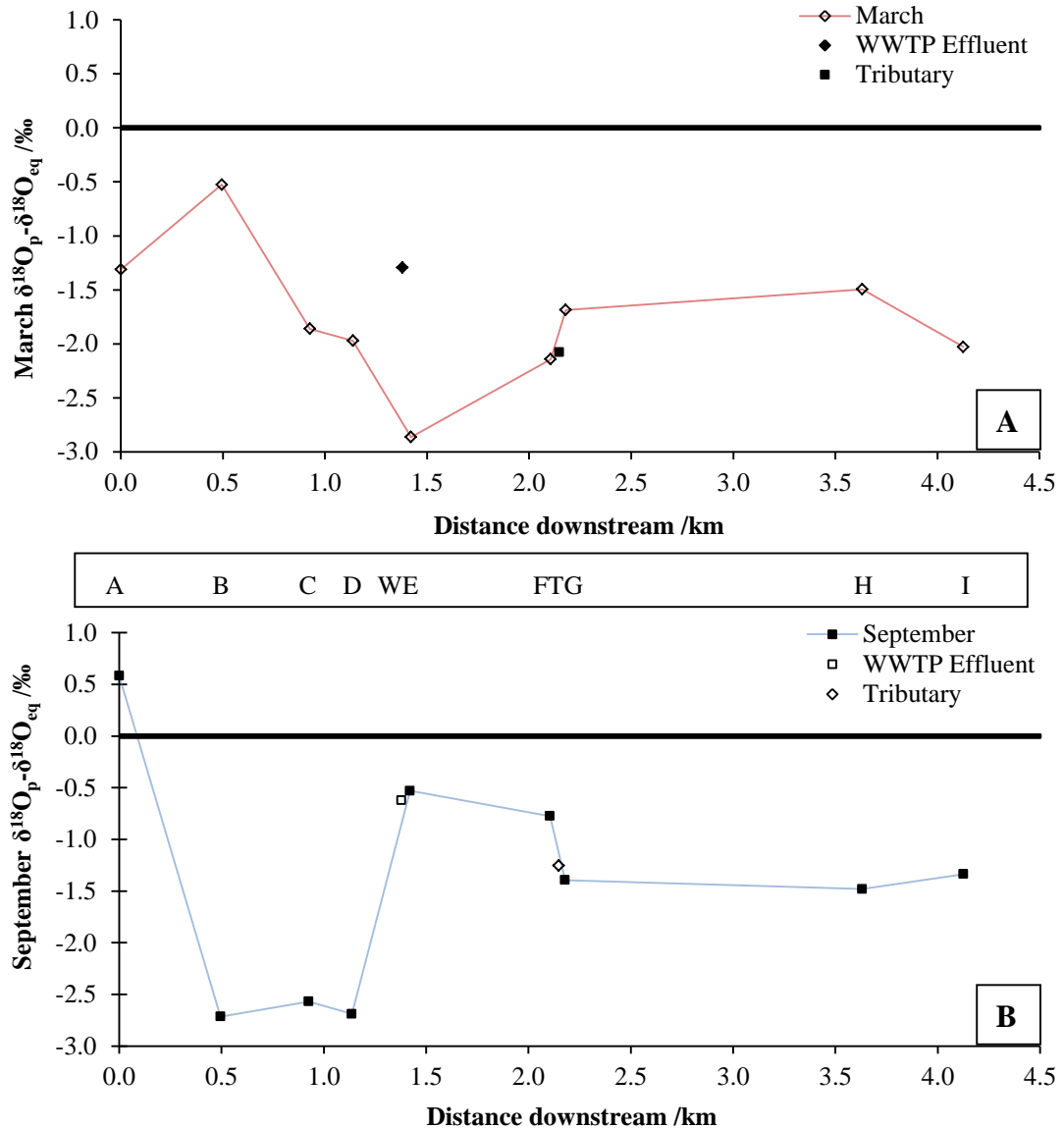


Figure 4.9: Difference between calculated equilibrium ($\delta^{18}\text{O}_{\text{eq}}$) based **Equation 4** and the mean measured $\delta^{18}\text{O}_{\text{p}}$ for sites in the River Beult catchment in March and September 2015. At $\delta^{18}\text{O}_{\text{p}} - \delta^{18}\text{O}_{\text{eq}} = 0$, $\delta^{18}\text{O}_{\text{p}}$ is assumed to be at temperature dependent equilibrium with $\delta^{18}\text{O}_{\text{w}}$. Main stem sites are connected with lines, inputs to the river are plotted at the point at which they would enter the main stem.

4.4 Discussion

The aim of this chapter was to evaluate the potential for $\delta^{18}\text{O}_{\text{p}}$ to be used as a tracer of P_i inputs to the headwater reaches of a river network and to identify the biogeochemical processes influencing the downstream transport of P_i within the river network. This aim led to two hypotheses:

- i) The input of P_i to a river from a point source (WWTP effluent) can be identified on the basis of an isotopically distinct $\delta^{18}O_p$ signature compared to upstream sources of P_i .
- ii) Metabolic processes will influence the downstream transport of P_i following input from a point source, leading to isotope effects or isotope fractionations that will enable the specific processes to be identified.

In order to test these hypotheses, river profiles of SRP (analogous to P_i) concentrations, in conjunction with $\delta^{18}O_p$ and $\delta^{18}O_{eq}$, were analysed on the River Beult. In all of the profiles there were differences between the March and September sampling campaigns. Below, the insights into in-river P biogeochemistry provided by these data are explored, in terms of both spatial changes along the in-river transects and the difference between seasons.

4.4.1 In-river phosphorus biogeochemistry revealed by bulk hydrochemical data

The SRP concentration profiles within the River Beult (**Figure 4.5**) from March and September 2015 demonstrated clear similarities. During both sampling events, SRP concentrations within the main river stem were noticeably influenced by the input of final effluent from Sutton Valence WWTP and by water from a tributary joining the main river stem. Specifically, SRP concentrations within the WWTP effluent were considerably higher than all upstream sites (A-D) in both sampling events, which resulted in elevated SRP concentrations in the river immediately downstream of the effluent input. This was especially evident under low flow conditions (September), when the in-river SRP concentration remained within $0.032 \text{ mg P.L}^{-1}$ of the final effluent SRP concentration up to 730 m downstream of the effluent input. In contrast, in samples collected during March 2015 SRP concentration at sample site E (40 m downstream) remained $0.351 \text{ mg P.L}^{-1}$ below that within the effluent. Therefore, under low flow conditions (September 2015), it appears that the final effluent from the WWTP was the primary determinant of in-river SRP concentration for a significant distance downstream of the effluent entry point into the river. Under higher flow conditions (March 2015), SRP concentrations downstream of Sutton Valence WWTP were governed by the combined effects of upstream sources and the input of final

effluent. The SRP data reported above are consistent with the findings reported by Goody *et al.* (2016) from an in-stream transect of more limited length, based on samples collected in September 2013 and January 2014. The dominant influence of WWTP effluent on in-river SRP concentration at site E under low flow conditions, alongside evidence of combined controls on downstream river conditions exerted by both upstream river water and effluent under high flow conditions, was also observed in the DOC, NO₃⁻ and electrical conductivity profiles reported in this chapter (**Table 4.2**). This pattern is characteristic of WWTP effluent-impacted streams within which, under low flow conditions in particular, in-river hydrochemical conditions can be largely, or indeed solely, determined by the properties of the effluent. Under higher flow conditions, effluent inputs are diluted to a greater extent by the larger volume of water delivered to main river stem from upstream areas of the catchment (Withers and Jarvie, 2008; Bowes *et al.*, 2015).

The impact of the tributary that entered the main stem of the River Beult between sample sites F and G is also revealed through changes in SRP concentration, in which sharp decreases in SRP concentration were observed between these sample sites in both sampling events. Changes in SRP concentration between sites F and G suggest that tributary water diluted water within the River Beult that was dominated by WWTP effluent at site F. Dilution effects, whether through the addition of storm water or more permanent features such as tributaries, are frequently observed in studies of nutrient cycling in freshwaters (e.g. Hooda *et al.*, 1997; Young *et al.*, 1999). Dilution is also supported by trends in DOC, NO₃⁻ and electrical conductivity profiles, each of which suggests that dilution occurs between sample sites F and G as a result of the input of tributary T to the main River Beult (**Table 4.2**). However, dilution effects as a result of tributary input cannot be the sole cause of changes in the concentration of SRP along the transect of the River Beult sampled for the purposes of this chapter. For example, a substantial decrease in SRP concentration occurred between sample sites A and B in September 2015, and between sample sites E and F in March 2015. Between these sites, no significant surface water tributary enters the River Beult. Furthermore, increases in SRP concentration were observed at other locations along the sampled transect, including between sample sites A and B in March 2015 and between sites C and D in September 2015, where no obvious tributary or effluent input occurred. Such changes in SRP concentration are associated with additional

sources of SRP or with biogeochemical processes that control the in-stream fate of SRP. These biogeochemical processes could include biological uptake of SRP, adsorption or chemical precipitation of SRP, or the regeneration of SRP from organic P compounds. However, without the use of an inherent tracer of P_i , it is impossible to differentiate between the multiple potential processes and sources that could be responsible for SRP concentration changes within a river. In this context, $\delta^{18}O_p$ may provide additional insights into the controls on SRP within river networks, alongside the importance of SRP from specific sources for metabolic processes operating within rivers. Therefore, subsequent sections of this chapter examine the additional insights into the controls on P within the River Beult that are provided through isotopic analysis.

4.4.2 Insights into the sources and biogeochemical cycling of P through stable isotope analysis

To illustrate the role that $\delta^{18}O_p$ can play in elucidating processes that alter the bulk P_i pool but cannot be determined by changes in SRP concentration alone, the sampled reach of the River Beult was considered as three separate sections:

- Section 1 (sites A-D): The first 1.14 km of the reach, ending with the last site (site D) upstream of the final effluent from Sutton Valence WWTP.
- Section 2 (sites D-F, W): Between distances 1.14 and 2.11 km, this reach includes site D – 240 m upstream of the WWTP effluent input (W), and sites E and F which are downstream of the input site by 40 and 730 m respectively.
- Section 3 (sites F-I, T): Between distances 2.11 and 4.13 km and including the input of tributary (T).

4.4.2.1 Section 1 (sites A-D)

This section flows through a predominantly rural setting where the main sources of P are associated with agriculture. Similar absolute $\delta^{18}O_p$ ranges for these sites were observed under both high and low flow conditions – 16.60-17.81‰ and 15.62-17.03‰ respectively. These data sit within the global range of anthropogenic fertilisers (15.5-25.3‰) reported in **Table 2.2** which would be expected for an

agriculturally dominated area, but were consistently lighter than samples collected from equivalent sites that are reported in Gooddy *et al.* (2016) (**Table 4.4**).

Table 4.4: Comparison of the key variables across the four directly comparable sample sites to Gooddy *et al.* (2016), in which low flow sampling was conducted in September 2013 and high flow sampling in January 2014.

		This study			Gooddy <i>et al.</i> , 2016			
Site Name		[SRP] mg P.L ⁻¹	$\delta^{18}\text{O}_p$ /‰	$\delta^{18}\text{O}_p - \delta^{18}\text{O}_{eq}$ /‰	Site Name	[SRP] mg P.L ⁻¹	$\delta^{18}\text{O}_p$ /‰	$\delta^{18}\text{O}_p - \delta^{18}\text{O}_{eq}$ /‰
Low flow	B	0.063	15.62	-0.53	SV1	2.090	16.7	0.1
	D	1.092	15.90	-1.97	SV2	1.296	16.6	-1.5
	W	1.799	16.13	-1.29	SV4	0.948	15.4	-0.8
	E	1.782	16.25	-2.86	SV7	0.948	15.1	-1.2
High flow	B	0.334	17.81	-2.72	SV1	0.181	18.6	0.1
	D	0.293	16.63	-2.69	SV2	0.301	19.0	0.5
	W	1.190	16.15	-0.62	SV4	1.036	16.8	-0.4
	E	0.839	15.10	-0.53	SV7	0.524	17.6	-0.7

Between sites A and B, the River Beult flowed through an underground culvert, although the majority of flow was diverted into an irrigation pond prior to entering the culvert during the September 2015 sampling. The large differences observed in the majority of measured variables (**Tables 4.2** and **4.3**) between these sites in both seasons suggest that further inputs to the stream occur within this underground section. This is evidenced, particularly in September, by the marked increase in $\delta^{18}\text{O}_w$ between sites A and B (**Figure 4.8**), suggesting that the changes are likely due to the introduction of a new water source, rather than biogeochemical processes. In terms of SRP and $\delta^{18}\text{O}_p$, this addition appears to be of a lower SRP concentration and $\delta^{18}\text{O}_p$ compared to site A under low flow conditions, whilst being slightly higher in SRP concentration and $\delta^{18}\text{O}_p$ under high flow conditions.

Under high flow conditions (March 2015), despite a relatively constant SRP concentration between sites B-D, there was a large decrease in $\delta^{18}\text{O}_p$ coupled with an increase in the difference between measured $\delta^{18}\text{O}_p$ and the theoretical equilibrium, $\delta^{18}\text{O}_{eq}$ (**Figure 4.9a**). Because the stable isotope composition of P_i changed between these sites, metabolism must have influenced the downstream transport of P, a fact that is not discernible from SRP concentration data alone. The increasing divergence between $\delta^{18}\text{O}_p$ and $\delta^{18}\text{O}_{eq}$ suggests that intracellular metabolism of P_i was not

responsible for the observed changes in $\delta^{18}\text{O}_p$ between sites B and D in March 2015. If intracellular metabolism had been dominant, river $\delta^{18}\text{O}_p$ would be expected to converge on the theoretical $\delta^{18}\text{O}_{\text{eq}}$ (Blake *et al.*, 1997; Puc at *et al.*, 2010; Chang and Blake, 2015). However, extracellular hydrolysis of P_{org} compounds has the potential to result in a decrease in $\delta^{18}\text{O}_p$ through two processes: inheritance effects and kinetic fractionation. Firstly, inheritance effects occur when a P_{org} compound is enzymatically hydrolysed to P_i and other by-products, with the resulting P_i molecule retaining a proportion of the O atoms from the original P_{org} molecule. The remaining O atoms in the resulting P_i atom that are not inherited from P_{org} are instead donated from the surrounding river water, with a kinetic fractionation operating in this process in favour of incorporation of ^{16}O in the P_i . Secondly, a kinetic fractionation occurs through reactions in which P_{org} molecules with different $\delta^{18}\text{O}$ composition have different rates of reaction, due to their isotopic composition (Blake *et al.*, 2005). Specifically, $\text{P}-^{18}\text{O}$ bonds are more thermodynamically stable relative to $\text{P}-^{16}\text{O}$ bonds, as they have lower ground state zero potential energies and therefore will have a higher activation energy relative to their ^{16}O equivalents (Hoefs, 2008). This results in isotopically lighter P_{org} molecules undergoing hydrolysis at a faster rate, due to a lower threshold energy level, and releasing P_i that is isotopically depleted, before any inheritance effect is considered, due to a lighter starting material. The magnitude of both of these effects is dependent on the $\delta^{18}\text{O}$ ratio of the initial P_{org} molecule. The resultant P_i molecule has a $\delta^{18}\text{O}_p$ between that of the source P_{org} molecule and $\delta^{18}\text{O}_w$ (Blake *et al.*, 1997; Colman *et al.*, 2005; Liang and Blake, 2006b). Due to the low mean $\delta^{18}\text{O}_w$ ratios in comparison to the $\delta^{18}\text{O}_p$ values observed in the River Beult, any change in $\delta^{18}\text{O}_p$ as a result of kinetic fractionation during regeneration of P_i from P_{org} would be expected to result in more negative $\delta^{18}\text{O}_p$ within bulk river samples, particularly if P_{org} molecules were isotopically similar or depleted compared to P_i , potentially resulting in the observed decrease in $\delta^{18}\text{O}_p$ between sites B and D in March 2015.

However, extracellular hydrolysis of P_{org} would be expected to increase in-stream SRP concentrations due to the P_i released in the hydrolysis process. An increase in SRP concentration was not observed between sites B and D in March 2015 (**Figure 4.5a**). P_{org} hydrolysis typically occurs in P_i -limited ecosystems to generate P_i to be utilised rapidly by biomass within the water column (Ammerman, 1991; Liang and Blake, 2006b), resulting in no observable change within extracellular SRP concentration.

Biological uptake of extracellular P_i is expected to impart a kinetic isotope effect, particularly over short timescales and where the reaction responsible for the isotope effect does not proceed to equilibrium (Habicht and Canfield, 1997; Blake *et al.*, 2005). However, the isotope effect associated with biological uptake of SRP would involve the preferential uptake of isotopically lighter P_i , i.e. $^{31}P^{16}O_4^{3-}$, compared to isotopically heavier ions, i.e. $^{31}P^{18}O_4^{3-}$. This would result in bulk river $\delta^{18}O_p$ becoming increasingly heavier and is therefore not consistent with the observed changes in river $\delta^{18}O_p$ between sites B and D in March 2015. However, the combined inheritance and kinetic fractionation associated with extracellular P_{org} hydrolysis may have masked any increase in $\delta^{18}O_p$ associated with biological uptake of P_i . Thus, a combination of extracellular hydrolysis of P_{org} and subsequent biological uptake of P_i could explain the trends in both SRP and $\delta^{18}O_p$ data observed between sites B and D on the River Beult in March 2015. This interpretation is further supported by N to P molar ratios which were all substantially greater than the threshold of 20:1 suggested to be indicative of P limitation (Sturner *et al.* (2008).

To evaluate the full role that extracellular hydrolysis of P_{org} played in this environment, the $\delta^{18}O$ of P_{org} compounds within the reach would need to be determined. To date, little research has been undertaken to directly determine $\delta^{18}O$ in P_{org} compounds, with one laboratory study focusing on the effects on $\delta^{18}O$ during different analytical approaches to P_{org} extraction (Liang and Blake, 2006a). Few studies have fully speciated P_{org} compounds in freshwater ecosystems and therefore knowledge of the relative concentration or lability of specific groups of P_{org} compounds in natural freshwater environments remains limited (Espinosa *et al.*, 1999; Turner *et al.*, 2002; Toor *et al.*, 2003; Cade-Menun *et al.*, 2006; Koopmans *et al.*, 2007). Further research is required to fully speciate and to separate P_{org} compounds within freshwaters, to enable $\delta^{18}O$ analyses to be performed on individual P_{org} compounds or classes. Thus, future research should focus on analysis of $\delta^{18}O$ within the phosphate moieties of P_{org} , to both better understand the cycling of P_{org} within aquatic ecosystems and to provide additional information to help interpret $\delta^{18}O_p$ within these ecosystems.

However, a further possibility is that P_i between sites B and D in March 2015 was not controlled predominantly by biological processes. Abiotically, bioavailable P can be

sorbed and desorbed to stream sediments, particularly if they are rich in iron oxides, and ion exchange occurs between the solid and liquid phases (Jarvie *et al.*, 2005; Jarvie *et al.*, 2006). Work by Jaisi *et al.* (2011) under aerobic conditions has shown that two abiotic isotope effects can be seen in two phase systems: a transient kinetic effect and abiotic ion exchange. Transient kinetic effects occur in the early stages of sorption and desorption, in which $^{31}\text{P}^{16}\text{O}_4^{3-}$ ions will be involved in these processes at a slightly faster rate than $^{31}\text{P}^{18}\text{O}_4^{3-}$ ions, leading to residual $\delta^{18}\text{O}_p$ in solution becoming progressively enriched isotopically during sorption and progressively depleted isotopically during desorption. The decrease in $\delta^{18}\text{O}_p$ supports the potential occurrence of desorption between sites B and D during March 2015, although this is not consistent with a relatively constant SRP concentration across the sites unless subsequent processes, such as biological uptake, acted to prevent increases in SRP concentration.

September 2015 represented low flow conditions within the River Beult and differences compared to high flow conditions were observed across sites B-D. In particular, SRP concentrations increased substantially between sites B and D with the most substantial increase between sites C and D, whereas SRP concentrations remained relatively constant between these sites in March 2015. There was also an increase in $\delta^{18}\text{O}_p$ between sites B and D, with relatively stable $\delta^{18}\text{O}_w$ and other hydrochemical parameters in September 2015. Whilst a relatively small shift in $\delta^{18}\text{O}_p$ towards $\delta^{18}\text{O}_{\text{eq}}$ was observed, this was likely driven by the change in water temperature and consequent change in the theoretical equilibrium value. If intracellular metabolism was dominant in this section, a stronger movement of $\delta^{18}\text{O}_p$ towards equilibrium and no net change in SRP concentration would have been expected. Although extracellular hydrolysis of P_{org} would generate an increase in SRP concentration, given the magnitude of the observed increase in SRP concentration it would be expected that $\delta^{18}\text{O}_p$ would be driven to isotopically lighter values as a result of this process, similar to patterns observed in March 2015. However, clearly if $\delta^{18}\text{O}$ of the source P_{org} molecule involved in hydrolysis was isotopically heavier than $\delta^{18}\text{O}_p$ within the river, an inheritance effect may have contributed to the observed increases in $\delta^{18}\text{O}_p$ between sites B and D in September 2015. Similarly, SRP regeneration within river bed sediments during microbial respiration of organic matter may have released P_i into the overlying water, increasing in-river SRP concentrations (Jaisi and

Blake, 2010; Goldhammer *et al.*, 2011a). SRP regeneration has also been shown to cause inheritance effects in regenerated P_i found in marine pore waters (Goldhammer *et al.*, 2011a), resulting in P_i that is in a state of disequilibrium. Consequently, SRP regeneration within the river bed sediments and release of disequilibrated P_i to the water column could result in the increase in both the SRP concentration and $\delta^{18}O_p$.

Finally, it might be the case that an additional source of P entered the river between sites C and D, leading to the substantial increase in SRP concentration alongside a clear decrease in DO and nitrate concentrations (**Table 4.2**), under low flow conditions. Any source of P entering the river at this point would also need to be associated with no substantial change in $\delta^{18}O_p$ or $\delta^{18}O_w$ compared to site C. Further, this potential input was not clearly indicated in the data collected in March 2015 under higher flow conditions. Taken together, these observations are consistent with groundwater discharge to the river. The addition of a nitrate-depleted water source between sites B and D that is only apparent under low flow conditions is also consistent with the findings of Goody *et al.* (2016). However, in the research reported by these authors, there was a 0.86‰ increase in $\delta^{18}O_w$ under low flow conditions between sites B (SV1) and D (SV2), resulting in $\delta^{18}O_w$ of -5.22‰ which is outside the -6 to -7‰ range that is typical for groundwater in this area (Darling *et al.*, 2003). The values of $\delta^{18}O_w$ reported in the current chapter for sites B to D in September 2015 range from -5.36 to -5.47‰, in agreement with those reported by Goody *et al.* (2016). Therefore, although much of the data is characteristic of an additional groundwater input, the $\delta^{18}O_w$ data is not consistent with a groundwater discharge to the river.

4.4.2.2 Section 2 (sites D-F, W)

Within this reach, the final effluent of Sutton Valence WWTP enters the River Beult. There appears to be little difference in the $\delta^{18}O_p$ signature of the effluent between samples collected in March compared to September 2015 ($\Delta = 0.02\text{‰}$), suggesting little evidence of seasonal or temperature-related effects that alter the absolute $\delta^{18}O_p$ value for the WWTP effluent. However, previous research at the same site reported greater variation in final effluent $\delta^{18}O_p$, with values of 15.4 and 16.8‰ under low flow (September) and high flow (January) conditions respectively (Goody *et al.*, 2016). However, the absolute $\delta^{18}O_p$ values reported in this chapter do fall within the range

reported by Goody *et al.* (2016) for the effluent from Sutton Valence WWTP, suggesting that $\delta^{18}\text{O}_p$ for this individual WWTP may be relatively constant. The global dataset for $\delta^{18}\text{O}_p$ from WWTP effluents is reported in **Table 2.1** and ranges from 8.4 to 18.4‰, with a mean $\delta^{18}\text{O}_p$ of 13.5‰ (Gruau *et al.*, 2005; Young *et al.*, 2009). Therefore, the effluent $\delta^{18}\text{O}_p$ values reported in this chapter are consistent with those found in other regions of the world. In order to be able to perform effective source tracing research using $\delta^{18}\text{O}_p$, it is essential that the isotopic composition of a source is constant or varies within a well-constrained range. Temporal and spatial variation might arise due to factors such as different sources of P to individual WWTPs (e.g. isotopic variation in P_i entering a WWTP from an urban area compared to a rural area, or a diurnal variation in P_i sources, or contrasting mixtures of hydrolysable P_{org} compounds that could impart differing inheritance effects on the effluent); different processes occurring within a WWTP (e.g. the presence/absence of P-stripping technology or differing biological treatment approaches which alter bulk P_i or hydrolyse P_{org}); and natural variations in both temperature and $\delta^{18}\text{O}_w$ which would alter the absolute $\delta^{18}\text{O}_p$ during intracellular metabolism. Whilst initial research from Sutton Valence WWTP, alongside other final effluent samples from around the world, suggests that WWTP effluents could be constrained in terms of variation in $\delta^{18}\text{O}_p$, further work is required to determine the extent of temporal or spatial effects on the $\delta^{18}\text{O}_p$ signature of WWTP effluents.

In order to be able to probe the in-river fate of P_i derived from a WWTP using stable isotope techniques, $\delta^{18}\text{O}_p$ within a final effluent sample must differ from $\delta^{18}\text{O}_p$ with a river immediately upstream of the final effluent discharge point. Little research to date has undertaken this type of coupled effluent-river water assessment. Therefore, the potential to use $\delta^{18}\text{O}_p$ to better understand the in-river fate of WWTP-derived P_i remains largely unknown. In the March 2015 sampling event, the difference in $\delta^{18}\text{O}_p$ was 0.48‰ between sites D (240 m upstream of the effluent input) and W (the WWTP final effluent), and in September 2015 the difference was 0.23‰. The analytical precision based on two standard errors of repeated Ag_3PO_4 standards was 0.3‰. This indicates that $\delta^{18}\text{O}_p$ in the WWTP effluent can be considered significantly different to upstream river water under high flow conditions, but under low flow conditions $\delta^{18}\text{O}_p$ within the effluent was similar to that within river water upstream of the WWTP and therefore cannot be used effectively to trace the in-river fate of WWTP-derived P_i . In

contrast, Goody *et al.* (2016) reported differences of 2.2 and 1.2‰ between effluent and upstream river water under high and low flow conditions respectively. Both WWTP effluent samples reported in this chapter were in disequilibrium with respect to $\delta^{18}\text{O}_{\text{eq}}$, with $\delta^{18}\text{O}_{\text{p}}$ being 1.29‰ lighter than $\delta^{18}\text{O}_{\text{eq}}$ under high flow conditions and 0.62‰ lighter than $\delta^{18}\text{O}_{\text{eq}}$ under low flow conditions. This is indicative either of an excess of P_i within the WWTP system, resulting in the incomplete intracellular cycling of influent P_i to the WWTP and retention of source $\delta^{18}\text{O}_{\text{p}}$ signatures, or that disequilibrium processes dominate within the WWTP, such as the regeneration of P_i from P_{org} . In previous research which focussed solely on final effluents from three French WWTPs, isotopic equilibrium was observed with respect to $\delta^{18}\text{O}_{\text{p}}$. However, the values of $\delta^{18}\text{O}_{\text{p}}$ within final effluent samples overlapped with the $\delta^{18}\text{O}_{\text{p}}$ of a phosphate builder within detergent; detergent-derived P_i was estimated to form 50-70% of the final WWTP effluent and it can be suggested that phosphate builders may make up a significant proportion of detergent-derived P_i , and thus, in the case of Gruau *et al.* (2005), the $\delta^{18}\text{O}_{\text{p}}$ in the effluent may have reflected the source signature for a major component of effluent.

Both the March and September 2015 sampling events demonstrated significant changes in the majority of in-river nutrient and isotope profiles between sites D, 240 m upstream of the WWTP effluent input, and E, 40 m downstream of the input. In September 2015, these profiles all reached, or tended towards, the corresponding value associated with the final effluent sample. This indicates that, under low flow conditions, WWTP effluent dominated in-river conditions and over-printed the effects of upstream agricultural sources. Subsequently, between sites E and F there was no obvious change in SRP concentration, $\delta^{18}\text{O}_{\text{p}}$ or N:P ratio. Although there were slight variations in the difference between $\delta^{18}\text{O}_{\text{p}}$ and $\delta^{18}\text{O}_{\text{eq}}$ in this section, samples always remained at least 0.5‰ offset from the theoretical equilibrium. This suggests little evidence of intracellular metabolism of P_i within this section of the River Beult during September 2015. Despite $\delta^{18}\text{O}_{\text{p}}$ within the WWTP effluent being within analytical precision of river water upstream of the effluent entry point, additional consideration of the difference between $\delta^{18}\text{O}_{\text{p}}$ and $\delta^{18}\text{O}_{\text{eq}}$ indicates that WWTP-derived P was not strongly coupled with intracellular metabolic processes within the river, at least over the 730 m reach of the River Beult between the effluent entry point and sample site F.

In rivers within the UK that are heavily influenced by the input of effluent from WWTPs, SRP concentrations peak in the period August to October and are lowest in March to May, as driven by variable dilution of the effluent across the hydrological year (Bowes *et al.*, 2011). This is consistent with the two sampling campaigns reported in this chapter, with SRP concentrations in September typically exceeding those in March. However, in March 2015, $\delta^{18}\text{O}_p$ at site E was substantially lower than both the WWTP effluent and the upstream river water at sample site D. Consequently, this cannot be the result of a simple mixing process between the upstream river water and WWTP effluent, because under conditions of simple mixing the $\delta^{18}\text{O}_p$ at site E would fall within the range defined by $\delta^{18}\text{O}_p$ at sites D and W. Thus, the change in $\delta^{18}\text{O}_p$ between sites D and E must be the product of one or more processes operating to influence $\delta^{18}\text{O}_p$ that are not revealed on the basis of hydrochemical data alone (**Table 4.2**), which are all consistent with a mixing effect controlling conditions at site E in March 2015. Processes that may be responsible for the observed decrease in river $\delta^{18}\text{O}_p$ and increased divergence between $\delta^{18}\text{O}_p$ and $\delta^{18}\text{O}_{eq}$ at site E compared to site D include extracellular hydrolysis of P_{org} , desorption of P_i from bed sediments and abiotic ion exchange with river bed sediments. Due to the magnitude and the rate of the $\delta^{18}\text{O}_p$ shift between sites D and E in March 2015, alongside the likely input of readily hydrolysable P_{org} compounds within the WWTP effluent, extracellular hydrolysis of P_{org} and the generation of isotopically depleted P_i through inheritance effects and/or a kinetic fractionation is likely to explain the changes in isotopic composition of P_i between sites D and E. These observations are in contrast to the September 2015 sampling event, which suggests that there were seasonal differences in the extent to which WWTP-derived P was linked to extracellular hydrolysis processes in the River Beult.

Subsequently, between sites E and F under high flow conditions (March 2015), SRP concentrations decreased steadily and $\delta^{18}\text{O}_p$ increased significantly whilst also moving towards $\delta^{18}\text{O}_{eq}$. Between these sample sites, there was only a slight increase in $\delta^{18}\text{O}_w$ and no observable change in temperature, suggesting that the movement of $\delta^{18}\text{O}_p$ towards equilibrium was caused by isotope fractionation influencing the P_i pool. Isotopically, this is consistent with intracellular metabolism occurring within this reach of the River Beult (Blake *et al.*, 1997; Puc at *et al.*, 2010; Chang and Blake, 2015). This is likely the result of the addition of readily available P_i from the WWTP

into a P-limited system, which was subsequently metabolised by primary producers in the river, resulting in isotopic fractionation and a shift in the isotopic composition of P_i toward that expected at theoretical equilibrium. There was also an increase in DOC and decrease in NO_3^- concentrations between sample sites E and F, which is consistent with increasing biomass concentrations and corresponding requirement for bioavailable P, because N:P remains greater than 20 despite the addition of P_i from the WWTP. In the case of intracellular metabolism alone, the in-stream SRP concentrations would not change. However, it is possible that biological uptake and intracellular storage of P_i also occurred within this reach of the River Beult, alongside intracellular metabolism, which would also contribute to increasing values of $\delta^{18}O_p$ and decreasing SRP concentration within river water.

Alternatively, a transient kinetic fractionation due to sorption could also explain an increasing aqueous $\delta^{18}O_p$ and a decrease in SRP concentrations (Jaisi *et al.*, 2011). A chemical analysis of in-river sediments would be a useful addition to this study to determine whether the sediment is iron oxide rich (i.e. has the potential to sorb P_i) and potentially P_i could also be extracted to determine the $\delta^{18}O_p$ of any sorbed P_i phases and see whether it is consistent with a sorption theory.

However, March is during the period of spring blooms (March to May) of phytobenthic organisms in the UK, where SRP concentrations and silica levels both decrease due to algal-related removal of both elements (Bowes and House, 2001; Bowes *et al.*, 2011). During this time, the demand for bioavailable P to support algal production is very high, providing further support to intracellular metabolism and biological uptake as the most likely processes responsible for changes in $\delta^{18}O_p$ in this section of the River Beult. Whether driven by intracellular metabolism or biological uptake, changes in $\delta^{18}O_p$ downstream of Sutton Valence WWTP in March 2015 are consistent with metabolic processes within the river being supported by P_i delivered from final effluent. The effects are observed for at least 700 m downstream of the WWTP, and cannot be robustly identified on the basis of SRP concentration changes alone. These data provide a strong example of the additional potential to probe the fate of P_i within rivers provided by analysis of $\delta^{18}O_p$.

4.4.2.3 Section 3 (sites F-I, T)

Across both March and September sampling events, hydrochemical data generally suggest that mixing between the tributary (T) and upstream river water from site F controlled conditions at site G. However, under high flow conditions (March), the $\delta^{18}\text{O}_p$ profile cannot be explained by mixing alone, because $\delta^{18}\text{O}_p$ at sample site G was heavier than that either at site F or within the tributary. Therefore, an additional process or water source must have influenced P_i between sites F and G under high flow conditions that was not revealed through analysis of hydrochemical data alone. Given the substantial decrease in SRP concentration between sites F and G in March 2015, an additional water source with high SRP concentration entering the River Beult between these sites is believed to be unlikely. The increase in $\delta^{18}\text{O}_p$ and narrowing of the difference between $\delta^{18}\text{O}_p$ and $\delta^{18}\text{O}_{eq}$ may reflect intracellular metabolism of P_i in this reach of the river, or the uptake and storage of P_i within biomass that results in a kinetic isotope effect in which the remaining extracellular P_i becomes isotopically enriched. Between sites G and H in March 2015, the continued increase in $\delta^{18}\text{O}_p$ and further approach of $\delta^{18}\text{O}_p$ towards $\delta^{18}\text{O}_{eq}$, coupled with no obvious change in SRP concentration, is consistent with continued intracellular metabolism of P_i . However, between sites H and I in March 2015, $\delta^{18}\text{O}_p$ decreased and moved further away from $\delta^{18}\text{O}_{eq}$. Because there was no significant change in either SRP concentration or $\delta^{18}\text{O}_w$, the isotopic changes in P_i between sites H and I are unlikely to be due to an additional source of SRP to the River Beult in this reach. This divergence from $\delta^{18}\text{O}_{eq}$ could be the result of abiotic ion exchange, a process in which systems are driven away from $\delta^{18}\text{O}_{eq}$ when aqueous P_i that may have been equilibrated metabolically is abiotically exchanged with P_i ions in the sorbed phase that is still at disequilibrium (Jaisi *et al.*, 2011). However, for a natural setting this process is very slow and therefore is likely to be masked if biological processes are occurring. The processes responsible for the isotopic changes between sites H and I in March 2015 currently remain unclear. Under low flow conditions (September 2015), there was a slight decrease in $\delta^{18}\text{O}_p$ and increase in the difference between $\delta^{18}\text{O}_p$ and $\delta^{18}\text{O}_{eq}$ between sites H and I, although these changes were very close to the analytical precision of the $\delta^{18}\text{O}_p$ method.

4.5 Conclusions

This chapter has shown that P_i derived from Sutton Valence WWTP was isotopically distinct from the upstream P_i under high flow conditions. However, under low flow conditions the difference in $\delta^{18}O_p$ was within the analytical precision of the TCEA-IRMS method. Therefore, the use of $\delta^{18}O_p$ as a tracer of WWTP effluent may be dependent on seasonal variations in river P cycling upstream of the effluent input. In addition, it has been shown that $\delta^{18}O_p$ can be used to detect differences in the in-river biological response to a WWTP effluent over two seasons in a calendar year. The use of $\delta^{18}O_p$ has revealed likely major biological pathways that influence P transport within the Beult that were masked in the hydrochemical data. For example, under high flow conditions in March 2015, extracellular hydrolysis of P_{org} to generate P_i can be determined which would have been interpreted as the physical mixing of two water bodies on the basis of the hydrochemical data alone. Similarly, isotopic evidence for intracellular metabolism, in combination with the biological uptake of P_i , downstream of the WWTP effluent input was also provided, processes which could not be robustly identified using changes in SRP concentration alone. In contrast, in September 2015 under low flow conditions, little isotopic evidence was present to support metabolic processes influencing in-river transport of P. Although it may not always be possible to determine the exact process that governs P transport within a specific river reach, the use of $\delta^{18}O_p$ in combination with hydrochemical data offers evidence for the presence or absence of certain processes that would not be possible to provide on the basis of hydrochemical data alone. In particular, it is possible to observe evidence of metabolic processes that influence the P_i pool that do not alter the bulk SRP concentration within a river, but still have a significant role in biogeochemical cycling of P within aquatic ecosystems.

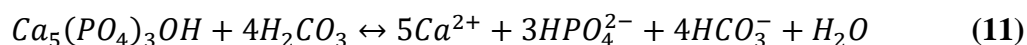
Chapter 5: Application of $\delta^{18}\text{O}_p$ to understand phosphorus sources and cycling within groundwater and a groundwater-fed stream

5.1 Introduction

Phosphate oxygen isotopes have the potential to act as an inherent tracer of the sources and biogeochemical cycling of P_i within, but also between, many ecosystems. However, the global database for $\delta^{18}\text{O}_p$ remains extremely limited and there are a number of ecosystem types in which the utility of $\delta^{18}\text{O}_p$ has yet to be fully assessed. In particular, there have only been three previous studies that have reported $\delta^{18}\text{O}_p$ in groundwaters (Blake *et al.*, 2001; McLaughlin *et al.*, 2006a; Young *et al.*, 2009), resulting in a very limited groundwater $\delta^{18}\text{O}_p$ dataset. In this context, the current chapter reports an application of the $\delta^{18}\text{O}_p$ method developed and reported in **Chapter 3** to groundwater samples derived from springs and boreholes, in order to extend the global library of groundwater- $\delta^{18}\text{O}_p$ through sampling of new aquifer units in the UK. Further, a freshwater river system fed by groundwater springs and, potentially, by groundwater discharge, is also examined to determine whether groundwater sources of P_i , alongside tracing of the subsequent in-river fate of groundwater-derived P_i , can be identified through the application of $\delta^{18}\text{O}_p$ analyses.

Groundwater is often perceived to have only low concentrations of dissolved P_i , due the low solubility of P_i resulting from two major processes (Schwartz and Zhang, 2003; Denver *et al.*, 2010). The first process is the potential for P_i to form metal-phosphate minerals with iron, calcium and aluminium ions, causing P_i to precipitate from solution (Aydin *et al.*, 2009). The second process is the tendency for P_i to sorb to the surface of a number of common minerals, in particular clays and metal

hydr(oxides) such as kaolinite, ferrihydrite and goethite (Edzwald *et al.*, 1976; Geelhoed *et al.*, 1997; Rhoton and Bigham, 2005). However, within some catchments groundwater may be an important source of P_i to surface water ecosystems. For example, depending on bedrock geology, geogenic P_i may be released into groundwater as a result of weathering or dissolution reactions; a common example being the weathering of apatite minerals (**Equation 11**) (Filippelli, 2008):



Apatite minerals can be found in all types of rock as an accessory mineral. However, apatite is commonly found in the form of detrital fluorapatite and authigenic carbonate-fluorapatite in sedimentary deposits and fluorapatite in igneous and metamorphic rocks (Filippelli, 2008; Denver *et al.*, 2010). Beyond apatite, other P-rich minerals include feldspar, phosphorite, vivianite and wavellite (Aydin *et al.*, 2009; Denver *et al.*, 2010). In the most abundant P rock deposits, known as phosphorites, P₂O₅ contents can reach 28-38% and these ores are mined and processed to create a range of products, including inorganic P fertilisers, with 75% of mining ores being found in sedimentary marine deposits. Alternatively, increased P_i concentrations in groundwater may be due to the existence of relatively young soils which contain fewer secondary minerals, meaning that these soils are less able to sorb P_i derived from activities at the ground surface (Boyle *et al.*, 2013; McGinley *et al.*, 2016). Finally, the presence of tile drains that increase the rate of movement of P_i within and through the soil system may also be responsible for increases in P_i concentration within groundwater (Sims *et al.*, 1998).

Despite the widespread assumption that P_i concentrations are not of concern within groundwater, there is emerging evidence to suggest that this represents an oversimplification. For example, it has been shown that many groundwater bodies within south eastern England, UK, have elevated median P_i concentrations (>50 µg P.L⁻¹) and groundwater within the Lower Greensand formation in southern England has P_i concentrations in the range <20 – 311 µg P.L⁻¹, with a mean concentration of 70 µg P.L⁻¹ (Shand *et al.*, 2003; Holman *et al.*, 2010). Within the Lower Greensand aquifer, P_i is thought to be derived from the dissolution of phosphatic nodules present in the lower part of this group (Ruffell, 1992). In addition, phosphatic nodules have also been reported in the Upper Greensand group, another important aquifer in

southern England, as well as in the Gault Clay which lies between the two Greensand groups (Parrish, 1990; Gale, 2012). These nodules can contain 40-60% calcium phosphate (Pigott, 1964). In addition, elevated P_i concentrations ($>30 \mu\text{g P.L}^{-1}$) have been observed in other aquifers, including in the mid-west Republic of Ireland and the east of Scotland, with potentially significant anthropogenic inputs of P_i to these aquifers linked to land use in the area from which groundwater recharge is derived (Holman *et al.*, 2010).

In locations where groundwater containing elevated P_i concentrations discharge to rivers or lakes, P_i concentrations within these surface water ecosystems may rise (Holman *et al.*, 2010; Hampton, 2012a, b). If P_i availability within these ecosystems limits primary production, then delivery of P_i from groundwater has the potential to adversely affect both the chemical and biological status of receiving waters (Holman *et al.*, 2008). However, further research is required to understand whether P_i derived from groundwater is directly linked to metabolism within surface water ecosystems. Furthermore, the understanding of whether P_i in groundwater that discharges to surface water was originally derived from geogenic sources or from human activity at the ground surface is critical for designing suitable management responses to address elevated P_i within surface water systems that receive groundwater discharge (Holman *et al.*, 2010; McDowell *et al.*, 2015).

In this context, an inherent tracer for P, such as $\delta^{18}\text{O}_p$, offers the potential to enhance understanding both of the sources of P entering groundwater and the role of groundwater-derived P_i within surface water ecosystems. However, groundwater has been analysed for $\delta^{18}\text{O}_p$ in only a very limited number of previous studies, with reported data ranging between 15.1 and 22.4‰, with a mean value of 18.6‰ ($n = 9$, $\sigma = 2.13\%$) (**Table 2.1**). The largest study to date sampled only five groundwater sites in Cape Cod, Massachusetts, USA, from a shallow glacial outwash aquifer that had been contaminated by sewage (Blake *et al.*, 2001). This research found evidence within the $\delta^{18}\text{O}_p$ data to suggest that biological processes within groundwater influenced P_i , but that the P_i pool had not reached thermodynamic equilibrium with $\delta^{18}\text{O}_w$ through intracellular metabolism. The contamination with sewage resulted in elevated P_i concentrations (30-108 μM) in the Cape Cod groundwater and the research suggested that complete metabolic turnover of P_i was limited by low dissolved organic

carbon (DOC) concentrations within groundwater. Therefore, it was speculated that in uncontaminated groundwater ($<5\mu\text{M P}_i$), low DOC concentrations would not be a limiting factor for metabolism and, consequently, that P_i within groundwater would be fully metabolised, resulting in $\delta^{18}\text{O}_p$ that was equal to the theoretical equilibrium value, $\delta^{18}\text{O}_{\text{eq}}$. Conversely, Young *et al.* (2009) found that $\delta^{18}\text{O}_p$ ratios of two groundwaters in the San Joaquin River system (California, USA) did not reflect significant biological processing, with +0.7 and -3.2‰ offsets between $\delta^{18}\text{O}_p$ and $\delta^{18}\text{O}_{\text{eq}}$ across two different well depths (4.4 and 32.8 m deep respectively). McLaughlin *et al.* (2006a) used $\delta^{18}\text{O}_p$ analysis in groundwater to explore the possibility that groundwater discharge influences P_i concentrations within Elkhorn Slough, California, USA. These authors suggested that a shift towards lower $\delta^{18}\text{O}_p$ within samples from the slough itself was the result of groundwater discharge. However, given that only two groundwater samples were analysed in this research, the potential for application of $\delta^{18}\text{O}_p$ analysis to help assess the role of groundwater discharge for P cycling within surface water ecosystems remains unclear. Fundamentally, a larger global library of $\delta^{18}\text{O}_p$ for groundwater is required. This expanded dataset would provide insight into whether $\delta^{18}\text{O}_p$ is consistent between groundwater in different geological and wider environmental settings, or whether there are typical variations in $\delta^{18}\text{O}_p$ depending on the geological or environmental setting.

In order for $\delta^{18}\text{O}_p$ to be an effective tracer of P_i source in groundwater, biological cycling of P within groundwater, and the impact of P_i following discharge of groundwater to surface water, groundwater $\delta^{18}\text{O}_p$ must be better constrained and must be distinct from P_i already present in surface water before discharge of P_i from groundwater. Therefore, this chapter is comprised of two components. Firstly, a survey of groundwater is reported to determine if groundwater $\delta^{18}\text{O}_p$ is consistent spatially and temporally, alongside whether $\delta^{18}\text{O}_p$ is distinct compared to the stable isotope composition of other sources of P. The hypothesis tested here is that groundwater $\delta^{18}\text{O}_p$ will vary significantly depending upon the sample type (boreholes versus springs) and the geological unit from which a sample is collected. Secondly, analysis is reported from an in-river transect within a catchment that includes a number of groundwater-fed springs and where the river flows over geological formations that are known to contain phosphatic nodules. The hypothesis for this

second component of the current chapter is that variation in $\delta^{18}\text{O}_p$ within an in-river transect provides evidence of the potential input, and subsequent in-stream fate, of groundwater-derived P_i that is not available without $\delta^{18}\text{O}_p$ analyses.

A secondary aim was to contribute to an in-field method comparison between **Methods 2** and **3** reported in **Chapter 3**. However, this comparison will be discussed in **Chapter 6**, with all data presented in the current chapter based solely on **Method 2**.

5.2 Methodology

The upper Wey catchment in Alton, Hampshire has been identified as a catchment that experiences elevated surface water P_i concentrations, despite the lack of obvious links to P_i sources associated with land use at the ground surface, such as intensive agriculture or wastewater treatment plants (WWTP) in the upper parts of the reach (Hampton, 2012a). This catchment lies in an area underlain by Upper Greensand and Chalk geological formations and is hypothesised to have a significant groundwater input to the surface water ecosystem, associated with groundwater discharge and groundwater-fed springs. Therefore, it was hypothesised that groundwater may be a significant contributor to the elevated concentrations of P_i within the river and that $\delta^{18}\text{O}_p$ could be used as a tracer to identify groundwater inputs of P_i to the river network.

5.2.1 Geological setting

The main geological units present in the study area (**Figure 5.1**), which cover both the upper Wey and Tillingbourne river catchments, all derive from the Cretaceous period, with the Lower Greensand Group representing the oldest sediments, and covered over time by the Gault formation, Upper Greensand formation and the Chalk group. These units are all sedimentary marine deposits and feature prominently across southern England, representing important regional aquifers (Edmunds and Kinniburgh, 1986; Shand *et al.*, 2003). The Lower Greensand group is comprised of bands of sandstone and clays (Ellison *et al.*, 2002). Two main units within this formation are the Hythe

Formation and the higher Folkestone Formation, separated by the Bargate and Sandgate Beds (bands of sandstone and silty and sandy clays). The Hythe Formation consists of fine to medium grained sands, and has chert nodules present within the top 30 m. Importantly, within this layer phosphatic nodules can be found (Ruffell, 1992), which maybe a significant source of P_i to groundwater within the region. In addition, the reworked phosphatic pebbles derived from the Hythe Beds (with diameters of up to 10 mm) have been found in the Bargate Beds. The Folkestone Formation is mainly comprised of similarly fine to medium grained sands, however this layer has four distinct clay strata and a number of iron horizons. The Upper Greensand formation is also a sedimentary unit, consisting of calcareous sandstone and siltstones, and was overlain by the Lower Chalk formation – the lower two units within this formation are the West Melbury Marly and the Zig Zag Chalk formations. In addition to the Lower Greensand formation, phosphate nodules have been reported within both the Upper Greensand formation and in the Gault Clay layer (Parrish, 1990; Gale, 2012).

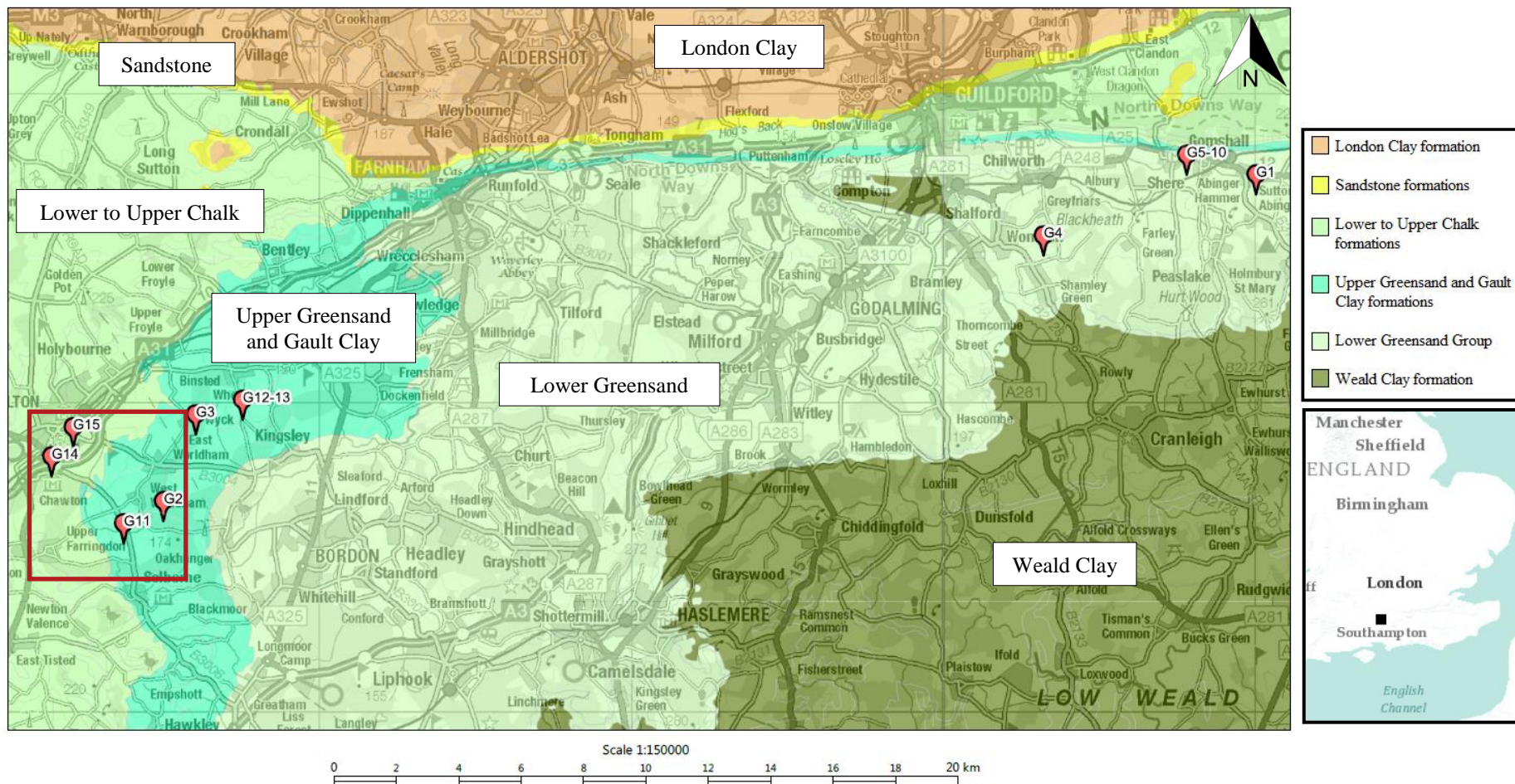


Figure 5.1: Geological map of the bedrock for the Alton and Godalming area, South England, UK. Groundwater samples (red arrows) are located within the upper Wey (G2, 3, 11-15) and Tillingbourne (G1, 4-10) river catchments and the ground surface is underlain by four different formations – Chalk formation in the west to the older Lower Greensand Group in the east. Stream samples are displayed in **Figure 5.2**, which is contained within the red box above. Printed with permission: Geological Map Data ©NERC 2016. © Crown Copyright and Database Right 2016. Ordnance Survey (Digimap Licence).

5.2.2 Groundwater survey

Table 5.1 and **Figure 5.1** report the groundwater sites used for two sampling campaigns, alongside a description of the type of sample that was collected and the main bedrock unit that each sample represents. A sample of Upper Greensand bedrock was also collected from site G3 in order to extract P_i and determine $\delta^{18}O_p$ for the P_i released during bedrock dissolution. As this dissolution process is abiotic, it can be hypothesised that no isotopic fractionation would occur. Therefore, the aqueous $\delta^{18}O_p$, following a liquid extraction using MilliQ water, would be expected to reflect that in the source bedrock material. Any difference found in $\delta^{18}O_p$ between the bedrock extracts and the groundwater samples would then be associated with an isotope fractionation within the groundwater system itself.

Table 5.1: Site descriptions for groundwater borehole and spring sample sites in the upper Wey and Tillingbourne catchments, alongside the bedrock unit from which each sample was derived.

Code	Name	Location	Sample type	Depth /m	Bedrock unit
G1	Water cress farm (PGWU 0984)	Kingfisher Farm Shop, Abinger Hammer	Spring source (sampled as culvert)	-	Lower Greensand, boundary of Hythe/Bargate Beds
G2	Manor Farm (PGWU 1958)	Nr Warner's Wood, Manor Farm, Selborne Road, Alton	Spring	-	Upper Greensand, close to Gault Clay
G3*	Wyck Place (PGWU 1996)	Wyck Place, Binsted	Spring	-	Emerges from base of Upper Greensand just above the Gault Clay
G4	Arunshead Farm (PGWU 1555)	Arunshead Farm, Shamley Green	Collection of 6 artesian boreholes (sampled as collection enters a brook)	10-25	Lower Greensand, close to Bargate Beds
G5	Netley 4 (PGWU 0853)	Netley Mill Pumping Station, Gomshall	Borehole	40	Folkestone Beds (Lower Greensand)
G6	Netley 1 (PGWU 0850)		Borehole	72	Folkestone and Hythe Beds (in bottom 9 m only) (Lower Greensand)
G7	Netley 2		Borehole	78-92	Hythe Beds (Lower Greensand)
G8	Netley 5		Borehole	78-92	Hythe Beds (Lower Greensand)
G9	Netley 6		Borehole	78-92	Hythe Beds (Lower Greensand)
G10	Netley 7		Borehole	78-92	Hythe Beds (Lower Greensand)
G11	Hartley Park (PGWU 1975)	Hartley Park Farm, Selborne Road, Alton	Borehole	Not known	Lower Greensand
G12	South Hays Cottage	South Hay, Nr Binsted	Borehole	11.85	Upper Greensand
G13	Colesons (SU7378)	South Hay, Nr Binsted,	Borehole	13	Upper Greensand
G14	Coors brewery (PGWU 1855)	A339/A31, Alton	Borehole	36.5	Lower Chalk and Upper Greensand
G15	Windmill Hill Pumping Station (PGWU 0561)	Windmill Hill, Alton	Borehole	164.5	Intersects Lower Chalk and Upper Greensand

PGWU codes refer to the sample codes on the Environment Agency network

*Location of bedrock sample used in rock extracts for $\delta^{18}\text{O}_p$ analysis

5.2.3 *In-river sampling for analysis of $\delta^{18}O_p$*

The Caker stream forms part of the upper Wey catchment and is located near Alton, Hampshire, England. The underlying geology of the in-stream sites is summarised in **Table 5.2** and **Figure 5.3**. The reach of the Caker stream analysed for the research reported in this chapter covered approximately 9 km (**Figure 5.5**), starting on an arable farm, before flowing through arable and grassland fields, and ending in the industrial/urban area of Alton. Located 160 m upstream of the final in-stream site was the entry point for the final effluent from Alton WWTP. Sample W in **Table 5.2** was collected from the outflow pipe at the WWTP, approximately 200 m prior to its entry into the river. Sample F was taken 160 m downstream of the final effluent entry point to the stream, on the assumption that the effluent would have mixed fully with stream water by this sample point.

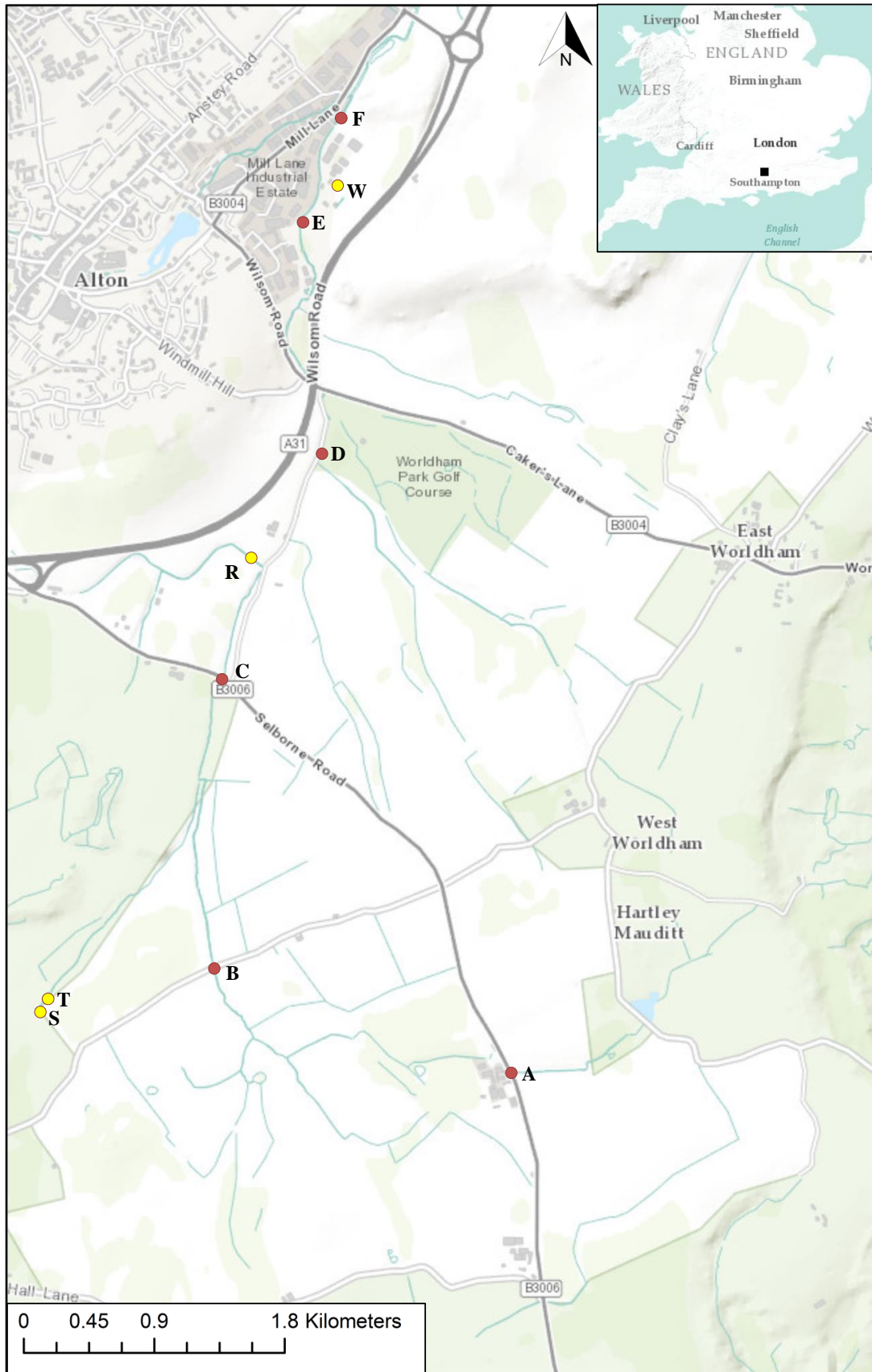


Figure 5.2: Location of sample sites along a tributary of the River Wey, Alton, UK. The direction of flow is from south to north and samples A-F are located along the main stem of the river, with four known additions to the main stream (yellow markers): S = a groundwater spring, T = the spring source 40 m downstream of S following input from a tile drain to the tributary, and W = a WWTP effluent that enters the river 160 m upstream of site F. Inset is for illustrative purposes only for the general location of the study site in Hampshire, England.

Table 5.2: Site descriptions for surface water sample sites in the upper Wey catchment and predominant land use directly surrounding each site.

	Sample site	Distance downstream from A /km	Predominant land use	Underlying bedrock formation
A	Main river	0.00	Agriculture	Upper Greensand Boundary of Upper Greensand and West Melbury Marly Chalk
B	Main river	2.69	Agriculture	Upper Greensand and West Melbury Marly Chalk
S	Groundwater spring	4.11*	Agriculture	West Melbury Marly Chalk
T	Spring and tile drain	4.11*	Agriculture	West Melbury Marly Chalk
C	Main river	4.81	Agriculture	West Melbury Marly Chalk
R	Tributary	5.67*	Agriculture	West Melbury Marly Chalk
D	Main river	6.58	Agriculture	West Melbury Marly Chalk
E	Main river	8.38	Urban	Zig Zag Chalk
W	WWTP effluent	9.03*	WWTP effluent	-
F	Main river	9.19	Urban	Zig Zag Chalk

*Point at which inflow enters the main stream. S and T are situated on a tributary 2 km upstream of its confluence with the stream and W was sampled from a pipe on the WWTP site, approximately 200 m from the final effluent discharge point to the stream.

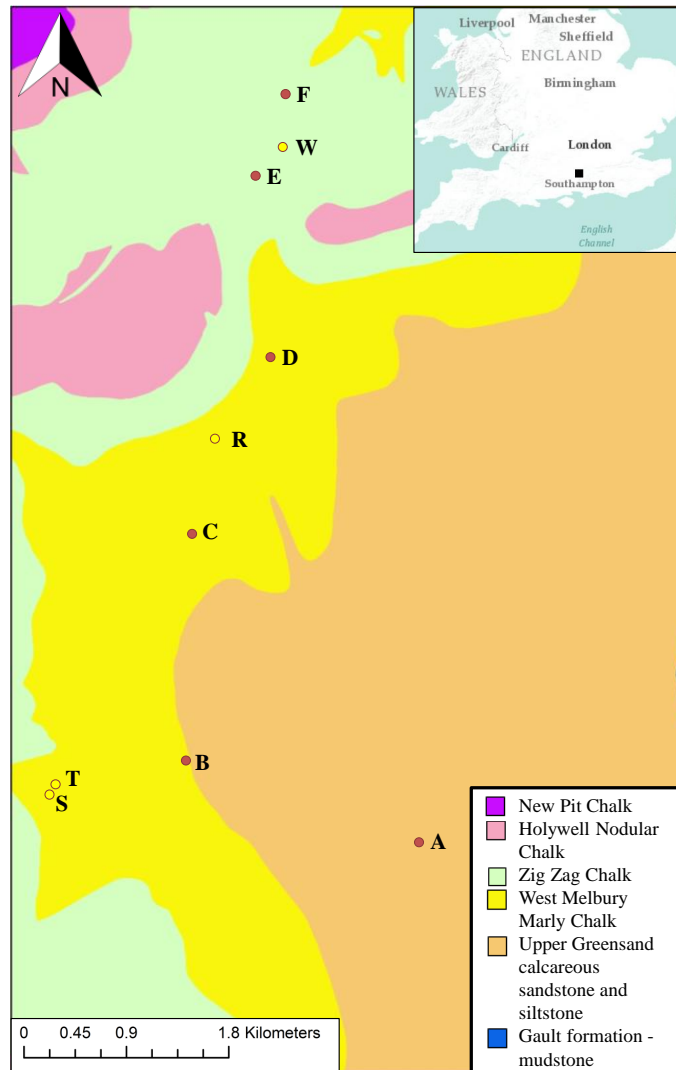


Figure 5.3: Underlying bedrock for surface water samples in the upper catchment of the River Wey, Alton, UK. Direction of surface water flow is from south to north.

5.2.4 *Field sampling campaigns*

Three sampling campaigns were conducted: June 2015 (02/06/2015 – groundwaters G1 and G4, as well as preliminary stream data from sites E, F and R (**Appendix A.2**); 03/06/15 – groundwaters G3, G14 and G15); early November 2015 (03/11/2015 – groundwaters G1, G4-10; 04/11/15 – groundwaters G2, G3, G11-13); and late November 2015 (27/11/2015 – stream sites A – F, S, T and W). Sample codes are listed in **Tables 5.1** and **5.2**, and locations are displayed in **Figures 5.1** and **5.2**.

5.2.5 *Sample collection and field measurements*

The volumes of sample for collection were determined prior to sampling using previous concentrations from similar sites analysed by the Environment Agency (Hampton, 2012b, a) as a guide to the volume of sample required to contain approximately 0.4-0.7 mg P, thereby producing sufficient Ag_3PO_4 to run triplicate measurements on the thermal combustion/elemental analyser isotope ratio mass spectrometer (TCEA-IRMS). The two November campaigns also included an in-field SRP test for sample sites at which no prior concentration data were held.

Water samples of 5-30 L for $\delta^{18}\text{O}_p$ analysis were collected from both stream and groundwater sites using a bucket and filtered in the field through 0.45 μm filter cartridges, using a peristaltic pump, into acid-washed high-density polyethylene containers. These samples were then stored at 4°C in a cold store before analysis. For groundwater samples collected from boreholes, the borehole was pumped prior to collection until the electrical conductivity, pH and dissolved oxygen readings were stable. If the pump tubing was capable of being attached directly to the borehole, this was achieved in preference to collecting the sample in a bucket; however, no attempt was made to avoid contact of groundwater samples with the atmosphere during collection. For both spring and stream sampling, all the collection sites were chosen where the water was flowing freely and the bucket was used to sample from the most actively flowing section of each channel. The location of the spring sample G3 was the most densely vegetated, however every effort was made to minimise surface contamination from soil and vegetation during collection – for example, after clearing

the majority of large vegetation from the sampling location, the spring was allowed to flow freely to rinse away any loose contamination before collection.

Water temperature was measured directly in the field using a Hanna Instruments handheld probe. An unfiltered sample was collected and analysed for electrical conductivity (EC), pH, reduction-oxidation potential (E_H) and dissolved oxygen (DO) concentration in the field using calibrated Mettler Toledo probes. Alkalinity was determined by an in-field bromocresol green colorimetric titration against 1.6N H_2SO_4 . Separate unfiltered (collected in amber vials) and filtered (0.45 μm syringe filtered, collected in 50 mL centrifuge tubes) sample aliquots were collected at each site and retained for $\delta^{18}O_w$ and nutrient analysis respectively, and stored at $<4^\circ C$ prior to analysis in the laboratory.

5.2.6 Analysis of nutrient concentrations

On 0.45 μm filtered sample aliquots, soluble reactive P (SRP) concentrations were determined using a phosphomolybdenum blue method on a Seal Analytical AQ2 discrete autoanalyser (LOD = 0.005 mg P.L⁻¹; analytical quality controls: matrix-matched SPEX CertiPrep WR1 (0.6 mg P.L⁻¹) and WR2 (0.3 mg P.L⁻¹)). Total dissolved P (TDP) concentrations were analysed similarly to SRP, following the digestion of samples in a 0.11M sulfuric acid (H_2SO_4) and 0.03M potassium persulfate ($K_2S_2O_8$) matrix. However, due to a time delay of several weeks in analysis for this component, the TDP concentrations indicated that sample deterioration had occurred prior to analysis, with lower TDP concentrations relative to the SRP concentrations which were processed immediately on returning to the laboratory. TDP loss is a known issue with delayed analysis (Kotlash and Chessman, 1998; Neal *et al.*, 2000); therefore, the TDP concentrations have not been included in this thesis. Dissolved organic carbon concentrations were analysed on acidified and sparged filtered samples using an Analytical Sciences Thermalox (LOD = 1.3 mg C.L⁻¹; analytical quality control: EAG REF162 (0.5, 5 and 15 mg C.L⁻¹)). Cl^- , F^- , $N-NO_3^-$, and $S-SO_4^{2-}$ concentrations in filtered samples were determined using ion chromatography on a Dionex ICS2500 (LOD = 0.03 mg Cl.L⁻¹, 0.0002 mg F.L⁻¹, 0.02 mg N.L⁻¹ and 0.07 mg S.L⁻¹ respectively; calibrated 0-10 mg N.L⁻¹; analytical

quality controls: SPEX CertiPrep WR1 (60 mg Cl.L⁻¹, 0.6 mg F.L⁻¹, 4 mg N.L⁻¹ and 10 mg S.L⁻¹) and WR2 (30 mg Cl.L⁻¹, 0.3 mg F.L⁻¹, 2 mg N.L⁻¹ and 5 mg S.L⁻¹).

5.2.7 Upper Greensand rock extracts

A sample of Upper Greensand bedrock was collected from site **G3**, and ground to a homogeneous powder using a planetary ball mill. Extraction of P_i from the ground bedrock sample was performed in 18.2 MΩ MilliQ water for 72 hours using a roller shaker, using 3 x 20.00 g of bedrock powder and 400 mL MilliQ water for a set of triplicate samples. The mixtures were filtered (0.45 μm) and the filtrate collected and analysed for SRP (mean concentrations: 1.130, 1.166 and 1.116 mg P.L⁻¹). The filtrate was subjected to **Method 3** (protocol described in **Section 3.5**) in order to precipitate Ag₃PO₄ prior to determination of δ¹⁸O_p.

5.2.8 δ¹⁸O_p and δ¹⁸O_w measurements

After P_i concentrations had been determined, the appropriate volume of sample to generate 0.7 mg P as Ag₃PO₄ was processed using **Method 2**, as described in **Section 4.2.5**. If sufficient sample volume remained, the sample was also run for Ag₃PO₄ using the revised **Method 3** (see **Chapter 3**).

Ag₃PO₄ samples were analysed for δ¹⁸O_p on an IsoPrime100 mass spectrometer coupled to a varioPYRO cube elemental analyser. 400 μg Ag₃PO₄ was weighed out in silver capsules alongside 800 μg carbon black, dried at 40°C overnight and converted to CO by pyrolysis in an ash crucible at 1450 °C. The resulting gases passed through Sicapent (phosphorus pentoxide) to remove water vapour. Subsequently, the CO is separated from other impurities, namely N₂, using a purge-and-trap system and helium carrier gas. ¹⁸O/¹⁶O is derived from the integrated mass 28 (¹²C¹⁶O) and 30 (¹²C¹⁸O; ¹⁴C¹⁶O; ¹³C¹⁷O) signals from the sample CO pulse, compared to those in an independently introduced pulse of pure CO reference gas. These ratios are then calibrated to the Vienna-Standard Mean Ocean Water (VSMOW) scale in per mille notation (‰) using standards – NBS127 (+9.3‰), EM Ag₃PO₄ (+21.7‰) and Acros Ag₃PO₄ (+14.2‰). Analytical precision based on two standard errors for repeat analysis of the quality control (Acros Ag₃PO₄) is better than ±0.3‰_{VSMOW}.

Unfiltered field samples were analysed for $\delta^{18}\text{O}_p$ using an equilibration method on an IsoPrime100 mass spectrometer coupled to an IsoPrime Multiflow inlet. 200 μL of heated (40°C) sample was left for ~ 15 hours to equilibrate with the equilibration CO_2 gas. The resulting headspace gas was then sampled and passed to the IsoPrime for isotopic analysis. $^{18}\text{O}/^{16}\text{O}$ ratios are then calibrated to the Vienna-Standard Mean Ocean Water (VSMOW) scale in per mille notation (‰) using standards – LEC LIGHT (-15.0‰) and LEC HEAVY (-1.5‰). The precision obtained for repeat analysis of the quality control (LEC TAP) is better than $\pm 0.15\text{‰}_{\text{VSMOW}}$.

The $\delta^{18}\text{O}_p$ value predicted for a system at thermodynamic equilibrium with $\delta^{18}\text{O}_w$ was calculated using **Equation 4** and is denoted as $\delta^{18}\text{O}_{\text{eq}}$ (Chang and Blake, 2015).

$$1000 \ln \alpha_{eq-w} = (14.43(\pm 0.39) \times 1000/T) - 26.54(\pm 1.33) \quad (4)$$

where T is in degrees Kelvin, and:

$$\alpha_{eq-w} = \frac{(\delta^{18}\text{O}_{eq} + 1000)}{(\delta^{18}\text{O}_w + 1000)} \quad (4a)$$

If the measured $\delta^{18}\text{O}_p$ is equal to $\delta^{18}\text{O}_{\text{eq}}$, $\delta^{18}\text{O}_p$ is assumed to be at thermodynamic equilibrium with $\delta^{18}\text{O}_w$.

5.3 Results

5.3.1 Analysis of groundwater samples and Upper Greensand bedrock extracts

Tables 5.3 and **5.4** report the hydrochemical and isotope data collected across both June and November 2015 sampling events. Elevated SRP concentrations were found within all groundwater samples, ranging from 0.025 to 1.130 mg P.L⁻¹, with a mean concentration of 0.494 mg P.L⁻¹. When considered separately, the groundwater extracted from the Lower and Upper Greensand formations had mean SRP concentrations of 0.544 and 0.415 mg P.L⁻¹ respectively. Concentrations were elevated in spring samples ($\bar{x} = 0.765$ mg P.L⁻¹) compared to borehole samples ($\bar{x} = 0.390$ mg P.L⁻¹). No correlation was found between SRP concentrations and Cl⁻

or SO_4^{2-} using a Spearman's correlation two-tail test, however a positive correlation was found between SRP and NO_3^- concentrations: $r_s = 0.504$, $p = 0.033$. Nitrate concentrations ranged from 0.17 to 10.73 mg N.L⁻¹ (**Figure 5.4**). Repeat samples from sites G1 and 4 remained relatively consistent across all nutrient parameters in both June and November 2015, with the exception of DOC concentrations which were significantly reduced in November. Whilst there was a similar observed decrease in DOC concentration between June and November 2015 at site G3, there were also increases in SRP, NO_3^- and SO_4^{2-} concentrations from 1.051 to 1.130 mg P.L⁻¹, 4.17 to 7.19 mg N.L⁻¹ and 9.17 to 10.74 mg S.L⁻¹ respectively.

Table 5.3: Dissolved (0.45µm) nutrient concentrations and temperatures of groundwater in the Wey and Tillingbourne catchments. Soluble reactive P (SRP) concentrations are given to 3 decimal places; chloride concentrations and temperatures to 1 decimal place; N:P as a molar ratio, electrical conductivity (EC), E_H and alkalinity to 3 significant figures and the remaining parameters to 2 decimal places.

Groundwaters	Sample type	Sample depth m	T °C	DO mg.L ⁻¹	pH	EC µS.c m ⁻¹	E _H mV	Alkalinity mg HCO ₃ .L ⁻¹	[SRP]	[NO ₃ ⁻]	[Cl ⁻]	[F ⁻]	[SO ₄ ²⁻]	[DOC]	Molar N:P	
									mg P .L ⁻¹	mg N.L ⁻¹	mg Cl .L ⁻¹	mg F .L ⁻¹	mg S.L ⁻¹	mg C.L ⁻¹		
June 2015	G1	Spring	n.a.	10.3	8.54	6.49	348	170	75.6	0.704	10.43	22.8	0.47	7.35	11.00	32.7
	G3	Spring	n.a.	13.6	10.17	7.87	588	-	292	1.051	4.17	20.6	0.24	9.17	3.96	8.77
	G4	Artesian borehole	10-25	10.9	9.71	6.37	271	203	34.1	0.907	5.31	20.5	0.38	6.92	5.38	12.9
	G14	Borehole	36.5	11.6	2.20	7.06	661	171	339	0.049	1.00	16.0	0.36	13.72	b.d.	45.3
	G15	Borehole	164.5	11.8	8.11	7.06	726	133	332	0.025	9.08	29.7	0.22	9.48	9.23	802
November 2015	G1	Spring	n.a.	10.1	-	-	-	70.7	-	0.732	10.08	23.6	0.45	7.50	b.d.	30.5
	G2	Spring	n.a.	10.3	-	-	-	249	-	0.210	4.46	19.8	0.35	13.36	2.11	47.0
	G3	Spring	n.a.	11.3	-	-	-	266	-	1.130	7.19	25.1	0.22	10.74	2.25	14.1
	G4	Artesian borehole	10-25	10.5	-	-	-	58.5	-	0.954	5.32	21.6	0.37	7.03	b.d.	12.3
	G5	Borehole	40	11.3	-	-	-	143	-	0.622	5.38	17.0	0.47	9.67	b.d.	19.1
	G6	Borehole	72	10.9	-	-	-	62.2	-	0.300	3.15	16.9	0.42	7.24	b.d.	23.2
	G7	Borehole	78-92	11.0	-	-	-	28.8	-	0.217	3.39	17.5	0.33	7.88	b.d.	34.6
	G8	Borehole	78-92	11.2	-	-	-	64.6	-	0.711	3.78	14.9	0.52	7.21	b.d.	11.8
	G9	Borehole	78-92	10.9	-	-	-	118	-	0.408	5.10	19.0	0.39	8.35	b.d.	27.6
	G10	Borehole	78-92	10.9	-	-	-	68.3	-	0.350	3.60	17.5	0.45	7.83	b.d.	22.6
	G11	Borehole	Not known	12.0	-	-	-	70.7	-	0.080	0.17	11.8	0.29	3.85	b.d.	4.75
	G12	Borehole	11.85	13.5	-	-	-	366	-	0.241	4.94	23.1	0.23	15.96	1.41	45.4
	G13	Borehole	13	11.3	-	-	-	329	-	0.201	2.24	20.2	0.41	23.46	3.04	24.6

n.a. = not applicable;

b.d. = below limit of detection;

- = not determined. In the case of November 2015, DO, pH, EC and alkalinity data were not collected due to the absence of field equipment.

Table 5.4: Oxygen isotope composition of phosphate ($\delta^{18}\text{O}_p$), water ($\delta^{18}\text{O}_w$) and the theoretical equilibrium ($\delta^{18}\text{O}_{eq}$) for borehole and spring samples in the Wey and Tillingbourne catchments and their respective geological settings. The oxygen yields from pyrolysis of Ag_3PO_4 precipitates are given to 1 decimal place, a pure Ag_3PO_4 molecule would contain 15.3% oxygen. Isotope compositions given to 2 decimal places.

Ground-waters	Sample type	Sample depth m	Bedrock unit	Mean	1 σ	n	Mean	Mean	$\delta^{18}\text{O}_{eq}$	$\delta^{18}\text{O}_p - \delta^{18}\text{O}_{eq}$	
				$\delta^{18}\text{O}_p$ ‰	‰		O yield %	$\delta^{18}\text{O}_w$ ‰	‰	‰	
June 2015	G1	Spring	n.a.	Lower Greensand, boundary of Hythe Bargate Beds	20.50	0.26	3	15.3	-6.88	17.62	2.88
	G3	Spring	n.a.	Base of Upper Greensand, above Gault Clay	17.02	0.11	3	14.3	-5.73	18.20	-1.18
	G4	Artesian borehole	10-25	Lower Greensand, close to Bargate Beds	19.21	0.06	3	15.5	-6.97	17.42	1.79
	G14	Borehole	36.5	Lower Chalk and Upper Greensand	n.d.	-	-	-	-5.78	-	-
	G15	Borehole	164.5	Lower Chalk and Upper Greensand	n.d.	-	-	-	-6.13	-	-
November 2015	G1	Spring	n.a.	Lower Greensand, boundary of Hythe Bargate Beds	20.13	0.26	3	15.4	-7.25	17.28	2.85
	G2	Spring	n.a.	Upper Greensand, close to Gault Clay	18.57	0.41	3	15.4	-6.49	18.02	0.55
	G3	Spring	n.a.	Base of Upper Greensand, above Gault Clay	17.65	0.14	3	15.6	-6.78	17.54	0.11
	G4	Artesian borehole	10-25	Lower Greensand, close to Bargate Beds	20.15	0.17	3	15.6	-6.64	17.83	2.32
	G5	Borehole	40	Folkestone Beds (Lower Greensand)	19.84	0.38	3	15.4	-7.15	17.16	2.68
	G6	Borehole	72	Folkestone and Hythe Beds (in bottom 9 m only) (Lower Greensand)	20.58	0.28	3	15.4	-6.98	17.41	3.17
	G7	Borehole	78-92	Hythe Beds (Lower Greensand)	20.13	0.21	3	14.9	-7.30	17.06	3.07
	G8	Borehole	78-92	Hythe Beds (Lower Greensand)	20.32	0.27	3	15.2	-7.26	17.07	3.25
	G9	Borehole	78-92	Hythe Beds (Lower Greensand)	20.07	0.46	3	15.1	-7.35	17.03	3.03
	G10	Borehole	78-92	Hythe Beds (Lower Greensand)	20.15	0.20	3	15.2	-7.09	17.29	2.86
	G11	Borehole	Not known	Lower Greensand only?	-	-	-	-	-6.70	-	-
	G12	Borehole	11.85	Upper Greensand	18.88	0.41	3	15.2	-6.48	17.45	1.43
	G13	Borehole	13	Upper Greensand	18.50	0.26	3	15.7	-6.45	17.88	0.62
Rock Extracts	n.a.	n.a.	Upper Greensand	18.19 [†]	0.43	9	15.1	-6.73	-	-	

n.a. = not applicable;

n.d. = not determined due to sample concentration being too low to yield sufficient Ag_3PO_4 for TCEA-IRMS analysis;

n = number of repeats for TCEA-IRMS analysis from one Ag_3PO_4 precipitate, with the exception of the rock extracts where n = 9 from 3 TCEA-IRMS analysis per triplicate Ag_3PO_4 precipitate;

* = MilliQ water in extracts;

[†] = Extracts underwent **Method 3** protocol, all other analyses reported in this chapter utilised **Method 2**.

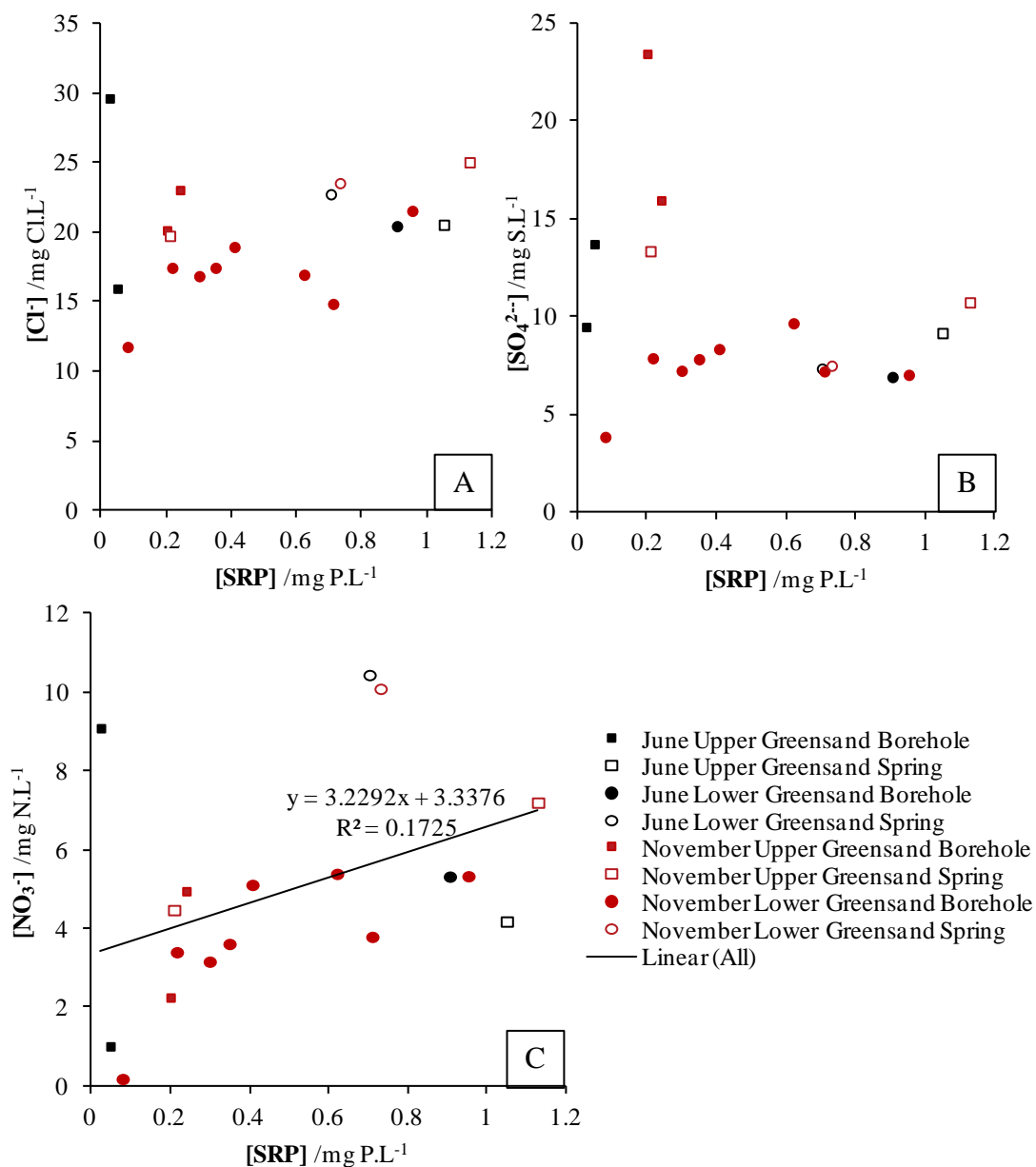


Figure 5.4: Groundwater SRP concentrations plotted against a) Cl⁻, b) SO₄²⁻ and c) NO₃⁻ concentrations. A significant correlation was found between SRP and NO₃⁻ concentrations, whilst no correlation was found for SRP with Cl⁻ or SO₄²⁻.

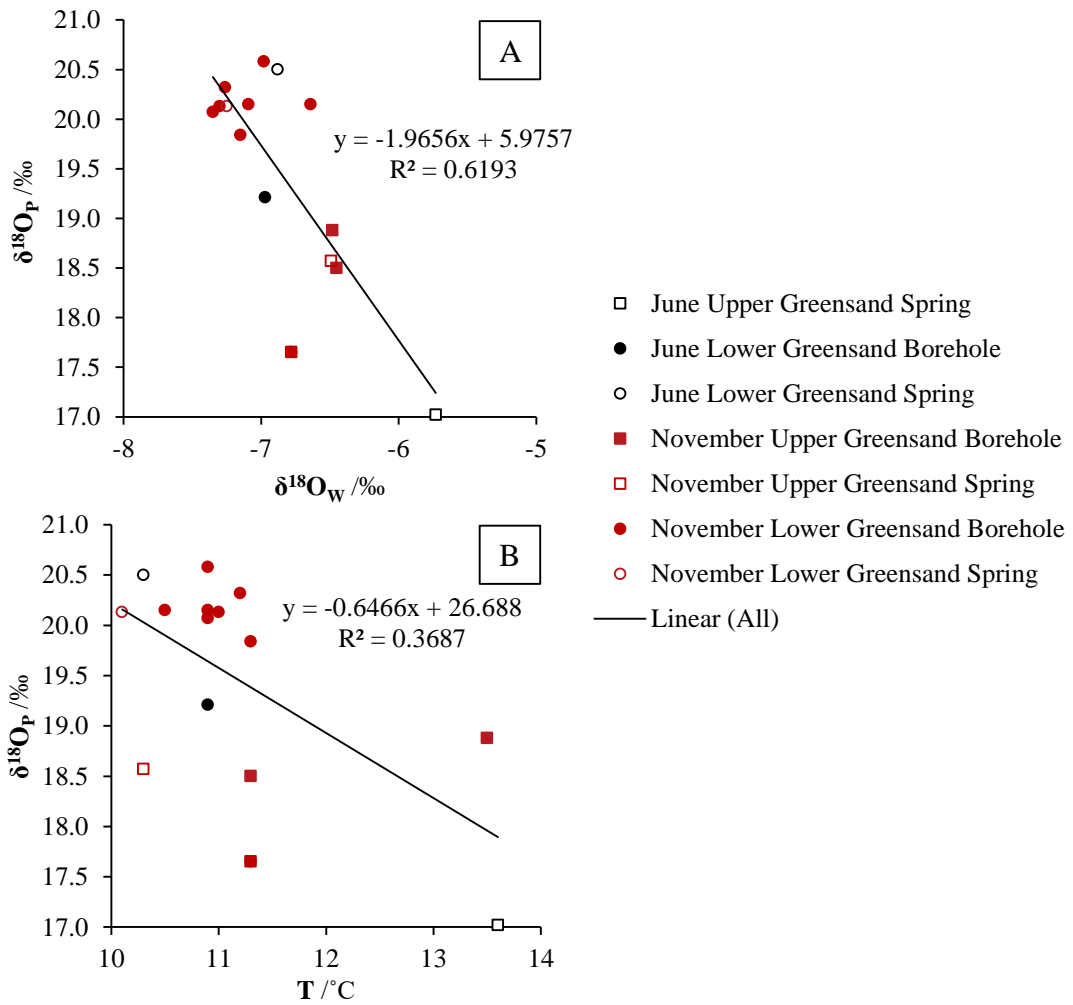


Figure 5.5: Comparison of groundwater $\delta^{18}O_p$ with a) $\delta^{18}O_w$ and b) water temperature. Inverse regression and significant correlations were found for both sets of variables. relationships were found in both cases.

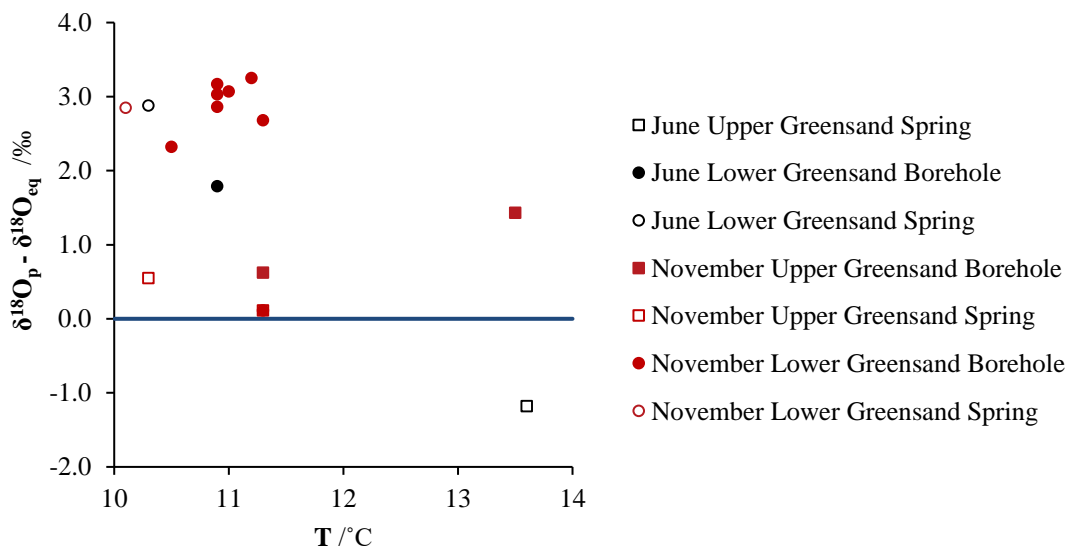


Figure 5.6: Comparison of groundwater $\delta^{18}O_p - \delta^{18}O_{eq}$ with water temperature. No significant correlation was found between the two variables in a Spearman's correlation test.

The mean value for $\delta^{18}\text{O}_p$ within groundwater samples was 19.44‰ ($1\sigma = 1.09\%$), with a range from 17.02 to 20.58‰. The majority of groundwater samples were in disequilibrium compared to $\delta^{18}\text{O}_{eq}$, ranging from -1.18 to +3.25‰ relative to $\delta^{18}\text{O}_{eq}$, with a mean difference of +1.96‰. An inverse relationship was observed between $\delta^{18}\text{O}_p$ and both $\delta^{18}\text{O}_w$ and water temperature, although no relationship was found between $\delta^{18}\text{O}_p - \delta^{18}\text{O}_{eq}$ and water temperature (**Figures 5.5 and 5.6**). This was supported by the results from a Spearman's correlation two-tail test in which no significant correlation was found between $\delta^{18}\text{O}_p - \delta^{18}\text{O}_{eq}$ and water temperature, whereas significant negative correlations were found between $\delta^{18}\text{O}_p$ and $\delta^{18}\text{O}_w$ ($r_s = -0.560$, $p = 0.030$) and $\delta^{18}\text{O}_p$ and water temperature ($r_s = -0.550$, $p = 0.034$). To determine if there was a significant difference between mean $\delta^{18}\text{O}_p$ of the different sample types (spring *vs.* borehole samples), a two-tail T-test was undertaken, with the results indicating any difference was not significant at a 95% confidence level. This was also true with respect to the difference between $\delta^{18}\text{O}_p$ and $\delta^{18}\text{O}_{eq}$ across spring *vs.* borehole samples. For the sites that were sampled in both June and November 2015, G1 had a slightly lighter $\delta^{18}\text{O}_p$ ratio in November compared to June, but a very similar difference compared to $\delta^{18}\text{O}_{eq}$; G3 and G4 had $\delta^{18}\text{O}_p$ values that increased by 1.55‰ and decreased by 1.56‰ respectively between June and November, with samples from both these sites demonstrating reduced differences between $\delta^{18}\text{O}_p$ and $\delta^{18}\text{O}_{eq}$ in November *vs.* June.

Differences between $\delta^{18}\text{O}_p$ in samples from the Lower Greensand and Upper Greensand units were significant when compared using a two-tail T-test: $t(13) = 6.83$, $p < 0.001$. This was also true for the difference between $\delta^{18}\text{O}_p$ and $\delta^{18}\text{O}_{eq}$ between the two units: $t(13) = 7.03$, $p < 0.001$. Therefore, average $\delta^{18}\text{O}_p$ in groundwater appeared to differ dependent on the bedrock geology, with mean $\delta^{18}\text{O}_p$ for the Lower and Upper Greensand units of 20.11‰ ($\sigma = 0.38\%$) and 18.12‰ ($\sigma = 0.77\%$) respectively. The mean difference between observed $\delta^{18}\text{O}_p$ and $\delta^{18}\text{O}_{eq}$ was +0.31‰ ($\sigma = 0.96\%$) for samples taken from the Upper Greensand and +2.79‰ ($\sigma = 0.44\%$) for samples from the Lower Greensand. The mean $\delta^{18}\text{O}_p$ from groundwater samples collected from the Upper Greensand (18.12‰) did not significantly differ from the $\delta^{18}\text{O}_p$ of the water extracts from the bedrock, which was only 0.07‰ heavier ($\bar{x} = 18.19\%$, $\sigma = 0.43\%$), although it should be noted that the extracts used the **Method 3** protocol (see **Section 6.1**). Conversely, there was a significant difference between the Lower Greensand

groundwater samples and the Upper Greensand bedrock extracts using a two-tail T-test: $t(11) = 7.44, p < 0.001$.

5.3.2 *Hydrochemical and isotopic data from surface water samples*

Values for selected field and laboratory parameters are reported in **Table 5.5**; all distances in **Table 5.5** and subsequent figures are quoted as downstream from site A, with the exception of sites S, T and W. The distances for these sites are quoted with respect to the point of input into the main stem of the Caker stream, i.e. site W = 9.03 km, where the WWTP final effluent outflow pipe enters the stream. Sites S and T are reported to be at 4.11 km, where the tributary they are located on joins the main stem with both sites situated approximately 2 km upstream of the confluence, with site S being a sample fed by a groundwater spring, and site T located 40 m downstream following the entry of an agricultural tile drain.

Table 5.5: Dissolved (0.45µm) nutrient concentrations and temperatures of surface water samples in the Wey catchment. Soluble reactive P (SRP) concentrations are given to 3 decimal places, temperature to 1 decimal place, alkalinity to 3 significant figures and the remaining parameters to 2 decimal places. Molar ratios of N (in the form of NO₃⁻) to P (in the form of SRP), and C (in form of alkalinity and DOC) to P (in the form of SRP) are given to 3 significant figures. Typically, N to P ratios also include ammonium concentrations but these were not determined in the laboratory, and thus potentially these ratios would have been higher if dissolved inorganic N had been determined (Sander and Moore, 1979).

		Distance	[P _i]	[DOC]	[NO ₃ ⁻]	T	Alkalinity	Molar ratio	Molar ratio
		downstream from site A	/mg P.L ⁻¹	/mg C.L ⁻¹	/mg N.L ⁻¹	°C	mg HCO ₃ .L ⁻¹	N:P	C(Alk+DOC):P
		/km							
November 2015	A	-	0.481	7.58	5.41	9.9	105	24.8	151
	B	2.69	0.310	4.96	5.03	10.3	190	35.9	353
	S*	4.11	0.018	1.64	7.43	11.1	312	898	8890
	T*	4.11	0.036	1.30	5.92	11.2	317	367	4600
	C	4.81	0.217	4.48	4.82	10.6	244	49.2	625
	D	6.58	0.166	4.09	3.98	10.8	207	52.9	695
	E	8.38	0.155	3.59	4.08	10.5	246	58.2	867
	W*	9.03	1.097	7.20	22.12	12.7	207	44.6	113
	F	9.19	0.789	5.62	16.13	12.2	207	45.2	152

b.d. = below LOD; *Sites S and T characterise the inputs from a tributary and are located 2 km upstream of the confluence with the main stream. Site W characterises the WWTP effluent input.

Table 5.5 and **Figure 5.7** report SRP concentrations, taken to be analogous to those of P_i for the purposes of this chapter. There was a monotonic decrease in P_i concentration with distance downstream along 8.4 km of the Caker stream between sample sites A and E. Between sample sites E and F, SRP concentration increased 5-fold, from 0.155 to 0.789 mg P.L⁻¹, following entry of final effluent from the WWTP into the main stem. A steady increase in water temperature was observed between sample sites A – D (**Figure 5.8**), before a small inflection between sites D and E. The input of WWTP effluent was associated with a sharp increase in water temperature between sites E and F. Both the NO₃⁻ and DOC profiles exhibited a steady decrease in concentration between sites A and E and, similarly to the water temperature profile, increased sharply between sites E and F in response to the input of WWTP effluent (**Table 5.5**). In both SRP and water temperature profiles, the input of the tributary characterised by sample sites S and T generally appears to have no significant impact on the water quality conditions in the main stem of the stream. However, alkalinity in the main stem did rise between sites B and C in response to the input of a tributary with a greater alkalinity, as characterised by S and T.

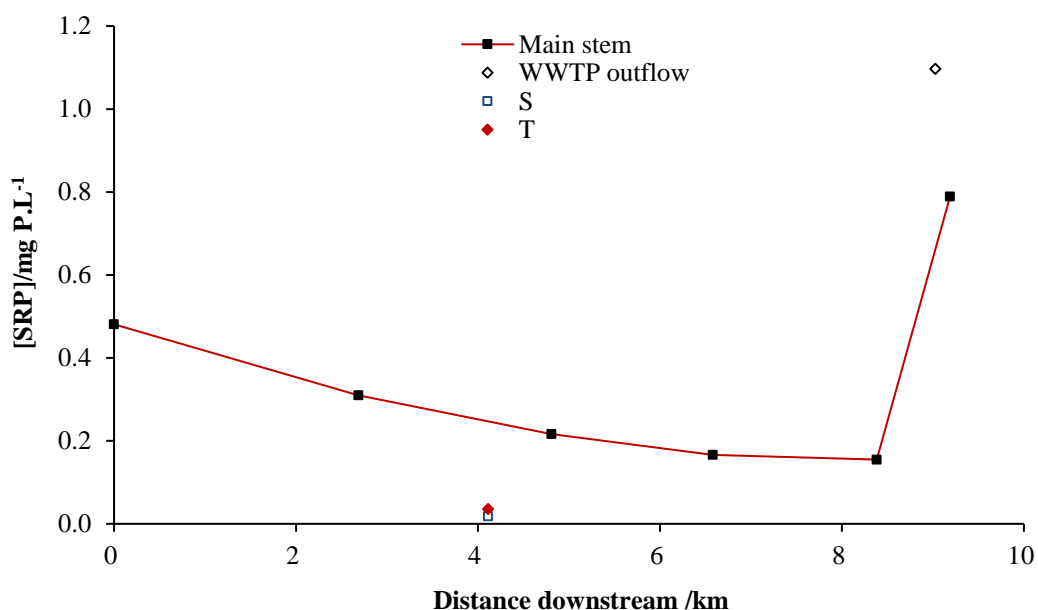


Figure 5.7: SRP concentrations downstream of site A on the Caker stream. Main stem sites are connected with lines; inputs to the stream are located at the point at which they would enter the main stem.

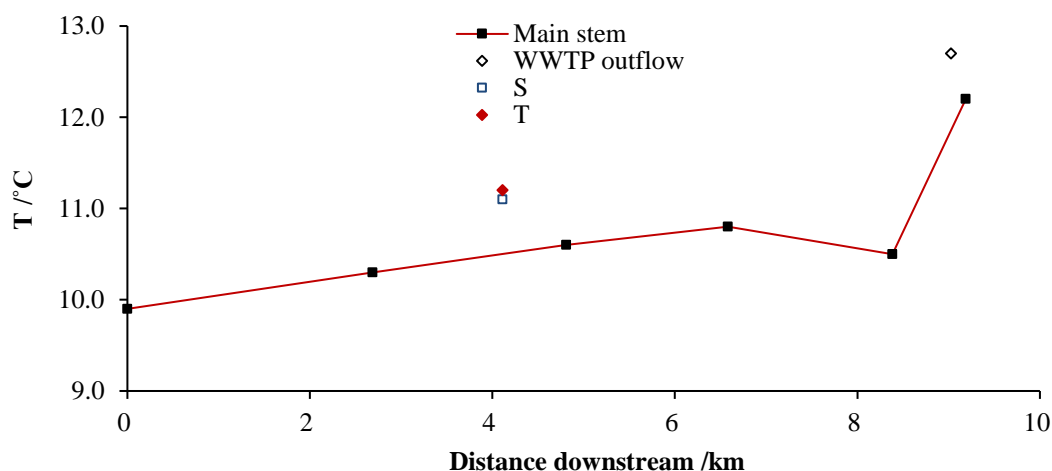


Figure 5.8: *In situ* surface water temperature downstream of site A on the Caker stream. Main stem sites are connected with lines; inputs to the stream are located at the point at which they would enter the main stem.

Table 5.5 also reports the molar ratio of N-NO₃ to P-SRP; all sites and inputs yielded a molar ratio greater than 20 with the lowest ratio being associated with the most upstream site, site A. The C:P molar ratios have also been calculated for carbon in the form of DOC and inorganic C (in the form of alkalinity). These ratios increased steadily downstream, such as the increase seen between sites C and D following the input of the tributary characterised by sites S and T. However, a substantial decrease was observed between sites E and F, following the addition of the low C:P WWTP effluent to the main river stem.

The stable oxygen isotope composition of P_i and H₂O also varied substantially along the in-stream transect. **Table 5.6** reports the measured isotope data, as well as the theoretical equilibrium $\delta^{18}\text{O}_{\text{eq}}$ calculated using **Equation 4**.

Table 5.6: Oxygen isotope composition of phosphate ($\delta^{18}\text{O}_p$), water ($\delta^{18}\text{O}_w$) and the theoretical equilibrium ($\delta^{18}\text{O}_{eq}$) for surface water samples from the Caker stream system. The oxygen yields from pyrolysis of Ag_3PO_4 precipitates are given to 1 decimal place, a pure Ag_3PO_4 molecule would contain 15.3% oxygen. Isotope compositions and distances downstream from site A given to 2 decimal places.

		Distance	Mean	n	1 σ	Mean	Mean	n	Range	$\delta^{18}\text{O}_{eq}$	$\delta^{18}\text{O}_p -$
		downstream	$\delta^{18}\text{O}_p$			O yield	$\delta^{18}\text{O}_w$		/1 σ [†]	/‰	$\delta^{18}\text{O}_{eq}$
		/km	/‰		/‰	/%	/‰		/‰	/‰	/‰
November 2015	A	-	18.73	3	0.16	15.2	-5.83	1	-	18.77	-0.04
	B	2.69	18.41	3	0.14	15.4	-6.01	1	-	18.51	-0.11
	S*	4.11	n.d.	-	-	-	-6.24	3	0.23	18.13	-
	T*	4.11	n.d.	-	-	-	-6.30	1	-	18.05	-
	C	4.81	18.17	3	0.26	15.4	-6.06	1	-	18.40	-0.24
	D	6.58	17.59	3	0.20	15.3	-6.13	1	-	18.30	-0.71
	E	8.38	18.70	3	0.21	15.2	-5.86	1	-	18.63	0.07
	W*	9.03	15.79	3	0.38	15.0	-6.53	1	-	17.54	-1.74
	F	9.19	16.07	3	0.07	15.4	-6.28	3	0.14	17.88	-1.81

n.d. = not determined due to sample concentration being too low to yield sufficient Ag_3PO_4 for TCEA-IRMS analysis;

[†]n is the number of repeats for TCEA-IRMS analysis from one Ag_3PO_4 precipitate. If n = 2, range is quoted, if n = 3 the uncertainty is 1 standard deviation;

*Sites S and T characterise the inputs from two tributaries and W the WWTP final effluent.

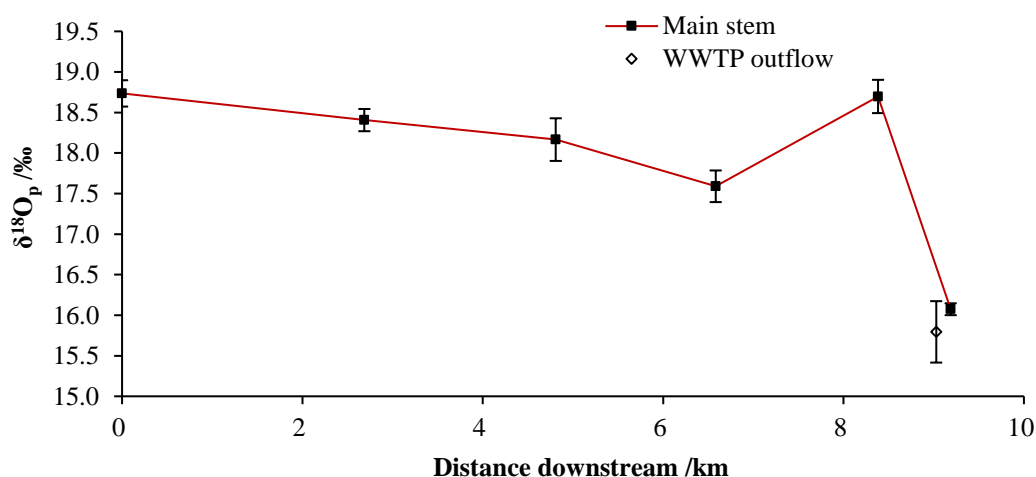


Figure 5.9: Mean $\delta^{18}\text{O}_p$ against distance downstream of site A on the Caker stream. Error bars display $\pm 1\sigma$ when samples were run in triplicate through the TCEA-IRMS. Analytical uncertainty based on 2 standard errors of the Acros Ag_3PO_4 standard measurements is $\pm 0.3\%$.

The measured $\delta^{18}\text{O}_p$ for surface samples (**Figure 5.9**) showed a steady decrease of 1.14‰ along 6.6 km of the in-stream transect between sample sites A and D. In contrast, over the 1.8 km between sample sites D and E, $\delta^{18}\text{O}_p$ increased by over 1‰ to reach 18.70‰. With the input of final effluent from the WWTP between sites E and F, there was a substantial decrease in $\delta^{18}\text{O}_p$ to 16.07‰ which is within one standard deviation of $\delta^{18}\text{O}_p$ determined for the final effluent from the WWTP. No isotope data

are available for sites S and T, due to extremely low concentrations of SRP in these samples and the insufficient mass of Ag_3PO_4 that could be recovered using the **Method 2** extraction procedure.

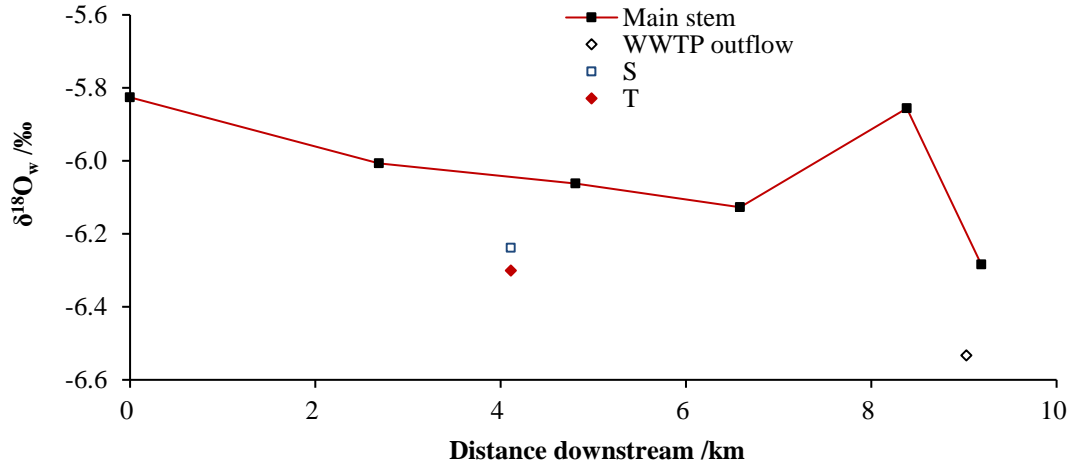


Figure 5.10: Mean $\delta^{18}\text{O}_w$ against distance downstream of site A on the Caker stream. Analytical uncertainty based on 2 standard errors of the LEC TAP standard measurements is $\pm 0.15\text{‰}$.

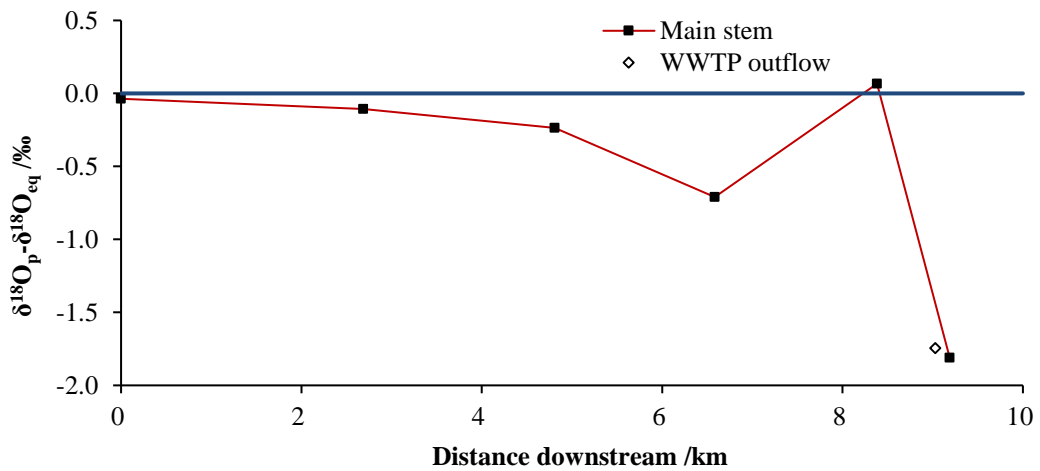


Figure 5.11: Difference between calculated equilibrium $\delta^{18}\text{O}_{eq}$ based on **Equation 4** and the mean $\delta^{18}\text{O}_p$ ratios for samples from the Caker stream. At $\delta^{18}\text{O}_p - \delta^{18}\text{O}_{eq} = 0$, $\delta^{18}\text{O}_p$ is assumed to be at temperature dependent equilibrium with $\delta^{18}\text{O}_w$.

Distinct patterns were also observed in both $\delta^{18}\text{O}_w$ (**Figure 5.10**) and $\delta^{18}\text{O}_{eq} - \delta^{18}\text{O}_p$ (**Figure 5.11**) profiles. The difference between $\delta^{18}\text{O}_{eq}$ and $\delta^{18}\text{O}_p$ increased steadily from -0.04 to -0.71‰ across sites A to D, before a substantial return towards equilibrium between sites D and E. The influence of WWTP effluent input between sites E and F was again evident in $\delta^{18}\text{O}_{eq} - \delta^{18}\text{O}_p$, which increased to approximately -1.8‰ at site F. The variation in $\delta^{18}\text{O}_w$ between sites followed almost exactly the pattern described above for $\delta^{18}\text{O}_{eq} - \delta^{18}\text{O}_p$. Despite a substantially lower $\delta^{18}\text{O}_w$ at

sample sites S and T, the input of this tributary to the main stream stem did not appear to significantly alter $\delta^{18}\text{O}_w$ between sample sites B and C.

5.4 Discussion

5.4.1 Characterising $\delta^{18}\text{O}_p$ within groundwater and assessing microbially-mediated cycling of P_i in groundwater using $\delta^{18}\text{O}_p$

Groundwater SRP concentrations were elevated in the vast majority of the samples reported in this chapter. These concentrations are consistent with other studies that have found elevated SRP concentrations in some groundwater in England, particularly in groundwater derived from the Lower Greensand formation (Shand *et al.*, 2003; Holman *et al.*, 2010). However, the mean SRP concentration for the Lower Greensand groundwater reported in this chapter ($\bar{x} = 0.544 \text{ mg P.L}^{-1}$) far exceeds the $<0.02\text{-}0.311 \text{ mg P.L}^{-1}$ range reported by Shand *et al.* (2003) for groundwater in the same geological unit. The two spring samples (G1) derived from this formation had a greater mean SRP concentration ($0.718 \text{ mg P.L}^{-1}$) relative to the borehole samples derived from this unit, alongside the highest NO_3^- concentrations, suggesting an additional source of P_i at the ground surface. The Lower Greensand group consists of bands of sandstones and clays (Ellison *et al.*, 2002); therefore differences in flow path dependent on the exact strata which the groundwater flows through, and consequently differences in residence times, could cause the resulting observed differences between the deeper borehole and surface spring samples.

Similarly, the mean SRP concentration in the Upper Greensand ($0.415 \text{ mg P.L}^{-1}$) was elevated in relation to many UK groundwaters, including previously reported P_i concentrations in Lower Greensand groundwaters (Shand *et al.*, 2003; Holman *et al.*, 2010). In addition, the G3 spring samples in the Upper Greensand formation were considerably more enriched in terms of SRP, NO_3^- and DOC concentrations than the borehole samples derived from this geological unit, although the G2 spring sample was more consistent with the borehole samples, suggesting that G3 may be influenced by additional source of P at the ground surface, but that G2 is more reflective of the

subsurface groundwater. The contrast between G2 and G3 also support that a difference in flow path could result in differences in the groundwater chemistry; for example, the flow path that G2 is derived from could have been more isolated from the surface than that for sample G3, with either more numerous or thicker layer(s) of Gault Clay overlying the pathway, reducing groundwater recharge along its flow path.

This suggests that one explanation for the elevated concentrations of P_i observed within groundwater derived from both the Lower and Upper Greensand formations is that P_i from sources at the ground surface are able to leach into groundwater. This is particularly supported by the elevated DOC concentrations observed in the June sampling from sites G4 and G15. Potential sources for this additional P_i include inorganic fertilisers, or leakage from sewage pipes or septic tanks. For all three possible sources, a strong positive linear correlation between NO_3^- and SRP could be hypothesised, as these sources contain NO_3^- alongside P_i . However, while a significant correlation was found between NO_3^- and P_i , only a weak linear regression was exhibited in **Figure 5.4c**. Nitrate concentrations from Lower Greensand borehole samples ranged from 0.17 to 5.38 mg N.L⁻¹, and mean SO_4^{2-} and Cl^- concentrations were 7.33 mg S.L⁻¹ and 17.41 mg Cl.L⁻¹ respectively; the concentrations of all three ions were consistent with the findings reported by Shand *et al.* (2003). Therefore, these nutrients, unlike the P_i concentrations, were not particularly elevated compared to Shand *et al.* (2003) and this is suggestive of the addition of a P_i -only source. Consequently, this does not suggest a surface-derived P_i source. One alternative source for elevated P_i concentration in groundwater from the Lower Greensand is the dissolution of phosphatic nodules contained with this formation, which can contain 40-60% calcium phosphate (Pigott, 1964).

Globally, only a total of nine data points for $\delta^{18}O_p$ in groundwater have been reported to date in the published literature. Therefore, the data included in this chapter represent a substantial addition to the worldwide library of stable isotope data related to P_i within groundwater. Although $\delta^{18}O_p$ across the groundwater samples reported in this chapter had a range of 3.56‰ (from 17.02 to 20.58‰), the data do lie within the range of 15.1 to 22.4‰ reported for groundwater in previous studies (Blake *et al.*, 2001; McLaughlin *et al.*, 2006a; Young *et al.*, 2009), suggesting some consistency across groundwater derived from different geographical locations and from different

geological units. When combined with previously published data for groundwater, the total number of groundwater samples for which $\delta^{18}\text{O}_p$ has been determined increases from 9 to 24, the mean $\delta^{18}\text{O}_p$ increases from 18.6 to 19.1‰ and the standard deviation decreases from 2.13 to 1.57‰. **Figure 5.12** summarises the range of $\delta^{18}\text{O}_p$ values reported in the literature from various environments. From these data, it is clear that there is overlap in the ranges of $\delta^{18}\text{O}_p$ across different samples types from the current data in published literature (see **Table 2.1**). For example, within the worldwide dataset the lower tail of groundwater overlaps with the heavier tail of both WWTP effluents and river waters. Therefore, from a worldwide perspective, groundwater may not present a distinct $\delta^{18}\text{O}_p$ compared to other freshwater ecosystems, which could adversely impact its utility as a tracer of P_i inputs from groundwater into surface water. However, whilst global-scale differentiation in $\delta^{18}\text{O}_p$ between individual sample types may not be realised, differences related to sources and/or cycling at more local scales may still exist, providing potential opportunities for application of $\delta^{18}\text{O}_p$ to address questions of P source and biogeochemical cycling (Gooddy *et al.*, 2015). Indeed, this is confirmed in **Figure 5.12** at the UK-scale based on the separation between $\delta^{18}\text{O}_p$ in groundwater samples and in final effluents from WWTPs that have been analysed in this thesis.

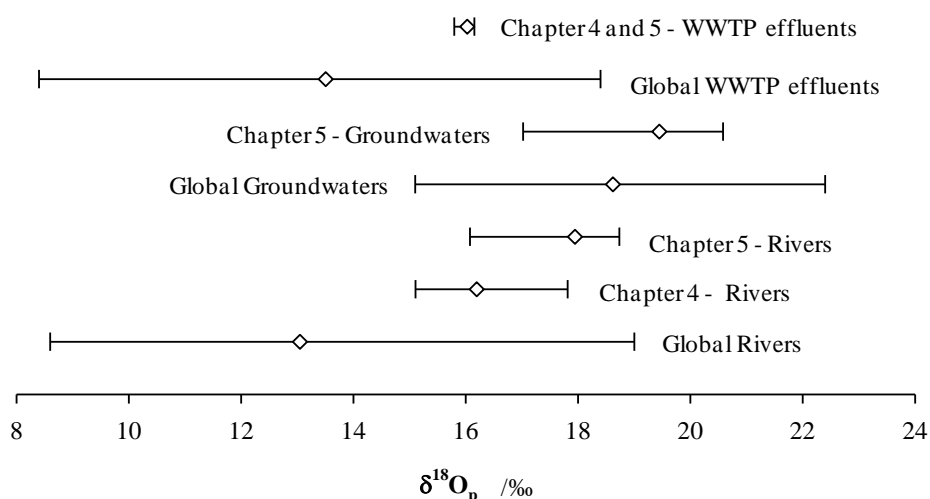


Figure 5.12: Global $\delta^{18}\text{O}_p$ ratios in relation to $\delta^{18}\text{O}_p$ data reported in **Chapters 4** and **5**. Mean values are represented by diamonds, and tails shown the range of all data. Global data derived from references within **Table 2.1** and Gooddy *et al.* (2016).

Despite the difference in SRP concentration between samples from springs and boreholes, there was no significant difference in $\delta^{18}\text{O}_p$ between these two sample types. This suggests that there is no significant alteration of $\delta^{18}\text{O}_p$ associated with

differences in residence time and/or transport pathway between borehole and spring samples. Furthermore, if a significant additional source of P_i was introduced at or close to the ground surface in the spring samples, leading to higher SRP concentration than in the borehole samples, this source must have been isotopically similar to that of the bulk groundwater P_i . However, $\delta^{18}O_p$ in groundwater did vary significantly dependent on the bedrock unit that a sample was collected from, with a mean difference between samples from the Upper Greensand (18.12‰, $1\sigma = 0.77\%$) and Lower Greensand (20.11‰, $1\sigma = 0.38\%$) of approximately 2‰. The $\delta^{18}O_p$ of samples from the Upper Greensand was also highly consistent with $\delta^{18}O_p$ from MilliQ water extracts of Upper Greensand rock material, that exhibited a mean $\delta^{18}O_p$ of 18.19‰ ($1\sigma = 0.43\%$). This suggests that groundwater P_i in this unit is likely to be derived abiotically from the bedrock material, for example through simple dissolution, with no significant fractionation or isotope effect within the groundwater itself. Whilst P_i may have been derived from the surface, the consistency between $\delta^{18}O_p$ in rock extracts and in groundwater samples, coupled the existence of confining clay layers within the region that could have prevented recharge from the surface reaching the groundwater, suggests that geogenic rather than anthropogenic sources of P to groundwater are more likely. However, further work is required to determine $\delta^{18}O_p$ for water-extractable P_i from other bedrock units, in order to establish whether this consistency between $\delta^{18}O_p$ in groundwater and in bedrock extracts is present in other geological formations. In addition, other potential mechanisms for the release of P_i from geogenic sources, such as acid dissolution, should be evaluated in terms of their likely impact on $\delta^{18}O_p$ of P_i released from bedrock. In conclusion, the combination of hydrochemical and stable isotope data indicates that geogenic sources may contribute to elevated concentrations of P_i in some geological units. Consequently, this raises questions about the fate of geogenic P_i in groundwater, and about the potential environmental impact of geogenic P_i if delivered to surface water ecosystems.

The groundwater $\delta^{18}O_p$ data reported within this chapter have a negative correlation and regression with $\delta^{18}O_w$ (**Figure 5.5a**), suggesting that isotopically heavier $\delta^{18}O_p$ was associated with samples in which $\delta^{18}O_w$ was isotopically lighter. This is inconsistent both with intracellular cycling of P_i and with extracellular hydrolysis of P_{org} as potential influences on $\delta^{18}O_p$ within groundwater because, under conditions in which these processes operated, a positive correlation between $\delta^{18}O_p$ and $\delta^{18}O_w$ would

be expected (Blake *et al.*, 2001). In addition, no significant correlation was observed between the difference $\delta^{18}\text{O}_p - \delta^{18}\text{O}_{eq}$ and water temperature (**Figure 5.6**). When compared to the theoretical equilibrium ($\delta^{18}\text{O}_{eq}$), P_i in groundwater appears to be in a state of isotopic disequilibrium, with a mean $\delta^{18}\text{O}_p - \delta^{18}\text{O}_{eq}$ value of +2.79 and +0.31‰ for the Lower and Upper Greensand samples respectively. Whilst it appears that the mean state of the Upper Greensand groundwater was much closer to $\delta^{18}\text{O}_{eq}$, the absolute difference across all samples from this unit ranged from -1.18 to +1.43‰, indicating that most individual samples were not close to equilibrium. There was no significant difference in $\delta^{18}\text{O}_p - \delta^{18}\text{O}_{eq}$ values across borehole and spring samples.

In comparison with previous studies, the fact that $\delta^{18}\text{O}_p$ in the vast majority of samples reported in the current chapter were not at temperature-dependent equilibrium with $\delta^{18}\text{O}_w$ is consistent with the findings of Young *et al.* (2009), who showed no evidence of intracellular metabolism of P_i within groundwater extracted from two different depths in the San Joaquin River system (California, USA). Conversely, Blake *et al.* (2001) did report a positive correlation between $\delta^{18}\text{O}_p$ and $\delta^{18}\text{O}_w$ as evidence to support biological activity influencing P_i within a shallow glacial outwash aquifer in Cape Cod, Massachusetts, USA. However, this study was conducted on a highly contaminated aquifer that had received sewage effluent and it was speculated that metabolic turnover of the P_i pool was stimulated by the delivery of dissolved organic carbon (DOC) associated with sewage. These authors speculated that in groundwater with low DOC concentrations, complete metabolic turnover of P_i would not occur. This appears to be consistent with the data reported in the current chapter, compounded by elevated P_i concentrations from geogenic sources, which results in little isotopic evidence for metabolic processes influencing $\delta^{18}\text{O}_p$ from groundwater samples in the Upper or Lower Greensand units. This suggests that source $\delta^{18}\text{O}_p$ signatures may persist within P_i in groundwater, rather than being rapidly over-printed by fractionations associated with metabolic processes.

5.4.2 Evidence for sources and biogeochemical cycling of P within the Caker stream

5.4.2.1 Phosphorus dynamics as interpreted from hydrochemical data

The SRP concentration profile of the river reach sampled within this chapter indicated a steady decrease along the main stem of the Caker stream, before a sharp increase coinciding with the input of WWTP effluent between sites E and F. This increase elevated the in-stream SRP concentration to $0.789 \text{ mg P.L}^{-1}$, only $0.308 \text{ mg P.L}^{-1}$ below that of the WWTP effluent itself, and coincided with substantial increases in both NO_3^- concentrations and surface water temperatures (**Table 5.5**). This is consistent with the findings reported in section **4.4.1**, alongside many previous studies, that demonstrate that significant influence of WWTP effluent on in-stream hydrochemical conditions, in particular through increases in SRP concentration to levels that reflect those within an effluent discharging to the stream (Bowes *et al.*, 2005; Carey and Migliaccio, 2009; Gammons *et al.*, 2010; Goody *et al.*, 2016).

The monotonic decrease in SRP concentration along the majority of the upper reach of the Caker stream (sites A to E) may suggest hydrological dilution, whereby a water source with lower SRP concentration than the main stream discharged to the stream, thereby reducing SRP concentration (Hooda *et al.*, 1997; Young *et al.*, 1999). In addition, the DOC concentration profile between sites A and E was similar to that described for SRP. Given that there was little precipitation during the sampling campaign, and thus overland flow was unlikely to be a significant input to the stream, two possible sources of water that may have been responsible for dilution remain, either surface water tributaries or groundwater. A number of tributaries form confluences with the Caker stream along the reach, with tributaries entering the main stem between every sample site with the exception of sites E and F between which the WWTP effluent is discharged. However, the concentration of SRP was only determined for one of the more major tributaries to the Caker stream (sites S and T), which was associated with a spring source and enters the main stem between sites B and C. Both sample sites S and T had very low SRP concentration (mean $0.027 \text{ mg P.L}^{-1}$), approximately $0.283 \text{ mg P.L}^{-1}$ below the concentration at site B upstream of the confluence with this tributary. Therefore, it is possible that the input of water from this tributary may have resulted in decreased SRP concentration within the main stream stem, resulting in the SRP concentration profiles in **Figure 5.7**. Given that most

tributaries within the catchment rise from groundwater springs and flow through similar land use covers, it could be argued that similar SRP concentrations may reasonably be expected within the other tributaries entering the main stem along this reach of the Caker stream. However, it would also be expected that a more stepped change in SRP concentration would be apparent along the reach, due to the individual inputs from tributaries that range in size, and potentially SRP concentration. In addition, the SRP concentrations found in the spring samples reported in **Section 5.3.1**, are considerably greater than those of sample sites S and T, therefore SRP concentrations could be variable in the tributaries joining the main Caker stream in this reach. Furthermore, the NO_3^- profile within the Caker stream was not consistent with dilution by surface water tributaries, with a decreasing concentration of NO_3^- between sites A and E despite a relatively high concentration of NO_3^- observed at sample sites S and T. This is not consistent with dilution by surface water tributaries, unless an alternative water source was entering the stream, or unless NO_3^- was being removed by in-stream biogeochemical processes, such as denitrification (Seitzinger, 1988; Mulholland *et al.*, 2008), within the main stream stem.

Alternatively, groundwater discharge along this reach of the Caker stream may have been responsible for the observed decreases in SRP concentration between sample sites A and E. The Caker stream rises on the Upper Greensand (sites A and B) and is underlain by chalk geology in the downstream section of the sampled reach (sites B-F). Although the Upper Greensand springs and boreholes measured in **Table 5.3** suggested the potential for elevated SRP concentrations in groundwater derived from this formation, every groundwater sample, except one, exhibited an SRP concentration below that observed at site A on the Caker stream, with some samples being extremely low in terms of P_i concentration (for example, G14: 0.049 and G15: 0.035 mg P.L^{-1}). The concentration of SRP in groundwater supports the hypothesis that groundwater discharge may have been responsible for dilution of SRP concentration within the Caker stream. Furthermore, the steady decrease in SRP concentration, suggesting a constant diffuse input along the reach, in combination with a stream water temperature profile that increases steadily between sites A and E, was consistent with groundwater discharge to the Caker stream (Constantz, 1998; Becker *et al.*, 2004).

However, without the use of inherent tracer for SRP, the cause of changes in SRP concentration along the in-stream transect cannot be properly explored. Concentration data provide little information about the fate of in-stream P_i , for example it is also possible that metabolic processes may have altered P_i concentration and produced the profile observed along the sampled reach of the Caker stream. Using the 166C:20N:1P molar ratio to indicate which nutrient element may have limited production within the system, all samples from the Caker stream would be considered as P_i -limited (Sterner *et al.*, 2008). In an ecosystem in a state of P_i -limitation, P_i addition to the system would be expected to stimulate biological activity, either through intracellular metabolism and/or biological uptake. These processes would lead to an isotopic fractionation or isotope effect influencing $\delta^{18}O_p$ alongside, in the case of intracellular metabolism, the approach of $\delta^{18}O_p$ towards $\delta^{18}O_{eq}$. Therefore, the use of $\delta^{18}O_p$ may provide additional insights into the importance of in-stream biogeochemical process for the fate of P_i along the sampled reach of the Caker stream.

5.4.2.2 Insights into the sources and biogeochemical cycling of P within the Caker stream through stable isotope analysis

Within the Caker stream, $\delta^{18}O_p$ decreased steadily from 18.73‰ at site A to 17.59‰ at site D. This downstream trend matched that observed in the concentration of SRP between the same sampling sites. Decreasing $\delta^{18}O_p$ along this reach either reflects the input of water to the stream with $\delta^{18}O_p$ that is isotopically lighter compared to that at site A, or the action of a process which leads to oxygen isotope fractionation or an isotope effect that produces isotopically lighter $\delta^{18}O_p$.

Groundwater from the Upper Greensand within the region had a mean $\delta^{18}O_p$ of 18.12‰ ($1\sigma = 0.77\%$), although the range of $\delta^{18}O_p$ from groundwater in this aquifer was 17.02 to 18.88‰. Coupled with SRP concentrations in the Upper Greensand groundwater, these stable isotope data confirm that groundwater discharge to the Caker stream may have been responsible for the observed $\delta^{18}O_p$ profile between sites A and E. Further support for potential groundwater discharge to the Caker stream is provided by $\delta^{18}O_w$ that also decreased steadily in the main stream stem between sites A and E, with $\delta^{18}O_w$ in groundwater samples from the Upper Greensand averaging 0.43‰ lower than at site A in the Caker stream. Despite substantially lower $\delta^{18}O_w$ in the tributary represented by sample sites S and T compared to the Caker stream, no

step change in $\delta^{18}\text{O}_w$ was observed between sites B and C as might be expected if the physical addition of this surface tributary were significantly influencing the hydrochemistry of the main stream stem. Because $\delta^{18}\text{O}_p$ within groundwater was relatively close to that at site A in the Caker stream, a substantial contribution from groundwater discharge to discharge within the Caker stream would have been required in order to produce the observed trend in $\delta^{18}\text{O}_p$ within the main stream stem. However, the $\delta^{18}\text{O}_p$ data reported in this chapter for groundwater derived from the Upper Greensand relate to only four samples collected from three different locations. Therefore, it remains possible that groundwater from other locations in the Upper Greensand is associated with more isotopically depleted $\delta^{18}\text{O}_p$, compared to the data reported here. A more extensive sampling campaign would be required to further characterise $\delta^{18}\text{O}_p$ in groundwater from the Upper Greensand. However, it is noted that $\delta^{18}\text{O}_p$ in bedrock extracts from the Upper Greensand averaged 18.19‰. Therefore, substantially depleted $\delta^{18}\text{O}_p$ in Upper Greensand groundwater would have to be associated with different $\delta^{18}\text{O}_p$ in source bedrock material across the aquifer unit and/or fractionation or isotope effects acting during the initial release of P_i from bedrock into solution or during subsequent transport of P_i within the aquifer.

The change in $\delta^{18}\text{O}_p$ within the Caker stream between sites D and E (a 1.11‰ increase) differs substantially compared to that observed between sites A and D. Therefore, coupled with the fact that SRP concentration decreased between sites D and E, it is extremely unlikely that $\delta^{18}\text{O}_p$ solely reflects groundwater discharge to the stream between these sites. An explanation based on continued groundwater discharge would require that groundwater with a substantially more enriched $\delta^{18}\text{O}_p$ than reported within this chapter discharged to the Caker stream. Alongside a substantial increase in $\delta^{18}\text{O}_p$ between D and E, a reversal in the patterns seen across upstream sample sites in terms of water temperature and $\delta^{18}\text{O}_w$ was observed. Taken together, these data suggest that a water source with lower P_i concentration and water temperature, alongside elevated $\delta^{18}\text{O}_w$, may have entered the Caker stream between sites D and E. However, further work would be required to identify this water source beyond the sampling undertaken for the current chapter.

Alternatively, the change in $\delta^{18}\text{O}_p$ between sample sites D and E on the Caker stream may also be consistent with intracellular cycling influencing the fate of P_i in this

reach. Between the same sample sites, the difference between $\delta^{18}\text{O}_p$ and the theoretical equilibrium, $\delta^{18}\text{O}_{eq}$, decreased to approximately -0.07‰. Whilst changes in $\delta^{18}\text{O}_w$ and water temperature between these sample sites will lead to changes in the value of $\delta^{18}\text{O}_{eq}$ (**Equation 4**), the change in absolute values of $\delta^{18}\text{O}_p$ also indicates that isotope fractionation or an isotope effect occurred, consistent with a metabolic process influencing the fate of P_i in this reach. The increase in $\delta^{18}\text{O}_p$ and movement toward $\delta^{18}\text{O}_{eq}$ are consistent with intracellular metabolism of P_i between sites D and E on the Caker stream. However, between sites A and D, the divergence of $\delta^{18}\text{O}_p$ from $\delta^{18}\text{O}_{eq}$ increased, alongside the decrease in absolute values of $\delta^{18}\text{O}_p$ described above. Intracellular metabolism cannot be the cause of this trend, due to the increasing movement of $\delta^{18}\text{O}_p$ away from $\delta^{18}\text{O}_{eq}$ (Puc at *et al.*, 2010; Chang and Blake, 2015). Uptake of extracellular P_i and incorporation into biomass results in a kinetic isotope effect, due to preferential uptake of isotopically lighter P_i isotopologues by microbial and plant communities, resulting in an increase in $\delta^{18}\text{O}_p$ within residual P_i in the extracellular environment, which is inconsistent with the in-stream $\delta^{18}\text{O}_p$ profile, alongside a decrease in SRP concentration (Blake *et al.*, 2005). Similarly, extracellular hydrolysis of P_{org} to yield P_i represents another metabolic process that could lead to change in $\delta^{18}\text{O}_p$. This process has the potential to cause a decrease in $\delta^{18}\text{O}_p$ within the extracellular environment, due to kinetic and/or inheritance isotope effects, with the resulting $\delta^{18}\text{O}_p$ lying between that of the P_{org} molecule and $\delta^{18}\text{O}_w$ (see **2.2.3** for further discussion) (Blake *et al.*, 1997; Colman *et al.*, 2005; Liang and Blake, 2006b). However, this process yields additional P_i , in contrast to the SRP profile observed between sites A and D on the Caker stream. Finally, abiotic ion exchange in which aqueous P_i is abiotically exchanged with P_i ions in the sorbed phase that may be at disequilibrium, can also result in disequilibrium isotope effects (Jaisi *et al.*, 2011). However, within natural ecosystems abiotic ion exchange occurs at a very slow rate and therefore is likely to be masked or overprinted by any biological processes that are altering the P_i pool. Therefore, it is unlikely to be a main driver of change observed within the $\delta^{18}\text{O}_p$ river profile. In conclusion, the gradual decrease in $\delta^{18}\text{O}_p$ between sites A and D on the Caker stream is most likely to reflect groundwater discharge to the stream along this reach, and thereby for groundwater-derived P that is isotopically depleted in $\delta^{18}\text{O}_p$ compared to conditions at site A.

5.5 Conclusions

Globally, only a total of nine data points for $\delta^{18}\text{O}_p$ in groundwater have been reported to date in the published literature. Therefore, the data included in this chapter represent a nearly threefold increase to the worldwide library of stable isotope data related to P_i within groundwater. In addition, the groundwater $\delta^{18}\text{O}_p$ signature has become more constrained – for example, within the Alton and Tillingbourne catchments in southern England, groundwater $\delta^{18}\text{O}_p$ exhibits consistency across sample locations and sample types within the same geology. However, $\delta^{18}\text{O}_p$ reflects the bedrock geology with lighter Upper Greensand (18.12‰, $1\sigma = 0.77\text{‰}$) and heavier Lower Greensand (20.11‰, $1\sigma = 0.38\text{‰}$), and notably the Upper Greensand groundwaters display little alteration to the bedrock material. This is essential knowledge for future studies where groundwater may be a significant P_i input. The very small difference in $\delta^{18}\text{O}_p$ between solid phase-extracted P_i and groundwater P_i within the Upper Greensand formation and a system in disequilibrium with respect to $\delta^{18}\text{O}_{\text{eq}}$ suggest that abiotic weathering dominates the P_i cycling within the groundwater. However, further work is required to determine the effects of seasonality, temperature and biological processing across a larger range of natural and contaminated sites.

In addition, this chapter has shown that by analysing $\delta^{18}\text{O}_p$ and $\delta^{18}\text{O}_w$, in conjunction with a classical hydrochemical approach, the groundwater discharge from an Upper Greensand aquifer may be shown to play an important role in P_i biogeochemical cycling within a small river catchment. However, for this study there was insufficient evidence to determine the cause of the deviation from $\delta^{18}\text{O}_{\text{eq}}$; although, similarly to **Chapter 4**, several common biogeochemical cycling processes have been ruled out which would not have been possible using a hydrochemical approach. **Chapter 6** will compare how $\delta^{18}\text{O}_p$ helped to elucidate the occurrence of biogeochemical processes that were masked in in-stream SRP concentration profiles and will explore how $\delta^{18}\text{O}_p$ may be used in future biogeochemical studies of P within freshwater ecosystems.

Chapter 6: Discussion and consideration of future requirements for $\delta^{18}\text{O}_p$ research

Analysis of $\delta^{18}\text{O}_p$ within P_i represents a novel, inherent and potentially powerful stable isotope tracer for biogeochemical research focussed on P. However, due to the challenges of robustly extracting P_i for $\delta^{18}\text{O}_p$ analyses from freshwater matrices, only a relatively limited number of studies have attempted to use $\delta^{18}\text{O}_p$ in order to assess the sources and metabolism of P_i in freshwater ecosystems (Blake *et al.*, 2001; Gruau *et al.*, 2005; McLaughlin *et al.*, 2006a; McLaughlin *et al.*, 2006c; Elsbury *et al.*, 2009; Young *et al.*, 2009; Li *et al.*, 2011). This thesis has sought to couple the development of new protocols for determination of $\delta^{18}\text{O}_p$ with application of these protocols within exemplar freshwater ecosystems. This was achieved through addressing the four key objectives of the thesis as formulated in **Chapter 1**:

1. To develop, optimise and test extraction protocols for analysis of $\delta^{18}\text{O}_p$ in surface water and groundwater matrices.
2. To determine $\delta^{18}\text{O}_p$ in river water, wastewater treatment plant (WWTP) effluent and groundwater to constrain $\delta^{18}\text{O}_p$ in potential sources of P_i to freshwater stream ecosystems.
3. To examine changes in $\delta^{18}\text{O}_p$ within river water as an indicator for the in-river fate of P_i derived from sources including WWTP final effluent and groundwater.
4. To determine whether $\delta^{18}\text{O}_p$ within groundwater can act as a tracer for the sources and metabolism of P_i within groundwater and the discharge of groundwater-derived P_i to surface water ecosystems.

In this chapter, the contribution made by the thesis towards addressing each of these objectives is first summarised. Subsequently, the chapter moves on to place the outcomes of the thesis in the broader context of research using $\delta^{18}\text{O}_p$ to address questions surrounding P biogeochemistry, and to consider key priorities for future development and application of this novel stable isotope technique.

6.1 Development of robust analytical protocols for $\delta^{18}\text{O}_p$ in freshwater matrices

Chapter 3 sought to address the first objective of the thesis by advancing the protocols available for analysis of $\delta^{18}\text{O}_p$ within freshwater matrices. **Figure 2.4** summarises five key protocols for $\delta^{18}\text{O}_p$ analysis in natural samples – three based on natural aqueous samples (McLaughlin *et al.*, 2004; Gruau *et al.*, 2005; Goldhammer *et al.*, 2011a) and two based on extracts of soil samples (Tamburini *et al.*, 2010; Weiner *et al.*, 2011). **Chapter 3** focussed on evaluating the McLaughlin *et al.* (2004) protocol that had originally been developed for marine waters when applied to freshwater matrices (**Figure 3.1**), and subsequently developing new sample processing stages as part of this protocol in order to more robustly determine $\delta^{18}\text{O}_p$ within freshwater samples.

To achieve this, **Method 3 (Figure 3.12)** was newly developed and evaluated within this thesis, whilst **Method 2 (Figure 3.7)**, which had previously been developed within the research group (Goody *et al.*, 2016) was further evaluated within this thesis. Both methods target the isolation of P_i from a freshwater matrix, with the use of specific DOM removal resins to reduce the probability of P_{org} hydrolysis, alongside the use of anion exchange resins to chromatographically separate P_i from competing oxyanions. Both methods use DAX8 resins, which also feature in the Weiner *et al.* (2011) and Tamburini *et al.* (2010) methods, to remove strongly hydrophobic organic matter from a matrix that is often attributed to humic and fulvic acids DOM (Carroll *et al.*, 2000). However, a key advance in both **Methods 2 and 3** compared to previously published protocols is the use of an anion exchange resin to concentrate and chromatographically isolate P_i from large volumes of water that potentially contain

substantial quantities of competing oxyanions, alongside P_i . **Method 3** also incorporates a second resin that targets DOM removal – ISOLUTE® ENV+ – specifically for polar analytes (Alonso *et al.*, 1999; Biotage, 2004). Importantly, this thesis developed **Method 3** to overcome a potentially important limitation of **Method 2**, in which variable sample volumes and matrix compositions must be loaded onto DAX-8 and anion exchange resins. This is a particular challenge in freshwater samples where the P_i concentration can vary significantly, meaning that the sample volume to be loaded onto a resin in order to generate sufficient Ag_3PO_4 also varies significantly, as does the composition of the sample matrix. Therefore, through the introduction of an initial MagIC precipitation, **Method 3** sought to ensure that a standardised matrix is subsequently loaded onto the DOM-removal and anion exchange resins.

Method 3 proved to generate $\delta^{18}O_p$ data with greater precision in laboratory trials (**Section 3.5**) compared to **Method 1** (the original McLaughlin *et al.* (2004) protocol). However, the mean $\delta^{18}O_p$ determined following precipitation of Ag_3PO_4 was isotopically lighter than that of the inorganic P_i spike added to test solutions. This inaccuracy was most likely due to the consistent loss of P_i during the loading of the anion exchange resin for all matrices used in the trials in **Section 3.5**. For example, using the WWTP matrix, 43.2% of the starting P_i mass was lost throughout all the resin stages (steps 3c-7c in **Figure 3.12**), of which the majority was found in the waste stream when loading the anion exchange resin (39.9% of starting mass of P_i). Minimal losses (~1%) were associated with the ENV+ and DAX8 resin stages. After further analysis, it was established that the increased total mass of acetic acid loaded onto the anion resin, relative to earlier trials described in **Section 3.4**, had prevented P_i from effectively sorbing to the solid phase anion exchange resin. Given the large proportion of P_i that did not bind to the anion exchange resin, an isotope effect associated with the loss of P_i during loading of the resin cannot be ruled out, and this potential isotope effect may have influenced the resulting $\delta^{18}O_p$ from the trials reported in **Section 3.5**. In addition, the low yields of Ag_3PO_4 that were periodically generated using **Method 3** resulted in an incomplete evaluation dataset within **Chapter 3**. In contrast, **Method 2** has been proven to combine accuracy and precision relative to **Method 1**, consistently generating sufficient Ag_3PO_4 yields for repeated isotope analyses. Therefore, **Chapters 4** and **5** applied **Method 2** universally to the samples. However,

where P_i concentration and sample volumes allowed, a repeat analysis was also performed using **Method 3**. In total, 28 samples were run in parallel through both **Methods 2** and **3** (**Table 6.1**), allowing for a comparison of the resulting isotope data. For these parallel analyses using **Methods 2** and **3**, the anion exchange resin conditions used within **Method 3** were altered to match those of **Method 2**. Specifically, the anion exchange resin volume was increased from 12.5 mL to 50 mL and the molarity of the KCl eluent was increased from 0.25M to 0.3M. In addition, the re-dissolved brucite samples generated in step 2c of **Method 3** (**Figure 3.12**) were diluted to 0.6%_{v/v} acetic acid to ensure the acetic acid concentration was similar to that used in previous trials described in **Section 3.4**. Following these adjustments, in most cases a sufficient mass of Ag_3PO_4 for triplicate TCEA-IRMS analysis was precipitated overcoming the limitations observed in terms of Ag_3PO_4 yield that were highlighted in **Chapter 2**. However, further method validation is required to determine if these changes in anion exchange resin conditions improved the accuracy and precision of **Method 3** against spiked test matrices as described in **Chapter 3**.

Table 6.1: Summary of sample codes which were run for $\delta^{18}O_p$ analysis with both **Methods 2** and **3** (see **Tables 4.1** and **5.2** for site descriptions).

Chapter 4		Chapter 5		
March 2015	September 2015	June 2015	Early November 2015	Late November 2015
A	A	G1	G1	A
D	C	G3	G2	W
W	D	G4	G3	F
	W	F	G4	
	E		G5	
	F		G6	
	T		G8	
	G		G12	
	H			
	I			

Figures 6.1 and **6.2** report comparisons of data derived from parallel analysis of samples using **Methods 2** and **3**. To determine if the two methods produced significantly different $\delta^{18}O_p$ for samples that were run in parallel, the data were subjected to a Shapiro-Wilk test for normality which showed **Method 3** data to be normally distributed, whilst **Method 2** data was not normally distributed. The Levene's test showed that the variances on the means (0.708) and medians (0.667) were not significantly different for data drawn from the two methods. Therefore, a

Wilcoxon Signed-Rank Test for paired samples was undertaken. This test showed that the median $\delta^{18}\text{O}_p$ generated using **Method 2** ($\tilde{x} = 16.62$, $n = 28$) was significantly higher compared to that generated using **Method 3** ($\tilde{x} = 16.03$): $T(n=28) = 26$, $p < 0.001$.

To determine if the two methods produced Ag_3PO_4 precipitates from field samples that differed significantly in terms of their purity, the oxygen yield of the samples that were run in parallel using both methods were subjected to a Shapiro-Wilk test for normality which showed that data from both **Methods 2** and **3** were not normally distributed. The Levene's test showed that the variances on the means (0.0525) and medians (0.0612) were not significantly different at a 95% confidence level. Therefore, a Wilcoxon Signed-Rank Test for paired samples was undertaken and showed that the median oxygen yields for Ag_3PO_4 precipitates generated using **Method 3** ($\tilde{x} = 15.33\%$, $\bar{x} = 15.27\%$, $n = 28$) and **Method 2** ($\tilde{x} = 15.37\%$, $\bar{x} = 15.30\%$) were not significantly different at a 95% confidence level. Both methods therefore appeared to generate pure Ag_3PO_4 with oxygen yields, except for one sample, within 10% of that expected based on pure Ag_3PO_4 (**Figure 6.1b**). Whilst oxygen yields greater than 15.3% suggest the presence of contaminant oxygen in an Ag_3PO_4 precipitate, potentially altering $\delta^{18}\text{O}_p$, oxygen yields less than 15.3% indicate that impurities are present in the Ag_3PO_4 but that these additional compounds do not contain any oxygen atoms. As the source of contamination is not oxygen-bearing, for example silver chloride, there should be no effect on $\delta^{18}\text{O}_p$. However, oxygen yields below the expected value may indicate a potential issue during the P_i extraction protocol, for example the incomplete precipitation of Ag_3PO_4 which could have imparted a fractionation P_i within the original sample.

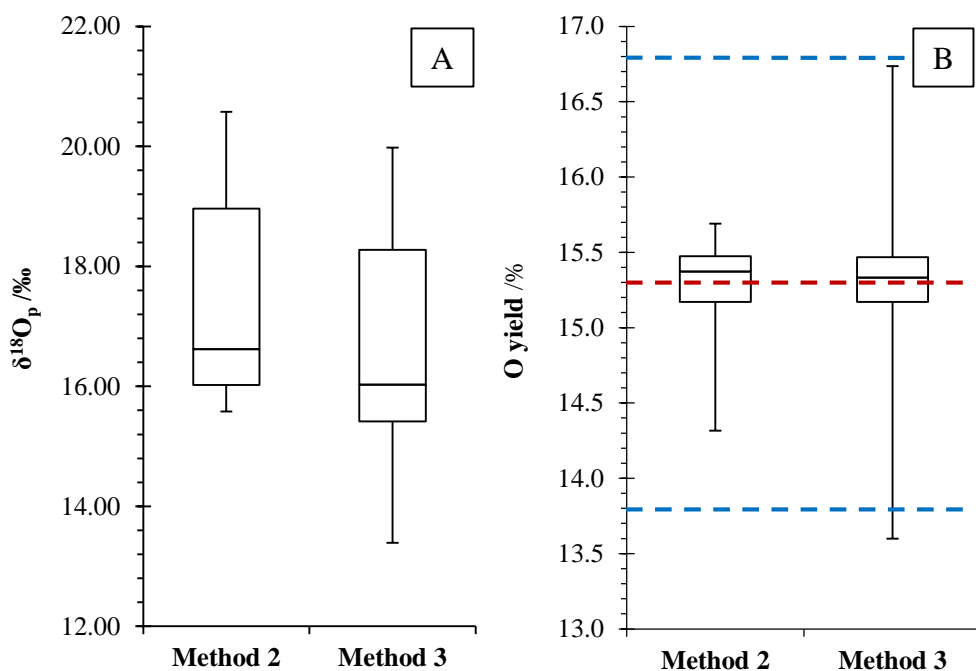


Figure 6.1: a) Boxplot of $\delta^{18}\text{O}_p$ ratios from repeat analyses of sample in **Chapter 4** and **5** using **Methods 2** and **3**. **Method 3** has a significantly lower median $\delta^{18}\text{O}_p$ and wider range. b) Boxplot of oxygen yield of Ag_3PO_4 precipitates from repeat analyses of **Chapter 4** and **5** samples using **Methods 2** and **3**. Both methods have very similar median yields very close to the expected theoretical yield of 15.3% (dashed red line, $\pm 10\%$ boundary blue lines), however **Method 3** has a wider range.

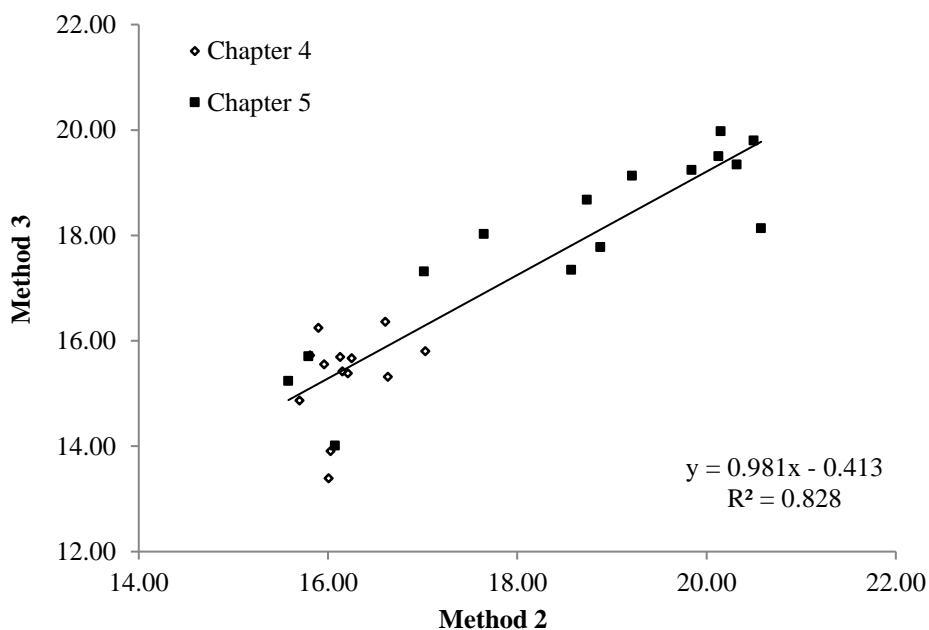


Figure 6.2: Scatterplot of $\delta^{18}\text{O}_p$ derived from samples collected as part of Chapters 4 and 5 and subsequently run using Methods 2 and 3. A linear regression between the two data sets yields the equation “Method 3 = 0.981*Method 2 – 0.413” ($R^2 = 0.828$).

The strong linear regression ($R^2 = 0.828$) between $\delta^{18}\text{O}_p$ for samples extracted with both **Methods 2** and **3** (**Figure 6.2**), suggests that there is a systematic difference between the two protocols. Therefore, the identification of P sources and of processes influencing the transport of P through the environment should be possible using either extraction method, because the relative changes in $\delta^{18}\text{O}_p$ will be maintained across a sample profile regardless of the method. **Figure 6.3** presents a direct comparison of $\delta^{18}\text{O}_p$ for the river profile with the greatest number of repeated samples, based on the September sampling campaign reported in **Section 4.3**. Whilst the general profile of $\delta^{18}\text{O}_p$ along this in-river transect is largely maintained across data derived from both **Methods 2** and **3**, a number of differences exist in terms of the absolute $\delta^{18}\text{O}_p$ data derived from each protocol. In particular, **Method 3** results in a larger range of $\delta^{18}\text{O}_p$ across the profile (2.86‰) compared to **Method 2** (1.40‰), as well as resulting in lower $\delta^{18}\text{O}_p$ values for WWTP effluent and tributary samples (16.13 and 16.01‰ for **Method 2**, and 15.70 and 13.39‰ for **Method 3**). These two specific data points, in combination with the full dataset reported in **Figure 6.1a**, suggest that **Method 3** generates absolute values of $\delta^{18}\text{O}_p$ that are lower compared to data derived from **Method 2**. This is consistent with the results from the validation trials reported in **Section 3.5**, indicating that the altered anion exchange resin conditions described above may have reduced the P_i loss during the loading of the anion exchange resin to allow a greater mass of Ag_3PO_4 to precipitate, but without a correlating increase in $\delta^{18}\text{O}_p$. This suggests that isotopic fractionation was not associated with the loss of P_i during the loading of the anion exchange resin. Therefore, isotopic fractionation may have occurred earlier in the process, for example during the loading of the ENV+ resin or during the acetic acid dissolution stage following the initial MagIC precipitation (steps 5c and 2c respectively in **Figure 3.12**), as these steps are not present in **Method 2**. Consequently, further method evaluation work is required to identify the step causing the observed $\delta^{18}\text{O}_p$ differences between both the KH_2PO_4 spike in **Section 3.5** and the **Method 2** protocol described within this chapter.

In terms of the extent to which the different methods influence the interpretation of the in-stream fate of P_i , it can be seen that in the in-stream patterns in $\delta^{18}\text{O}_p$ are generally very similar for P_i extracted from both **Methods 2** and **3**, however samples extracted using **Method 3** exhibit a greater range of $\delta^{18}\text{O}_p$ (**Figure 6.3**). This similarity in pattern is even clearer when comparing the difference between $\delta^{18}\text{O}_p$ and $\delta^{18}\text{O}_{\text{eq}}$

(**Figure 6.4**), suggesting that the two protocols may differ in absolute $\delta^{18}\text{O}_p$ values but that they are in agreement with respect to the general direction of change of $\delta^{18}\text{O}_p$ - $\delta^{18}\text{O}_{eq}$, thus there is a consistent interpretation of the influence of intracellular metabolism in the $\delta^{18}\text{O}_p$ profile. For example for **Chapter 4** samples, through both protocols the addition of WWTP effluent to the main stream at 1.38 km appears to overprint the upstream $\delta^{18}\text{O}_p$ so that the in-stream $\delta^{18}\text{O}_p$ at site E reflects that of the WWTP final effluent. However, this is associated with an in-stream increase in $\delta^{18}\text{O}_p$ using **Method 2** and a decrease in $\delta^{18}\text{O}_p$ with **Method 3**. However, there is a difference in pattern immediately after the tributary input (2.11-2.18 km), with in-stream $\delta^{18}\text{O}_p$ deflecting towards the $\delta^{18}\text{O}_p$ of the tributary for **Method 2**, but diverging from the measured tributary $\delta^{18}\text{O}_p$ with **Method 3**. Interpretation of the stable isotope and hydrochemical data for **Method 2** suggested this deflection was due to a physical mixing of the main river with the incoming tributary, and consequently a deflection towards the addition to the stream. Conversely, the divergence from the tributary input using **Method 3** is consistent with the pattern surrounding the tributary that was observed in the March campaign using **Method 2**, which was attributed to a potential increase in intracellular metabolism immediately after the tributary confluence or a transient kinetic isotope effect due to sorption of P_i to the river sediments. Following the mixing of the tributary, there are consistent differences across the two methods in terms of downstream changes in $\delta^{18}\text{O}_p$. Therefore, the interpretation of the in-river fate of P_i based on $\delta^{18}\text{O}_p$ analysis would remain consistent.

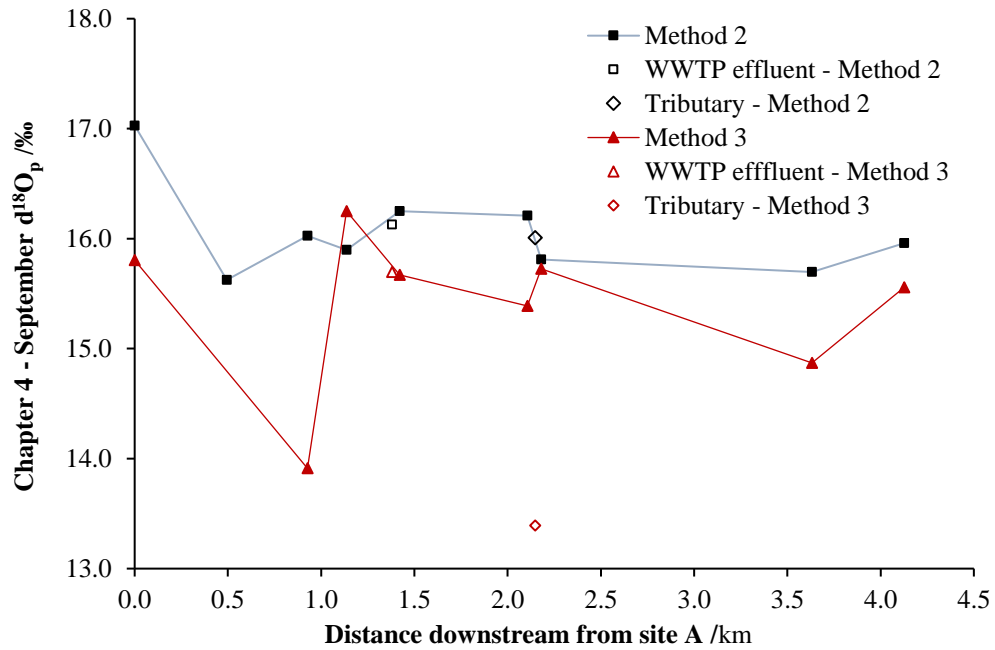


Figure 6.3: Mean $\delta^{18}\text{O}_p$ ratios against distance downstream from site A. Analytical uncertainty based on 2 standard errors of the Acros Ag_3PO_4 standard measurements is $\pm 0.3\%$. Main river stem samples are connected with lines; **Method 2** samples are drawn in black and **Method 3** in red.

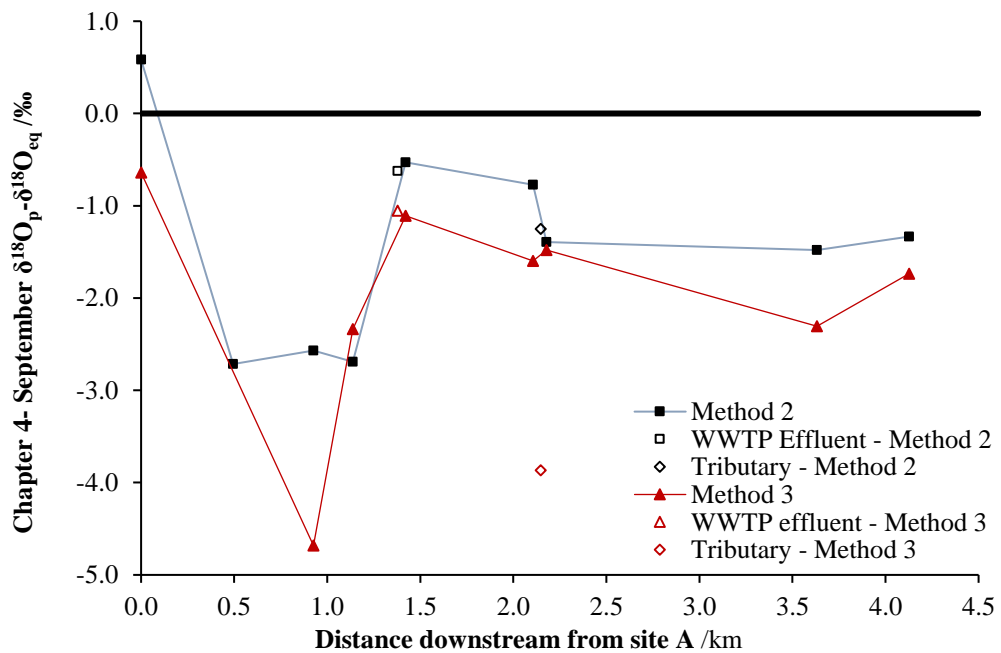


Figure 6.4: Difference between mean $\delta^{18}\text{O}_p$ ratios and theoretical equilibrium $\delta^{18}\text{O}_{eq}$ values. At $\delta^{18}\text{O}_p - \delta^{18}\text{O}_{eq} = 0$, there is no difference between the theoretical and measured values. Main river stem samples are connected with lines; **Method 2** samples are drawn in black and **Method 3** in red.

From the results reported above and within **Chapter 3**, it appears that a systematic difference in $\delta^{18}\text{O}_p$ is generated depending on whether Ag_3PO_4 is precipitated using **Method 2** or **3**. However, both methods generate Ag_3PO_4 that appears to be free of

contaminant oxygen and there is a strong linear relationship between $\delta^{18}\text{O}_p$ data derived from each method. For freshwater matrices, both methods provide a more accurate determination of $\delta^{18}\text{O}_p$ than can be derived from the original extraction protocol (**Method 1**, (McLaughlin *et al.*, 2004)), and would therefore be preferred to ensure the accuracy of $\delta^{18}\text{O}_p$ from freshwater matrices. However, further research is required to better constrain the reasons for the apparent differences in absolute $\delta^{18}\text{O}_p$ derived from **Methods 2** and **3**. In particular, additional method evaluation using KH_2PO_4 spiking as described in **Chapter 3** should be undertaken, but using the altered anion exchange resin conditions that were utilised for the field sample comparison described above. This appears to have overcome the low Ag_3PO_4 yield reported from **Method 3** in **Section 3.5** which may have been responsible for an isotope fractionation or effect, thereby leading to differences between observed $\delta^{18}\text{O}_p$ and the $\delta^{18}\text{O}_p$ of directly pyrolysed KH_2PO_4 (**Figure 3.14**). It is also recommended that a spiked KH_2PO_4 sample is run as a “blank” during laboratory analyses to ensure that, where possible, issues can be identified within the methods and to ensure accuracy and precision are maintained across multiple sample runs. In addition, other analytical methods, such as scanning electron microscopy, could reveal the exact nature of potential contaminants within Ag_3PO_4 precipitates derived from multiple methods.

6.2 Constraining $\delta^{18}\text{O}_p$ within sources of P_i to freshwater ecosystems

When the results from the application of $\delta^{18}\text{O}_p$ reported in this thesis are compared to the existing worldwide library of $\delta^{18}\text{O}_p$ (**Table 2.1** and **Figure 5.12**), it is clear that the data within this thesis are consistent with the ranges of $\delta^{18}\text{O}_p$ previously reported in published literature. No $\delta^{18}\text{O}_p$ data point from **Chapters 4** and **5** lies outside the range of previously published data at a worldwide scale, suggesting that there is general consistency between the data reported here and the worldwide $\delta^{18}\text{O}_p$ dataset.

Furthermore, the second objective of this thesis was to constrain $\delta^{18}\text{O}_p$ in potential sources of P_i to freshwater stream ecosystems, in order to determine how the case study stream systems may be impacted by additions of P_i from these sources. A very

narrow range of $\delta^{18}\text{O}_p$ in WWTP effluents was observed within this thesis (0.4‰) in comparison to that reported in the worldwide dataset (10‰). The worldwide dataset in **Table 2.1** is derived from only three published studies based on effluents from six WWTPs – 16.6–18.4‰, from three WWTPs in France (Gruau *et al.*, 2005), 8.4–13.6‰, from three WWTPs in the USA – in California, Idaho and Ohio (Young *et al.*, 2009) and 8.4 – 11.1‰, from the same Californian WWTP as Young *et al.* (2009), USA (McLaughlin *et al.*, 2006c). Therefore, there appears to be a potential spatial difference in the stable isotope composition of P_i in WWTP effluents; this could be due to differences in technology, P_i sources to WWTPs or flow rates. For example, McLaughlin *et al.* (2006c) noted that a 2.7‰ difference was found for two samples that had been collected under two different effluent outflow rates – high flow (8.4‰) and low flow (11.1‰). Variation in effluent- $\delta^{18}\text{O}_p$ could also arise from differences in the technology and treatment processing of sewage within a WWTP that could impart different $\delta^{18}\text{O}_p$ signatures, such as the presence/absence of P-stripping technology or differing biological treatment approaches which alter bulk P_i or hydrolyse P_{org} . However, the variation may have also derived from differences in the influents to the individual WWTPs. For example, isotopic variation in P_i entering a WWTP from an urban area compared to a rural area, or a diurnal variation in P_i sources, or contrasting mixtures of hydrolysable P_{org} compounds that could impart differing inheritance effects on $\delta^{18}\text{O}_p$ within the effluent. In addition, natural geographical variations in both temperature and $\delta^{18}\text{O}_w$ would equilibrate with P_i to yield differing $\delta^{18}\text{O}_p$ ratios during intracellular metabolism.

In order to be able to perform effective source tracking using $\delta^{18}\text{O}_p$, it is essential that the isotopic composition of a source is constant or varies within a well-constrained range over time. Therefore, further work needs to be conducted to constrain the range of $\delta^{18}\text{O}_p$ in WWTP effluents and to understand the factors responsible for variation in $\delta^{18}\text{O}_p$ across different WWTP effluents. As was noted in **Chapter 4**, despite the very narrow range in $\delta^{18}\text{O}_p$ reported between seasons in this thesis, a greater variation in $\delta^{18}\text{O}_p$ within the effluent from Sutton Valence WWTP (range of 1.4‰) was previously reported across two seasons by Goody *et al.* (2016). However, in the context of the existing worldwide dataset, a 1.4‰ range is relatively consistent, which suggests that $\delta^{18}\text{O}_p$ could be used consistently as a marker of the input of P_i from Sutton Valence WWTP. Therefore, for specific catchment studies that contain a discharging WWTP,

WWTP effluents should be fully characterised as part of the study. This should also provide the basis for greater understanding of the magnitude and causes of local-scale variations in $\delta^{18}\text{O}_p$ from WWTP effluents.

Worldwide, there are few published groundwater $\delta^{18}\text{O}_p$ studies and the current work reported in **Chapter 5** of this thesis has increased the worldwide groundwater dataset almost threefold, with the addition of 15 data points across 12 different locations within the Lower and Upper Greensand geological units of the UK. Prior to the groundwater survey reported in **Chapter 5**, the worldwide mean $\delta^{18}\text{O}_p$ of groundwater was 18.6‰ ($\sigma = 2.13\%$, $n = 9$), with a range of 15.1 to 22.4‰. The addition of **Chapter 5** increases the mean $\delta^{18}\text{O}_p$ to 19.1‰ and decreases the standard deviation to 1.57‰ ($n = 24$), however the range was not altered as every sample reported within this thesis fell within the worldwide range reported in **Table 2.1**. However, $\delta^{18}\text{O}_p$ in groundwater did vary significantly dependent on the bedrock unit that a sample was collected from, with a mean difference of approximately 2‰ between samples from the Upper Greensand (18.12‰, $1\sigma = 0.77\%$) and Lower Greensand (20.11‰, $1\sigma = 0.38\%$). Therefore, further groundwater surveys should be conducted to constrain groundwater $\delta^{18}\text{O}_p$ across significant geological units, particularly those that may discharge to surface waters. In addition, the $\delta^{18}\text{O}_p$ of samples from the Upper Greensand was also highly consistent with $\delta^{18}\text{O}_p$ from MilliQ water extracts of Upper Greensand rock material, that exhibited a mean $\delta^{18}\text{O}_p$ of 18.19‰ ($1\sigma = 0.43\%$). Given the very small difference in $\delta^{18}\text{O}_p$ between solid phase-extracted P_i and groundwater P_i within the Upper Greensand formation, alongside the persistence of disequilibrium in $\delta^{18}\text{O}_p$ in the Upper Greensand groundwater with respect to $\delta^{18}\text{O}_{eq}$, it may be suggested that abiotic weathering dominates the P_i cycling within groundwater in this formation. However, further work is required to determine whether variations in groundwater $\delta^{18}\text{O}_p$, and in the difference between $\delta^{18}\text{O}_p$ and $\delta^{18}\text{O}_{eq}$, are associated with seasonal, temperature and biological processing effects across a larger range of groundwater aquifers, including those that have received significant groundwater recharge containing high surface P_i concentrations, or significant P_i contamination (e.g. septic tank leakages).

Although there are overlaps in terms of $\delta^{18}\text{O}_p$ across individual sources of P and individual water types, as indicated in **Table 2.1** and **Figure 5.12** and similar plots in

Young *et al.* (2009) and Goody *et al.* (2015), this does not necessarily limit the application of $\delta^{18}\text{O}_p$ in regional or more local studies, in which the range of $\delta^{18}\text{O}_p$ across individual sources of P and water types may be significantly narrower than within the worldwide dataset. For example, there was no overlap between $\delta^{18}\text{O}_p$ in groundwater (**Chapter 5**) and $\delta^{18}\text{O}_p$ within WWTP effluents (**Chapter 4 and 5**) within this thesis, despite the fact that on a worldwide scale there is significant overlap between these two potential sources of P within river ecosystems. Similar observations have also been made by Gruau *et al.* (2005) who determined that $\delta^{18}\text{O}_p$ within WWTP effluents (16.6–18.4‰) were significantly lower than that of artificial fertilisers used within the same area in Brittany, France (19.6–23.1‰). However, overlapping $\delta^{18}\text{O}_p$ at more local scales may still confound research. Young *et al.* (2009) report artificial fertilisers with ratios from 15.5 to 22.3‰, dependent on the geological source of the fertiliser, a range that overlapped with other potential P_i sources including aerosols, detergents, toothpaste, and soil and faeces leachates. Therefore, within research that seeks to adopt $\delta^{18}\text{O}_p$ as an approach to differentiate between sources of P_i , efforts must be made to fully characterise potentially major sources of P_i at local scales, rather than relying on a global $\delta^{18}\text{O}_p$ mean.

6.3 Providing insights into biogeochemical processes controlling P cycling with $\delta^{18}\text{O}_p$

Objectives 3 and 4 of this thesis examined how $\delta^{18}\text{O}_p$ can be used to provide additional insights into biogeochemical processes that control the cycling of P within aquatic environments that cannot be derived from traditional, concentration-based studies alone. Research on P_i has grown significantly since its role in eutrophication became evident (Correll, 1999; Ruttenger, 2003; Schindler *et al.*, 2016) and since the imposition of regulations to reduce inputs of bioavailable P to aquatic ecosystems such as the European Union Water Framework Directive (WFD) and the United States Clean Water Act (U.S. Senate, 1972; European Parliament, 2000). This has led to significant changes, such as a 90% reduction in SRP being released from WWTPs in the Thames catchment (Bowes *et al.*, 2014). However, despite these reductions in P_i from WWTPs, and subsequent decreases within in-river P_i concentrations, this has not

also always led to changes within the primary producer communities within freshwaters, or the recovery has occurred over a prolonged period of time (May and Spears, 2011; Spears *et al.*, 2011). This demonstrates the uncertainty in understanding of how P_i from specific sources is, or is not, linked to metabolism within streams and rivers. Furthermore, there remain considerable legacy P pools in the environment, particularly in western Europe (Sattari *et al.*, 2012; Rowe *et al.*, 2015). Remobilisation of P from this legacy pool may continue to input significant quantities of P into aquatic ecosystems, for years to decades after the initial input of P to a terrestrial ecosystem, delaying the restoration of aquatic systems (Haygarth *et al.*, 2014; Powers *et al.*, 2016). Therefore, the ability to determine how P is cycled through aquatic environments is key to understanding how to best to mitigate against P_i inputs and to create sustainable P usage schemes. The use of $\delta^{18}O_p$ as an inherent tracer of biogeochemical processing might highlight which freshwater ecosystems are most vulnerable to additions of bioavailable P_i , e.g. by determining the presence or absence of biological cycling, and thus which ecosystems would have the greatest benefit from investments to reduce P_i inputs within the catchment. This would create a greater efficiency and efficacy for catchment restoration funding.

This thesis reports a number of cases in which $\delta^{18}O_p$ analysis provides additional insights into the mechanisms governing in-river cycling of P that are masked when considering in-river P concentration profiles alone. For example, in **Chapter 4** the seasonal contrast in intracellular metabolism of WWTP-derived P_i , inferred from **Figures 4.5, 4.7 and 4.9**, being observed under high flow conditions, whereas under low flow conditions, little isotopic evidence was present to support metabolic processes influencing in-river transport of P. Intracellular metabolism, a process that does not significantly alter the in-stream SRP concentration, would not have been determined through only the analysis of the hydrochemical data. Similarly, under high flow conditions, extracellular hydrolysis of P_{org} to generate P_i can be determined through isotopic analyses, which would have been interpreted as the physical mixing of two water bodies on the basis of the hydrochemical data. In addition, potential lines of evidence for abiotic processes have also been found within the isotopic profiles; for example within the upper reach of the **Chapter 5** in-stream profile, $\delta^{18}O_p$ diverged from $\delta^{18}O_{eq}$ (**Figure 5.11**) suggesting a possible disequilibrium effect through an abiotic ion exchange in which aqueous P_i is abiotically exchanged with P_i ions in the

sorbed phase that may be at disequilibrium (Jaisi *et al.*, 2011). However, within natural ecosystems abiotic ion exchange typically occurs at a very slow rate and therefore, in general, is likely to be masked or overprinted by any biological processes that are altering the P_i pool. Furthermore, in the upper reaches of the Caker stream in **Chapter 5**, the gradual decreases in $\delta^{18}O_p$, $\delta^{18}O_w$ and SRP concentrations (**Figures 5.9, 5.10 and 5.7**) all support the hypothesis that groundwater discharge into the river is an important P_i source, thus determining a more direct relationship between the two water bodies. Therefore, $\delta^{18}O_p$ can also provide potential evidence of naturally derived inputs to freshwater river systems, such as the dissolution of phosphatic nodules in the bedrock. This evidence could be used to support a decision to not remediate a P_i -rich river if it could be proved that any elevation in in-stream P_i concentration, relative to other catchments or regulatory controls, was the result of natural inputs to the ecosystem.

Additionally, there appears to be little biological processing of groundwater P_i within the Upper Greensand geological formation, resulting in $\delta^{18}O_p$ values close to that of water extracts from the parent bedrock material (**Figure 5.6 and Table 5.4**). This is consistent with the findings of Young *et al.* (2009), who showed no evidence of intracellular metabolism of P_i , but is inconsistent with those of Blake *et al.* (2001), who reported a positive correlation between $\delta^{18}O_p$ and $\delta^{18}O_w$ as evidence to support biological activity influencing P_i within a shallow glacial outwash aquifer. However, with both the published data and the data reported in **Chapter 5**, insights into the cycling of P within groundwaters, particularly in relation to the presence of intracellular metabolism, would not have been possible solely from the analysis of hydrochemical concentration profiles. However, the use of $\delta^{18}O_p$, in conjunction with $\delta^{18}O_w$, T and $\delta^{18}O_{eq}$ has allowed a greater insight into the occurrence or absence of biological processing. Another study that showed that $\delta^{18}O_p$ could determine processes and sources that cannot be explained by concentration studies alone was that of Lake Erie in which no increased influx of P_i to the lake water body had been observed, but P_i concentrations were increasing within the water column (Elsbury *et al.*, 2009). This P_i concentration increase could not be explained using traditional tools, such as mass balances of P sources, however $\delta^{18}O_p$ analyses provided evidence of a heavy end-member P_i source being introduced to the system which was

hypothesised as the remineralisation of ^{18}O -enriched P_{org} within the bed sediments, followed by release of P_i from the lake sediment to the water column.

In **Chapter 4**, contrasting seasonal evidence for intracellular metabolism occurring immediately downstream of a WWTP effluent discharge point was reported, based on $\delta^{18}\text{O}_p$. The data were consistent with intracellular metabolism of P during a sampling campaign in spring (March), but the $\delta^{18}\text{O}_p$ data suggested that intracellular metabolism was reduced during the autumn sampling campaign (September). This has been suggested to reflect the difference between the period of UK spring blooms (March to May) of phyto-benthic organisms (dominated by diatoms), where SRP concentrations and silica levels both decrease due to algal-related removal of both elements, compared to an autumn sampling campaign (Bowes and House, 2001; Bowes *et al.*, 2011). During this time, the demand for bioavailable P to support algal production is very high, promoting biological cycling processes such as intracellular metabolism and biological uptake. Seasonal differences were also observed by Li *et al.* (2011) within a freshwater wetland in the Everglades National Park, USA. The authors found that $\delta^{18}\text{O}_p$ was enriched in the colder, winter months relative to samples collected in summer. These seasonal effects could have been imparted through differences either in the metabolic activity within the wetland system, or in timings of artificial P_i fertilisers which had been shown to be a major source of P_i to the wetland ecosystem. This suggests that there are seasonal variations in the extent to which anthropogenically-derived P_i is metabolised following P_i point sources, which has been evidenced through $\delta^{18}\text{O}_p$ analysis. However, further investigation is required to determine the prevalence of these seasonal effects and whether they are predictable both temporally and spatially. Furthermore, it is often assumed that there is a need to reduce the P_i inputs from point sources due to their potential role in controlling downstream water quality and in stimulating eutrophication (Smith and Schindler, 2009). However, if it can be shown through $\delta^{18}\text{O}_p$ that in-river processing does not necessarily occur downstream of a point source, investment in P removal technologies would be more efficient and effective at alternative locations where $\delta^{18}\text{O}_p$ data suggest strong coupling between WWTP effluent and in-river metabolism (which would result in a profile similar to that of the Scenario A in **Figure 4.1** – a conceptual model for WWTP inputs to a strongly P_i limited ecosystem). When used in combination with stable isotope studies of nitrogen and carbon species, $\delta^{18}\text{O}_p$ analyses may provide

insights into whether P is the limiting nutrient for primary producers within rivers and stream, or whether other nutrients such as N or silica limit or co-limit production, or are indeed affected by factors such as wind speed, temperature or light availability (Hecky and Kilham, 1988; Pilkaitytė and Razinkovas, 2006; Conley *et al.*, 2009; Xu *et al.*, 2010; Gooddy *et al.*, 2016). However, this does not exclude the possibility that a point source could contribute significantly to P_i loads delivered to downstream ecosystems such as lakes, in which a reduction in the P_i load would be beneficial.

Therefore, an efficient and effective use of $\delta^{18}O_p$ protocols could determine which rivers are most vulnerable to P_i inputs through the uptake of P_i or evidence of SRP regeneration, P_{org} hydrolysis and intracellular metabolism. This could result in a more direct targeting of nutrient management schemes on catchments that demonstrate a greater sensitivity to the addition of P_i , and those that are likely to respond most rapidly to changes in P delivery. In addition, if $\delta^{18}O_p$ could be used to trace an input through the system, e.g. an artificial fertiliser through a farm system, there is potential for a greater understanding of how that input interacts and is utilised through the system. In the case of a fertiliser, this may result in the realisation of the most economical and cost-effective quantity of fertiliser required to support agriculture, without resulting in an increase of legacy P within the soils or excess drainage into the river system. For example, inputs of P from artificial fertilisers in the Everglades Agricultural Area (EAA) have contributed to mean concentrations of P in runoff being 20-fold greater than in non-agricultural areas of the national park (Li *et al.*, 2011). If a more efficient use of artificial fertilisers could be achieved, then demand for mineral P will be reduced and consequently, the uncertainty over mineral P reserves will lessen. This is particularly important given securing access to P remains a globally-significant issue due to the lack of effective P recycling within urban and agricultural areas, the lack of a suitable alternative source and a limited number of geographical locations of mineral reserves (Beardsley, 2011).

Furthermore, by increasing our understanding of P biogeochemical cycling within aquatic environments, we can begin to address the modelled $0.27 \text{ Tg } P_i\text{-P}\cdot\text{yr}^{-1}$ that is exported by rivers to coastal regions in Europe, 92% of which is derived from anthropogenic sources (Harrison *et al.*, 2010). Addressing this perturbation of natural aquatic P biogeochemical cycles should help to reduce the severity and range of

undesirable ecosystem changes, including increases in primary production, shifts in community composition, increased frequency of algal blooms and hypoxia, and reduced biodiversity (Sondergaard and Jeppesen, 2007; Smith and Schindler, 2009).

6.4 Future priorities to develop research using $\delta^{18}\text{O}_p$

The use of $\delta^{18}\text{O}_p$ in research examining P cycling in natural ecosystems is at an embryonic stage, particularly with respect to freshwater ecosystems. This stable isotope tracer has the potential to offer new insights into both the relative importance of different sources of P to ecosystems, and the extent to which P from individual sources is linked to metabolic activity within ecosystems. These insights would have important implications for understanding the reaction mechanisms controlling P biogeochemistry in nature, and for the design and targeting of future policies and practices to deliver more sustainable stewardship of P. This thesis concludes by highlighting future priorities for $\delta^{18}\text{O}_p$ research that would help realise the full potential of this novel approach.

6.4.1 *The utility of $\delta^{18}\text{O}_p$ to provide insight into biogeochemical processes controlling P cycling*

Due to our relatively limited understanding of the sources and reaction mechanisms controlling biogeochemical cycling of P within natural ecosystems (Blake *et al.*, 2005; Slomp, 2011), further studies using $\delta^{18}\text{O}_p$ across all aquatic environments would help to elucidate the biogeochemical pathways that govern the fate of P within the environment. However, $\delta^{18}\text{O}_p$ will not act as a conservative tracer for the sources of P to an ecosystem where metabolic reactions significantly influence the P cycle. Whilst clearly a constraint on source apportionment studies, the isotope fractionations that occur alongside metabolic processes provide the opportunity to use $\delta^{18}\text{O}_p$ to explore the reaction mechanisms controlling P cycling. Specifically, the balance between equilibrium and disequilibrium fractionations can provide insight into the relative importance of intracellular metabolism of P_i versus the extracellular regeneration of P_i from P_{org} . This requires future research to determine and interpret variations in $\delta^{18}\text{O}_p$,

both through time (for example, from inter-annual or seasonal cycles to event-driven variations within lake or river ecosystems) and through space (for example, tracking downstream changes in $\delta^{18}\text{O}_p$ associated with point or diffuse inputs of P to aquatic ecosystems).

In particular, the use of ^{18}O -labelled P_i could help elucidate reaction mechanisms that govern the fate of P in freshwater environments. ^{18}O -labels have been shown to be an effective tool in understanding reaction mechanisms within a laboratory setting (Liang and Blake, 2006b). The benefit of using a stable isotope labelled molecule in the environment is that the label can be manufactured such that it is far removed in terms of $\delta^{18}\text{O}$ from other sources within the catchment, and due to its stability will not degrade over time unlike its equivalent radio-label – ^{32}P ($t_{1/2} = 14.36$ days) and ^{33}P ($t_{1/2} = 25.34$ days) (Smith *et al.*, 2011). The use of labelled ^{18}O - P_i would allow tracing studies to be performed which could help distinguish physical pathways and reaction mechanisms for P biogeochemical processes within terrestrial and freshwater environments. For example, the internal loading of legacy P has been highlighted as a major concern for continuing algal blooms in a number of lakes despite extensive remediation and reduction of P_i inputs (Nürnberg *et al.*, 2013; Bormans *et al.*, 2015; North *et al.*, 2015). Internal loading describes the release of P compounds from bed sediments within a lake, and has been found to contribute over 80% of the total P load during summer months (Steinman *et al.*, 2009). The use of a labelled P_i system could provide important insights into how P is recycled within a holomictic lake system; particularly with a focus on the release of P from bed sediments into the hypolimnion when the lake is thermally stratified and the subsequent delivery of P-rich hypolimnion water to the surface during spring or autumn turnovers. This could be achieved through the release of labelled P_i into lake bottom sediments, and the tracking of $\delta^{18}\text{O}_p$ within the water column throughout the year, but with a focus on turnover times within a lake to determine the rate and extent to which P_i is exported from the lake sediments and mixed with the lake water. A second possibility would be to track the export of ^{18}O -labelled fertiliser P_i from its input onto agricultural land to a receiving water body, and its subsequent transport downstream to determine the fate and biogeochemical cycling of fertiliser-derived P_i .

6.4.2 Determination of $\delta^{18}\text{O}$ in P_{org} molecules

Compared to the volume of research that has focussed on P_i , very little is known about the concentration or the cycling of specific groups of P_{org} compounds in natural freshwater environments (Espinosa *et al.*, 1999; Turner *et al.*, 2002; Toor *et al.*, 2003; Cade-Menun *et al.*, 2006; Koopmans *et al.*, 2007). Further, there remains insufficient research that has fully speciated the P_{org} compounds found in freshwaters; however some research has begun to explore the use of $\delta^{18}\text{O}$ in P_{org} molecules in a laboratory setting (Liang and Blake, 2006a; Sandy *et al.*, 2013). This analytical gap remains to be addressed by future research, particularly considering the potential role of P_{org} as a factor influencing $\delta^{18}\text{O}_p$ in P_i within freshwaters following hydrolysis of P_{org} . Once full speciation and separation of P_{org} within waters is achieved, $\delta^{18}\text{O}$ analyses could be performed on individual P_{org} compounds or classes. This could be achieved through the separation of P_{org} compounds into fractions using high performance liquid chromatography, followed by ultraviolet radiation of each fraction to hydrolyse P_{org} to P_i without imparting an isotopic fractionation during the extraction process (Liang and Blake, 2006a), and finally the precipitation of the released P_i as Ag_3PO_4 . However, further investigations would be required to model the isotope effects of the water oxygen atoms that may be incorporated within the released P_i molecule, as to date the magnitude of the fractionation factor associated with this process has only been quantified for two classes of P_{org} (Liang and Blake, 2006a). Thus, following the analytical development for the analysis of $\delta^{18}\text{O}$ within the phosphate moieties of P_{org} , $\delta^{18}\text{O}_p$ could be used to understand the cycling of P_{org} within aquatic ecosystems. This would allow research to bridge the gap between P_i and P_{org} and more fully understand how these species interact with each other, for example how specific P_{org} compounds are accessed to support metabolisms by organisms across ecosystems that differ in the extent to which they are P_i -limited.

6.4.3 *Couple $\delta^{18}\text{O}_p$ with parallel techniques to develop an integrated isotope framework across C, N and P cycles.*

Whilst analysis of $\delta^{18}\text{O}_p$ is beginning to emerge as a research tool in aquatic ecosystems, parallel stable isotope techniques have a longer history of application for N ($^{15}\text{N}/^{14}\text{N}$ in ammonium and $^{15}\text{N}/^{14}\text{N}$, $^{18}\text{O}/^{16}\text{O}$ in nitrate) and for C ($^{13}\text{C}/^{12}\text{C}$). Coupling analysis of $\delta^{18}\text{O}_p$ with that of stable isotopes in N and C compounds would potentially offer new insights into process interactions between C, N and P biogeochemistry. A coupled stable isotope framework could draw on natural abundance approaches or, ultimately, on isotopic labelling studies based on production of labelled $\delta^{18}\text{O}_p$ to complement isotopically labelled sources of N and C. Finally, by coupling stable isotope and radioisotope techniques, processes that govern the cycling of P across both the short and long term within aquatic ecosystems could be more readily constrained (for recent examples see McLaughlin et al., 2013 and Goody, 2016).

References

- Alexander, R.B., E.W. Boyer, R.A. Smith, G.E. Schwarz & R.B. Moore. 2007. The role of headwater streams in downstream water quality. *Journal of the American Water Resources Association*. **43**, 41
- Alonso, M.C., M. Castillo & D. Barcelo. 1999. Solid phase extraction procedure of polar benzene- and naphthalenesulfonates in industrial effluents followed by unequivocal determination with ion pair chromatography/electrospray-mass spectrometry. *Analytical Chemistry*. **71**, 2586
- Amer, F., D.R. Bouldin, C.A. Black & F.R. Duke. 1955. Characterization of soil phosphorus by anion exchange resin adsorption and P³²-equilibration. *Plant and Soil*. **6**, 391
- Aminot, A. & R. Kerouel. 2004. Dissolved organic carbon, nitrogen and phosphorus in the N-E Atlantic and the N-W Mediterranean with particular reference to non-refractory fractions and degradation. *Deep-Sea Research Part I- Oceanographic Research Papers*. **51**, 1975
- Ammerman, J.W. 1991. Role of ecto-phosphohydrolases in phosphorus regeneration in estuarine and coastal ecosystems. *Microbial Enzymes in Aquatic Environments*. 165
- Ammerman, J.W. & F. Azam. 1985. Bacterial 5'-nucleotidase in aquatic ecosystems: a novel mechanism of phosphorus regeneration. *Science*. **227**, 1338
- Angert, A., T. Weiner, S. Mazeh & M. Sternberg. 2012. Soil phosphate stable oxygen isotopes across rainfall and bedrock gradients. *Environmental Science and Technology*. **46**, 2156
- Angert, A., T. Weiner, S. Mazeh, F. Tamburini, E. Frossard, S.M. Bernasconi & M. Sternberg. 2011. Seasonal variability of soil phosphate stable oxygen isotopes in rainfall manipulation experiments. *Geochimica et Cosmochimica Acta*. **75**, 4216

- Aydin, I., S. Imamoglu, F. Aydin, A. Saydut & C. Hamamci. 2009. Determination of mineral phosphate species in sedimentary phosphate rock in Mardin, SE Anatolia, Turkey by sequential extraction. *Microchemical Journal*. **91**, 63
- Ayliffe, L.K., H.H. Veeh & A.R. Chivas. 1992. Oxygen isotopes of phosphate and the origin of island apatite deposits. *Earth and Planetary Science Letters*. **108**, 119
- Beardsley, T.M. 2011. Peak phosphorus. *Bioscience*. **61**, 91
- Becker, M.W., T. Georgian, H. Ambrose, J. Siniscalchi & K. Fredrick. 2004. Estimating flow and flux of ground water discharge using water temperature and velocity. *Journal of Hydrology*. **296**, 221
- Benda, L., M.A. Hassan, M. Church & C.L. May. 2005. Geomorphology of steep-land headwaters: the transition from hillslopes to channels. *Journal of the American Water Resources Association*. **41**, 835
- Bender, M.L. 1960. Mechanisms of catalysis of nucleophilic reactions of carboxylic acid derivatives. *Chemical Reviews*. **60**, 53
- Benitez-Nelson, C.R. 2000. The biogeochemical cycling of phosphorus in marine systems. *Earth-Science Reviews*. **51**, 109
- Benitez-Nelson, C.R. & K.O. Buesseler. 1998. Measurement of cosmogenic ³²P and ³³P activities in rainwater and seawater. *Analytical Chemistry*. **70**, 64
- Benitez-Nelson, C.R. & K.O. Buesseler. 1999. Variability of inorganic and organic phosphorus turnover rates in the coastal ocean. *Nature*. **398**, 502
- Beveridge, N.A.S. & N.J. Shackleton. 1994. Carbon isotopes in recent planktonic-foraminifera - a record of anthropogenic CO₂ invasion of the surface ocean. *Earth and Planetary Science Letters*. **126**, 259
- Biotage. 2004. *Technical Note 109: Method Development in Solid Phase Extraction using ISOLUTE® ENV+ SPE Columns for the Extraction of Aqueous Samples* [Online]. Biotage. Available: http://www.biotage.com/literature/download/1767_tn109rev11.4_isolute_env_aqueous_samples1.pdf [Accessed 23/03/16]
- Björkman, K. & D.M. Karl. 1994. Bioavailability of inorganic and organic phosphorus-compounds to natural assemblages of microorganisms in Hawaiian coastal waters. *Marine Ecology Progress Series*. **111**, 265

- Bjorkman, K.M. & D.M. Karl. 2005. Presence of dissolved nucleotides in the North Pacific Subtropical Gyre and their role in cycling of dissolved organic phosphorus. *Aquatic Microbial Ecology*. **39**, 193
- Blake, R.E., J.C. Alt & A.M. Martini. 2001. Oxygen isotope ratios of PO₄: An inorganic indicator of enzymatic activity and P metabolism and a new biomarker in the search for life. *Proceedings of the National Academy of Sciences of the USA*. **98**, 2148
- Blake, R.E., J.R. O'Neil & G.A. Garcia. 1997. Oxygen isotope systematics of biologically mediated reactions of phosphate: I. Microbial degradation of organophosphorus compounds. *Geochimica et Cosmochimica Acta*. **61**, 4411
- Blake, R.E., J.R. O'Neil & A.V. Surkov. 2005. Biogeochemical cycling of phosphorus: Insights from oxygen isotope effects of phosphoenzymes. *American Journal of Science*. **305**, 596
- Bormans, M., B. Maršálek & D. Jančula. 2015. Controlling internal phosphorus loading in lakes by physical methods to reduce cyanobacterial blooms: a review. *Aquatic Ecology*. **50**, 407
- Bowes, M.J., J. Hilton, G.P. Irons & D.D. Hornby. 2005. The relative contribution of sewage and diffuse phosphorus sources in the River Avon catchment, southern England: implications for nutrient management. *Science of the Total Environment*. **344**, 67
- Bowes, M.J. & W.A. House. 2001. Phosphorus and dissolved silicon dynamics in the River Swale catchment, UK: a mass-balance approach. *Hydrological Processes*. **15**, 261
- Bowes, M.J., H.P. Jarvie, S.J. Halliday, R.A. Skeffington, A.J. Wade, M. Loewenthal, E. Gozzard, J.R. Newman & E.J. Palmer-Felgate. 2015. Characterising phosphorus and nitrate inputs to a rural river using high-frequency concentration-flow relationships. *Science of the Total Environment*. **511**, 608
- Bowes, M.J., H.P. Jarvie, P.S. Naden, G.H. Old, P.M. Scarlett, C. Roberts, L.K. Armstrong, S.A. Harman, H.D. Wickham & A.L. Collins. 2014. Identifying priorities for nutrient mitigation using river concentration–flow relationships: The Thames basin, UK. *Journal of Hydrology*. **517**, 1
- Bowes, M.J., J.T. Smith, H.P. Jarvie & C. Neal. 2008. Modelling of phosphorus inputs to rivers from diffuse and point sources. *Science of the Total Environment*. **395**, 125

- Bowes, M.J., J.T. Smith, C. Neal, D.V. Leach, P.M. Scarlett, H.D. Wickham, S.A. Harman, L.K. Armstrong, J. Davy-Bowker, M. Haft & C.E. Davies. 2011. Changes in water quality of the River Frome (UK) from 1965 to 2009: is phosphorus mitigation finally working? *Science of the Total Environment*. **409**, 3418
- Boyle, J.F., R.C. Chiverrell, S.A. Norton & A.J. Plater. 2013. A leaky model of long-term soil phosphorus dynamics. *Global Biogeochemical Cycles*. **27**, 516
- Brand, W.A. 2004. Mass spectrometer hardware for analyzing stable isotope ratios. In: De Groot, P.A. (ed.) *Handbook of Stable Isotope Analytical Techniques*. Oxford, UK: Elsevier. 835-858
- Bryant, J.D., B. Luz & P.N. Froelich. 1994. Oxygen isotopic composition of fossil horse tooth phosphate as a record of continental paleoclimate. *Palaeogeography Palaeoclimatology Palaeoecology*. **107**, 303
- Cade-Menun, B.J., J.A. Navaratnam & M.R. Walbridge. 2006. Characterizing dissolved and particulate phosphorus in water with P-31 nuclear magnetic resonance spectroscopy. *Environmental Science and Technology*. **40**, 7874
- Carey, R.O. & K.W. Migliaccio. 2009. Contribution of wastewater treatment plant effluents to nutrient dynamics in aquatic systems: a review. *Environmental Management*. **44**, 205
- Carroll, T., S. King, S.R. Gray, B.A. Bolto & N.A. Booker. 2000. The fouling of microfiltration membranes by NOM after coagulation treatment. *Water Research*. **34**, 2861
- Chang, S.J. & R.E. Blake. 2015. Precise calibration of equilibrium oxygen isotope fractionations between dissolved phosphate and water from 3 to 37 degrees C. *Geochimica et Cosmochimica Acta*. **150**, 314
- Childers, D.L., J. Corman, M. Edwards & J.J. Elser. 2011. Sustainability challenges of phosphorus and food: solutions from closing the human phosphorus cycle. *Bioscience*. **61**, 117
- Chróst, R.J. 1991. Environmental control of the synthesis and activity of aquatic microbial ectoenzymes. In: Chróst, R.J. (ed.) *Microbial Enzymes in Aquatic Environments*. New York, USA: Springer. 29-59
- Clark, L.L., E.D. Ingall & R. Benner. 1998. Marine phosphorus is selectively remineralized. *Nature*. **393**, 426

- Cohn, M. 1958. Phosphate-water exchange reaction catalyzed by inorganic pyrophosphatase of yeast. *Journal of Biological Chemistry*. **230**, 369
- Colman, A.S. 2002. *The oxygen composition of dissolved inorganic phosphate and the marine phosphorus cycle*. Ph.D. dissertation, Yale University
- Colman, A.S., R.E. Blake, D.M. Karl, M.L. Fogel & K.K. Turekian. 2005. Marine phosphate oxygen isotopes and organic matter remineralization in the oceans. *Proceedings of the National Academy of Sciences USA*. **102**, 13023
- Conley, D.J., H.W. Paerl, R.W. Howarth, D.F. Boesch, S.P. Seitzinger, K.E. Havens, C. Lancelot & G.E. Likens. 2009. Controlling eutrophication: nitrogen and phosphorus. *Science*. **323**, 1014
- Constantz, J. 1998. Interaction between stream temperature, streamflow, and groundwater exchanges in alpine streams. *Water Resources Research*. **34**, 1609
- Cooperman, B.S., A.A. Baykov & R. Lahti. 1992. Evolutionary conservation of the active-site of soluble inorganic pyrophosphatase. *Trends in Biochemical Sciences*. **17**, 262
- Cordell, D., J.O. Drangert & S. White. 2009. The story of phosphorus: global food security and food for thought. *Global Environmental Change-Human and Policy Dimensions*. **19**, 292
- Cordell, D., A. Rosemarin, J.J. Schroder & A.L. Smit. 2011. Towards global phosphorus security: a systems framework for phosphorus recovery and reuse options. *Chemosphere*. **84**, 747
- Cordell, D. & S. White. 2011. Peak phosphorus: clarifying the key issues of a vigorous debate about long-term phosphorus security. *Sustainability*. **3**, 2027
- Correll, D.L. 1999. Phosphorus: a rate limiting nutrient in surface waters. *Poultry Science*. **78**, 674
- Council Directive 91/271/EEC of 21 May 1991 concerning urban waste-water treatment. *Official Journal of the European Communities* L 135, 30.5.91, 40-52
- Cox Jr, J.R. & O.B. Ramsay. 1964. Mechanisms of nucleophilic substitution in phosphate esters. *Chemical Reviews*. **64**, 317

- Darling, W.G., A.H. Bath & J.C. Talbot. 2003. The O & H stable isotopic composition of fresh waters in the British Isles. 2. Surface waters and groundwater. *Hydrology and Earth System Sciences*. **7**, 183
- Davies, C.W. & A.L. Jones. 1955. The precipitation of silver chloride from aqueous solutions. Part 2 - kinetics of growth of seed crystals. *Transactions of the Faraday Society*. **51**, 812
- de Laeter, J.R., J.K. Böhlke, P. de Bièvre, H. Hidaka, H.S. Peiser, K.J.R. Rosman & P.D.P. Taylor. 2003. Atomic weights of the elements: review 2000. *Pure Applied Chemistry*. **75**, 683
- Demadis, K.D., E. Mavredaki, A. Stathouloupoulou, E. Neofotistou & C. Mantzaridis. 2007. Industrial water systems: problems, challenges and solutions for the process industries. *Desalination*. **213**, 38
- Denver, J., C.A. Cravotta III, S.W. Ator & B.D. Lindsey. 2010. Contributions of phosphorus from groundwater to streams in the Piedmont, Blue Ridge, and Valley and Ridge Physiographic Provinces, Eastern United States. *U.S. Geological Survey. Scientific Investigations Report 2010-5176*, 1
- Dettman, D.L., M.J. Kohn, J. Quade, F.J. Ryerson, T.P. Ojha & S. Hamidullah. 2001. Seasonal stable isotope evidence for a strong Asian monsoon throughout the past 10.7 m.y. *Geology*. **29**, 31
- Dillon, P.J. & W.B. Kirchner. 1975. Effects of geology and land-use on export of phosphorus from watersheds. *Water Research*. **9**, 135
- Ding, S., D. Xu, Q. Sun, H. Yin & C. Zhang. 2010. Measurement of dissolved reactive phosphorus using the diffusive gradients in thin films technique with a high-capacity binding phase. *Environmental Science and Technology*. **44**, 8169
- Doering, P.H., C.A. Oviatt, B.L. Nowicki, E.G. Klos & L.W. Reed. 1995. Phosphorus and nitrogen limitation of primary production in a simulated estuarine gradient. *Marine Ecology Progress Series*. **124**, 271
- Edmunds, W.M. & D.G. Kinniburgh. 1986. The susceptibility of UK groundwaters to acidic deposition. *Journal of the Geological Society*. **143**, 707
- Edzwald, J.K., D.C. Toensing & M.C.-Y. Leung. 1976. Phosphate adsorption reactions with clay minerals. *Environmental Science and Technology*. **10**, 485

- Ellison, R.A., I.T. Williamson & A.J. Humpage. 2002. Geology of the Guildford district - a brief explanation of the geological map. *Sheet Explanation of the British Geological Survey*. 1: 50 000 Sheet 285 Guildford (England and Wales)
- Elsbury, K.E., A. Paytan, N.E. Ostrom, C. Kendall, M.B. Young, K. McLaughlin, M.E. Rollog & S. Watson. 2009. Using oxygen isotopes of phosphate to trace phosphorus sources and cycling in Lake Erie. *Environmental Science and Technology*. **43**, 3108
- Elser, J. & E. Bennett. 2011. A broken biogeochemical cycle. *Nature*. **478**, 29
- Elser, J.J. & R.P. Hassett. 1994. A stoichiometric analysis of the zooplankton-phytoplankton interaction in marine and fresh-water ecosystems. *Nature*. **370**, 211
- Environment Agency. 2009. Nitrate concentrations in rivers: 1995-2008. http://data.defra.gov.uk/env/iwfg10_nitrate_river_200911.csv.
- European Parliament, 2000. Establishing a framework for community action in the field of water policy. *Directive EC/2000/60*. EU, Brussels
- Espinosa, M., B. Turner & P.M. Haygarth. 1999. Preconcentration and separation of trace phosphorus compounds in soil leachate. *Journal of Environmental Quality*. **28**, 1497
- Filippelli, G.M. 2008. The global phosphorus cycle: past, present, and future. *Elements*. **4**, 89
- Firsching, F. 1961. Precipitation of silver phosphate from homogeneous solution. *Analytical Chemistry*. **33**, 873
- Fourel, F., F. Martineau, C. Lecuyer, H.J. Kupka, L. Lange, C. Ojeimi & M. Seed. 2011. $^{18}\text{O}/^{16}\text{O}$ ratio measurements of inorganic and organic materials by elemental analysis-pyrolysis-isotope ratio mass spectrometry continuous-flow techniques. *Rapid Communications in Mass Spectrometry*. **25**, 2691
- Fricke, H.C., W.C. Clyde, J.R. O'Neil & P.D. Gingerich. 1998. Evidence for rapid climate change in North America during the latest Paleocene thermal maximum: oxygen isotope compositions of biogenic phosphate from the Bighorn Basin (Wyoming). *Earth and Planetary Science Letters*. **160**, 193

- Fricke, H.C. & J.R. O'Neil. 1996. Inter- and intra-tooth variation in the oxygen isotope composition of mammalian tooth enamel phosphate: implications for palaeoclimatological and palaeobiological research. *Palaeogeography Palaeoclimatology Palaeoecology*. **126**, 91
- Gajewski, E., D.K. Steckler & R.N. Goldberg. 1986. Thermodynamics of the hydrolysis of adenosine 5'-triphosphate to adenosine 5'-diphosphate. *Journal of Biological Chemistry*. **261**, 2733
- Gale, A.S. 2012. Early Cretaceous: rifting and sedimentation before the flood. In: Woodcock, N.H. & Strachan, R.A. (eds.) *Geological History of Britain and Ireland*. Oxford, UK: Wiley-Blackwell. 347-364
- Gammons, C.H., J.N. Babcock, S.R. Parker & S.R. Poulson. 2010. Diel cycling and stable isotopes of dissolved oxygen, dissolved inorganic carbon, and nitrogenous species in a stream receiving treated municipal sewage. *Chemical Geology*. **283**, 44
- Geelhoed, J.S., T. Hiemstra & W.H. van Riemsdijk. 1997. Phosphate and sulfate adsorption on goethite: single anion and competitive adsorption. *Geochimica et Cosmochimica Acta*. **61**, 2389
- Goldhammer, T., B. Brunner, S.M. Bernasconi, T.G. Ferdelman & M. Zabel. 2011a. Phosphate oxygen isotopes: insights into sedimentary phosphorus cycling from the Benguela upwelling system. *Geochimica et Cosmochimica Acta*. **75**, 3741
- Goldhammer, T., T. Max, B. Brunner, F. Einsiedl & M. Zabel. 2011b. Marine sediment pore-water profiles of phosphate $\delta^{18}\text{O}$ using a refined micro-extraction. *Limnology and Oceanography: Methods*. **9**, 110
- Gooddy, D.C., D.J. Lapworth, M.J. Ascott, S.A. Bennett, T.H.E. Heaton & B.W.J. Surridge. 2015. Isotopic fingerprint for phosphorus in drinking water supplies. *Environmental Science and Technology*. **49**, 9020
- Gooddy, D.C., D.J. Lapworth, S.A. Bennett, T.H.E. Heaton, P.J. Williams & B.W.J. Surridge. 2016. A multi-stable isotope framework to understand eutrophication in aquatic ecosystems. *Water Research*. **88**, 623
- Gross, A., A. Nishri & A. Angert. 2013. Use of phosphate oxygen isotopes for identifying atmospheric-P sources: a case study at Lake Kinneret. *Environmental Science and Technology*. **47**, 2721

- Gruau, G., M. Legeas, C. Riou, E. Gallacier, F. Martineau & O. Hénin. 2005. The oxygen isotope composition of dissolved anthropogenic phosphates: a new tool for eutrophication research? *Water Research*. **39**, 232
- Habicht, K.S. & D.E. Canfield. 1997. Sulfur isotope fractionation during bacterial sulfate reduction in organic-rich sediments. *Geochimica et Cosmochimica Acta*. **61**, 5351
- Halas, S., G. Skrzypek, W. Meier-Augenstein, A. Pelc & H.F. Kemp. 2011. Inter-laboratory calibration of new silver orthophosphate comparison materials for the stable oxygen isotope analysis of phosphates. *Rapid Communications in Mass Spectrometry*. **25**, 579
- Hampton, C. 2012a. Groundwater – surface water interaction: Alton Upper Greensand *GB40601G600100 – North Wey (Alton to Tilford) GB106039017830. *Unpublished internal report, Environment Agency*.
- Hampton, C. 2012b. Groundwater – surface water interaction: Godalming Lower Greensand GB40602G601900 –Tillingbourne GB106039017840. *Unpublished internal report, Environment Agency*.
- Harrison, J.A., A.F. Bouwman, E. Mayorga & S. Seitzinger. 2010. Magnitudes and sources of dissolved inorganic phosphorus inputs to surface fresh waters and the coastal zone: A new global model. *Global Biogeochemical Cycles*. **24**, GB1003
- Harvey, E.T., S. Kratzer & A. Andersson. 2015. Relationships between colored dissolved organic matter and dissolved organic carbon in different coastal gradients of the Baltic Sea. *Ambio*. **44 Suppl 3**, 392
- Haygarth, P.M., H.P. Jarvie, S.M. Powers, A.N. Sharpley, J.J. Elser, J.B. Shen, H.M. Peterson, N.I. Chan, N.J.K. Howden, T. Burt, F. Worrall, F.S. Zhang & X.J. Liu. 2014. Sustainable phosphorus management and the need for a long-term perspective: the legacy hypothesis. *Environmental Science and Technology*. **48**, 8417
- Hecky, R.E., P. Campbell & L.L. Hendzel. 1993. The stoichiometry of carbon, nitrogen, and phosphorus in particulate matter of lakes and oceans. *Limnology and Oceanography*. **38**, 709
- Hecky, R.E. & P. Kilham. 1988. Nutrient limitation of phytoplankton in fresh-water and marine environments - a review of recent-evidence on the effects of enrichment. *Limnology and Oceanography*. **33**, 796

- Hoefs, J. 2008. Theoretical and experimental principles. *In: Hoefs, J. Stable Isotope Geochemistry*. Berlin Heidelberg: Springer-Verlag. 1-33
- Holman, I.P., N.J. Howden, P. Bellamy, N. Willby, M.J. Whelan & M. Rivas-Casado. 2010. An assessment of the risk to surface water ecosystems of groundwater P in the UK and Ireland. *Science of the Total Environment*. **408**, 1847
- Holman, I.P., M.J. Whelan, N.J.K. Howden, P.H. Bellamy, N.J. Willby, M. Rivas-Casado & P. McConvey. 2008. Phosphorus in groundwater – an overlooked contributor to eutrophication? *Hydrological Processes*. **22**, 5121
- Holt, M.S., K.K. Fox, M. Daniel & H. Buckland. 2003. Linear alkylbenzene sulfonate and boron monitoring in four catchments in the UK contribution to GREAT-ER #11. *Science of the Total Environment*. **314**, 271
- Hooda, P.S., M. Moynagh, I.F. Svoboda, M. Thurlow, M. Stewart, M. Thomson & H.A. Anderson. 1997. Soil and land use effects on phosphorus in six streams draining small agricultural catchments in Scotland. *Soil Use and Management*. **13**, 196
- Howarth, R.W. & R. Marino. 2006. Nitrogen as the limiting nutrient for eutrophication in coastal marine ecosystems: Evolving views over three decades. *Limnology and Oceanography*. **51**, 364
- Jaisi, D.P. & R.E. Blake. 2010. Tracing sources and cycling of phosphorus in Peru Margin sediments using oxygen isotopes in authigenic and detrital phosphates. *Geochimica et Cosmochimica Acta*. **74**, 3199
- Jaisi, D.P., R.E. Blake & R.K. Kukkadapu. 2010. Fractionation of oxygen isotopes in phosphate during its interactions with iron oxides. *Geochimica et Cosmochimica Acta*. **74**, 1309
- Jaisi, D.P., R.K. Kukkadapu, L.M. Stout, T. Varga & R.E. Blake. 2011. Biotic and abiotic pathways of phosphorus cycling in minerals and sediments: insights from oxygen isotope ratios in phosphate. *Environmental Science and Technology*. **45**, 6254
- Jarvie, H.P., M.D. Jürgens, R.J. Williams, C. Neal, J.J.L. Davies, C. Barrett & J. White. 2005. Role of river bed sediments as sources and sinks of phosphorus across two major eutrophic UK river basins: the Hampshire Avon and Herefordshire Wye. *Journal of Hydrology*. **304**, 51

- Jarvie, H.P., C. Neal, M.D. Jürgens, E.J. Sutton, M. Neal, H.D. Wickham, L.K. Hill, S.A. Harman, J.J.L. Davies, A. Warwick, C. Barrett, J. Griffiths, A. Binley, N. Swannack & N. McIntyre. 2006. Within-river nutrient processing in chalk streams: The Pang and Lambourn, UK. *Journal of Hydrology*. **330**, 101
- Jarvie, H.P., C. Neal, A. Warwick, J. White, M. Neal, H.D. Wickham, L.K. Hill & M.C. Andrews. 2002. Phosphorus uptake into algal biofilms in a lowland chalk river. *Science of the Total Environment*. **282**, 353
- Jarvie, H.P., A.N. Sharpley, B. Spears, A.R. Buda, L. May & P.J. Kleinman. 2013. Water quality remediation faces unprecedented challenges from "legacy phosphorus". *Environmental Science and Technology*. **47**, 8997
- Jasinski, S.M. 2012. Phosphate Rock. *Mineral Commodity Summaries*, U.S. Geological Survey
<http://minerals.usgs.gov/minerals/pubs/commodity/phosphate_rock/mcs-2012-phosp.pdf>
- Jorgensen, C., H.S. Jensen, F.O. Andersen, S. Egemose & K. Reitzel. 2011. Occurrence of orthophosphate monoesters in lake sediments: significance of myo- and scyllo-inositol hexakisphosphate. *Journal of Environmental Monitoring*. **13**, 2328
- Karhu, J. & S. Epstein. 1986. The implication of the oxygen isotope records in coexisting cherts and phosphates. *Geochimica et Cosmochimica Acta*. **50**, 1745
- Karl, D.M. 2000. Aquatic ecology - phosphorus, the staff of life. *Nature*. **406**, 31
- Karl, D.M. & G. Tien. 1992. Magic: A sensitive and precise method for measuring dissolved phosphorus in aquatic environments. *Limnology and Oceanography*. **37**, 105
- Karl, D.M. & G. Tien. 1997. Temporal variability in dissolved phosphorus concentrations in the subtropical North Pacific Ocean. *Marine Chemistry*. **56**, 77
- Kolodny, Y., B. Luz & O. Navon. 1983. Oxygen isotope variations in phosphate of biogenic apatites. 1. Fish bone apatite - rechecking the rules of the game. *Earth and Planetary Science Letters*. **64**, 398
- Koopmans, G.F., W.J. Chardon & R.W. McDowell. 2007. Phosphorus movement and speciation in a sandy soil profile after long-term animal manure applications. *Journal of Environmental Quality*. **36**, 305

- Kornberg, A. 1999. Inorganic polyphosphate: a molecule of many functions. *In*: Schroder, H.C. & Muller, W.E.G. (eds.) *Inorganic Polyphosphates*. Berlin Heidelberg: Springer. 1-18
- Kornexl, B.E., M. Gehre, R. Höfling & R.A. Werner. 1999. On-line $\delta^{18}\text{O}$ measurement of organic and inorganic substances. *Rapid Communications in Mass Spectrometry*. **13**, 1685
- Kotlash, A.R. & B.C. Chessman. 1998. Effects of water sample preservation and storage on nitrogen and phosphorus determinations: implications for the use of automated sampling equipment. *Water Research*. **32**, 3731
- Koziet, J. 1997. Isotope ratio mass spectrometric method for the on-line determination of oxygen-18 in organic matter. *Journal of Mass Spectrometry*. **32**, 103
- Krom, M.D., N. Kress, S. Brenner & L.I. Gordon. 1991. Phosphorus limitation of primary productivity in the Eastern Mediterranean sea. *Limnology and Oceanography*. **36**, 424
- Kubo, A., M. Yamamoto-Kawai & J. Kanda. 2015. Seasonal variations in concentration and lability of dissolved organic carbon in Tokyo Bay. *Biogeosciences*. **12**, 269
- LaPorte, D.F., C. Holmden, W.P. Patterson, T. Prokopiuk & B.M. Eglington. 2009. Oxygen isotope analysis of phosphate: improved precision using TC/EA CF-IRMS. *Journal of Mass Spectrometry*. **44**, 879
- Lapworth, D.J., D.C. Gooddy, D. Allen, P.J. Williams, T.H.E. Heaton, F. Kent & R. Penn. 2009. Phosphate sources in the Beult catchment, Kent - a multi technique approach. *British Geological Survey Internal Report*. 41
- Lécuyer, C. 2004. Oxygen isotope analysis of phosphate. *In*: De Groot, P.A. (ed.) *Handbook of Stable Isotope Analytical Techniques*. China: Elsevier. 482-496
- Lécuyer, C., F. Fourel, F. Martineau, R. Amiot, A. Bernard, V. Daux, G. Escarguel & J. Morrison. 2007. High-precision determination of $^{18}\text{O}/^{16}\text{O}$ ratios of silver phosphate by EA-pyrolysis-IRMS continuous flow technique. *Journal of Mass Spectrometry*. **42**, 36
- Lécuyer, C., P. Grandjean, J.R. O'Neil, H. Cappetta & F. Martineau. 1993. Thermal excursions in the ocean at the Cretaceous-Tertiary boundary (Northern Morocco) - $\delta^{18}\text{O}$ record of phosphatic fish debris. *Palaeogeography Palaeoclimatology Palaeoecology*. **105**, 235

- Lécuyer, C., P. Grandjean, F. Paris, M. Robardet & D. Robineau. 1996. Deciphering "temperature" and "salinity" from biogenic phosphates: the $\delta^{18}\text{O}$ of coexisting fishes and mammals of the Middle Miocene sea of western France. *Palaeogeography Palaeoclimatology Palaeoecology*. **126**, 61
- Levine, S.N., M.P. Stainton & D.W. Schindler. 1986. A radiotracer study of phosphorus cycling in a eutrophic Canadian Shield lake, Lake-227, Northwestern Ontario. *Canadian Journal of Fisheries and Aquatic Sciences*. **43**, 366
- Li, X., Y. Wang, J. Stern & B.H. Cu. 2011. Isotopic evidence for the source and fate of phosphorus in Everglades wetland ecosystems. *Applied Geochemistry*. **26**, 688
- Liang, Y. & R.E. Blake. 2006a. Oxygen isotope composition of phosphate in organic compounds: isotope effects of extraction methods. *Organic Geochemistry*. **37**, 1263
- Liang, Y. & R.E. Blake. 2006b. Oxygen isotope signature of P_i regeneration from organic compounds by phosphomonoesterases and photooxidation. *Geochimica et Cosmochimica Acta*. **70**, 3957
- Liang, Y. & R.E. Blake. 2007. Oxygen isotope fractionation between apatite and aqueous-phase phosphate: 20–45 °C. *Chemical Geology*. **238**, 121
- Liu, Y., G. Villalba, R.U. Ayres & H. Schroder. 2008. Global phosphorus flows and environmental impacts from a consumption perspective. *Journal of Industrial Ecology*. **12**, 229
- Longinelli, A., M. Bartelloni & G. Cortecci. 1976. Isotopic cycle of oceanic phosphate. 1. *Earth and Planetary Science Letters*. **32**, 389
- Longinelli, A. & S. Nuti. 1973. Revised phosphate-water isotopic temperature scale. *Earth and Planetary Science Letters*. **19**, 373
- Ma, H.Z., H.E. Allen & Y.J. Yin. 2001. Characterization of isolated fractions of dissolved organic matter from natural waters and a wastewater effluent. *Water Research*. **35**, 985
- Manahan, S.E. 2004. Fundamentals of Aquatic Chemistry. *Environmental Chemistry*. 8 ed. USA: CRC Press. 68

- Markel, D., Y. Kolodny, B. Luz & A. Nishri. 1994. Phosphorus cycling and phosphorus sources in Lake Kinneret: tracing by oxygen isotopes in phosphate. *Israel Journal of Earth Sciences*. **43**, 165
- May, L. & B.M. Spears. 2011. Managing ecosystem services at Loch Leven, Scotland, UK: actions, impacts and unintended consequences. *Hydrobiologia*. **681**, 117
- McDowell, R.W., N. Cox, C.J. Daughney, D. Wheeler & M. Moreau. 2015. A national assessment of the potential linkage between soil, and surface and groundwater concentrations of phosphorus. *JAWRA Journal of the American Water Resources Association*. **51**, 992
- McGinley, P.M., K.C. Masarik, M.B. Gotkowitz & D.J. Mechenich. 2016. Impact of anthropogenic geochemical change and aquifer geology on groundwater phosphorus concentrations. *Applied Geochemistry*. **72**, 1
- McLaughlin, K., S. Silva, C. Kendall, H. Stuart-Williams & A. Paytan. 2004. A precise method for the analysis of $\delta^{18}\text{O}$ of dissolved inorganic phosphate in seawater. *Limnology and Oceanography: Methods*. **2**, 202
- McLaughlin, K., B.J. Cade-Menun & A. Paytan. 2006a. The oxygen isotopic composition of phosphate in Elkhorn Slough, California: a tracer for phosphate sources. *Estuarine Coastal and Shelf Science*. **70**, 499
- McLaughlin, K., F. Chavez, J.T. Pennington & A. Paytan. 2006b. A time series investigation of the oxygen isotopic composition of dissolved inorganic phosphate in Monterey Bay, California. *Limnology and Oceanography*. **51**, 2370
- McLaughlin, K., C. Kendall, S.R. Silva, M. Young & A. Paytan. 2006c. Phosphate oxygen isotope ratios as a tracer for sources and cycling of phosphate in North San Francisco Bay, California. *Journal of Geophysical Research-Biogeosciences*. **111**, G03003
- McLaughlin, K., A. Paytan, C. Kendall & S. Silva. 2006d. Oxygen isotopes of phosphatic compounds – application for marine particulate matter, sediments and soils. *Marine Chemistry*. **98**, 148
- McLaughlin, K., J.A. Sohm, G.A. Cutter, M.W. Lomas & A. Paytan. 2013. Phosphorus cycling in the Sargasso Sea: Investigation using the oxygen isotopic composition of phosphate, enzyme-labelled fluorescence, and turnover times. *Global Biogeochemical Cycles*. **27**, 375

- Meier-Augenstein, W. 1999. Applied gas chromatography coupled to isotope ratio mass spectrometry. *Journal of Chromatography A*. **842**, 351
- Monbet, P., I.D. McKelvie & P.J. Worsfold. 2009. Dissolved organic phosphorus speciation in the waters of the Tamar estuary (SW England). *Geochimica et Cosmochimica Acta*. **73**, 1027
- Monteith, D.T., C.D. Evans, P.A. Henrys, G.L. Simpson & I.A. Malcolm. 2014. Trends in the hydrochemistry of acid-sensitive surface waters in the UK 1988–2008. *Ecological Indicators*. **37**, 287
- Mooney-Slater, R.C.L. 1962. Polymorphic forms of bismuth phosphate. *Zeitschrift für Kristallographie*. **117**, 371
- Mulholland, P.J., A.M. Helton, G.C. Poole, R.O. Hall, S.K. Hamilton, B.J. Peterson, J.L. Tank, L.R. Ashkenas, L.W. Cooper, C.N. Dahm, W.K. Dodds, S.E. Findlay, S.V. Gregory, N.B. Grimm, S.L. Johnson, W.H. McDowell, J.L. Meyer, H.M. Valett, J.R. Webster, C.P. Arango, J.J. Beaulieu, M.J. Bernot, A.J. Burgin, C.L. Crenshaw, L.T. Johnson, B.R. Niederlehner, J.M. O'Brien, J.D. Potter, R.W. Sheibley, D.J. Sobota & S.M. Thomas. 2008. Stream denitrification across biomes and its response to anthropogenic nitrate loading. *Nature*. **452**, 202
- Murphy, J. & J.P. Riley. 1962. A modified single solution method for determination of phosphate in natural waters. *Analytica Chimica Acta*. **27**, 31
- Nakai, N. & M.L. Jensen. 1964. The kinetic isotope effect in the bacterial reduction and oxidation of sulfur. *Geochimica et Cosmochimica Acta*. **28**, 1893
- Neal, C., H.P. Jarvie, S.M. Howarth, P.G. Whitehead, R.J. Williams, M. Neal, M. Harrow & H. Wickham. 2000a. The water quality of the River Kennet: initial observations on a lowland chalk stream impacted by sewage inputs and phosphorus remediation. *Science of the Total Environment*. **251**, 477
- Neal, C., H.P. Jarvie, B. Whitton & J. Gemmel. 2000b. The water quality of the River Wear, north-east England. *Science of the Total Environment*. **251**, 153
- Neal, C., H.P. Jarvie, M. Neal, L. Hill & H. Wickham. 2006. Nitrate concentrations in river waters of the upper Thames and its tributaries. *Science of the Total Environment*. **365**, 15

- Newton, R. & S. Bottrell. 2007. Stable isotopes of carbon and sulphur as indicators of environmental change: past and present. *Journal of the Geological Society*. **164**, 691
- North, R.L., J. Johansson, D.M. Vandergucht, L.E. Doig, K. Liber, K.-E. Lindenschmidt, H. Baulch & J.J. Hudson. 2015. Evidence for internal phosphorus loading in a large prairie reservoir (Lake Diefenbaker, Saskatchewan). *Journal of Great Lakes Research*. **41**, 91
- Nowack, B. 2003. Environmental chemistry of phosphonates. *Water Research*. **37**, 2533
- Nürnberg, G.K., L.A. Molot, E. O'Connor, H. Jarjanazi, J. Winter & J. Young. 2013. Evidence for internal phosphorus loading, hypoxia and effects on phytoplankton in partially polymictic Lake Simcoe, Ontario. *Journal of Great Lakes Research*. **39**, 259
- O'Neil, J.R., T.W. Vennemann & W.F. McKenzie. 2003. Effects of speciation on equilibrium fractionations and rates of oxygen isotope exchange between $\text{PO}_{4(\text{aq})}$ and H_2O . *Geochimica et Cosmochimica Acta*. **67**, 3135
- Ott, C. & H. Rechberger. 2012. The European phosphorus balance. *Resources, Conservation and Recycling*. **60**, 159
- Parrish, J.T. 1990. Paleooceanographic and paleoclimatic setting of the Miocene phosphogenic episode. In: Burnett, W.C. & Riggs, S.R. (eds.) *Phosphate Deposits of the World*. Cambridge, UK: Cambridge University Press. 223-240
- Pennington, J.T. & F.P. Chavez. 2000. Seasonal fluctuations of temperature, salinity, nitrate, chlorophyll and primary production at station H3/M1 over 1989-1996 in Monterey Bay, California. *Deep-Sea Research Part II-Topical Studies in Oceanography*. **47**, 947
- Peterson, B.J., W.M. Wollheim, P.J. Mulholland, J.R. Webster, J.L. Meyer, J.L. Tank, E. Marti, W.B. Bowden, H.M. Valett, A.E. Hershey, W.H. McDowell, W.K. Dodds, S.K. Hamilton, S. Gregory & D.D. Morrall. 2001. Control of nitrogen export from watersheds by headwater streams. *Science*. **292**, 86
- Pigott, C.D. 1964. Nettles as indicators of soil conditions. *New Scientist*. **375**, 230
- Pilkaitytė, R. & A. Razinkovas. 2006. Factors controlling phytoplankton blooms in a temperate estuary: nutrient limitation and physical forcing. *Hydrobiologia*. **555**, 41

- Powers, S.M., T.W. Bruulsema, T.P. Burt, N.I. Chan, J.J. Elser, P.M. Haygarth, N.J.K. Howden, H.P. Jarvie, Y. Lyu, H.M. Peterson, A.N. Sharpley, J.B. Shen, F. Worrall & F.S. Zhang. 2016. Long-term accumulation and transport of anthropogenic phosphorus in three river basins. *Nature Geoscience*. **9**, 353
- Pucéat, E., M.M. Joachimski, A. Bouilloux, F. Monna, A. Bonin, S. Motreuil, P. Morinière, S. Hénard, J. Mourin, G. Dera & D. Quesne. 2010. Revised phosphate-water fractionation equation reassessing paleotemperatures derived from biogenic apatite. *Earth and Planetary Science Letters*. **298**, 135
- Redfield, A.C., B.H. Ketchum & F.A. Richards. 1963. The influence of organisms on the composition of sea-water. In: Hill, M.N. (ed.) *Global Coastal Ocean*. USA: John Wiley & Sons, Inc. 26-77
- Rhoton, F.E. & J.M. Bigham. 2005. Phosphate adsorption by ferrihydrite-amended soils. *Journal of Environmental Quality*. **34**, 890
- Rowe, H., P.J.A. Withers, P. Baas, N.I. Chan, D. Doody, J. Holiman, B. Jacobs, H. Li, G.K. MacDonald, R. McDowell, A.N. Sharpley, J. Shen, W. Taheri, M. Wallenstein & M.N. Weintraub. 2015. Integrating legacy soil phosphorus into sustainable nutrient management strategies for future food, bioenergy and water security. *Nutrient Cycling in Agroecosystems*. **104**, 393
- Ruffell, A.H. 1992. Correlation of the Hythe Beds Formation (Lower Greensand Group: early-mid-Aptian), southern England. *Proceedings of the Geologists' Association*. **103**, 273
- Ruttenberg, K.C. 2003. 8.13 - The global phosphorus cycle. *Treatise on Geochemistry*. **8: Biogeochemistry**, 585
- Salonen, K., R.J. Jones, H. de Haan & M. James. 1994. Radiotracer study of phosphorus uptake by plankton and redistribution in the water column of a small humic lake. *Limnology and Oceanography*. **39**, 69
- Sander, F. & E. Moore. 1979. Significance of ammonia in determining N:P ratio of sea water off Barbados, West Indies. *Marine Biology*. **55**, 17
- Sandy, E.H., R.E. Blake, S.J. Chang, Y. Jun & C. Yu. 2013. Oxygen isotope signature of UV degradation of glyphosate and phosphonoacetate: Tracing sources and cycling of phosphonates. *Journal of Hazardous Materials*. **260**, 947

- Sattari, S.Z., A.F. Bouwman, K.E. Giller & M.K. van Ittersum. 2012. Residual soil phosphorus as the missing piece in the global phosphorus crisis puzzle. *Proceedings of the National Academy of Sciences of the USA*. **109**, 6348
- Schindler, D.W. 1974. Eutrophication and recovery in experimental lakes - implications for lake management. *Science*. **184**, 897
- Schindler, D.W., S.R. Carpenter, S.C. Chapra, R.E. Hecky & D.M. Orihel. 2016. Reducing phosphorus to curb lake eutrophication is a success. *Environmental Science and Technology*. **50**, 8923
- Schwartz, F.W. & H. Zhang. 2003. *Fundamentals of Ground Water*. New York, USA, John Wiley & Sons
- Scott, T.M., J.B. Rose, T.M. Jenkins, S.R. Farrah & J. Lukasik. 2002. Microbial source tracking: current methodology and future directions. *Applied and Environmental Microbiology*. **68**, 5796
- Seitzinger, S.P. 1988. Denitrification in freshwater and coastal marine ecosystems: ecological and geochemical significance. *Limnology and Oceanography*. **33**, 702
- Seyhan, D., H.P. Weikard & E. van Ierland. 2012. An economic model of long-term phosphorus extraction and recycling. *Resources Conservation and Recycling*. **61**, 103
- Shand, P., J. Cobbing, R. Tyler-Whittle, A.F. Tooth & A. Lancaster. 2003. Baseline Report Series 9: The Lower Greensand of southern England. *British Geological Survey Commissioned Report*. No. CR/03/273N
- Shemesh, A. & Y. Kolodny. 1988. Oxygen isotope variations in phosphorites from the Southeastern Tethys. *Israel Journal of Earth Sciences*. **37**, 1
- SI 2000 No. 3184. Water Supply (Water Quality) Regulations 2000. *SI 2000 No. 3184*. England and Wales
- Simpson, J.M., J.W. Santo Domingo & D.J. Reasoner. 2002. Microbial source tracking: state of the science. *Environmental Science and Technology*. **36**, 5279

- Sims, J.T., R.R. Simard & B.C. Joern. 1998. Phosphorus loss in agricultural drainage: historical perspective and current research. *Journal of Environmental Quality*. **27**, 277
- Slomp, C.P. 2011. Give more priority to phosphorus studies. *Nature*. **478**, 459
- Smith, J.T., M.J. Bowes & C.R. Cailes. 2011. A review and model assessment of ³²P and ³³P uptake to biota in freshwater systems. *Journal of Environmental Radioactivity*. **102**, 317
- Smith, S.V., S. Serruya, Y. Geifman & T. Berman. 1989. Internal sources and sinks of water, P, N, Ca, and Cl in Lake Kinneret, Israel. *Limnology and Oceanography*. **34**, 1202
- Smith, V.H. & D.W. Schindler. 2009. Eutrophication science: where do we go from here? *Trends in Ecology & Evolution*. **24**, 201
- Smith, V.H., G.D. Tilman & J.C. Nekola. 1999. Eutrophication: impacts of excess nutrient inputs on freshwater, marine, and terrestrial ecosystems. *Environmental Pollution*. **100**, 179
- Sondergaard, M. & E. Jeppesen. 2007. Anthropogenic impacts on lake and stream ecosystems, and approaches to restoration. *Journal of Applied Ecology*. **44**, 1089
- Spears, B.M., L. Carvalho, R. Perkins, A. Kirika & D.M. Paterson. 2011. Long-term variation and regulation of internal phosphorus loading in Loch Leven. *Hydrobiologia*. **681**, 23
- Steinman, A., X. Chu & M. Ogdahl. 2009. Spatial and temporal variability of internal and external phosphorus loads in Mona Lake, Michigan. *Aquatic Ecology*. **43**, 1
- Stephan, E. 2000. Oxygen isotope analysis of animal bone phosphate: Method refinement, influence of consolidants, and reconstruction of palaeotemperatures for Holocene sites. *Journal of Archaeological Science*. **27**, 523
- Sterner, R.W., T. Andersen, J.J. Elser, D.O. Hessen, J.M. Hood, E. McCauley & J. Urabe. 2008. Scale-dependent carbon : nitrogen : phosphorus seston stoichiometry in marine and freshwaters. *Limnology and Oceanography*. **53**, 1169

- Stuart, M.E., P.J. Chilton, J.H. Kinniburgh & D.M. Cooper. 2007. Screening for long-term trends in groundwater nitrate monitoring data. *Quarterly Journal of Engineering Geology and Hydrogeology*. **40**, 361
- Sutcliffe, D. 1998. The ionic composition of surface waters in the English Lake District, related to bedrock geology, with some singular facts and speculation on the existence of mineral-rich groundwaters. *Freshwater Forum*. **11**, 30
- Tamburini, F., S.M. Bernasconi, A. Angert, T. Weiner & E. Frossard. 2010. A method for the analysis of the $\delta^{18}\text{O}$ of inorganic phosphate extracted from soils with HCl. *European Journal of Soil Science*. **61**, 1025
- Tamburini, F., V. Pfahler, E.K. Bunemann, K. Guelland, S.M. Bernasconi & E. Frossard. 2012. Oxygen isotopes unravel the role of microorganisms in phosphate cycling in soils. *Environmental Science and Technology*. **46**, 5956
- Tamburini, F., V. Pfahler, C. von Sperber, E. Frossard & S. Bernasconi. 2014. Oxygen isotopes for unravelling phosphorus transformations in the soil-plant system: a review. *Soil Science Society of America Journal*. **78**, 38
- Thingstad, T.F., E.F. Skjoldal & R.A. Bohne. 1993. Phosphorus cycling and algal-bacterial competition in Sandsfjord, Western Norway. *Marine Ecology-Progress Series*. **99**, 239
- Thomson-Bulldis, A. & D. Karl. 1998. Application of a novel method for phosphorus determinations in the oligotrophic North Pacific Ocean. *Limnology and Oceanography*. **43**, 1565
- Toor, G.S., L.M. Condron, H.J. Di, K.C. Cameron & B.J. Cade-Menun. 2003. Characterization of organic phosphorus in leachate from a grassland soil. *Soil Biology and Biochemistry*. **35**, 1317
- Tudge, A.P. 1960. A method of analysis of oxygen isotopes in orthophosphate - its use in the measurement of paleotemperatures. *Geochimica et Cosmochimica Acta*. **18**, 81
- Turner, B., I. McKelvie & P.M. Haygarth. 2002. Characterisation of water-extractable soil organic phosphorus by phosphatase hydrolysis. *Soil Biology & Biochemistry*. **34**, 27
- Turner, B.L. & P.M. Haygarth. 2005. Phosphatase activity in temperate pasture soils: Potential regulation of labile organic phosphorus turnover by phosphodiesterase activity. *Science of the Total Environment*. **344**, 27

- U.S. Senate. 1972. *Clean Water Act*. 33 U.S.C. §1251
- Vaccari, D.A. & N. Strigul. 2011. Extrapolating phosphorus production to estimate resource reserves. *Chemosphere*. **84**, 792
- Vennemann, T.W., H.C. Fricke, R.E. Blake, J.R. O'Neil & A. Colman. 2002. Oxygen isotope analysis of phosphates: a comparison of techniques for analysis of Ag_3PO_4 . *Chemical Geology*. **185**, 321
- Weiner, T., S. Mazeh, F. Tamburini, E. Frossard, S.M. Bernasconi, T. Chiti & A. Angert. 2011. A method for analyzing the $\delta^{18}\text{O}$ of resin-extractable soil inorganic phosphate. *Rapid Communications in Mass Spectrometry*. **25**, 624
- Whiticar, M.J. 1999. Carbon and hydrogen isotope systematics of bacterial formation and oxidation of methane. *Chemical Geology*. **161**, 291
- Wipfli, M.S., J.S. Richardson & R.J. Naiman. 2007. Ecological linkages between headwaters and downstream ecosystems: transport of organic matter, invertebrates, and wood down headwater channels. *Journal of the American Water Resources Association*. **43**, 72
- Withers, P.J., K.C. van Dijk, T.S. Neset, T. Nesme, O. Oenema, G.H. Rubaek, O.F. Schoumans, B. Smit & S. Pellerin. 2015. Stewardship to tackle global phosphorus inefficiency: the case of Europe. *Ambio*. **44 Suppl 2**, S193
- Withers, P.J.A. & H.P. Jarvie. 2008. Delivery and cycling of phosphorus in rivers: a review. *Science of the Total Environment*. **400**, 379
- Worsfold, P.J., P. Monbet, A.D. Tappin, M.F. Fitzsimons, D.A. Stiles & I.D. McKelvie. 2008. Characterisation and quantification of organic phosphorus and organic nitrogen components in aquatic systems: a review. *Analytica Chimica Acta*. **624**, 37
- Wu, J.F., W. Sunda, E.A. Boyle & D.M. Karl. 2000. Phosphate depletion in the western North Atlantic Ocean. *Science*. **289**, 759
- Xu, H., H.W. Paerl, B.Q. Qin, G.W. Zhu & G. Gao. 2010. Nitrogen and phosphorus inputs control phytoplankton growth in eutrophic Lake Taihu, China. *Limnology and Oceanography*. **55**, 420

- Young, K., G.K. Morse, M.D. Scrimshaw, J.H. Kinniburgh, C.L. MacLeod & J.N. Lester. 1999. The relation between phosphorus and eutrophication in the Thames Catchment, UK. *Science of the Total Environment*. **228**, 157
- Young, M.B., K. McLaughlin, C. Kendall, W. Stringfellow, M. Rollog, K. Elsbury, E. Donald & A. Paytan. 2009. Characterizing the oxygen isotopic composition of phosphate sources to aquatic ecosystems. *Environmental Science and Technology*. **43**, 5190
- Zhang, H., W. Davison, R. Gadi & T. Kobayashi. 1998. In situ measurement of dissolved phosphorus in natural waters using DGT. *Analytica Chimica Acta*. **370**, 29
- Zohar, I., A. Shaviv, T. Klass, K. Roberts & A. Paytan. 2010. Method for the analysis of oxygen isotopic composition of soil phosphate fractions. *Environmental Science and Technology*. **44**, 7583

Appendix

A.1 Supplementary elution profiling for Chapter 3

To ensure that the new conditions for the loading and elution of the anion exchange resin for **Method 3**, set out in **Section 3.5.2**, allowed full P_i adsorption to the resin and that P_i was effectively separated during the anion exchange resin elution, triplicate spiked MilliQ matrices – consisting of 0.6%_{v/v} acetic acid, 0.7 mg $P-PO_4.L^{-1}$, 11.2 mg $N-NO_3.L^{-1}$ and 3.3 mg $S-SO_4.L^{-1}$ – were loaded and eluted using the new conditions. The waste streams from the loading of the resins were collected and analysed for P_i , and were all below detection limits. The subsequent elution profiles exhibited a clear separation of P_i from SO_4^{2-} and almost complete P_i mass recovery was achieved (**Figure A.1**).

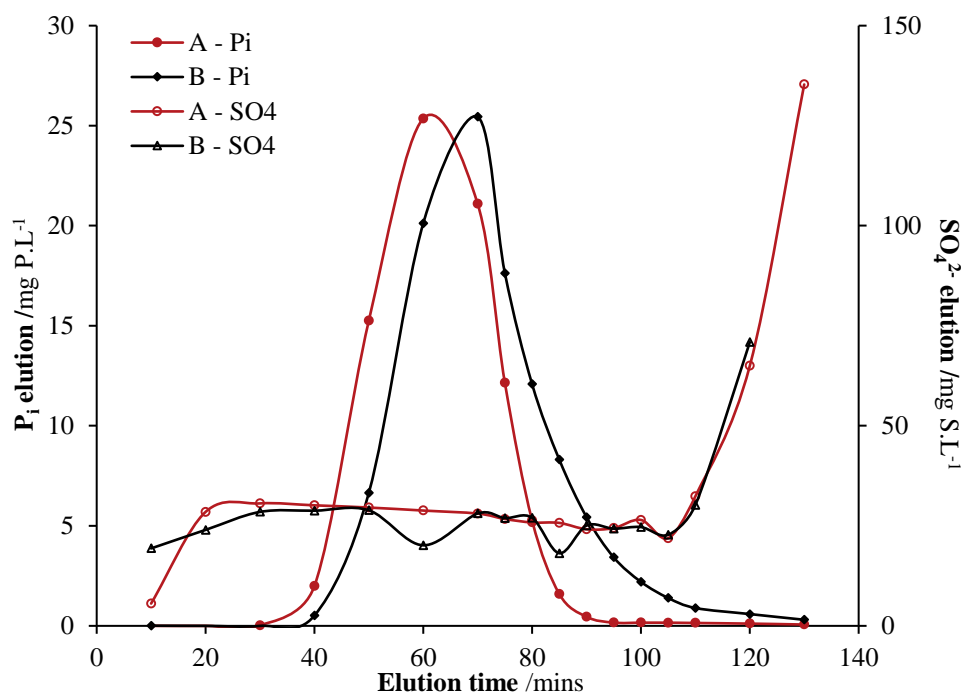


Figure A.1: Elution profiles for Cl^- -form anion exchange resins using 0.3M KCl with an elution rate of $1 mL.min^{-1}$ in two duplicate columns - A and B.

A.2 Supplementary field data for Chapter 5

For the in-stream field campaign presented in **Chapter 5**, an initial sampling trip was conducted in June 2015, alongside the first groundwater sampling campaign. This resulted in supplementary data surrounding two of sites described and measured in **Chapter 5** (sites E and F), as well as a new site R, being tested. Sample descriptions for all three sites are provided in **Table 5.2**, and their respective locations and geologies in **Figures 5.2** and **5.3**. **Table A.1** summarises the hydrochemical and stable isotope data collected during this initial sampling trip.

Table A.1: Dissolved (0.45 μ m) nutrient concentrations and stable isotopic data of supplementary surface water samples in the Wey catchment. Soluble reactive P (SRP) concentrations are given to 3 decimal places, temperature to 1 decimal place, alkalinity to 3 significant figures and the distance downstream and nitrate concentration to 2 decimal places. Molar ratios of N (in the form of NO₃⁻) to P (in the form of SRP), and C (in form of alkalinity and DOC) to P (in the form of SRP) are given to 3 significant figures. Oxygen isotope composition of phosphate ($\delta^{18}\text{O}_p$), water ($\delta^{18}\text{O}_w$) and the theoretical equilibrium ($\delta^{18}\text{O}_{eq}$) are given to 2 decimal places. The oxygen yields from pyrolysis of Ag₃PO₄ precipitates are given to 1 decimal place, a pure Ag₃PO₄ molecule would contain 15.3% oxygen.

		R	E	F
Distance downstream from A	/km	5.67*	8.38	9.19
[P_i]	mg P.L ⁻¹	0.072	0.034	0.958
[DOC]	/mg C.L ⁻¹	3.73	5.11	22.80
[NO₃⁻]	/mg N.L ⁻¹	3.63	4.92	20.14
T	°C	17.2	12.2	15.1
Alkalinity	mg HCO ₃ .L ⁻¹	334.0	295.6	209.7
Molar ratio N:P		112	320	46.5
Molar ratio C(Alk+DOC):P		4800	172	2490
Mean $\delta^{18}\text{O}_p$	/‰	17.22	n.d.	15.58
1σ (n)	/‰	0.35 (3)	n.d.	0.09 (3)
Mean $\delta^{18}\text{O}_w$	/‰	-5.70	-5.75	-5.73
Range (n)	/‰	0.01 (2)	n.d. (1)	0.08 (2)
$\delta^{18}\text{O}_{eq}$	/‰	17.59	18.43	17.93
$\delta^{18}\text{O}_p - \delta^{18}\text{O}_{eq}$	/‰	-0.37	n.d.	-2.35

n.d. = not determined; *Site R characterises the input from a tributary that enters the main stem at 5.67 km downstream from site A.